Mixed NNLO QCD×EW radiative corrections to W/Z production and decay

Dissertation

zur Erlangung des Doktorgrades
der Fakultät für Mathematik und Physik der

Albert-Ludwigs-Universität
Freiburg im Breisgau

vorgelegt von

Jan Schwarz

August 2023

Dekan: Prof. Dr. Michael Thoss
Referent: Prof. Dr. Stefan Dittmaier
Korreferent: PD Dr. Heidi Rzehak
Tag der mündlichen Prüfung: 1.12.2023

Contents

Chapter 1
Introduction

The identification of the fundamental constituents of matter and the description of interactions between these constituents is the main goal of particle physics. In the 1970s particle physicists formalized the so-called Standard Model (SM) of particle physics and ever since predictions made by the SM have been tested in a variety of experiments. So far, experimental results and theoretical predictions based on the SM show remarkable agreement. The SM is therefore arguably one of the most if not the most successful and predictive theory in physics ever created, and its theoretical completion in the 1970s marked a big step towards a theoretical description of the fundamental constituents of matter and their interactions.
The constituents of matter included in the SM are grouped into three generations of spin-$\frac{1}{2}$ particles, each generation containing two quarks, one neutral lepton-neutrino, and one charged lepton. These three generations differ only in the masses of the contained particles but otherwise carry identical quantum numbers. Three out of the four known forces acting on fermionic matter are incorporated in the SM and are mediated by spin-1 gauge bosons, where the photon mediates the electromagnetic force, the $W^{\pm}$ and Z bosons mediate the weak force, and eight gluons the strong force. The interaction of the eight gluons with themselves and with the quarks is described by the theory of Quantum Chromodynamics (QCD). The description of the weak and electromagnetic interactions mediated by the photon, the $W^{\pm}$ bosons, and Z boson is unified in the Glashow-Salam-Weinberg (GSW) model [1–4]. The Higgs boson is introduced as part of the so-called Higgsmechanism used to produce mass terms for the [5–8] massive $W^{\pm}$ and Z bosons, which where observed experimentally in 1982, without breaking the gauge symmetry of the GSW model. The discovery of a scalar particle with properties of the SM Higgs boson in 2012 [9, 10] at the Large Hadron Collider (LHC) at CERN completed the experimental search for particles predicted by the SM. Even though the predictions of the SM are in remarkable agreement with experimental results, there are some shortcomings or experimental observations that the SM cannot explain. The most obvious one is the missing description of the gravitational force. But also the origin of dark matter or the experimentally observed matter-anti-matter asymmetry in the universe are problems that cannot be solved by the SM. Therefore, the SM in its current form cannot be the ultimate description of Nature.

The most prominent experimental facility in high-energy physics used to test theoretical

predictions made by the SM and also potential theoretical extensions of it, is the LHC. The proton–proton collider started its research program in 2010 at a collision energy of 7 TeV. After a shutdown in 2022 it became operational again operating at a collision energy of 13.6 TeV. Due to its high cross section and clean experimental signature the Drell–Yan-like production of lepton pairs is among the most important standard-candle processes at the LHC [11–14] and can be used for both detector calibration and luminosity monitoring. Moreover, these processes provide the opportunity to gain insight on the mass and width of W bosons, they allow the search for new gauge bosons in the high-mass range, and the W charge asymmetry and the rapidity distributions of the Z boson can be used to constraint fits of the parton distribution functions (PDFs) [15]. Furthermore, Drell–Yan processes allow for the determination of precision observables in the vicinity of the Z resonance such as the effective weak mixing angle [16, 17], which can be extracted from the forward–backward asymmetry, A_{FB}. If we consider the long list of physical insights that can be gained by studying only DY processes—and of course there are many more processes that can be used to test different predictions by the SM, e.g. vector-boson-scattering—it becomes clear that with the discovery of the Higgs boson in 2012 the story of particle physics and the SM was and still is far from completed. In recent years, the focus of experimental searches at the LHC partly shifted from a rather broad investigation of the features predicted by the SM, i.e. findig all predicted particles, towards the strive for gaining more knowledge on the more subtle predictions by the SM that require more experimental accuracy, such as the measurement of the mass and width of the W boson or triple or quartic gauge couplings in multi-boson processes.

In order to perform precision tests of the Standard Model, theoretical predictions have to match the accuracy of the high-precision measurements mentioned above. This means that the calculation of higher-order corrections to DY processes is needed. Current state-of-the-art calculations involve electroweak fixed-order corrections up to next-to-leading order (NLO) [18–30] and leading higher-order effects from multiple photon emissions or of universal origin [26, 28, 29, 31, 32]. Fixed-order QCD calculations for inclusive observables are available up to next-to-next-to-next-to-leading order ($\mathrm{N^3LO}$) [33] whereas for differential observables predictions up to next-to-next-to-leading (NNLO) order [34–41] were made. These QCD corrections are supplemented by the calculation of threshold effects studied up to $\mathrm{N^3LO}$ accuracy [42, 43] and by resuming large logarithms occurring due to soft-gluon emissions at small transverse momentum [44–53]. It is commonly agreed that the calculation of $\mathcal{O}(\alpha_{\mathrm{s}}\alpha)$ corrections is needed in order to achieve the accuracy goal of minimizing the uncertainty on the W-boson mass to around 8 MeV [54]. This motivates the effort in recent years of calculating $\mathcal{O}(\alpha_{\mathrm{s}}\alpha)$ corrections to DY processes. To reduce the complexity of calculations and avoid at the time unknown two-loop box integrals the so-called pole approximation (PA) was used in [55, 56] to get a handle on these corrections. Applying the PA it is possible to classify corrections in a gauge-invariant way into so-called factorizable corrections that include corrections to the production and decay modes and non-factorizable corrections obtained from contributions including a soft photon that connects the production and decay of the intermediate W/Z boson. In [55] it has been shown that the non-factorizable contributions are phenomenologically negligible and in [56] that factorizable corrections of type "initial–final" lead to a mass shift of the W-boson mass of $\mathcal{O}(10\ \mathrm{MeV})$, proving the relevance of $\mathcal{O}(\alpha_{\mathrm{s}}\alpha)$ corrections in order to

achieve the targeted accuracy goal mentioned before. Quite recently the first complete calculations of differential $\mathcal{O}(\alpha_s\alpha)$ corrections to DY-like off-shell W/Z production were obtained [57, 58].
The only class of gauge-invariant corrections of $\mathcal{O}(\alpha_s\alpha)$ in the context of the PA that had not been calculated at the time of [56] are the initial–initial type corrections. It is one of the subjects of this thesis to complete the PA for the neutral-current DY process by calculating the remaining initial–initial type corrections and further study their impact on the forward–backward asymmetry A_{FB} of neutral-current DY processes in the resonance region of the intermediate Z boson. To our best knowledge, this is the first time that the impact of $\mathcal{O}(\alpha_s\alpha)$ corrections on the numerically challenging forward–backward asymmetry has been studied as there are no published results.
We have applied the PA and calculated the previously missing initial–initial type $\mathcal{O}(\alpha_s\alpha)$ corrections to the neutral-current DY processes in PA. This gauge-invariant part of the full set of $\mathcal{O}(\alpha_s\alpha)$ corrections in PA contains contributions where the corrections are solely contained in the production mode of the Z boson and include genuine two-loop virtual–virtual corrections, real–virtual corrections, and double-real $\mathcal{O}(\alpha_s\alpha_{phot})$ corrections. Furthermore, we also study the effect of the $\mathcal{O}(\alpha_s\alpha)$ corrections on the transverse-momentum and invariant-mass spectrum of the Z boson.

Since physics beyond the SM might also show up in the tails of invariant-mass or transverse-momentum distributions outside the resonance regions, it is important to provide information about the size of $\mathcal{O}(\alpha_s\alpha)$ corrections beyond the PA. A first step towards a calculation of the full $\mathcal{O}(\alpha_s\alpha)$ corrections to off-shell DY processes is the calculation of the gauge-invariant $\mathcal{O}(N_f\alpha_s\alpha)$ two-loop corrections to single W/Z-boson production which are enhanced by the number of fermion flavours N_f in the SM and result from diagrams including closed fermion loops and additional gluon exchange or radiation. Besides corrections containing one-particle-irreducible two-loop (sub)diagrams the $\mathcal{O}(N_f\alpha_s\alpha)$ corrections also contain reducible contributions which either involve a product of two one-loop subdiagrams or one-loop subdiagrams with an additional possibly unresolved QCD parton in the final state. We have evaluated the $\mathcal{O}(N_f\alpha_s\alpha)$ corrections to single W/Z-boson production in a fully differential manner and studied their effect on the (transverse) invariant-mass and transverse-momentum spectra of the W and Z boson, respectively. The calculation of virtual corrections of $\mathcal{O}(N_f\alpha_s\alpha)$ involves the issue of extending a gauge-invariant scheme for treating the W/Z resonance to this order. To solve this problem, we describe the generalization of the complex-mass scheme [59] (see also Ref. [60]), which is a standard method for a gauge-invariant treatment of resonances at NLO, for the application to W/Z resonances at $\mathcal{O}(\alpha_s\alpha)$.

This thesis is structured as follows:

- We start with an overview over the SM in Section 2.1, and its renormalization is part of Section 2.2. The renormalization of the electroweak sector defined by the GSW model using the on-shell scheme, the renormalization of QCD in the so-called $\overline{\text{MS}}$ scheme, and also different electroweak input-parameter schemes are discussed. Moreover, Chapter 2 contains a short review of the treatment of unstable particles in quantum field theory (QFT) and the complexified version of the on-shell scheme.

- In Chapter 3 we discuss factorization properties of amplitudes in infrared(IR)-singular limits including corrections up to next-to-next-to-leading order (NNLO). The properties shown there are the basis for the construction of "antenna subtraction terms", which is the content of Chapter 4.
- Chapter 5 is devoted to the calculation of $\mathcal{O}(N_f\alpha_s\alpha)$ two-loop corrections to DY-like W/Z-boson production. Before giving an overview over the different $\mathcal{O}(N_f\alpha_s\alpha)$ corrections to the squared amplitude we start with a short review of properties of the DY processes at leading order (LO), followed by a discussion of IR and ultraviolet (UV) singularities present at $\mathcal{O}(N_f\alpha_s\alpha)$ and their cancellation using antenna subtraction, and the extension of the complexified version of the on-shell renormalization scheme to $\mathcal{O}(\alpha_s\alpha)$.
- In Chapter 6 we begin with the discussion of the PA for processes with a single resonance and proceed with an overview over the classification of $\mathcal{O}(\alpha_s\alpha)$ corrections to DY-like Z production in PA into gauge-invariant parts. This is followed by the calculation of the various contributions to the initial–initial type corrections and an extensive discussion of NNLO antenna subtraction terms needed to cancel IR singularities.
- We conclude with a summary and outlook in Chapter 7.
- In the appendices we summarize some conventions and give auxiliary functions relevant for Chapter 5 and Chapter 6 in App. D and App. E, respectively. App. B contains a short overview over the kinematics relevant at hadron colliders.

Note the slightly unconventional ordering of starting with the discussion of the calculation of the $\mathcal{O}(N_f\alpha_s\alpha)$ corrections to off-shell DY processes and a subsequent discussion of $\mathcal{O}(\alpha_s\alpha)$ initial–initial corrections to DY-like Z production in PA. We organize the thesis in this way as the $\mathcal{O}(N_f\alpha_s\alpha)$ corrections contain vertex counterterm contributions which will also be included in the calculation of the $\mathcal{O}(\alpha_s\alpha)$ initial–initial corrections.

Chapter 2

The Standard Model and its renormalization

2.1 The Standard Model of particle physics

The Standard Model of particle physics (SM) is a relativistic quantum field theory that describes three out of the four known fundamental forces, namely the strong, the weak, and the electromagnetic forces. At small distances, or equivalently at large energies, the gravitational force is extremely small compared to the other three fundamental interactions and therefore negligible, which explains the applicability of the Standard Model in the description of physics at scales relevant for, e.g., particle colliders. The physics of strong interactions is described by quantum chromodynamics (QCD) [61–63] based on the non-abelian gauge group $SU(3)_C$. The Glashow–Salam–Weinberg model (GSW) [1–4], based on the spontaneously broken gauge group $SU(2)_W \times U(1)_Y$, provides a unified description of electromagnetic and weak interactions. This renders the Standard Model a spontaneously broken non-abelian gauge theory with gauge group,

$$SU(3)_C \times SU(2)_W \times U(1)_Y, \tag{2.1}$$

describing the continuous internal symmetries of the SM. The non-vanishing masses of the $W^{\pm}$ and Z gauge bosons of the GSW model are theoretically introduced by employing the mechanism of spontaneous symmetry breaking (SSB), allowing for the generation of mass terms without the explicit violation of gauge symmetries. This mechanism breaks the $SU(2)_W \times U(1)_Y$ symmetry of the GSW model spontaneously to the electromagnetic $U(1)_{EM}$ symmetry, so that the photon as the mediator of the electromagnetic force remains massless.

The quantum particle states of the SM are elements of an infinite-dimensional Hilbert space and are classified according to unitary infinite-dimensional irreducible representations of the Poincaré group introducing the mass m and the spin s of the particles as quantum numbers. The corresponding quantum fields belong to finite-dimensional irreducible representations of the Lorentz group. As the SM is formulated as a relativistic quantum field theory, the quantum fields are the relevant objects for the description of the dynamics of the SM. The fermionic fields are related to particles making up matter,

	generation							
	1	2	3	Q	$I^3_{\mathrm{W}}(\Psi_i^L)$	$I^3_{\mathrm{W}}(\Psi_i^R)$	$Y_{\mathrm{W}}(\Psi_i^L)$	$Y_{\mathrm{W}}(\Psi_i^R)$
charged leptons Ψ_L	e	μ	τ	-1	$-\frac{1}{2}$	0	-1	-2
neutral leptons Ψ_ν	ν_e	ν_μ	ν_τ	0	$+\frac{1}{2}$	-	-1	-
u-type quarks Ψ_u	u	c	t	$+\frac{2}{3}$	$+\frac{1}{2}$	0	$+\frac{1}{3}$	$+\frac{4}{3}$
d-type quarks Ψ_d	d	s	b	$-\frac{1}{3}$	$-\frac{1}{2}$	0	$+\frac{1}{3}$	$+\frac{2}{3}$

Table 2.1: The electroweak quantum numbers of the fermionic matter content of the SM, which is classified into three generations and a higher generation indicates a higher mass.

and bosonic fields correspond to particles mediating forces between the fermions. The dynamics of all SM fields follows from the Poincaré-invariant Lagrangian density,

$$\mathcal{L}_{\mathrm{SM}} = \mathcal{L}_{\mathrm{YM}} + \mathcal{L}_{\mathrm{Higgs}} + \mathcal{L}_{\mathrm{ferm}} + \mathcal{L}_{\mathrm{Yukawa}}, \tag{2.2}$$

which receives contributions from terms that describe the dynamics of fermionic ($\mathcal{L}_{\mathrm{ferm}}$) and bosonic ($\mathcal{L}_{\mathrm{YM}}$) fields, the breaking of the electroweak symmetry in order to introduce mass terms for the massive gauge bosons ($\mathcal{L}_{\mathrm{Higgs}}$), and the generation of mass terms for fermions ($\mathcal{L}_{\mathrm{Yukawa}}$). All of these contributions will be discussed individually in the following sections.

Fermions, local gauge invariance, and the Yang–Mills Lagrangian

The fermionic spin-$\frac{1}{2}$ particle content of Standard Model includes three generations of fermions, where each generation of fermions is an identical copy of the other generations except for the masses of the fermions, which increase with the generation. In principle it is not necessary to fix a certain number of fermion generations theoretically. However, as the flavour sector is the only source of the experimentally observed CP violation, one needs at least three fermion generations within the SM to incorporate this experimental observation. The SM fermions, divided into three generations, can be further classified according to the $SU(3)_C$ representation they belong to. The first class of particles transforms in the singlet representation of $SU(3)_C$ and are the so-called leptons. They include three electrically neutral particles, the neutrinos ν, and three electrically charged leptons l. The second group of particles transforms in the fundamental representation of $SU(3)_C$ and are the so-called quarks. The group of quarks is again subdivided by their electric charge into up-type u and down-type d quarks. Quarks are not observed as free particles, but confined into bound states called hadrons. The fermionic particle content of the SM is shown in Table 2.1.

The fermionic fields are elements of the Dirac representation of the Lorentz group and can be projected onto their left-chiral $(\frac{1}{2}, 0)$ and right-chiral $(0, \frac{1}{2})$ parts by using chirality projectors, $\omega_\pm = \frac{1}{2}(1 \pm \gamma_5)$ (see App. A for a definition of γ_5),

$$\Psi_L(x) = \omega_- \Psi(x) = \begin{pmatrix} \tilde{\Psi}_L(x) \\ 0 \end{pmatrix}, \quad \Psi_R(x) = \omega_+ \Psi(x) = \begin{pmatrix} 0 \\ \tilde{\Psi}_R(x) \end{pmatrix}, \tag{2.3}$$

where the spinor $\tilde{\Psi}_R$ ($\tilde{\Psi}_L$) is an element of the right-chiral $(0, \frac{1}{2})$ (left-chiral $(\frac{1}{2}, 0)$) spinor representation of the Lorentz group (see also App. A for more details on Weyl spinors). The experimentally observed parity violation is theoretically implemented in the SM by using different representations of the weak gauge group, $SU(2)_W$, in the left- and the right-handed components. The left-handed fields transform in the fundamental representation, whereas the right-handed fields are $SU(2)_W$ singlets. Therefore, right-handed fields do not couple to the gauge bosons of $SU(2)_W$.

The kinetic part of the fermionic Lagrangian is given by

$$\mathcal{L}_{\text{ferm,kin}} = \sum_{i=1}^{3} \left(\bar{\boldsymbol{\Psi}}^L_{L'_i} \partial\!\!\!/ \boldsymbol{\Psi}^L_{L'_i} + l'^R_i \partial\!\!\!/ l'^R_i + \bar{\boldsymbol{\Psi}}^L_{Q'_i} \partial\!\!\!/ \boldsymbol{\Psi}^L_{Q'_i} + d'^R_i \partial\!\!\!/ d'^R_i + u'^R_i \partial\!\!\!/ u'^R_i \right) \tag{2.4}$$

where $\partial\!\!\!/$ is defined in (A.11) and we have introduced weak isospin doublets for the left-handed fermions,

$$\boldsymbol{\Psi}^L_{L'_i} = \begin{pmatrix} \nu'^L_i \\ l'^L_i \end{pmatrix}, \qquad \boldsymbol{\Psi}^L_{Q'_i} = \begin{pmatrix} u'^L_i \\ d'^L_i \end{pmatrix}, \tag{2.5}$$

with i denoting the generation and the primes indicating that the fields are interaction eigenstates. Mass terms in the Lagrangian for the fermionic matter content will be discussed below, since a naive introduction of them would violate gauge invariance due to the different representations of left- and right-chiral fields. The guiding principle when constructing interaction terms of fermions and bosons is the demand on local gauge invariance of the Lagrangian. The kinetic Lagrangian in (2.4) is, however, only invariant under global gauge transformation of the fermionic fields $\boldsymbol{\Psi}(x)$,

$$\boldsymbol{\Psi}(x) \to U(\boldsymbol{\theta}_C, \boldsymbol{\theta}_W, \theta_Y)\boldsymbol{\Psi}(x) = \exp(-\mathrm{i}g_S\theta^a_C\hat{T}^a_C + \mathrm{i}g_2\theta^j_W\hat{T}^j_W - \mathrm{i}g_1\theta_Y\hat{T}_Y)\boldsymbol{\Psi}(x), \tag{2.6}$$

but not under the corresponding local gauge transformation where the global gauge parameters $\boldsymbol{\theta_C}$ of $SU(3)_C$, $\boldsymbol{\theta_W}$ of $SU(2)_W$, and θ_Y of $U(1)_Y$, also depend on x, respectively. Note that the form of the generators, $\hat{T}^a_C$, $\hat{T}^j_W$, and $\hat{T}_Y$, of the Lie algebras depends on the representation the fields $\boldsymbol{\Psi}(x)$ belong to. Local gauge invariance of the kinetic part of fermionic Lagrangian is obtained by replacing the ordinary derivative by the covariant derivative

$$D_\mu = \partial_\mu + \mathrm{i}g_s G^a_\mu(x)\hat{T}^a_C - \mathrm{i}g_2 W^j_\mu(x)\hat{T}^j_W + \mathrm{i}g_1 B_\mu(x)\hat{T}_Y, \tag{2.7}$$

where the vector fields B_μ, W^j_μ $(j = 1, 2, 3)$, and G^a_μ $(a = 1, \ldots, 8)$, introduced in the covariant derivative, are the gauge fields corresponding to gauge bosons. These fields have the following behaviour under gauge transformations,

$$B_\mu \to B_\mu + \partial_\mu\theta_Y(x), \tag{2.8}$$

$$W^j_\mu\hat{T}^j_W \to U_W(\boldsymbol{\theta}_W(x))\left(W^j_\mu\hat{T}^j_W + \frac{\mathrm{i}}{g}\partial_\mu\right)U_W(\boldsymbol{\theta}_W(x))^\dagger, \tag{2.9}$$

$$G^a_\mu\hat{T}^a_C \to U_C(\boldsymbol{\theta}_C(x))\left(G^a_\mu\hat{T}^a_C + \frac{\mathrm{i}}{g_s}\partial_\mu\right)U_C(\boldsymbol{\theta}_C(x))^\dagger. \tag{2.10}$$

The combination of covariant derivative and fermionic field transforms according to

$$D_\mu \Psi(x) \to U(\boldsymbol{\theta}(x)) D_\mu \Psi(x). \tag{2.11}$$

Replacing the ordinary derivative by the covariant derivative in order to obtain a Lagrangian that is invariant under local gauge transformations leads to a Lagrangian which includes the kinetic part of the fermionic Lagrangian but also interaction terms between the fermions and the gauge bosons,

$$\begin{aligned}\mathcal{L}_{\text{ferm}} = \sum_{i=1}^{3} \Bigg[& \bar{\boldsymbol{\Psi}}^L_{L'_i} \Big(\not{\partial} - \mathrm{i} g_2 \not{W}^a \tau^a + \mathrm{i} g_1 \frac{Y_L}{2} \not{B} \Big) \boldsymbol{\Psi}^L_{L'_i} + l'^R_i \Big(\not{\partial} + \mathrm{i} g_1 \frac{Y_l}{2} \not{B} \Big) l'^R_i \\ & + \bar{\boldsymbol{\Psi}}^L_{Q'_i} \Big(\not{\partial} + \mathrm{i} g_s \not{G}^a \frac{\lambda^a}{2} - \mathrm{i} g_2 \not{W}^a \tau^a + \mathrm{i} g_1 \frac{Y_Q}{2} \not{B} \Big) \boldsymbol{\Psi}^L_{Q'_i} + \\ & + d'^R_i \Big(\not{\partial} + \mathrm{i} g_s \not{G}^a \frac{\lambda^a}{2} + \mathrm{i} g_1 \frac{Y_d}{2} \not{B} \Big) d'^R_i + u'^R_i \Big(\not{\partial} + \mathrm{i} g_s \not{G}^a \frac{\lambda^a}{2} + \mathrm{i} g_1 \frac{Y_u}{2} \not{B} \Big) u'^R_i \Bigg].\end{aligned} \tag{2.12}$$

In (2.12) we have replaced the Lie algebra generators according to the representation of the gauge groups the fermions belong to, which means that $\hat{T}^a_C$ is replaced by the Gell-Mann matrices $\frac{\lambda^a}{2}$ for quarks, $\hat{T}_Y$ by the number $\frac{Y_W}{2}$, where Y_W is the so-called weak hypercharge, and $\hat{T}^j_W$ either by normalized Pauli matrices $\tau^j = I^j_W = \frac{\sigma^j}{2}$ (for left-handed fields) or by $\hat{T}^j_W = 0$ (for right-handed fields). Using the Gell-Mann–Nishijima relation (which will be motivated in the next section),

$$Q = I^3_W + \frac{Y_W}{2}, \tag{2.13}$$

the weak hypercharges, Y_W, are chosen such that the fields obtain the correct electric charges

$$Q l'_i = -1 l'_i, \qquad Q \nu'_i = 0, \qquad Q u'_i = +\frac{2}{3} u'_i, \qquad Q d'_i = -\frac{1}{3} d'_i. \tag{2.14}$$

The dynamics of the gauge fields present in the SM, introduced as part of the covariant derivative, is described by the Yang–Mills Lagrangian,

$$\mathcal{L}_{\text{YM}} = -\frac{1}{4} G^a_{\mu\nu} G^{a,\mu\nu} - \frac{1}{4} W^i_{\mu\nu} W^{i,\mu\nu} - \frac{1}{4} B_{\mu\nu} B^{\mu\nu}, \tag{2.15}$$

where the field-strength tensors are defined as,

$$\begin{aligned} G^a_{\mu\nu} &= \partial_\mu G^a_\nu - \partial_\nu G^a_\mu - g_s f^{abc} G^b_\mu G^c_\nu, \\ W^j_{\mu\nu} &= \partial_\mu W^j_\nu - \partial_\nu W^j_\mu + g_2 \varepsilon^{jkl} W^k_\mu W^l_\nu, \\ B_{\mu\nu} &= \partial_\mu B_\nu - \partial_\nu B_\mu. \end{aligned} \tag{2.16}$$

The non-abelian nature of $SU(3)_C$ and $SU(2)_W$ manifests itself by the non-commutativity of the corresponding generators of the respective Lie algebra

$$\left[T^a, T^b \right] = c^{abc}\, T^c, \tag{2.17}$$

where c^{abc} has to be replaced by the structure constant of the gauge group the generators, T^a, are associated to. The non-abelian structure of $SU(3)_C$ and $SU(2)_W$ leads to non-vanishing structure constants. When the corresponding field-strength tensors are squared in the Yang-Mills Lagrangian, these terms proportional to the structure constants then result in self-interaction terms of the gauge bosons associated to $SU(3)_C$ and $SU(2)_W$. Due to the abelian nature of the $U(1)_Y$ gauge group no such self-interaction terms are generated in the Yang-Mills Lagrangian.
Using the behaviour of the covariant derivative under gauge transformations given in Eq. (2.11), and the relation of the field-strength tensors to the commutator of covariant derivatives,

$$[D_\mu, D_\nu] = \mathrm{i}g_s G^a_{\mu\nu}\hat{T}^a_C - \mathrm{i}g_2 W^j_{\mu\nu}\hat{T}^j_W + \mathrm{i}g_1 B_{\mu\nu}, \tag{2.18}$$

one obtains the behaviour of the field-strength tensors under gauge transformation which can be used to verify the gauge invariance of the Lagrangian $\mathcal{L}_{\mathrm{YM}}$ in (2.15).

Higgs part

The naive introduction of mass terms in the SM Lagrangian is not possible, as they would spoil gauge invariance. The mechanism of spontaneous symmetry breaking offers a solution to this problem by introducing a complex scalar colour-neutral weak-isospin doublet,

$$\Phi(x) = \begin{pmatrix} \phi^+(x) \\ \phi^0(x) \end{pmatrix}, \tag{2.19}$$

with a non-vanishing vacuum expectation value (vev). Choosing a certain vacuum state Φ_0 breaks the full symmetry group $SU(2)_W \times U(1)_Y$ of the Lagrangian. Expanding the scalar isospin doublet Φ around the chosen vev $\Phi(x) = \Phi_0 + \varphi(x)$ introduces the Higgs field and two would-be Goldstone bosons as part of $\varphi(x)$. By choosing the vev Φ_0 properly, the Lagrangian in terms of the fluctuating field around the vev $\varphi(x)$ and the vev Φ_0 will have only a residual $U(1)_{EM}$ gauge symmetry instead of the full electroweak gauge symmetry group. Terms within the Lagrangian that include the vev Φ_0 provide the desired mass terms for the $W^\pm$ and Z boson. It is, however, important to mention that the Lagrangian in terms of the original scalar isospin doublet $\Phi(x)$ still has the full $SU(2)_W \times U(1)_Y$ gauge symmetry, it is just not obvious when writing the Lagrangian in terms of $\varphi(x)$. The generation of mass terms for gauge bosons using spontaneous symmetry breaking, also known as "Higgs mechanism", is discussed in more detail in the following.

Renormalizability and gauge invariance constrain the allowed terms for the Lagrangian of the scalar isospin doublet Φ, leading to

$$\mathcal{L}_{\mathrm{Higgs}} = (D_\mu\Phi)^\dagger(D^\mu\Phi) - V(\Phi), \tag{2.20}$$

with the potential

$$V(\Phi) = -\mu^2\Phi^\dagger\Phi + \frac{\lambda}{4}\big(\Phi^\dagger\Phi\big)^2, \quad \mu^2, \lambda > 0. \tag{2.21}$$

Higher powers of $\Phi^\dagger\Phi$ are not allowed as they would lead to a coupling with negative mass dimension and therefore contradict the requirement of renormalizability. The parameters λ and μ^2 are chosen such that the scalar field develops a nonzero vev, Φ_0, which is the minimum of the potential $V(\Phi)$ at $|\Phi| \neq 0$ and is determined by the condition

$$\Phi_0^\dagger\Phi_0 = \frac{2\mu^2}{\lambda} \equiv \frac{v^2}{2}. \tag{2.22}$$

As mentioned above, by choosing the vacuum state properly, one can break the $SU(2)_W \times U(1)_Y$ down to a $U(1)_{EM}$ symmetry. As we will see below, a possible choice that leads to this behaviour is given by

$$\langle\Phi\rangle = \Phi_0 = \begin{pmatrix} 0 \\ \frac{v}{\sqrt{2}} \end{pmatrix}. \tag{2.23}$$

Fluctuations around this ground state can be parametrized by

$$\Phi(x) = \begin{pmatrix} 0 \\ \frac{v}{\sqrt{2}} \end{pmatrix} + \begin{pmatrix} \phi^+(x) \\ \frac{1}{\sqrt{2}}(H(x) + \mathrm{i}\chi(x)) \end{pmatrix} = \Phi_0 + \varphi(x), \tag{2.24}$$

where the real field H corresponds to the neutral spin-0 Higgs particle with mass

$$M_H = \sqrt{2}\mu. \tag{2.25}$$

The real field χ, the complex field ϕ^+, and its adjoint ϕ^- correspond to unphysical would-be Goldstone bosons, which provide the necessary longitudinal degrees of freedom to render the weak gauge bosons W, Z massive. Inserting the field Φ, expanded around its vev given in (2.24), into the Lagrangian $\mathcal{L}_{\text{Higgs}}$, we obtain the Lagrangian in terms of the Higgs boson and the would-be Goldstone bosons,

$$\mathcal{L}_{\text{Higgs}} = \frac{1}{2}(\partial_\mu H)(\partial^\mu H) - \mu^2 H^2 + \mathcal{L}_{\text{Mass}} + \text{“interaction terms”}. \tag{2.26}$$

The mass terms for the massive gauge bosons are produced from contributions that only include the vev Φ_0,

$$\begin{aligned} \mathcal{L}_{\text{Mass}} =& (D_\mu\Phi_0)^\dagger(D^\mu\Phi_0) \\ =& \frac{1}{4}\frac{v^2}{2}\left(g_2^2\sum_{a=1}^{2} W_\mu^a W^{a,\mu} + (g_2 W_\mu^3 + g_1 B_\mu)(g_2 W^{3,\mu} + g_1 B^\mu)\right). \end{aligned} \tag{2.27}$$

In order to obtain a diagonal mass matrix we rotate the fields W_μ^3 and B_μ into the A_μ and Z_μ fields and additionally define the electromagnetic charge eigenstates $W_\mu^\pm$ by,

$$\begin{pmatrix} A_\mu \\ Z_\mu \end{pmatrix} = \begin{pmatrix} \cos\theta_W & -\sin\theta_W \\ \sin\theta_W & \cos\theta_W \end{pmatrix} \begin{pmatrix} B_\mu \\ W_\mu^3 \end{pmatrix}, \qquad W_\mu^\pm = \frac{1}{\sqrt{2}}(W_\mu^1 \pm \mathrm{i}W_\mu^2), \tag{2.28}$$

where the weak mixing angle θ_W is fixed according to

$$\cos\theta_W = \frac{g_2}{\sqrt{g_2^2 + g_1^2}}. \tag{2.29}$$

Using $I^{\pm} = I^1_W \pm \mathrm{i} I^2_W$, we are now able to show that the Lagrangian including the mass terms for the gauge bosons from above does not include a mass term for the photon. We start by rewriting the covariant derivative in terms of the rotated fields,

$$D_\mu = \partial_\mu - \mathrm{i}\frac{g_2}{\sqrt{2}} \sum_{\pm} W^{\pm}_\mu I^{\pm} - \mathrm{i}\frac{1}{\sqrt{g_1^2+g_2^2}} Z_\mu \left(g_2^2 I^3_W - g_1^2 \frac{Y_W}{2} \right) - \mathrm{i}\frac{g_1 g_2}{\sqrt{g_1^2+g_2^2}} Q A_\mu, \quad (2.30)$$

where we have identified the electric charge Q by

$$Q = I^3_W + \frac{Y_W}{2}. \quad (2.31)$$

Note that the last equation motivates the Gell-Mann–Nishijima relation that we already introduced in (2.13). We now observe that the combination of gauge group generators, which we identified with the electric charge Q and are multiplied with the field A_μ in the covariant derivative, vanishes when applied to the vev chosen before,

$$Q\,\Phi_0 = \left(I^3_W + \frac{Y_W}{2} \right) \Phi_0 = \begin{pmatrix} 1 & 0 \\ 0 & 0 \end{pmatrix} \begin{pmatrix} 0 \\ \frac{v}{\sqrt{2}} \end{pmatrix} = 0. \quad (2.32)$$

Therefore, we conclude that there is no term in $(D_\mu \Phi_0)^\dagger (D^\mu \Phi_0)$, that corresponds to a mass term for the photonic field A_μ and the photon indeed remains massless. As mentioned above, the fields $W^{\pm}_\mu(x)$ turn out to be eigenstates of the charge operator Q with eigenvalues ± 1. The masses of the gauge bosons are identified in $(D_\mu \Phi_0)^\dagger (D^\mu \Phi_0)$ as,

$$M_W = g_2 \frac{v}{2}, \quad M_Z = \frac{v}{2}\sqrt{g_1^2+g_2^2}, \quad M_A = 0. \quad (2.33)$$

Identifying the electric unit charge with the coupling of the photonic field A_μ to charged fermions, one obtains

$$e = \frac{g_1 g_2}{\sqrt{g_1^2+g_2^2}}. \quad (2.34)$$

After choosing the specific ground state Φ_0, expanding around this ground state $\Phi(x) = \Phi_0 + \varphi(x)$, and rewriting $\mathcal{L}_{\text{Higgs}}$ in terms of $\varphi(x)$, the result is invariant under the simultaneous gauge transformation

$$\begin{aligned} \varphi(x) &\to \exp\Big(\mathrm{i} e Q \theta(x) \Big) \varphi(x) \\ A_\mu(x) &\to A_\mu + \partial_\mu \theta(x), \end{aligned} \quad (2.35)$$

since there is no mass term for the field A_μ. This means that the original $SU(2)_W \times U(1)_Y$ symmetry has been broken down to the $U(1)_{EM}$ symmetry.

Fermion masses

The experimentally observed parity violation is implemented in the SM by assigning different representations of $SU(2)_W$ to the left- and right-chiral parts of fermionic fields.

The introduction of a naive mass term would mix left- and right-handed components of fermionic fields and therefore violate gauge invariance of the Lagrangian. Also in the fermionic sector the $SU(2)_W$ Higgs doublet is the key ingredient in the generation of mass terms. However, in contrast to the bosonic sector, where the interplay of the non-vanishing vev of the Higgs doublet with the covariant derivative leads to mass terms for the massive vector bosons, in the fermionic sector mass terms are generated via the introduction of Yukawa couplings of the left-handed isospin doublets, the right-handed fermions, and the Higgs doublet,

$$\mathcal{L}_{\text{Yukawa}} = -\sum_{i,j}\left(G^l_{ij}\bar{\Psi}^L_{L'_i}\Phi\ l'^R_j + G^u_{ij}\bar{\Psi}^L_{Q'_i}\Phi^c\ u'^R_j + G^d_{ij}\bar{\Psi}^L_{Q'_i}\Phi\ d'^R_j + \text{h.c.}\right), \tag{2.36}$$

where we used the charge conjugate of the Higgs doublet

$$\Phi^c = \begin{pmatrix}(\phi^0)^*\\ -\phi^-\end{pmatrix} \tag{2.37}$$

and the Yukawa couplings G^f, $f = l, u, d$, are complex 3×3 matrices in generation space. The mass terms for fermions are obtained by splitting the Higgs doublet into its vev and the fields fluctuating around the vev (2.24), $\Phi(x) = \Phi_0 + \varphi(x)$. The terms in (2.36) including the vev then produce the fermionic mass terms,

$$\mathcal{L}_{\text{Mass,f}} = -M_f\bar{f}_L f'_R + \text{h.c.} = \frac{1}{\sqrt{2}}v\bar{f}'_L G^f f'_R + \text{h.c.},\ \text{with}\ f' = l', u', d'. \tag{2.38}$$

In order to obtain diagonal mass matrices one can use biunitary transformations,

$$\text{diag}(m_{f_i}) = \frac{v}{\sqrt{2}}U^L_f G^f U^{R\dagger}_f. \tag{2.39}$$

The "physical fermion fields" correspond to mass eigenstates and are obtained by applying the unitary matrices $U^{L/R}_f$ to the primed fields that correspond to eigenstates of the gauge interactions

$$\Psi^L_{f_i} = \sum_{k=1}^{3} U^L_{f,ik}\Psi^L_{f'_k}, \qquad f^R_i = \sum_{k=1}^{3} U^R_{f,ik}f'^R_k. \tag{2.40}$$

Since neutrinos are assumed to be massless in the SM, we can choose the same unitary transformation for the neutrinos as for the leptons, $U^L_\nu = U^L_l$, so that U^L_l drops out off the Lagrangian. In the quark sector the transformation matrices $U^{R/L}_{u/d}$ drop out in interaction terms in the Lagrangian that are flavour diagonal. However, in the $W^\pm_\mu$ coupling terms,

$$\frac{g_2}{\sqrt{2}}(\bar{u}^L W^+ d^L + \bar{d}^L W^- u^L), \tag{2.41}$$

and also in $\phi^+\bar{u}d$ and $\phi^-\bar{d}u$ interaction terms present in (2.36) the transformation matrices do not cancel and instead introduce the Cabibbo–Kobayashi–Maskawa (CKM) matrix,

$$\mathbf{V}_{CMK} = U^L_u U^{L\dagger}_d. \tag{2.42}$$

The CKM matrix can be parametrized by four parameters, one complex phase and three angles. The complex phase used to parametrize the CKM matrix is the only source of $\mathcal{CP}$ violation in the SM.

Quantization

When using functional integrals to quantize gauge theories one is obliged to introduce a gauge-fixing prescription to handle divergent contributions to the path integral, originating from physically equivalent field configurations, which are related by gauge transformations. The Fadeev–Popov procedure [64] can be used to split off the infinite gauge-invariant volume of the local gauge group from the functional integral. After normalization of the path integral this infinite factor drops out.

Using the Fadeev–Popov procedure, the gauge-symmetry-breaking contribution is introduced as an additional term in the Lagrangian, $\mathcal{L}_{\text{fix}}$, which is added to the SM Lagrangian and allows for the extraction of the infinite gauge-invariant volume of the local gauge group. The introduction of the additional term, $\mathcal{L}_{\text{fix}}$, is compensated by the Faddeev–Popov Lagrangian, $\mathcal{L}_{\text{FP}}$, which ensures that each representative field configuration of a "gauge orbit" is taken into account with the correct weight. In total, this leads to an effective SM Lagrangian of the form

$$\mathcal{L}_{\text{SM,eff}} = \mathcal{L}_{\text{SM}} + \mathcal{L}_{\text{fix}} + \mathcal{L}_{\text{FP}}. \tag{2.43}$$

The gauge-fixing Lagrangian is given in terms of gauge-fixing functionals,

$$\mathcal{L}_{\text{fix}} = -\frac{1}{2\xi_A}(f^A)^2 - \frac{1}{2\xi_Z}(f^Z)^2 - \frac{1}{2\xi_G}(f^{G,a})^2 - \frac{1}{\xi_W} f^+ f^-, \tag{2.44}$$

which are, in case of the SM, typically chosen as,

$$\begin{aligned} f^Z &= \partial^\mu Z_\mu - \mathrm{i}\xi'_Z M_Z \chi^\pm, & f^A &= \partial^\mu A_\mu, \\ f^\pm &= \partial^\mu W^\pm_\mu \mp \mathrm{i}\xi'_W M_W \phi^\pm, & f^{G,a} &= \partial^\mu G^a_\mu. \end{aligned} \tag{2.45}$$

By using the 't Hooft-Feynman gauge, $\xi_V^{(\prime)} = 1$ $(V = A, Z, W, G)$, the masses of the unphysical would-be Nambu–Goldstone bosons reduce to the masses of corresponding physical bosons, $M_{\phi^\pm} \to M_W$ and $M_\chi \to M_Z$. Moreover, the mixing terms of would-be Goldstone fields and gauge bosons in the electroweak Lagrangian can be canceled against terms in the gauge-fixing Lagrangian using the 't Hooft-Feynman gauge and the gauge-boson propagators reduce to the form

$$\Delta^V_{\mu\nu}(p) = \frac{-\mathrm{i}\, g_{\mu\nu}}{p^2 - M_V^2 + \mathrm{i}0}. \tag{2.46}$$

The Faddeev-Popov Lagrangian $\mathcal{L}_{\text{FP}}$ is given in terms of so-called ghosts u^a and $\bar{u}^a$, which are Grassmann-valued scalar fields and correspond to unphysical states. Explicitly the Faddeev-Popov Lagrangian reads

$$\mathcal{L}_{\text{FP}} = -\bar{u}^a M^{ab} u^b, \ (a, b = \pm, Z, A). \tag{2.47}$$

The operator M^{ab} is given by the variation of the gauge-fixing functionals (2.45) with respect to infinitesimal gauge parameters $\delta\theta^a$,

$$M^{ab}(x)\delta(x-y) = \frac{\delta f_a(x)}{\delta\theta^b(y)}. \tag{2.48}$$

2.2 Renormalization

A Lagrangian of a given model depends on a certain number of independent input parameters which have to be determined by experiment. These parameters are usually chosen such that they have a physical meaning directly related to experimental measurable quantities or because chosing them is theoretically motivated. Precision measurements of strong and electroweak processes, however, require the calculation of higher-order corrections to tree-level approximations within the SM. Including these corrections in theoretical predictions changes the relation between parameters of the SM Lagrangian at tree level, called the "bare" parameters (denoted by a subscript "0"), and observables and therefore spoils the direct relation between these parameters and physical quantities.
Additionally, higher-order corrections contain loop diagrams that introduce so-called ultraviolet (UV) divergent contributions to theoretical predictions, which are a result of regions included in the corresponding loop integrals, where the loop momenta tend towards infinity. It was shown by 't Hooft [65] that gauge theories are renormalizable, i.e. that both for unbroken and spontaneously broken gauge theories it is possible to eliminate all UV divergences in observable quantities (cross sections or decay widths) in all orders of perturbation theory by absorbing them into a finite set of renormalization constants, which are introduced by reparametrizing the bare parameters $\{g_{1,0}, \dots, g_{n,0}\}$ in terms of UV-divergent renormalization constants $\{Z_{g_1}, \dots, Z_{g_n}\}$ and finite renormalized parameters $\{g_1, \dots, g_n\}$. We use a multiplicative renormalization, i.e. we reparametrize all bare parameters, $g_{i,0}$, in the SM Lagrangian by $g_{i,0} = Z_{g_i} g_i$ and expand the renormalization constant, $Z_{g_i} = 1 + \delta Z_{g_i} + \mathcal{O}(g_i^2)$, using perturbation theory. Applying this renormalization transformation to the bare parameters of the SM Lagrangian, one can split the bare Lagrangian, $\mathcal{L}_{SM,0}$, into a part containing only renormalized input parameters, $\mathcal{L}_{SM}$, and a counterterm part that contains renormalized input parameters and renormalization constants, $\delta\mathcal{L}_{SM}$. In total we have,

$$\mathcal{L}_{SM,0}(g_{1,0}, \dots) = \mathcal{L}_{SM}(g_1, \dots) + \delta\mathcal{L}_{SM}(g_1, \dots), \tag{2.49}$$

where $\delta\mathcal{L}_{SM}$ is the so-called counterterm Lagrangian containing all renormalization constants δZ_{g_i} and $\mathcal{L}_{SM}$ is obtained by the replacement $g_{i,0} \to g_i$ in $\mathcal{L}_{SM,0}$. As input parameters of the Lagrangian we choose the electromagnetic and strong couplings, the masses of the fermions and gauge bosons, and the CKM matrix $\mathbf{V}_0$:

$$e_0, g_{s,0}, m_{f,i,0}, M_{W,0}, M_{Z,0}, M_{H,0}, \mathbf{V}_0. \tag{2.50}$$

For these input parameters we introduce the following renormalization transformations,

$$\begin{aligned} e_0 &= (1 + \delta Z_e)e, & M^2_{H,0} &= M^2_H + \delta M^2_H, \\ M^2_{W,0} &= M^2_W + \delta M^2_W, & m_{f,i,0} &= m_{f,i} + \delta m_{f,i}, \\ M^2_{Z,0} &= M^2_Z + \delta M^2_Z, & V_{ij,0} &= V_{ij} + \delta V_{ij}. \end{aligned} \tag{2.51}$$

Renormalizing the parameters of the SM Lagrangian is sufficient to obtain UV-finite S-matrix elements, but in order to get finite Green's functions as well, one has to renormalize

the fields in the same way as described above for the parameters. The field renormalization transformations read

$$\begin{aligned}
W_0^\pm =& \sqrt{Z_W} W^\pm = (1 + \frac{1}{2}\delta Z_W) W^\pm, \\
\begin{pmatrix} Z_0 \\ A_0 \end{pmatrix} =& \begin{pmatrix} Z_{ZZ}^{1/2} & Z_{ZA}^{1/2} \\ Z_{AZ}^{1/2} & Z_{AA}^{1/2} \end{pmatrix} \begin{pmatrix} Z \\ A \end{pmatrix} = \begin{pmatrix} 1 + \frac{1}{2}\delta Z_{ZZ} & \frac{1}{2}\delta Z_{ZA} \\ \frac{1}{2}\delta Z_{AZ} & 1 + \frac{1}{2}\delta Z_{AA} \end{pmatrix} \begin{pmatrix} Z \\ A \end{pmatrix}, \\
H_0 =& \sqrt{Z_H} H = (1 + \frac{1}{2}\delta Z_H) H, \\
f_{i,0}^\tau =& \sqrt{Z_{ij}^{f,\tau}} f_j^\tau = (\delta_{ij} + \frac{1}{2}\delta Z_{ij}^{f,\tau}) f_j^\tau, \quad \tau = R, L.
\end{aligned} \tag{2.52}$$

By demanding that the UV divergences have to cancel in Green's functions, only the UV divergent parts of the renormalization constants are fixed, whereas the finite parts of the renormalization constants have to be fixed by additional constraints, known as "renormalization conditions". Choosing a set of renormalization conditions defines a "renormalization scheme". By using the so-called "on-shell renormalization scheme" [66–69] we can restore the physical meaning of the renormalized parameters after including higher-order corrections and relate these parameters to quantities that are directly measurable in experiments. Before absorbing the UV-divergent contributions into the renormalization constants and fixing the finite parts of the renormalization constants by choosing a renormalization scheme, one needs a regularization procedure which maps the divergences to finite expressions and reproduces the divergences in some limit. Throughout this work we use dimensional regularization [70, 71] (see App. C for a short recapitulation).

2.2.1 On-shell renormalization scheme

The renormalization conditions in the on-shell scheme are chosen such that the renormalized parameters are directly related to physical parameters and external fields are on their mass shell. As a consequence the renormalized electric charge is equal to the classical electromagnetic charge occurring in the on-shell $\gamma e^+ e^-$ vertex for vanishing photon momentum. In addition to the renormalizeation transformations in (2.51) and (2.52), another finite renormalization transformation is introduced to fix the vacuum expectation value (vev) at the true value by using an additional renormalization constant δt.

By fixing the zeroes of renormalized one-particle two-point vertex functions, $\hat{\Gamma}^{ab}$, to be equal to the physical masses,

$$\mathrm{Re}\hat{\Gamma}^{ff}(p) u_f(p)\Big|_{p^2=m_f^2} = 0, \tag{2.53}$$

$$\mathrm{Re}\hat{\Gamma}_{\mu\nu}^{V\tilde{V}}(p) \varepsilon^\nu(p)\Big|_{p^2=M_V^2} = 0, \quad V, \tilde{V} \in \{A, W, Z\}, \tag{2.54}$$

one ensures that the propagators as the inverse of two-point vertex functions have their pole at the location of the physical masses of particles. The spinor $u(p)$ and polarization

vector $\varepsilon^\nu(p)$ project onto physical degrees of freedom of on-shell fermions and gauge bosons, respectively, in the corresponding two-point functions,

$\hat{\Gamma}^f_{ij}(p)$ $=$ 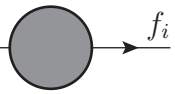 (2.55)

$$= \mathrm{i}\delta_{ij}(\not{p} - m_i) + \mathrm{i}\left[\not{p}\omega_-\hat{\Sigma}^{f,L}_{ij}(p^2) + \not{p}\omega_+\hat{\Sigma}^{f,R}_{ij}(p^2) + (m_{f,i}\omega_- + m_{f,j}\omega_+)\hat{\Sigma}^{f,S}_{ij}(p^2)\right],$$

$$\hat{\Gamma}^H(p) = \mathrm{i}(p^2 - M_H^2) + \mathrm{i}\hat{\Sigma}^H(p^2),$$

$$\hat{\Gamma}^{WW}_{\mu\nu}(p) = -\mathrm{i}g_{\mu\nu}(p^2 - M_W^2) - \mathrm{i}\left(g_{\mu\nu} - \frac{p_\mu p_\nu}{p^2}\right)\hat{\Sigma}^{WW}_T(p^2) - \mathrm{i}\frac{p_\mu p_\nu}{p^2}\hat{\Sigma}^{WW}_L(p^2),$$

$$\hat{\Gamma}^{V\tilde{V}}_{\mu\nu}(p) = -\mathrm{i}g_{\mu\nu}(p^2 - M_V^2)\delta_{V\tilde{V}} - \mathrm{i}\left(g_{\mu\nu} - \frac{p_\mu p_\nu}{p^2}\right)\hat{\Sigma}^{V\tilde{V}}_T(p^2) - \mathrm{i}\frac{p_\mu p_\nu}{p^2}\hat{\Sigma}^{V\tilde{V}}_L(p^2),$$

where $V, \tilde{V} \in \{A, Z\}$ and $M_A^2 = 0$. Note that we write renormalized quantities with the superscript $\hat{}$ in order to distinguish them from unrenormalized quantities. In the renormalized fermion two-point functions, $\hat{\Sigma}^{f,S}_{ij}$ denotes the scalar and $\hat{\Sigma}^{f,L}_{ij}$, $\hat{\Sigma}^{f,R}_{ij}$ the left- and right-handed vector parts of the fermion self-energies. The longitudinal and transversal parts of the boson self-energies $\Sigma^{V\tilde{V}'}$ ($V^{(\prime)} = A, Z, W$) are denoted by $\Sigma^{V\tilde{V}'}_L$ and $\Sigma^{V\tilde{V}'}_T$, respectively.

To obtain finite Green's functions we also renormalize wave functions and demand that on-shell external particles have the canonical normalization as in the free theory and for this reason force the residues of the renormalized propagators to be 1. This fixes the finite parts of the wave-function renormalization constants and translates into the following renormalization conditions,

$$\lim_{p^2\to m_f^2} \frac{\not{p} + m_f}{p^2 - m_f^2}\mathrm{Re}\hat{\Gamma}^{ff}(p)u_f(p) = -u_f(p), \tag{2.56}$$

$$\lim_{p^2\to M_V^2} \frac{1}{p^2 - M_V^2}\mathrm{Re}\hat{\Gamma}^{V\tilde{V}}_{\mu\nu}(p)\varepsilon^\mu(p) = \varepsilon_\mu(p), \tag{2.57}$$

$$\lim_{p^2\to M_H^2} \frac{1}{p^2 - M_H^2}\mathrm{Re}\hat{\Gamma}^H(p) = \mathrm{i}. \tag{2.58}$$

As a consequence of the renormalization conditions for the wave functions no self-energy diagrams on external legs have to be taken into account when calculating renormalized amplitudes. Inserting the renormalized two-point functions into the renormalization conditions (2.54) and (2.58), one obtains the following bosonic renormalization constants [72],

$$\delta M_W^2 = \widetilde{\mathrm{Re}}\,\Sigma^W_T(M_W^2), \quad \delta Z_W = -\mathrm{Re}\,\frac{\partial\Sigma^W_T(k^2)}{\partial k^2}\bigg|_{k^2=M_W^2},$$

$$\delta M_Z^2 = \mathrm{Re}\,\Sigma_T^{ZZ}(M_Z^2), \quad \delta Z_{ZZ} = -\mathrm{Re}\,\frac{\partial \Sigma_T^{ZZ}(k^2)}{\partial k^2}\bigg|_{k^2=M_Z^2},$$

$$\delta Z_{AZ} = -2\mathrm{Re}\,\frac{\Sigma_T^{AZ}(M_Z^2)}{M_Z^2}, \quad \delta Z_{ZA} = 2\frac{\Sigma_T^{AZ}(0)}{M_Z^2}, \tag{2.59}$$

$$\delta Z_{AA} = -\frac{\partial \Sigma_T^{AA}(k^2)}{\partial k^2}\bigg|_{k^2=0},$$

$$\delta M_H^2 = \mathrm{Re}\,\Sigma^H(M_H^2), \quad \delta Z_H = -\mathrm{Re}\,\frac{\partial \Sigma^H(k^2)}{\partial k^2}\bigg|_{k^2=M_H^2}.$$

For the fermionic sector the renormalization constants are given by

$$\begin{aligned}
\delta m_{f,i} &= \frac{m_{f,i}}{2}\widetilde{\mathrm{Re}}\left(\Sigma_{ii}^{f,L}(m_{f,i}^2) + \Sigma_{ii}^{f,R}(m_{f,i}^2) + 2\Sigma_{ii}^{f,S}({m_{f,i}}^2)\right),\\
\delta Z_{ij}^{f,L} &= \frac{2}{m_{f,i}^2 - m_{f,j}^2}\widetilde{\mathrm{Re}}\left[m_{f,j}^2\Sigma_{ij}^{f,L}(m_{f,j}^2) + m_{f,i}m_{f,j}\Sigma_{ij}^{f,R}(m_{f,j}^2)\right.\\
&\qquad \left. +(m_{f,i}^2 + m_{f,j}^2)\Sigma_{ij}^{f,S}(m_{f,j}^2)\right], \qquad i \neq j,\\
\delta Z_{ij}^{f,R} &= \frac{2}{m_{f,i}^2 - m_{f,j}^2}\widetilde{\mathrm{Re}}\left[m_{f,j}^2\Sigma_{ij}^{f,R}(m_{f,j}^2) + m_{f,i}m_{f,j}\Sigma_{ij}^{f,L}(m_{f,j}^2)\right.\\
&\qquad \left. +2m_{f,i}m_{f,j}\Sigma_{ij}^{f,S}(m_{f,j}^2)\right], \qquad i \neq j,\\
\delta Z_{ii}^{f,L} &= -\widetilde{\mathrm{Re}}\,\Sigma_{ii}^{f,L}(m_{f,i}^2) - m_{f,i}^2\frac{\partial}{\partial p^2}\widetilde{\mathrm{Re}}\left[\Sigma_{ii}^{f,L}(p^2) + \Sigma_{ii}^{f,R}(p^2) + 2\Sigma_{ii}^{f,S}(p^2)\right]\Big|_{p^2=m_{f,i}^2},\\
\delta Z_{ii}^{f,R} &= -\widetilde{\mathrm{Re}}\,\Sigma_{ii}^{f,R}(m_{f,i}^2) - m_{f,i}^2\frac{\partial}{\partial p^2}\widetilde{\mathrm{Re}}\left[\Sigma_{ii}^{f,L}(p^2) + \Sigma_{ii}^{f,R}(p^2) + 2\Sigma_{ii}^{f,S}(p^2)\right]\Big|_{p^2=m_{f,i}^2}.
\end{aligned} \tag{2.60}$$

Note that longitudinal parts of bosonic self-energies do not occur in renormalization constants as the polarization vector $\varepsilon^\nu(p)$ projects on the transversal degrees of freedom. The operator $\widetilde{\mathrm{Re}}$ is only applied to quantities that depend on the quark mixing matrix at one loop. It returns the real part of its argument but does not act on quark mixing matrix elements appearing in the expression where $\widetilde{\mathrm{Re}}$ is applied to.
The renormalization transformations of the sine and cosine of the weak mixing angle are given by,

$$c_{W,0} = c_W + \delta c_W, \qquad s_{W,0} = s_W + \delta s_W. \tag{2.61}$$

As the weak mixing angle is derived from the masses of the massive vector bosons,

$$c_W^2 = 1 - s_W^2 = \frac{M_W^2}{M_Z^2}, \tag{2.62}$$

its renormalization constants are related to the W and Z boson self-energies,

$$\frac{\delta c_W}{c_W} = -\frac{s_W^2}{c_W^2}\frac{\delta s_W}{s_W} = \frac{1}{2}\mathrm{Re}\left(\frac{\Sigma_T^{WW}(M_W^2)}{M_W^2} - \frac{\Sigma_T^{ZZ}(M_Z^2)}{M_Z^2}\right). \tag{2.63}$$

The CKM matrix appears in the quark–W-boson couplings at leading order as a consequence of the transformation of bare weak interaction eigenstates, f_0', into bare mass eigenstates, $f_0 = U_{f,0}^L f_0'$, via the unitary matrices $U_{f,0}^L$, $f = u, d$. Due to the renormalization transformation at next-to-leading order in the on-shell scheme,

$$f_{i,0}^L = (1 + \frac{1}{2}\delta Z_{ij}^{f,L}) f_j^L, \tag{2.64}$$

the higher-order mass eigenstates, f^L, are rotated by the anti-Hermitian part $\delta Z^{f,AH} = \frac{1}{2}(\delta Z^{f,L} - \delta Z^{f,L\dagger})$ of $\delta Z^{f,L}$,

$$f^L = (Z^{f,L})^{-\frac{1}{2}} U_{f,0}^L (Z^{f,L})^{\frac{1}{2}} f' = U_{f,0}^L \left(1 + \frac{1}{2}Z^{f,L} - \frac{1}{2}Z^{f,L\dagger}\right) f'. \tag{2.65}$$

To obtain mass eigenstates also after the renormalization transformation at next-to-leading order, this rotation has to be compensated by the introduction of a renormalization constant for the CKM matrix,

$$\delta V_{ij} = \frac{1}{2}\left(\delta Z_{ik}^{u,AH\dagger} V_{0,kj} + V_{0,ik}\delta Z_{kj}^{d,AH}\right). \tag{2.66}$$

The renormalization condition for the electric charge e is defined so that the coupling in a scattering process of a photon on a physical electron with zero momentum transfer of the photon is given by the classical electric charge, i.e. the renormalized photon-electron vertex,

$\hat{\Gamma}_\mu^{ff\gamma}(k, p, -p') =$

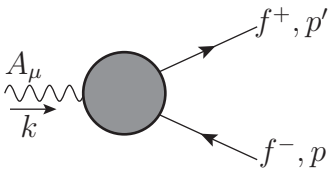

, (2.67)

gets no higher-order corrections,

$$\bar{u}(p)\hat{\Gamma}_\mu^{ff\gamma}(k = 0, p, -p)u(p)\Big|_{p^2=m_f^2} = \mathrm{i}e\bar{u}(p)\gamma_\mu u(p). \tag{2.68}$$

Note that in $\hat{\Gamma}_\mu^{ff\gamma}$ no external-leg corrections have to be considered due to the choice of the field renormalization conditions. Applying this renormalization condition leads to [72]

$$\delta Z_e = \frac{1}{2}\frac{\partial \Sigma_T^{AA}(k^2)}{\partial k^2}\Big|_{k^2=0} - \frac{s_W}{c_W}\frac{\Sigma_T^{AZ}(0)}{M_Z^2}. \tag{2.69}$$

The vev of the Higgs field, $v = \frac{2\mu}{\sqrt{\lambda}}$, leads to a vanishing Higgs tadpole t at leading order

$$t = v\left(\mu^2 - \frac{\lambda}{4}v^2\right) = 0, \tag{2.70}$$

which is determined from the term in the SM Lagrangian $\mathcal{L}_{SM}$ that is linear in the Higgs field,

$$\mathcal{L}_{tadpole} = t \cdot H. \tag{2.71}$$

If v is the "correct" vacuum, i.e. it fulfills (2.22), t as a function of v has to vanish and (2.70) can be seen as a definition of the "true" value of the vev v. At next-to-leading order the Higgs tadpole t gets non-vanishing loop corrections from vector bosons, fermions, and scalars in the loop. The scalar isospin doublet Φ introduced in (2.19) is renormalized via $\Phi_0 = \sqrt{Z_\Phi}\Phi$, with $Z_\Phi = Z_H$. Using (2.24) we see that the vev and the Higgs field H acquire the same renormalization constant $\delta Z_\Phi = \delta Z_H$ which means that determining the renormalization constant of the Higgs field renders the vev finite. In order to restore the renormalized vev as the actual minimum of the effective Higgs potential we introduce an additional renormalization transformation $t = t_0 + \delta t$ and use the renormalization condition $t \stackrel{!}{=} 0$ leading to

$$\mathrm{i}\,\delta t = -\mathrm{i}\,t_0 = (-1)\cdot$$  . (2.72)

In this way we cancel all higher-order contributions to the tadpole, and the finite vev of the renormalized theory is indeed the actual minimum of the effective Higgs potential.

2.2.2 $\overline{\mathrm{MS}}$ scheme and running of α_s

The application of the on-shell scheme for calculations in QCD is not reasonable as quarks and gluons are confined within hadronic bound states, meaning that the parameters of the QCD Lagrangian are not directly related to measurable quantities. This motivates the application of the so-called modified minimal subtraction ($\overline{\mathrm{MS}}$) scheme in QCD calculations. In this scheme, at the one-loop level one subtracts the $1/\varepsilon$ pole together with a universal constant, $\frac{1}{\varepsilon} - \gamma_E + \ln(4\pi)$, into the renormalization constants. In the $\overline{\mathrm{MS}}$ scheme renormalized loop amplitudes depend on the renormalization scale μ (see (C.2) in App. C for more details on dimensional regularization), since the renormalization constants have no dependence on μ, and therefore the counterterm diagrams do not cancel the renormalization scale in loop amplitudes. In the calculation of a physical quantity this scale dependence should drop out, which leads to the introduction of a running coupling constant. The dependence of the running coupling on the renormalization scale is dictated by the fact that the explicit dependence of physical quantities on the renormalization scale has to cancel. Following Ref. [73], we will now discuss how this running is implemented in the case of the strong coupling constant α_S.

We consider a dimensionless physical observable R that depends exactly on one energy scale Q. Assuming the scale Q to be bigger than any other dimensionful parameters entering the process implies that all involved quark masses can be set to zero. As a dimensionless quantity, R can only depend on Q^2/μ^2, where μ is introduced in the process of the renormalization of R which is necessary due to potential UV divergences present in higher-order corrections to physical observables. This second mass scale μ is associated to the point at which the strong coupling is measured. Moreover, as discussed above, we introduce an implicit dependence of R on μ by the running of the coupling $\alpha_S(\mu^2)$. The independence of the physical observable R on the arbitrary renormalization scale is expressed in the following equation,

$$\mu^2 \frac{d}{d\mu^2} R(Q^2/\mu^2, \alpha_S) = \left[\mu^2 \frac{\partial}{\partial \mu^2} + \mu^2 \frac{\partial \alpha_S}{\partial \mu^2} \frac{\partial}{\partial \alpha_S} \right] R = 0. \tag{2.73}$$

Introducing the so-called β-function,

$$\beta(\alpha_S) = \mu^2 \frac{\partial \alpha_S}{\partial \mu^2}, \tag{2.74}$$

which describes the rate of variation of the renormalized coupling at a fixed scale μ, i.e. the running of the coupling, we can can rewrite (2.73) as,

$$\left[-\frac{\partial}{\partial t} + \beta(\alpha_S) \frac{\partial}{\partial \alpha_S} \right] R(e^t, \alpha_S) = 0, \qquad t = \ln\left(\frac{Q^2}{\mu^2}\right). \tag{2.75}$$

One solution to the last equation is given by $R(1, \alpha_S(Q^2))$ which implies that the energy dependence of R is fully determined by the running coupling $\alpha_S(Q^2)$. The perturbative expansion of the QCD β-function has the following form,

$$\beta(\alpha_S) = -b\alpha_S^2(1 + b'\alpha_S + b''\alpha_S^2 + \mathcal{O}(\alpha_S^3)). \tag{2.76}$$

The coefficients in the expansion depend on the number of active quark flavours, n_f, and are given by [74],

$$\begin{aligned} b &= \frac{33 - 2n_f}{12\pi}, \\ b' &= \frac{153 - 19n_f}{2\pi(33 - 2n_f)}, \\ b'' &= \frac{77139 - 15099n_f + 325n_f^2}{288\pi^2(33 - 2n_f)}. \end{aligned} \tag{2.77}$$

At next-to-leading-order the differential equation (2.76) reads

$$\mu^2 \frac{\partial \alpha_S}{\partial \mu^2} = -b\alpha_S^2. \tag{2.78}$$

The solution of this equation,

$$\frac{1}{\alpha_S(Q^2)} - \frac{1}{\alpha_S(\mu^2)} = b \ln\left(\frac{Q^2}{\mu^2}\right) \Rightarrow \alpha_S(Q^2) = \frac{\alpha_S(\mu^2)}{1 + \alpha_S(\mu^2) b \ln(Q^2/\mu^2)}, \tag{2.79}$$

describes the running of α_S at this order in perturbation theory. Asymptotic freedom, i.e. the fact the strong coupling constant becomes smaller at large energies or small distances, is a consequence of the fact that for $n_f \leq 16$, the coefficient b is larger than zero. This implies that for larger energy scales Q^2 the coupling becomes smaller allowing for the treatment of QCD in a perturbative way at large energies.

2.3 Electroweak input-parameter scheme

In the previous section the electromagnetic coupling was defined in the Thomson limit, meaning that all corrections to the photon-electron vertex vanish on-shell and for vanishing photon momentum transfer. In this scheme, called the "$\alpha(0)$-scheme", theoretical predictions for electroweak radiative corrections to high-energy cross sections and decay widths (without photons) include logarithms $\sim \log(m_f^2/s)$ of light fermion masses, m_f. These logarithms originate from loop corrections to the photon vacuum polarization, $\Pi_{AA}(0)$, and lead to large radiative corrections at the relevant energy scales of high-energy experiments. By the introduction of a running electromagnetic coupling constant,

$$\alpha(0) \to \alpha(s) = \frac{\alpha(0)}{1 + \Delta\alpha(s)}, \tag{2.80}$$

the large logarithms, contained in $\Delta\alpha(s)$, can be absorbed into leading-order predictions. In the "$\alpha(M_Z)$-scheme", the scale of the running coupling $\alpha(s)$ is chosen to be at the mass of the Z boson, $s = M_Z^2$,

$$\alpha(0) \to \frac{\alpha(0)}{1 + \Delta\alpha(M_Z^2)}, \tag{2.81}$$

with the UV-finite quantity,

$$\Delta\alpha(M_Z) = \Pi_{AA}^{f\neq t}(0) - \mathrm{Re}\Pi_{AA}^{f\neq t}(M_Z^2). \tag{2.82}$$

Additionally, one has to modify the charge renormalization constant,

$$\delta Z_e^{\alpha(M_Z)} = \delta Z_e^{\alpha(0)} - \frac{1}{2}\Delta\alpha(M_Z), \tag{2.83}$$

since otherwise, corrections related to $\Delta\alpha(M_Z^2)$ would be counted twice in electroweak 1-loop corrections.
In the so-called "G_μ-scheme", the electromagnetic coupling constant is derived from the Fermi constant G_μ. In this scheme, the leading-order relation between the Fermi constant and the electromagnetic coupling constant,

$$G_\mu = \frac{\pi\alpha(0)}{\sqrt{2}s_w^2 M_W^2}, \tag{2.84}$$

is used as a definition of the electromagnetic coupling. The Fermi constant is obtained from the measurement of the muon lifetime [75] by using the following relation,

$$\frac{1}{\tau_\mu} = \frac{G_\mu^2 m_\mu^2}{192\pi^3}\left(1 - \frac{8m_e^2}{m_\mu^2}\right)\left[1 + \frac{3}{5}\frac{m_\mu^2}{m_W^2} + \frac{\alpha}{2\pi}\left(\frac{25}{4} - \pi^2\right)\right], \tag{2.85}$$

where the photonic corrections to the muon lifetime within the Fermi theory are given by the terms proportional to α. Including higher-order corrections to the muon decay, the LO relation between G_μ and $\alpha(0)$ in (2.84) is modified to [72, 75]

$$G_\mu = \frac{\pi\alpha(0)}{\sqrt{2}s_w^2 M_W^2}(1+\Delta r), \tag{2.86}$$

where Δr summarizes higher-order corrections to the muon decay obtained in the Fermi model except for the photonic corrections which are already contained in the definition of G_μ in Eq. (2.85). The UV-finite quantity Δr is given by,

$$\begin{aligned}\Delta r =& \Pi^{AA}(0) - \frac{c_W^2}{s_W^2}\left(\frac{\Sigma_T^{ZZ}(M_Z^2)}{M_Z^2} - \frac{\Sigma_T^{W}(M_W^2)}{M_W^2}\right) + \frac{\Sigma_T^{W}(0) - \Sigma_T^{W}(M_W^2)}{M_W^2} \\ &+ 2\frac{c_W}{s_W}\frac{\Sigma_T^{AZ}(0)}{M_Z^2} + \frac{\alpha}{4\pi s_W^2}\left(6 + \frac{7-4s_W^2}{2s_W^2}\log c_W^2\right),\end{aligned} \tag{2.87}$$

and leads to a corresponding electromagnetic coupling in the "G_μ-scheme" given by

$$\alpha(0) \longrightarrow \alpha_{G_\mu} = \frac{\sqrt{2}G_\mu M_W^2 s_w^2}{\pi} = \alpha(0)(1+\Delta r). \tag{2.88}$$

As in the "$\alpha(M_Z)$-scheme", the charge renormalization constant has to be modified in the following way,

$$\delta Z_e^{\alpha(0)} \longrightarrow \delta Z_e^{G_\mu} = \delta Z_e^{\alpha(0)} - \frac{1}{2}\Delta r. \tag{2.89}$$

The logarithms of the small fermion masses contained in the charge renormalization constant, $\delta Z_e^{\alpha(0)}$, are therefore cancelled in $\delta Z_e^{G_\mu}$ by $\Pi^{AA}(0)$ in Δr. In this way, the large logarithms are removed from the radiative corrections and absorbed into the coupling constant, α_{G_μ}.

2.4 Treatment of unstable particles in QFT

The lifetime of unstable elementary particles within the SM such as the Higgs or the W/Z boson are typically to short to be measured directly in detectors and only leave their imprint as resonances in the measurement of their decay products. The lifetime, τ_{V}, of an unstable particle V can then be obtained by the extraction of the total decay width, $\Gamma_{\mathrm{V}} = 1/\tau_{\mathrm{V}}$, from the Breit–Wigner-like resonance in invariant-mass or transverse-mass spectra of the decay products. As instability effects in the propagation of particles arise in quantum field theory only as higher-order effects, we need to resum one-particle irreducible self-energy contributions into the propagators in order to obtain a theoretical description of the Breit–Wigner-like resonances. This resummation of higher-order effects leads to a mixing of perturbative orders between corrections of self-energy type, which are resummed to all orders, and corrections that are not of self-energy type which are due to their complexity in practice calculated only to a finite order in perturbation theory. However,

as gauge independence and unitarity hold order-by-order in perturbation theory, this mixing leads to potentially gauge dependent results of S-matrix elements. In this work, we will use two different approaches in order to solve these conceptual problems. The first approach, the so-called complex-mass scheme, is discussed in the next section. The pole approximation, introduced in Section 6, is another possibility to introduce instability effects in a gauge-invariant way and leads to simplifications of theoretical calculations by reducing the number of allowed Feynman diagrams. This is achieved by insisting that the unstable particle under consideration is produced nearly on-shell, which also guarantees gauge independence. However, this restriction induced by the pole approximation limits the predictivity of calculations using the pole approximation to the resonance region of the unstable particle.

2.4.1 Preliminaries

Before the discussion of methods that circumvent conceptual issues arising from the resummation of higher-order effects combined with a truncation of the perturbative series, we first introduce the idea of a Dyson summation to introduce instability effects in propagators, which also addresses the issue of properly defining the mass and width of unstable particles. This will eventually also allow us to understand the relation between definitions of mass and width in different schemes. For simplicity in the following we consider only the case of the Higgs boson, but the discussion can also be applied to the EW gauge bosons of the Standard Model. For a more complete discussion of unstable particles and their theoretical implementation in perturbative calculations we refer to [60].

Dyson resummation of one-particle irreducible self-energy corrections to the Higgs propagator $G^{\mathrm{H}}(p^2)$ leads to,

$$\begin{aligned} G^{\mathrm{H}}(p^2) &= -[\Gamma^{\mathrm{H}}(p,-p)]^{-1} = \frac{\mathrm{i}}{p^2 - M^2_{\mathrm{H},0}} + \frac{\mathrm{i}}{p^2 - M^2_{\mathrm{H},0}} \mathrm{i}\Sigma^{\mathrm{H}}(p^2) \frac{\mathrm{i}}{p^2 - M^2_{\mathrm{H},0}} + \cdots \\ &= \frac{\mathrm{i}}{p^2 - M^2_{\mathrm{H},0}} \sum_{n=0}^{\infty} \left(- \frac{\Sigma^{\mathrm{H}}(p^2)}{p^2 - M^2_{\mathrm{H},0}} \right)^n = \frac{\mathrm{i}}{p^2 - M^2_{\mathrm{H},0} + \Sigma^{\mathrm{H}}(p^2)}, \end{aligned} \tag{2.90}$$

where Σ^{H} is the unrenormalized self-energy of the Higgs boson. In order to eliminate the bare mass $M_{\mathrm{H},0}$ of the Higgs boson from the propagator we can use the renormalization transformation of Higgs mass (2.51),

$$M^2_{\mathrm{H},0} = \; M^2_{\mathrm{H}} + \delta M^2_{\mathrm{H}}. \tag{2.91}$$

The renormalization condition (2.54) in the OS scheme, leads to the renormalization constant given in (2.59)

$$\delta M^2_{\mathrm{H,OS}} = \mathrm{Re}\, \Sigma^{\mathrm{H}}(M^2_{\mathrm{H,OS}}), \tag{2.92}$$

which implies that in the OS scheme the bare mass and the renormalized mass of the Higgs boson are related by

$$M^2_{\mathrm{H,OS}} - M^2_{\mathrm{H},0} + \mathrm{Re}\{\Sigma^{\mathrm{H}}(M^2_{\mathrm{H,OS}})\} = 0. \tag{2.93}$$

We can use the last equation to eliminate the bare mass in the the Dyson summed propagator in (2.90) and obtain,

$$G^{\mathrm{H}}(p^2) = \frac{\mathrm{i}}{p^2 - M^2_{\mathrm{H},0} + \Sigma^{\mathrm{H}}(p^2)} = \frac{\mathrm{i}}{p^2 - M^2_{\mathrm{H,OS}} - \mathrm{Re}\{\Sigma^{\mathrm{H}}(M^2_{\mathrm{H,OS}})\} + \Sigma^{\mathrm{H}}(p^2)}$$
$$\widetilde{p^2 \to M^2_{\mathrm{H,OS}}} \; \frac{1}{(p^2 - M^2_{\mathrm{H,OS}})[1 + \mathrm{Re}\{\Sigma^{\mathrm{H}\prime}(M^2_{\mathrm{H,OS}})\}] + \mathrm{i}\mathrm{Im}\{\Sigma^{\mathrm{H}}(M^2_{\mathrm{H,OS}})\} + \ldots}. \tag{2.94}$$

In the resonance region, $p^2 \approx M^2_{\mathrm{H,OS}}$, this is equivalent to

$$G^{\mathrm{H}}(p^2) = \frac{iR_{\mathrm{OS}}}{p^2 - M^2_{\mathrm{H,OS}} + \mathrm{i}M_{\mathrm{H,OS}}\Gamma_{\mathrm{H,OS}}}, \tag{2.95}$$

where we have used the definition,

$$R_{\mathrm{OS}} = \frac{1}{1 + \mathrm{Re}\{\Sigma^{\mathrm{H}\prime}(M^2_{\mathrm{H,OS}})\}}, \quad \Gamma_{\mathrm{H,OS}} = \frac{R_{\mathrm{OS}}\,\mathrm{Im}\{\Sigma^{\mathrm{H}}(M^2_{\mathrm{H,OS}})\}}{M_{\mathrm{H,OS}}}. \tag{2.96}$$

The square of this propagator generates the Breit–Wigner shape of the resonance of the Higgs boson in the invariant-mass spectrum of its decay products. Therefore, we now have identified the quantities that define the location and the width of the Breit–Wigner-shaped resonance as the mass, $M^2_{\mathrm{H,OS}}$, and the width, $\Gamma_{\mathrm{H,OS}}$, respectively.

If we choose to renormalize also the wave-functions in the OS scheme, we additionally get the wave-function renormalization constant in the denominator of the propagator (2.94),

$$\begin{aligned} G^{\mathrm{H}}(p^2) &= \frac{\mathrm{i}}{p^2 - M^2_{\mathrm{H,OS}} - \mathrm{Re}\{\Sigma^{\mathrm{H}}(M^2_{\mathrm{H,OS}})\} + (p^2 - M^2_{\mathrm{H,OS}})\,\delta Z_{\mathrm{H,OS}} + \Sigma^{\mathrm{H}}(p^2)} \\ &= \frac{\mathrm{i}}{p^2 - M^2_{\mathrm{H,OS}} + \hat{\Sigma}^{\mathrm{H}}(p^2)}, \end{aligned} \tag{2.97}$$

which then leads to the following behaviour in the vicinity of the resonance,

$$G^{\mathrm{H}}(p^2) \; \widetilde{p^2 \to M^2_{\mathrm{H,OS}}} \; \frac{\mathrm{i}}{(p^2 - M^2_{\mathrm{H,OS}})[1 + \underbrace{\mathrm{Re}\{\Sigma^{\mathrm{H}\prime}(M^2_{\mathrm{H,OS}})\} + \delta Z_{\mathrm{H,OS}}}_{=0}] + \mathrm{i}\mathrm{Im}\{\Sigma^{\mathrm{H}}(M^2_{\mathrm{H,OS}})\} + \ldots}. \tag{2.98}$$

Using (2.59), we see that the residue of the propagator, $\mathrm{i}R_{\mathrm{OS}}$, simply reduces to the complex unit, $\mathrm{i}R_{\mathrm{OS}} = \mathrm{i}$, which is a consequence of the renormalization condition (2.58), off course.

In the next section we will discuss the so-called complex-mass scheme where one determines the renormalization constant of the mass of the Higgs boson from the full self-energy instead of just using its real part as in the OS scheme. Instead of (2.93) this leads to an equation,

$$\mu^2_{\mathrm{H}} - M^2_{\mathrm{H},0} + \Sigma^{\mathrm{H}}(\mu^2_{\mathrm{H}}) = 0, \tag{2.99}$$

which determines the so-called pole mass $M_{\mathrm{H},0}$ and pole width $\Gamma_{\mathrm{H,pole}}$, respectively defined as the real and imaginary part of the complex pole μ_{H}^2 of the Dyson summed propagator,

$$\mu_{\mathrm{H}}^2 = M_{\mathrm{H,pole}}^2 - \mathrm{i}M_{\mathrm{H,pole}}\Gamma_{\mathrm{H,pole}}. \tag{2.100}$$

In the pole scheme, the behaviour of the Dyson summed propagator in the resonance region is then given by

$$G^{\mathrm{H}}(p^2) = \frac{1}{p^2 - \mu_{\mathrm{H}}^2 + \Sigma^{\mathrm{H}}(p^2) - \Sigma^{\mathrm{H}}(\mu_{\mathrm{H}}^2)} \;\widetilde{p^2\to\mu_{\mathrm{H}}^2}\; \frac{1}{(p^2 - \mu_{\mathrm{H}}^2)[1 + \Sigma^{\mathrm{H}\prime}(\mu_{\mathrm{H}}^2)] + \ldots}. \tag{2.101}$$

When including wave function renormalization, the behaviour of the propagator in the pole scheme is given by

$$G^{\mathrm{H}}(p^2) \;\widetilde{p^2\to\mu_{\mathrm{H}}^2}\; \frac{1}{(p^2 - \mu_{\mathrm{H}}^2) + \ldots}, \tag{2.102}$$

in the resonance region.

In the analysis of LEP data measured in the vicinity of the Z- or W-boson resonances a running-width scheme has been used [60]. In particular, the OS masses of the W and Z boson were measured in this scheme, where for $p^2 \sim M_V^2$ the imaginary part of the renormalized Dyson-summed self-energy in (2.97) is approximated by

$$\mathrm{Im}\{\hat{\Sigma}^{\mathrm{V}}(p^2)\} = \gamma_{\mathrm{V}}\, p^2\theta(p^2), \quad \gamma_{\mathrm{V}} = \frac{\Gamma_{\mathrm{V,OS}}}{M_{\mathrm{V,OS}}}, \quad \mathrm{V} = \mathrm{W}, \mathrm{Z}. \tag{2.103}$$

However, as the pole-scheme leads to a gauge-invariant definition of the pole mass and width [76–78], we are going to use this scheme within this thesis instead of the running width scheme. To do this, we need to understand the conversion from the OS masses to pole masses. By rewriting the denominator of the propagator using the running width and comparing the result to the denominator in (2.102),

$$\begin{aligned}
p^2 - M_{\mathrm{V,OS}}^2 + \mathrm{i}\gamma_{\mathrm{V}}p^2 &= p^2 + \mathrm{i}\gamma_{\mathrm{V}}p^2 - M_{\mathrm{V,OS}}^2\frac{1 - \mathrm{i}\gamma_{\mathrm{V}}}{1 - \mathrm{i}\gamma_{\mathrm{V}}} \\
&= (1 + \mathrm{i}\gamma_{\mathrm{V}})\, p^2 - \frac{M_{\mathrm{V,OS}}^2 - \mathrm{i}M_{\mathrm{V,OS}}\Gamma_{\mathrm{V,OS}}}{1 - \mathrm{i}\gamma_{\mathrm{V}}} \\
&= (1 + \mathrm{i}\gamma_{\mathrm{V}}) \left(p^2 - \frac{M_{\mathrm{V,OS}}^2}{1 + \gamma_{\mathrm{V}}^2} - \mathrm{i}\frac{M_{\mathrm{V,OS}}}{\sqrt{1 + \gamma_{\mathrm{V}}^2}}\frac{\Gamma_{\mathrm{V,OS}}}{\sqrt{1 + \gamma_{\mathrm{V}}^2}}\right) \\
&\overset{!}{=} (1 + \mathrm{i}\gamma_{\mathrm{V}})\,(p^2 - \mu_{\mathrm{V}}^2),
\end{aligned} \tag{2.104}$$

we can identify the real and imaginary part of the complex pole of the propagator, μ_{V}, as the mass and width in the pole scheme in terms of the OS quantities [60],

$$M_V = \frac{M_{V,\mathrm{OS}}}{\sqrt{1 + \Gamma_{V,\mathrm{OS}}^2/M_{V,\mathrm{OS}}^2}}, \qquad \Gamma_V = \frac{\Gamma_{V,\mathrm{OS}}}{\sqrt{1 + \Gamma_{V,\mathrm{OS}}^2/M_{V,\mathrm{OS}}^2}}. \tag{2.105}$$

2.4.2 Complex-mass scheme

In the complex-mass scheme [59, 60, 79, 80] one identifies the mass square of an unstable particle b with the location of the complex pole,

$$\mu_b^2 = M_b^2 - \mathrm{i}M_b\Gamma_b, \qquad b = \mathrm{W}, \mathrm{Z}, \mathrm{H} \tag{2.106}$$

of its resummed propagator in (2.101). In order to preserve gauge invariance, the complex mass square has to be used not only in the propagator, but also in derived quantities, such as couplings involving the weak mixing angle θ_W contained in

$$c_\mathrm{w}^2 = 1 - s_\mathrm{w}^2 = \frac{\mu_\mathrm{W}^2}{\mu_\mathrm{Z}^2}, \tag{2.107}$$

where we used the abbreviations $c_\mathrm{w} = \cos\theta_\mathrm{W}$ and $s_\mathrm{w} = \sin\theta_\mathrm{W}$. The complex-mass scheme can be seen as an analytic continuation of the masses of the unstable particles in the Standard Model into the complex plane. Therefore, as the gauge-boson masses are only modified by an analytic continuation, relations that do not involve complex conjugation are not affected by the consistent use of complex masses, which leads to the validity of e.g. Ward and Slavnov–Taylor identities in the complex mass scheme.

In the following, we limit the discussion of the complex-mass scheme to the massive spin-1 gauge bosons of the Standard Model, even though the complex-mass scheme is also applicable to obtain a gauge-invariant description of width effects of the Higgs boson or massive fermions [60].

At NLO, the complex-mass scheme can be obtained by replacing the bare squared mass of an unstable particle by a complex squared mass and the corresponding renormalization constant,

$$M_{V,0}^2 = \mu_V^2 + \delta\mu_V^2, \qquad V = \mathrm{W}, \mathrm{Z}. \tag{2.108}$$

As the bare mass is real the mass renormalization constant also has to be a complex quantity,

$$\mathrm{Im}\{\mu_V^2\} = -\mathrm{Im}\{\delta\mu_V^2\}. \tag{2.109}$$

In principle the imaginary part of the complex squared mass of an unstable particle is not an independent parameter of the theory, as it follows from the imaginary part of the corresponding self-energy via the optical theorem,

$$M_V\Gamma_V = \mathrm{Im}\{\Sigma_V(M_V^2 - \mathrm{i}M_V\Gamma_V)\}. \tag{2.110}$$

However, the imaginary part of the complex squared mass is obtained by adding and subtracting the imaginary part (2.109) from the Standard Model Lagrangian, where the added part becomes part of the mass, $M_{V,0}^2 \to \mu_V^2$, shifting it from the real axis into the complex plane and the subtracted imaginary part becomes the imaginary part of the corresponding mass-renormalization constant. Therefore, effectively we do not change the

Lagrangian and gauge invariance relations remain unchanged independent of the imaginary part that is added and subtracted. As a consequence it is therefore legit to use, e.g., also empirical values for the decay width appearing in the imaginary part.

Since the renormalization constants acquire an imaginary part in the complex-mass scheme, the renormalized self-energies of the electroweak gauge bosons are generalized to take the following form,

$$\begin{aligned}
\hat{\Sigma}^{\mathrm{W}}_{\mathrm{T}}(k^2) &= \Sigma^{\mathrm{W}}_{\mathrm{T}}(k^2) - \delta\mu^2_{\mathrm{W}} + (k^2 - \mu^2_{\mathrm{W}})\delta\mathcal{Z}_{\mathrm{W}}, \\
\hat{\Sigma}^{\mathrm{ZZ}}_{\mathrm{T}}(k^2) &= \Sigma^{\mathrm{ZZ}}_{\mathrm{T}}(k^2) - \delta\mu^2_{\mathrm{Z}} + (k^2 - \mu^2_{\mathrm{Z}})\delta\mathcal{Z}_{\mathrm{ZZ}}, \\
\hat{\Sigma}^{\mathrm{AA}}_{\mathrm{T}}(k^2) &= \Sigma^{\mathrm{AA}}_{\mathrm{T}}(k^2) + k^2\delta\mathcal{Z}_{\mathrm{AA}}, \\
\hat{\Sigma}^{\mathrm{AZ}}_{\mathrm{T}}(k^2) &= \Sigma^{\mathrm{AZ}}_{\mathrm{T}}(k^2) + k^2\frac{1}{2}\delta\mathcal{Z}_{\mathrm{AZ}} + (k^2 - \mu^2_{\mathrm{Z}})\frac{1}{2}\delta\mathcal{Z}_{\mathrm{ZA}},
\end{aligned} \tag{2.111}$$

where the requirement that the complex masses of unstable particles are identified with the location of the complex pole of the corresponding resummed propagators—of similar form as (2.101)—leads to generalized renormalization conditions compared to the on-shell scheme,

$$\begin{aligned}
\hat{\Sigma}^{\mathrm{W}}_{\mathrm{T}}(\mu^2_{\mathrm{W}}) &= 0, \qquad & \hat{\Sigma}^{\mathrm{ZZ}}_{\mathrm{T}}(\mu^2_{\mathrm{Z}}) &= 0, & \\
\hat{\Sigma}^{\mathrm{AZ}}_{\mathrm{T}}(0) &= 0, \qquad & \hat{\Sigma}^{\mathrm{AZ}}_{\mathrm{T}}(\mu^2_{\mathrm{Z}}) &= 0, & \\
\hat{\Sigma}'^{\mathrm{W}}_{\mathrm{T}}(\mu^2_{\mathrm{W}}) &= 0, \qquad & \hat{\Sigma}'^{\mathrm{ZZ}}_{\mathrm{T}}(\mu^2_{\mathrm{Z}}) &= 0, \qquad & \hat{\Sigma}'^{\mathrm{AA}}_{\mathrm{T}}(0) = 0.
\end{aligned} \tag{2.112}$$

These renormalization conditions lead to renormalization constants that depend on self-energies evaluated at complex squared masses,

$$\begin{aligned}
\delta\mu^2_{\mathrm{W}} &= \Sigma^{W}_{\mathrm{T}}(\mu^2_{\mathrm{W}}), \qquad & \delta\mu^2_{\mathrm{Z}} &= \Sigma^{ZZ}_{\mathrm{T}}(\mu^2_{\mathrm{Z}}), \\
\delta\mathcal{Z}_{W} &= -\Sigma'^{W}_{\mathrm{T}}(\mu^2_{\mathrm{W}}), & & \\
\delta\mathcal{Z}_{ZA} &= \frac{2}{\mu^2_{\mathrm{Z}}}\Sigma^{AZ}_{\mathrm{T}}(0), \qquad & \delta\mathcal{Z}_{AZ} &= -\frac{2}{\mu^2_{\mathrm{Z}}}\Sigma^{AZ}_{\mathrm{T}}(\mu^2_{\mathrm{Z}}),
\end{aligned} \tag{2.113}$$

$$\begin{aligned}
\delta\mathcal{Z}_{ZZ} &= -\Sigma'^{ZZ}_{\mathrm{T}}(\mu^2_{\mathrm{Z}}), \qquad & \delta\mathcal{Z}_{AA} &= -\Sigma'^{AA}_{\mathrm{T}}(0).
\end{aligned} \tag{2.114}$$

One can show (see Section 6 in [81]) that for sufficiently large squared masses M_V^2 and small widths Γ_V—as it is the case for unstable particles in the SM—the process of adding an imaginary part to the real masses, $M_V^2 \to \mu_V^2$ (i.e. $\Gamma_V = 0 \to \Gamma_V \neq 0$), leads to a crossing of the branch cut of two-point functions that appear in the calculation of the self-energies. Therefore, in general, the two-point functions have to be evaluated on the second Riemann sheet [81]. However, as the widths of the unstable particles present in the SM are small compared to their masses, one can circumvent this problem by expanding the self-energies about the real squared masses [60],

$$\begin{aligned}
\Sigma(\mu_V^2) &= \Sigma(M_V^2) + (\mu_V^2 - M_V^2)\Sigma'(M_V^2) \;+\; \mathcal{O}\left((\mu_V^2 - M_V^2)^2\right) \\
&= \Sigma(M_V^2) - \mathrm{i}M_V\Gamma_V\Sigma'(M_V^2) \;+\; \mathcal{O}\left((M_V\Gamma_V)^2\right).
\end{aligned} \tag{2.115}$$

The complex renormalization constants are modified by the expansion according to,

$$\delta\mu_V^2 = \Sigma(M_V^2) + (\mu_V^2 - M_V^2)\Sigma'(M_V^2) + \mathcal{O}(\alpha^3), \qquad \delta\mathcal{Z}_V = -\Sigma'(M_V^2) + \mathcal{O}(\alpha^2), \tag{2.116}$$

which leads to the following simplified renormalization constant of the SM weak gauge bosons in the complex mass scheme,

$$\begin{aligned}
\delta\mu_{\mathrm{W}}^2 &= \Sigma_{\mathrm{T}}^{W}(M_{\mathrm{W}}^2) + (\mu_{\mathrm{W}}^2 - M_{\mathrm{W}}^2)\Sigma_{\mathrm{T}}'^{W}(M_{\mathrm{W}}^2) + c_{\mathrm{T}}^{\mathrm{W}}, \\
\delta\mu_{\mathrm{Z}}^2 &= \Sigma_{\mathrm{T}}^{ZZ}(M_{\mathrm{Z}}^2) + (\mu_{\mathrm{Z}}^2 - M_{\mathrm{Z}}^2)\Sigma_{\mathrm{T}}'^{ZZ}(M_{\mathrm{Z}}^2),
\end{aligned} \tag{2.117}$$

$$\begin{aligned}
\delta\mathcal{Z}_W &= -\Sigma_{\mathrm{T}}'^{W}(M_{\mathrm{W}}^2), \qquad \delta\mathcal{Z}_{ZA} = \frac{2}{\mu_{\mathrm{Z}}^2}\Sigma_{\mathrm{T}}^{AZ}(0), \\
\delta\mathcal{Z}_{AZ} &= -\frac{2}{M_{\mathrm{Z}}^2}\Sigma_{\mathrm{T}}^{AZ}(M_{\mathrm{Z}}^2) + \left(\frac{\mu_{\mathrm{Z}}^2}{M_{\mathrm{Z}}^2} - 1\right)\delta\mathcal{Z}_{ZA}, \\
\delta\mathcal{Z}_{ZZ} &= -\Sigma_{\mathrm{T}}'^{ZZ}(M_{\mathrm{Z}}^2).
\end{aligned} \tag{2.118}$$

Note that the wave-function renormalization constants are only expanded up to $\mathcal{O}(\alpha^2)$, since they are always multiplied by $(k^2 - \mu_V^2) = \mathcal{O}(\alpha)$, for $k^2 \approx M_V^2$, in the renormalized self-energies (2.111). The additional term in the mass renormalization constant of the W boson,

$$c_{\mathrm{T}}^{\mathrm{W}} \;=\; \frac{\mathrm{i}\alpha}{\pi} M_{\mathrm{W}}\Gamma_{\mathrm{W}} \;=\; \frac{\alpha}{\pi}(M_{\mathrm{W}}^2 - \mu_{\mathrm{W}}^2), \tag{2.119}$$

is the result of the presence of contributions to the self-energy of the W boson involving a virtual photon leading to a branch point at $k^2 = \mu_W^2$.
Since the weak mixing angle is a derived quantity (see (2.107)), also its renormalization constant is fixed by the renormalization constants of the weak gauge bosons,

$$\frac{\delta s_{\mathrm{w}}}{s_{\mathrm{w}}} = -\frac{c_{\mathrm{w}}^2}{s_{\mathrm{w}}^2}\frac{\delta c_{\mathrm{w}}}{c_{\mathrm{w}}} = -\frac{c_{\mathrm{w}}^2}{2s_{\mathrm{w}}^2}\left(\frac{\delta\mu_{\mathrm{W}}^2}{\mu_{\mathrm{W}}^2} - \frac{\delta\mu_{\mathrm{Z}}^2}{\mu_{\mathrm{Z}}^2}\right). \tag{2.120}$$

The charge renormalzation constant is still defined in the Thomson limit and also becomes complex in the complex-mass scheme,

$$\delta Z_e = \frac{1}{2}\Sigma_{\mathrm{T}}'^{AA}(0) - \frac{s_{\mathrm{w}}}{c_{\mathrm{w}}}\frac{\Sigma_{\mathrm{T}}^{AZ}(0)}{\mu_{\mathrm{Z}}^2}. \tag{2.121}$$

In this work we will apply the complex-mass scheme in the context of calculating $\mathcal{O}(N_f\alpha_{\mathrm{s}}\alpha)$ corrections. The extension of the complex-mass scheme to this perturbative order will be discussed in Section 5.2.3.1.

Chapter 3

Infrared singularities and factorization properties of NNLO amplitudes

3.1 Colour ordering, extraction of "abelian gluons", and abelianization

In this section we discuss the reduction of general QCD colour factors to products of SU(3) generators in the fundamental representation, which then allows for the identification of so-called colour-ordered partial amplitudes. For the specific process $\gamma^* \to q(p_1)\bar{q}(p_2)g(p_3)g(p_4)$ we specifically construct the colour-ordered partial amplitudes and use them to calculate the corresponding squared amplitude. This explicit construction enables us to extract the relevant parts of the squared matrix element of the full NNLO double real QCD correction, $\gamma^* \to q(p_1)\bar{q}(p_2)g(p_3)g(p_4)$, to the process $\gamma^* \to q(p_1)\bar{q}(p_2)$, in order to get the NNLO QCD×QED correction, i.e. to extract the "abelian gluon" part of the full QCD×QCD result. Here and in the following an "abelian gluon" denotes a gluon that couples only to quarks and does not couple to other gluons, i.e. in the abelian gluon part no gluonic tripple or quartic gauge couplings are include. This knowledge can then be used to identify the relevant parts of NNLO QCD×QCD antenna functions when calculating NNLO QCD×QED corrections.

We start our discussion with a general n-parton QCD (tree-level) amplitude

$$\mathcal{M}_n^{c_1,\ldots,c_n,s_1,\ldots,s_n}(p_1,\ldots,p_n), \tag{3.1}$$

which is a function of the external momenta $p_1,\ldots,p_n$, the colour indices $c_1,\ldots,c_n$, and spin indices $s_1,\ldots,s_n$. It is possible to decompose general QCD amplitudes into a sum of products of two functions, one of these functions describing the colour structure $\mathcal{C}_m(c_1,\ldots,c_n)$ in (3.1), and the other containing information about the kinematics corresponding to the colour structure,

$$\mathcal{M}_n^{c_1,\ldots,c_n,s_1,\ldots,s_n}(p_1,\ldots,p_n) = \sum_m \mathcal{C}_m(c_1,\ldots,c_n)\mathcal{M}_{n,\mathcal{C}_m}^{s_1,\ldots,s_n}(p_1,\ldots,p_n). \tag{3.2}$$

The explicit structure of the appearing functions depends on the multiplicity and the kind of the involved particles in the scattering process described by the matrix element.

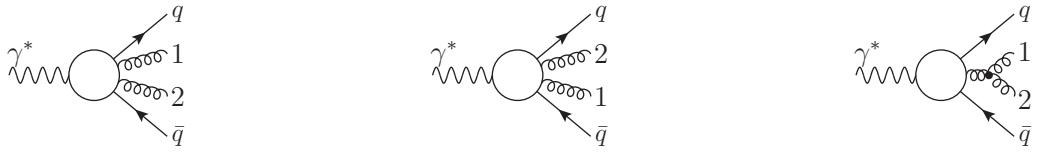

(a) $\mathcal{M}^{\mathrm{a}}_{12}$ (b) $\mathcal{M}^{\mathrm{a}}_{21}$ (c) $\mathcal{M}^{\mathrm{na}}$

Figure 3.1: Feynman diagrams relevant for the process $\gamma^* \to q\bar{q}gg$. The white blob indicates tree structures including no tripple gluon couplings, i.e. it includes only what we refer to as "abelian gluons".

However, by first rewriting the SU(3) structure functions in terms of generators in the fundamental representation,

$$f^{abc} = -2i\mathrm{Tr}([t^a, t^b]t^c), \tag{3.3}$$

and subsequently applying the Fiertz identity

$$t^a_{ij}t^a_{kl} = \frac{1}{2}(\delta_{il}\delta_{jk} - \frac{1}{N}\delta_{ij}\delta_{kl}), \tag{3.4}$$

it is possible to reduce amplitudes $\mathcal{M}_{q_{i_1}\bar{q}_{i_2}(n-2)g}$—the indices denote the external particles involved in the scattering process that is described by the matrix element—with an external quark–antiquark pair and $(n-2)$ external gluons to a factorized form, where the colour functions $\mathcal{C}_m(c_1, \ldots, c_n)$ reduce to a simple product of generators in the fundamental representation,

$$\mathcal{M}_{q_{i_1}\bar{q}_{i_2}(n-2)g} = \sum_{\sigma\in S_{n-2}} (t^{a_{\sigma_1}} \cdots t^{a_{\sigma_{n-2}}})_{i_1 i_2} \mathcal{M}^{s_{\sigma_1},\ldots,s_{\sigma_n}}_{A,(n-2)g,\mathcal{C}_\sigma}(p_q, p_{\sigma_1}, \ldots, p_{\sigma_{n-2}}, p_{\bar{q}}), \tag{3.5}$$

where the open indices i_1, i_2 of the colour functions are the fundamental colour indices carried by the quarks. The sum in (3.5) runs over permutations of $n-2$ elements, i.e. permutations σ that are elements of the symmetric group S_{n-2}, and the amplitudes $\mathcal{M}_{A,(n-2)g,\mathcal{C}_\sigma}$ multiplied with the colour functions in (3.5) are the so-called colour-ordered partial amplitudes that correspond to a certain colour function $\mathcal{C}_\sigma = t^{a_{\sigma_1}} \cdots t^{a_{\sigma_{n-2}}}$.

We now proceed to explicitly construct the decomposition (3.5) for the process

$$\gamma^* \to q(p_1)\bar{q}(p_2)g(p_3)g(p_4), \tag{3.6}$$

which is the process used for the construction of some of the antenna functions relevant for this work. The following discussion of colour decomposition applied to the specific process above is similar to a discussion in [82]. We will see in this example how the abelian gluon part of the squared matrix element, corresponding to the process above and accordingly also of the corresponding antenna function, can be extracted. The relevant Feynman diagrams are shown in Fig. 3.1 and include two contributions with no gluon self-coupling (abelian part) and one contribution including such a coupling (non-abelian part),

$$\mathcal{M}^0_{q_i\bar{q}_j gg} = \mathcal{M}^{\mathrm{a}}_{12} + \mathcal{M}^{\mathrm{a}}_{21} + \mathcal{M}^{\mathrm{na}}. \tag{3.7}$$

The last term on the right-hand side of (3.7) describes the non-abelian part, which can be decomposed into a partial amplitude and the colour structure,

$$\mathcal{M}^{\mathrm{na}} = it^a_{ij} f^{aa_1a_2} \mathcal{M}_{t\cdot f} = [(t^{a_1}t^{a_2})_{ij} - (t^{a_2}t^{a_1})_{ij}]\mathcal{M}_{t\cdot f}, \tag{3.8}$$

where in the second equality we have used (3.3) and (3.4). For the abelian contributions to the amplitude the decomposition into colour structures and kinematics leads to,

$$\mathcal{M}^{\mathrm{a}}_{12} = (t^{a_1}t^{a_2})_{ij}\mathcal{M}_{t^1t^2}, \tag{3.9}$$

$$\mathcal{M}^{\mathrm{a}}_{21} = (t^{a_2}t^{a_1})_{ij}\mathcal{M}_{t^2t^1}. \tag{3.10}$$

Having now reduced all colour structures present in (3.7) to a sum of products of SU(3) generators in the fundamental representation,

$$\mathcal{M}^0_{q_i\bar{q}_j gg} = (t^{a_1}t^{a_2})_{ij}\left(\mathcal{M}_{t^1t^2} + \mathcal{M}_{t\cdot f}\right) + (t^{a_2}t^{a_1})_{ij}\left(\mathcal{M}_{t^2t^1} - \mathcal{M}_{t\cdot f}\right), \tag{3.11}$$

we can identify the colour-ordered partial amplitudes

$$\mathcal{M}^0_{A,q_i\bar{q}_j gg}(q,1_g,2_g,\bar{q}) \equiv \mathcal{M}_{t^1t^2} + \mathcal{M}_{t\cdot f}, \tag{3.12}$$

$$\mathcal{M}^0_{A,q_i\bar{q}_j gg}(q,2_g,1_g,\bar{q}) \equiv \mathcal{M}_{t^2t^1} - \mathcal{M}_{t\cdot f}. \tag{3.13}$$

In terms of the colour-ordered partial amplitudes the colour-summed squared matrix element is given by

$$\begin{aligned}|\mathcal{M}^0_{q_i\bar{q}_j gg}|^2 =& \frac{1}{4}N(N^2-1)\Big(1-\frac{1}{N^2}\Big)\sum_{k,l\in P(1,2)}|\mathcal{M}^0_{A,q_i\bar{q}_j gg}(q,k_g,l_g,\bar{q})|^2 \\ &- \frac{1}{4}N(N^2-1)\frac{1}{N^2}\Big\{\mathcal{M}^0_{A,q_i\bar{q}_j gg}(q,1_g,2_g,\bar{q})^*\mathcal{M}^0_{A,q_i\bar{q}_j gg}(q,2_g,1_g,\bar{q}) \\ &\qquad + \mathcal{M}^0_{A,q_i\bar{q}_j gg}(q,2_g,1_g,\bar{q})^*\mathcal{M}^0_{A,q_i\bar{q}_j gg}(q,1_g,2_g,\bar{q})\Big\},\end{aligned} \tag{3.14}$$

where the colour-ordered part in the first line of (3.14) has a leading and subleading colour contribution originating from the prefactor $1-\frac{1}{N^2}$, whereas the part without colour ordering, i.e. the part including products of the two different partial amplitudes, is subleading in colour due to the prefactor $\frac{1}{N^2}$. If we collect terms in the last equation that have the same scaling behaviour in N we obtain,

$$\begin{aligned}|\mathcal{M}^0_{q_i\bar{q}_j gg}|^2 =& \frac{1}{4}N(N^2-1)\Big\{\sum_{k,l\in P(1,2)}|\mathcal{M}^0_{A,q_i\bar{q}_j gg}(q,k_g,l_g,\bar{q})|^2 \\ &- \frac{1}{N^2}\big|\mathcal{M}^0_{A,q_i\bar{q}_j gg}(q,1_g,2_g,\bar{q}) + \mathcal{M}^0_{A,q_i\bar{q}_j gg}(q,2_g,1_g,\bar{q})\big|^2\Big\}.\end{aligned} \tag{3.15}$$

The subleading colour part of (3.15) is given by the sum of the two colour-ordered partial amplitudes and is therefore symmetric under the exchange of the two gluons, $1_g \leftrightarrow 2_g$. This means that one of the gluons in the subleading colour part effectively behaves QED-like,

$$\mathcal{M}(q,1_g,2^\gamma_g,\bar{q}) \equiv \mathcal{M}^0_{A,q_i\bar{q}_j gg}(q,1_g,2_g,\bar{q}) + \mathcal{M}^0_{A,q_i\bar{q}_j gg}(q,2_g,1_g,\bar{q}), \tag{3.16}$$

and no non-abelian QCD couplings are included in this part. The notation 2_g^γ indicates, that the emission pattern of this gluon is not ordered and therefore behaves like a photon, while the other gluon still has an orderd emission (which is not relevant for amplitudes involving only two gluons). The radiating quark–antiquark pair are the only "colour neighbours" of the photon-like gluon, 2_g^γ, which is not colour connected to the other gluon, 1_g. Therefore, the limits where the photon-like gluon becomes unresolved only lead to IR singularities if the gluon is unresolved with respect to the quark–antiquark pair. In the discussion of infrared singularities of colour-ordered amplitudes in the following Section 3.2 we can implicitly include also the amplitude $\mathcal{M}(q, 1_g, 2_g^\gamma, \bar{q})$ with an abelian gluon due to its simple singularity structure. This is crucial for the construction of subtraction terms using antenna subtraction in later chapters.

The squared amplitude (3.15) is an illustrative example of the fact that the subleading colour part of a NNLO QCD×QCD calculation is sufficient in order to extract the needed information relevant for NNLO QED×QCD calculations. We will make use of this fact frequently when constructing subtraction terms relevant for this work.

3.1.1 Abelianization

Based on the previous section we will now derive a simple replacement rule that can be used to obtain QCD×QED corrections from the subleading colour part of QCD×QCD corrections. In order to do this, we follow the same steps that we already made in the last section, but this time for the process,

$$\gamma^* \to q(p_1)\bar{q}(p_2)g(p_3)\gamma(p_4).$$

In this case the colour-ordered amplitude is given by

$$\mathcal{M}^0_{q_i\bar{q}_j g\gamma} = t^a_{ij} Q_q \left(\mathcal{M}_{t^1 t^2} + \mathcal{M}_{t^2 t^1}\right)\Big|_{g_s^2 \to e g_s}, \tag{3.17}$$

where the colour-ordered subamplitudes, $\mathcal{M}_{t^i t^j}$, are the same as in the previous section, but we have to replace one of the QCD coupling factors, $t^k_{ij} g_s$, by the elementary charge, $Q_q e$. If we now compare the colour factors of the squared amplitude in the QCD×QED case,

$$|\mathcal{M}^0_{q_i\bar{q}_j g\gamma}|^2 = \frac{1}{2} N (N - \frac{1}{N}) Q_q^2 \left|\mathcal{M}_{t^1 t^2} + \mathcal{M}_{t^2 t^1}\right|^2\Big|_{g_s^4 \to e^2 g_s^2},$$

to the colour factors of the subleading colour part of the squared amplitude (3.15) in the QCD×QCD case,

$$\begin{aligned} |\mathcal{M}^0_{q_i\bar{q}_j gg}|^2\Big|_{\text{subleading}} &= -\frac{1}{4}(N - \frac{1}{N})|\mathcal{M}^0_{A,q_i\bar{q}_j gg}(q, 1_g, 2_g, \bar{q}) + \mathcal{M}^0_{A,q_i\bar{q}_j gg}(q, 2_g, 1_g, \bar{q})|^2 \\ &= -\frac{1}{4}(N - \frac{1}{N})|\mathcal{M}_{t^1 t^2} + \mathcal{M}_{t^2 t^1}|^2, \end{aligned}$$

we can read off the simple conversion rule to obtain the QCD×QED corrections:

- To obtain the subleading-colour contribution collect all terms proportional to $\frac{1}{N^2}$ (with respect to leading colour) of the squared QCD×QCD amplitude, where the terms in the squared amplitude have to be ordered according to their scaling behaviour in N as in (3.15).
- Apply the following replacement to the subleading-colour contribution,

$$\alpha_s^2 \to (-2N)\alpha_s \alpha Q_q^2. \tag{3.18}$$

This procedure is also known as abelianization.

3.2 Infrared singularities and factorization properties of colour-ordered amplitudes

Ultraviolet divergences arise in higher-order loop corrections in the limit of infinite loop momenta and are treated in the course of renormalization of the input parameters and fields of a given theory. In addition the UV divergences, also the finite-momentum regions of loop integrals can contain singular configurations, depending on the momenta and masses of the particles involved in the respective integrals. The so-called Landau equations [83] describe the conditions on the kinematic properties of the involved particle four-momenta that need to be fulfilled such that an integral develops singularities for finite loop momenta. The Landau equations depend on the four-momenta and masses of the external particles and also of virtual particles in the loop. Solutions of the Landau equations that depend only on the squares of external momenta but not on their orientation are called infrared (IR) divergences. In the following sections we describe the relevant configurations that lead to IR singularities at NLO and NNLO. We also discuss the factorization properties of squared colour-ordered partial amplitudes (as in (3.5)) in these singular limits. Since this work will mainly deal with the subleading colour parts of NNLO QCD corrections, it is important to note, as discussed in the previous section, that the factorization properties of leading-colour contributions to squared amplitudes are also applicable to the subleading-colour contributions relevant for this work.

Infrared singularities in one-loop amplitudes

One-loop amplitudes can contain two different kinds of IR singularities. In the SM, "soft" IR singularities are the result of the exchange of a massless virtual boson between two external on-shell particles. The integration over the region where the loop momentum, associated to the exchanged massless particle, is much smaller than any relevant scale of the theory is the origin of soft singularities in loop integrals. An illustration of the configuration that leads to a soft singularity is given in the left diagram of Fig. 3.2. The second kind of IR singularities present in one-loop amplitudes are the so-called "collinear" singularties, which originate from the region of the loop integral where two adjacent massless virtual particles are collinear to the momentum of their common external massless on-shell particle, as depicted in right diagram in Fig. 3.2. When using dimensional regularization

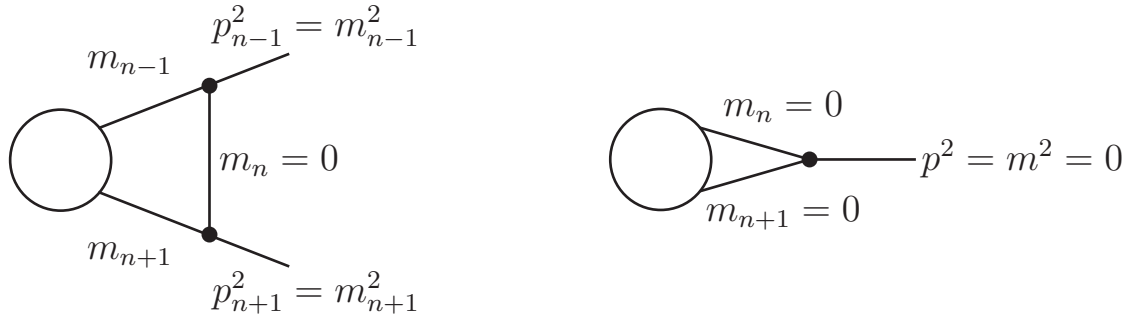

Figure 3.2: The two configurations in one-loop amplitudes that lead to soft (left diagram) or collinear (right diagram) IR singularities.

both collinear and soft singularities lead to $\frac{1}{\epsilon}$ poles. Regions of the loop integration where soft and collinear singularities overlap lead to $\frac{1}{\epsilon^2}$ poles.

To extract the IR-divergent part of amplitudes we introduce the operators $\mathcal{P}oles$ and $\mathcal{F}inite$. The $\mathcal{P}oles$ operator acts on one-loop amplitudes and returns their pole structure in terms of the colour-ordered two-particle IR singularity operators [84],

$$\begin{aligned}
\boldsymbol{I}^{(1)}_{q\bar{q}}(\epsilon, s_{q\bar{q}}) &= -\frac{e^{\epsilon\gamma}}{2\Gamma(1-\epsilon)}\left[\frac{1}{\epsilon^2}+\frac{3}{2\epsilon}\right](-s_{q\bar{q}})^{-\epsilon}\,,\\
\boldsymbol{I}^{(1)}_{qg}(\epsilon, s_{qg}) &= -\frac{e^{\epsilon\gamma}}{2\Gamma(1-\epsilon)}\left[\frac{1}{\epsilon^2}+\frac{5}{3\epsilon}\right](-s_{qg})^{-\epsilon}\,,\\
\boldsymbol{I}^{(1)}_{gg}(\epsilon, s_{gg}) &= -\frac{e^{\epsilon\gamma}}{2\Gamma(1-\epsilon)}\left[\frac{1}{\epsilon^2}+\frac{11}{6\epsilon}\right](-s_{gg})^{-\epsilon}\,,\\
\boldsymbol{I}^{(1)}_{q\bar{q},N_F}(\epsilon, s_{q\bar{q}}) &= 0\,,\\
\boldsymbol{I}^{(1)}_{qg,N_F}(\epsilon, s_{qg}) &= \frac{e^{\epsilon\gamma}}{2\Gamma(1-\epsilon)}\,\frac{1}{6\epsilon}\,(-s_{qg})^{-\epsilon}\,,\\
\boldsymbol{I}^{(1)}_{gg,N_F}(\epsilon, s_{gg}) &= \frac{e^{\epsilon\gamma}}{2\Gamma(1-\epsilon)}\,\frac{1}{3\epsilon}\,(-s_{gg})^{-\epsilon}\,.
\end{aligned} \tag{3.19}$$

The action of the $\mathcal{F}inite$ operator on loop amplitudes is defined by

$$\mathcal{F}inite(\mathcal{X}) = \mathcal{X} - \mathcal{P}oles(\mathcal{X}). \tag{3.20}$$

Contrary to what the naming convention of the operator $\mathcal{P}oles(\mathcal{X})$ might suggest, the two-particle IR singularity operators in (3.19) also contain finite parts of the form $\epsilon^n \log^n(-s)$, which result from the expansion of the terms $(-s)^{-\epsilon}$ combined with the poles included in the singularity operators.

For one-loop colour-ordered partial amplitudes the IR pole structure is given by

$$\mathcal{P}oles\Big(2\mathrm{Re}\big\{(\mathcal{M}^0_n)^*\,\mathcal{M}^1_n\big\}\Big) = 2\mathrm{Re}\{\boldsymbol{I}^{(1)}_n(\epsilon;\{p_i\}^n_{i=1})\}\cdot|M^0_n(\{p_i\}^n_{i=1})|^2, \tag{3.21}$$

where we introduced the notation $\{p_i\}^n_{i=1} = \{p_1,\ldots,p_n\}$ and the colour-ordered singularity operator, $\boldsymbol{I}^{(1)}_n$, is the sum of two-particle IR singularity operators of colour-connected

pairs $\mathcal{C}$,

$$\boldsymbol{I}_n^{(1)}(\epsilon;\{p_i\}_{i=1}^n) = \sum_{i,j\in\mathcal{C}} \boldsymbol{I}_{ij}^{(1)}(\epsilon, s_{ij}), \tag{3.22}$$

where $s_{ij} = (p_i + p_j)^2$ and the set of tuples $\mathcal{C}$ is defined as

$$\mathcal{C} = \{(i,j)|i,j = 1,\ldots,n,\ i \neq j,\ \text{and } i,j \text{ are colour connected}\}. \tag{3.23}$$

Single-unresolved limits of tree-level squared amplitudes at NLO

The factorization of squared amplitudes in IR-singular limits into a process-independent singular factor and a process-dependent reduced squared matrix element is a key ingredient in the calculation of perturbative corrections. Different prescriptions, such as two-cutoff slicing [85, 86] or subtraction schemes, allow for a independent calculation of real and virtual contributions at NLO and heavily rely on these factorization properties. In [60], both two-cutoff slicing and subtraction schemes applicable to NLO calculations are discussed in detail.

In real emission amplitudes $\mathcal{M}_{n+1}^0$ which include the radiation of an additional particle compared to the leading order process involving n partons, a soft singularity is the result of the emission of a photon or gluon with momentum p_i in the limit of vanishing momentum, $p_i^\mu \to 0$. The behaviour of colour-ordered real emission squared partial amplitudes in this limit is described by the process-independent eikonal factor, J_{ijk}, and the underlying born squared matrix element,

$$|\mathcal{M}_{n+1}^0(\cdots, p_i, p_j, p_k, \cdots)|^2 \underset{p_j\to 0}{\sim} J_{ijk}|\mathcal{M}_n^0(\cdots, p_i, p_k, \cdots)|^2, \tag{3.24}$$

where the eikonal current is given by,

$$J_{ijk} = \frac{2s_{ik}}{s_{ij}s_{jk}}. \tag{3.25}$$

Note that we consider partial amplitudes in (3.24) and as a consequence no colour factors appear. To parametrize the limit where the momenta p_j and p_k become collinear we use the so-called "Sudakov parametrization" and introduce a light-like vector $p_{(jk)}$, $p_{(jk)}^2 = 0$, which denotes the collinear direction, a light-like vector n, and the transverse component $k_\perp$, such that $k_\perp p_{(jk)} = k_\perp n = 0$. In terms of these momenta,

$$\begin{aligned} p_j^\mu &= z p_{(jk)}^\mu + k_\perp^\mu - \frac{k_\perp^2}{z}\frac{n^\mu}{2\,p_{(jk)}\cdot n}, \\ p_k^\mu &= (1-z) p_{(jk)}^\mu - k_\perp^\mu - \frac{k_\perp^2}{1-z}\frac{n^\mu}{2\,p_{(jk)}\cdot n}, \end{aligned} \tag{3.26}$$

the collinear limit of p_j and p_k is obtained for $k_\perp \to 0$. In case of a collinear (anti-)quark-gluon pair with momenta p_j, p_k, respectively, the colour-ordered squared partial matrix element behaves as,

$$|\mathcal{M}_{n+1}^0(\cdots, p_j, p_k, \cdots)|^2 \underset{p_j\|p_k}{\sim} \frac{1}{s_{jk}} P_{jk\to(jk)}|\mathcal{M}_n^0(\cdots, p_{(jk)}, \cdots)|^2, \tag{3.27}$$

where $P_{jk\to(jk)}$ are the polarization-averaged splitting functions, known as Altarelli–Parisi splitting functions [87]. The collinear limit of a quark–antiquark pair of matching flavour or of two gluons,

$$|\mathcal{M}^0_{n+1}(\cdots,p_j,p_k,\cdots)|^2 \underset{p_j\|p_k}{\sim} \frac{1}{s_{jk}} P^{\mu\nu}_{jk\to(jk)} |\mathcal{M}^0_n(\cdots,p_{(jk)},\cdots)|^2_{\mu\nu}, \tag{3.28}$$

does not lead to a fully factorized form, but instead includes spin correlations that lead to contractions between universal tensorial splitting functions and the colour-ordered squared born matrix elements. However, it is possible to rewrite the contraction between the tensorial splitting functions and the squared born matrix elements in terms of the spin-averaged splitting functions plus additional angular terms,

$$|\mathcal{M}^0_{n+1}(\cdots,p_j,p_k,\cdots)|^2 \underset{p_j\|p_k}{\sim} \frac{1}{s_{jk}} P^{\mu\nu}_{jk\to(jk)} |\mathcal{M}^0_n(\cdots,p_{(jk)},\cdots)|^2_{\mu\nu} \tag{3.29}$$

$$= \frac{1}{s_{jk}} P_{jk\to(jk)} |\mathcal{M}^0_n(\cdots,p_{(jk)},\cdots)|^2 + \text{angular terms}. \tag{3.30}$$

The angular terms vanish when integrating over the azimuthal angle ϕ, which is part of the phase-space integral and parametrizes the azimuthal angle of $k_\perp$ around the collinear direction $p_{(jk)}$. Angular terms are also relevant in the construction of subtraction terms in the context of antenna subtraction and will be discussed in more detail in Section 4.3. In conventional dimensional regularization, where gluons have $d-2$ and fermions two polarizations, the spin-averaged final-final splitting functions [84] are given by

$$\begin{aligned}
P_{qg\to Q} &= \frac{1+(1-z)^2-\epsilon z^2}{z}, \\
P_{q\bar{q}\to G} &= \frac{z^2+(1-z)^2-\epsilon}{1-\epsilon}, \\
P_{gg\to G} &= 2\left(\frac{z}{1-z}+\frac{1-z}{z}+z(1-z)\right).
\end{aligned} \tag{3.31}$$

Note that the splitting functions do not include any colour factors as we consider limits of colour-ordered squared subamplitudes. If one of the particles involved in the collinear limits is contained in the initial state, say with momentum p_i, of a colour-ordered squared amplituded the following initial–final splitting functions have to be used,

$$\begin{aligned}
P_{gq\leftarrow Q}(z) &= \frac{1}{1-z}\frac{1}{1-\epsilon} P_{qg\to Q}(1-z), \\
P_{qg\leftarrow Q}(z) &= \frac{1}{1-z} P_{qg\to Q}(z), \\
P_{q\bar{q}\leftarrow G}(z) &= \frac{1-\epsilon}{1-z} P_{q\bar{q}\to G}(z), \\
P_{gg\leftarrow G}(z) &= \frac{1}{1-z} P_{gg\to G}(z),
\end{aligned} \tag{3.32}$$

where the momentum fraction z now describes the splitting of the initial-state momentum, p_i, into the composite momentum, $p_{(jk)} = (1-z)p_i$, and the momentum of the second

particle, $p_j = zp_i$, involved in the splitting. The additional factors of $1-\epsilon$ compared to the final–finial splitting functions are due to the different averaging factors for gluons and quarks in the initial state,

$$\frac{\#\text{helicities}_{\text{gluons}}}{\#\text{helicities}_{\text{quarks}}} = \frac{d-2}{2} = 1-\epsilon. \tag{3.33}$$

3.2.1 Factorization properties of colour-ordered amplitudes at NNLO

In this section we extend the discussion of factorization properties of colour-ordered squared subamplitudes from NLO to NNLO. At this order of perturbation theory one has to consider double-real, real–virtual, and double-virtual contributions with $(n+2)$, $(n+1)$, and n partons in the final state compared to the leading-order process, respectively. The real–virtual corrections include, in addition to the real radiation, a one-loop correction, whereas the double-virtual contribution does not include any real radiation, but instead two-loop corrections. These new structures in the calculation of squared amplitudes present at NNLO lead to additional ingredients needed to formulate the factorization properties of amplitudes at this perturbative order.

Infrared singularities in two-loop amplitudes

The two-loop correction to the squared amplitude not only includes the contribution from the genuine two-loop correction projected onto the born amplitude, but also the squared one-loop correction,

$$M_n^2(\{p_i\}_{i=1}^n) = 2\text{Re}\{\mathcal{M}_n^0(\{p_i\}_{i=1}^n)^*\,\mathcal{M}_n^2(\{p_i\}_{i=1}^n)\} + |\mathcal{M}_n^1(\{p_i\}_{i=1}^n)|^2. \tag{3.34}$$

The IR pole structure of one-loop colour-ordered partial amplitudes (3.21),

$$\mathcal{M}_n^1(\{p_i\}_{i=1}^n) = \boldsymbol{I}_n^{(1)}(\epsilon;\{p_i\}_{i=1}^n)\mathcal{M}_n^0(\{p_i\}_{i=1}^n) + \mathcal{M}_n^{1,\text{fin}}(\{p_i\}_{i=1}^n), \tag{3.35}$$

can be used to obtain the pole structure of the squared one-loop term

$$\begin{aligned}\mathcal{P}oles\,|\mathcal{M}_n^1|^2 =& \mathcal{P}oles\Big((\mathcal{M}_n^0)^*\boldsymbol{I}_n^{(1)\,\dagger}\boldsymbol{I}_n^{(1)}\mathcal{M}_n^0 + 2\text{Re}\big\{(\mathcal{M}_n^{1,\text{fin}})^*\boldsymbol{I}_n^{(1)}\mathcal{M}_n^0\big\} + |\mathcal{M}_n^{1,\text{fin}}|^2\Big)\\ =&(\mathcal{M}_n^0)^*\boldsymbol{I}_n^{(1)\,\dagger}\boldsymbol{I}_n^{(1)}\mathcal{M}_n^0 + 2\text{Re}\big\{(\mathcal{M}_n^{1,\text{fin}})^*\boldsymbol{I}_n^{(1)}\mathcal{M}_n^0\big\}\\ =&\text{Re}\big\{2\,(\mathcal{M}_n^1)^*\boldsymbol{I}_n^{(1)}\mathcal{M}_n^0 - (\mathcal{M}_n^0)^*\boldsymbol{I}_n^{(1)\,\dagger}\boldsymbol{I}_n^{(1)}\mathcal{M}_n^0\big\}.\end{aligned} \tag{3.36}$$

This can be combined with the IR pole structure of the genuine two-loop contribution projected onto the born matrix element [88],

$$\begin{aligned}\mathcal{P}oles\Big(2\text{Re}\big\{(\mathcal{M}_n^0)^*\,\mathcal{M}_n^2\big\}\Big) =& 2\text{Re}\Bigg\{\boldsymbol{I}_n^{(1)}(\epsilon;\{p_i\}_{i=1}^n)\Big(M_n^1(\{p_i\}_{i=1}^n) - \frac{\beta_0}{\epsilon}M_n^0(\{p_i\}_{i=1}^n)\Big)\\ &-\frac{1}{2}\boldsymbol{I}_n^{(1)}(\epsilon;\{p_i\}_{i=1}^n)^2 M_n^0(\{p_i\}_{i=1}^n)\end{aligned}$$

$$+e^{-\epsilon\gamma}\frac{\Gamma(1-2\epsilon)}{\Gamma(1-\epsilon)}\left(\frac{\beta_0}{\epsilon}+K\right)\boldsymbol{I}_n^{(1)}(2\epsilon;\{p_i\}_{i=1}^n)M_n^0(\{p_i\}_{i=1}^n)$$
$$+\boldsymbol{H}^{(2)}(\epsilon)M_n^0(\{p_i\}_{i=1}^n)\Bigg\}, \tag{3.37}$$

to obtain the complete IR pole structure of the two-loop correction to the colour-ordered squared matrix element,

$$\mathcal{P}oles\big(M_n^2(\{p_i\}_{i=1}^n)\big)=\mathcal{P}oles\Big(2\mathrm{Re}\big\{(\mathcal{M}_n^0)^*\,\mathcal{M}_n^2\big\}\Big)+\mathcal{P}oles\,|\mathcal{M}_n^1|^2, \tag{3.38}$$

where the form of the function $\boldsymbol{H}^{(2)}(\epsilon)$ and the constant K in (3.37) depend on the particle content of the considered process [88].

Single-unresolved limits including one-loop amplitudes

In the soft limit one-loop squared colour-ordered partial matrix elements factorize into two parts,

$$M_{n+1}^1(\cdots,p_i,p_j,p_k,\cdots)\underset{p_j\to 0}{\sim}J_{ijk}^0M_n^1(\cdots,p_i,p_k,\cdots)+J_{ijk}^1|\mathcal{M}_n^0(\cdots,p_i,p_k,\cdots)|^2, \tag{3.39}$$

where the first part includes the leading-order eikonal current multiplied with the colour-ordered one-loop correction to the squared amplitude,

$$M_n^1(\{p_i\}_{i=1}^n)=2\mathrm{Re}\{\mathcal{M}_n^0(\{p_i\}_{i=1}^n)^*\cdot\mathcal{M}_n^1(\{p_i\}_{i=1}^n)\}, \tag{3.40}$$

whereas the second part in (3.39) contains the one-loop soft radiation function J_{ijk}^1, which is not present at NLO and its definition can be found in [89]. The collinear limit of one-loop squared partial matrix elements leads to a similar factorization behavior,

$$M_{n+1}^1(\cdots,p_j,p_k,\cdots)\underset{p_j\|p_k}{\sim}\frac{1}{s_{jk}}\big(P_{jk\to(jk)}M_n^1(\cdots,p_{(jk)},\cdots)$$
$$+P_{jk\to(jk)}^1|\mathcal{M}_n^0(\cdots,p_{(jk)},\cdots)|^2\big), \tag{3.41}$$

where the first term involves a leading-order splitting function and the second term a one-loop spin-averaged splitting function $P_{jk\to(jk)}^1$ [89]. These factorization patterns are relevant for the construction of subtraction terms for real–virtual NNLO corrections.

Double soft unresolved limits

For two soft adjacent gluons in the colour-ordered amplitude with momenta p_j,p_k, the squared colour-ordered partial matrix element factorizes into a soft function J_{ijkl} [90], which is independent of the particle type of the hard radiators i,l, and the underlying squared born matrix element,

$$|\mathcal{M}_{n+2}^0(\cdots,p_i,p_j,p_k,p_l,\cdots)|^2\underset{p_j,p_k\to 0}{\sim}J_{ijkl}|\mathcal{M}_n^0(\cdots,p_i,p_l,\cdots)|^2. \tag{3.42}$$

If the two soft adjacent particles form a quark-antiquark pair with momenta p_j, p_k, originating from a soft gluon, then the factorization is given by,

$$|\mathcal{M}^0_{n+2}(\cdots, p_i, p_j, p_k, p_l, \cdots)|^2 \underset{p_j, p_k \to 0}{\sim} J_{il}(p_j, p_k)|\mathcal{M}^0_n(\cdots, p_i, p_l, \cdots)|^2, \tag{3.43}$$

where the soft functions relevant for both cases can be found in [84]. In other cases, where the unresolved partons are separated by a hard radiator in the colour-ordered partial amplitudes, the singular behaviour of amplitudes can be obtained by a twofold application of the NLO soft factorization equation.

Double collinear unresolved limits

If two adjacent particles in the colour-ordered amplitude with momenta p_j, p_k become collinear to a hard radiator which is adjacent to at least one of the two particles j or k the colour-ordered squared partial matrix element factorizes according to [91],

$$|\mathcal{M}^0_{n+2}(\cdots, p_i, p_j, p_k, \cdots)|^2 \underset{p_i || p_j || p_k}{\sim} P_{ijk \to (ijk)}|\mathcal{M}^0_n(\cdots, p_{(ijk)}, \cdots)|^2. \tag{3.44}$$

This limit corresponds to a triple collinear limit. There are seven different triple collinear splitting functions relevant at NNLO, which all can be found in [84,91]. In the case where the particles j and k are collinear with different hard partons and not with each other, the limit of this configuration can be obtained by an twofold iteration of the NLO collinear factorization formula.

Soft-collinear unresolved limits

When two adjacent particles in the colour-ordered partial matrix element become unresolved between a common set of hard radiators and one of the unresolved partons is soft while the other is collinear to one of the hard radiators, one obtains the following factorization pattern [91],

$$|\mathcal{M}^0_{n+2}(\cdots, p_i, p_j, p_k, p_l, \cdots)|^2 \underset{p_j \to 0, p_k || p_l}{\sim} J_{i;jkl} \frac{1}{s_{kl}} P_{kl \to (kl)}|\mathcal{M}^0_n(\cdots, p_i, p_{(kl)}, \cdots)|^2, \tag{3.45}$$

where the soft-collinear factor $J_{i;jkl}$ can be found e.g. in [84] and $P_{kl \to (kl)}$ is a leading-order splitting function. In other cases, where the unresolved partons are separated by a hard radiator, the singular behaviour of amplitudes in soft-collinear limits can be obtained by an application of the NLO soft and collinear factorization formulas.

3.3 The parton model and mass factorization

The elementary particles described by QCD (gluons and quarks) are not observable as free asymptotic states, but instead are confined within colourless bound states. This fact prevented us from using an on-shell renormalization scheme in Section 2.2.2 and lead us to the application the $\overline{\text{MS}}$ renormalization scheme in QCD. This renormalization scheme applied in QCD calculations eventually leads to the running coupling constant, which, in turn, leads to the applicability of perturbation theory to QCD calculations at high

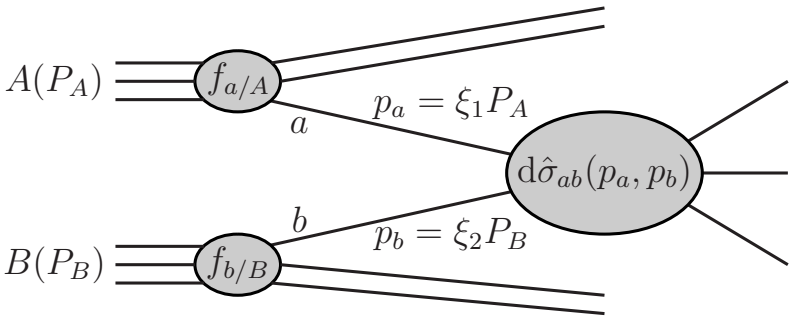

Figure 3.3: A schematic representation of the hadronic scattering of two hadrons A and B, where only the two partons a and b take part in the hard scattering process.

energies. However, on the other hand, it also implies the breakdown of any perturbative QCD calculation at small scales of the order of the confinement scale, Λ_{QCD}. Therefore, the description of hadrons relies on models, where the so-called "parton model" is amongst the most prominent ones. As perturbative QCD calculation fail to predict the structure of models for hadrons, their properties have to be determined from experimental input.

The parton model [92, 93] describes hadrons as composed objects of so-called partons in an infinite momentum frame, which allows for the neglect of the masses of hadrons and its constituents. The assumption of an infinite momentum frame limits the applicability of the parton model to high-energy interactions, but the time dilatation in this frame also justifies the assumption of a constant number density of partons and frozen internal interactions within the hadron during the short time span of interactions of hadronic collisions. One can further assume that at high energies the interaction between hadrons actually is an interaction between individual partons, as shown in Fig. 3.3, where each parton a carries a momentum fraction $p_a = \xi_1 P_A$, $0 < \xi_1 < 1$, of hadron A which carries momentum P_A. The probability to find a parton of type a that carries the longitudinal momentum fraction ξ_1 of parton A is described by the parton distribution function (PDF) $f^{(0)}_{a/A}(\xi_1)$. The hard scattering process of the individual partons, characterized by a momentum transfer much larger than Λ_{QCD}, is assumed to be calculable using perturbation theory. The hadronic cross section for the scattering of two hadrons A and B is given by the sum over all partonic cross sections, convoluted with the corresponding PDFs,

$$\sigma_{\mathrm{LO}}(P_A, P_B) = \sum_{a,b} \int_0^1 \frac{\mathrm{d}\xi_1}{\xi_1} \int_0^1 \frac{\mathrm{d}\xi_2}{\xi_2} f^{(0)}_{a/A}(\xi_1) f^{(0)}_{b/B}(\xi_2)\, \mathrm{d}\hat{\sigma}^{(0)}_{\mathrm{LO},ab}(\xi_1 P_A, \xi_2 P_B). \tag{3.46}$$

The superscript $^{(0)}$ indicates the bare cross section and PDFs in the context of "renormalized" PDFs, the exact meaning of which will be explained in the following section. Note that it does not necessarily refer to the leading order cross section, $\mathrm{d}\hat{\sigma}_{\mathrm{LO},ab}$. We will only consider proton–proton (i.e. $A = B = P$ in Fig. 3.3) collisions in this work and will therefore omit the index identifying the parent parton a PDF belongs to, $f^{(0)}_a(\xi_1) \equiv f^{(0)}_{a/P}(\xi_1)$, and implicitly assume that in an expression as (3.46) each of the two PDFs correspond to one of the two colliding protons.

The QCD-improved parton model up to NNLO

The mechanism leading to the cancellation of IR singularities between real and virtual corrections to cross section is described by the Kinoshita–Lee–Nauenberg (KLN) theorem and is based on the unitarity of the S-matrix. Therefore, the applicability of the theorem relies on the level of inclusiveness of all external states that are degenerate in energy. Collinear initial-state radiation, however, modifies the momentum entering the hard scattering process and therefore spoils the inclusive treatment of external states. As the parton model assumes all partons to be massless, these collinear emissions in the initial state lead to uncancelled singularities (which is why (3.46) has to be restricted to leading order). As a result, the extension of the naive parton model to NLO and NNLO perturbative QCD calculations requires the application of a procedure similar to renormalization in order to absorb the uncancelled collinear singularities into the PDFs. In the following we discuss the redefinition of PDFs used to absorb the remaining singularities. For more information on the matter we refer to [94, 95], which we will follow closely.

In order to absorb the collinear divergences that remain in the sum of real and virtual corrections in NLO and NNLO QCD predictions, we introduce the so-called mass factorization kernels Γ_{ab}, the inverse of which are the analogue of renormalization constants in the renormalization procedure applied to absorb UV divergences. The mass factorization kernel convoluted with the bare PDF, $f_a^{(0)}$, defines the "physical" or "renormalized" PDF which will be fitted to data,

$$f_a(\xi, \mu_{\mathrm{F}}^2) = \left[f_b^{(0)} \otimes \Gamma_{ba} \right] (\xi, \mu_{\mathrm{F}}^2) \equiv \int dx\, dy\; f_b^{(0)}(x) \Gamma_{ba}(y, \mu_{\mathrm{F}}^2) \delta(\xi - xy). \tag{3.47}$$

As in renormalization, we assume that the bare PDFs $f_a^{(0)}$ and the mass factorization kernels Γ_{ab} are potentially divergent quantities such that the physical PDFs f_a are finite. Furthermore, the so-called factorization scale, μ_{F}, is introduced to separate soft long-distance hadronic from hard short-distance partonic physics. In qualitative terms, partons radiated in collinear initial-state splittings with transverse momentum greater than the factorization scale are attributed to the hard scattering process, whereas a transverse momentum below the factorization scale indicates a splitting within the hadron. For simplicity, we set the factorization scale equal to the renormalization scale μ introduced in Section 2.2.2

$$\mu_{\mathrm{F}} = \mu. \tag{3.48}$$

In this work, the perturbative expansion of mass factorization kernel, Γ_{ba}, is relevant up to two-loop order,

$$\Gamma_{ba}(x, \mu_{\mathrm{F}}^2) = \delta_{ba}\delta(1-x) + \left(\frac{\alpha_s(\mu_{\mathrm{F}})}{2\pi} \right) \Gamma_{ba}^1(x) + \left(\frac{\alpha_s(\mu_{\mathrm{F}})}{2\pi} \right)^2 \Gamma_{ba}^2(x) + \mathcal{O}(\alpha_s^3). \tag{3.49}$$

The demand that all remaining collinear IR singularities have to be cancelled by the introduction of the mass factorization kernels only fixes the divergent part of the coefficients in the expansion of the kernels and there is, in analogy to renormalization, freedom in the choice of the respective finite terms. Choosing certain finite parts defines a factorization

scheme. In this work we will use the $\overline{\text{MS}}$ scheme, where the coefficients of the perturbative series up to two-loop order are given by

$$\Gamma^{(1)}_{ba}(x) = -\frac{1}{\epsilon}\, p^0_{ba}(x), \tag{3.50}$$

$$\Gamma^{(2)}_{ba}(x) = \frac{1}{2\epsilon^2}\left[\sum_c \left[p^0_{bc}\otimes p^0_{ca}\right](x) + 2\beta_0\, p^0_{ba}(x)\right] - \frac{1}{2\epsilon}\, p^1_{ba}(x), \tag{3.51}$$

where the four-dimensional colour ordered splitting kernels p^0_{ab}, p^1_{ab} can be found in [96]. The coefficient β_i of the perturbative expansion of the β-function,

$$\frac{1}{2\pi}\beta(\alpha_s) = -\beta_0\left(\frac{\alpha_s(\mu_{\rm F}^2)}{2\pi}\right)^2 - \beta_1\left(\frac{\alpha_s(\mu_{\rm F}^2)}{2\pi}\right)^3 - \beta_2\left(\frac{\alpha_s(\mu_{\rm F}^2)}{2\pi}\right)^4 + \mathcal{O}(\alpha_s(\mu_{\rm F}^2)^5) \tag{3.52}$$

can be obtained from the expansion given in (2.76) and (2.77) by

$$\beta_0 = 2\pi b, \quad \beta_1 = 2\pi b'\beta_0, \quad \beta_2 = (2\pi)^2 b''\beta_0. \tag{3.53}$$

By inverting (3.47) order by order in perturbation theory one can obtain the bare PDF in terms of the renormalized PDF as,

$$f^{(0)}_a(\xi) = \left[f_b\otimes\Gamma^{-1}_{ba}\right](\xi) = \int dx\, dy\; f_b(x,\mu_{\rm F}^2)\Gamma^{-1}_{ba}(y,\mu_{\rm F}^2)\delta(\xi - xy), \tag{3.54}$$

where the inverse of the mass factorization kernels is given by,

$$\begin{aligned}\Gamma^{-1}_{ba}(y,\mu_{\rm F}^2) &= \delta_{ba}\delta(1-y) - \left(\frac{\alpha_s(\mu_{\rm F})}{2\pi}\right)\Gamma^{(1)}_{ba}(y) \\ &\quad - \left(\frac{\alpha_s(\mu_{\rm F})}{2\pi}\right)^2\left[\Gamma^{(2)}_{ba}(y) - \sum_c\left[\Gamma^{(1)}_{bc}\otimes\Gamma^{(1)}_{ca}\right](y)\right] + \mathcal{O}(\alpha_s^3),\end{aligned} \tag{3.55}$$

as can be seen by explicit insertion of (3.54) and(3.55) in (3.47). Note that (3.54) is the analogue of the multiplicative renormalization transformation used to cancel UV divergences.

If we replace the bare PDFs in (3.46) by the physical PDFs using (3.54) we obtain

$$\mathrm{d}\sigma(P_A,P_B) = \sum_{i,j}\int\frac{d\xi_1}{\xi_1}\frac{d\xi_2}{\xi_2} f_i(\xi_1,\mu_{\rm F}^2) f_j(\xi_2,\mu_{\rm F}^2)\,\mathrm{d}\hat{\sigma}_{ij}(\xi_1 P_A,\xi_2 P_B), \tag{3.56}$$

where the IR-finite mass-factorized partonic cross section is given by

$$\mathrm{d}\hat{\sigma}_{ij}(\xi_1 P_A,\xi_2 P_B) = \int\frac{\mathrm{d}x_1}{x_1}\int\frac{\mathrm{d}x_2}{x_2}\Gamma^{-1}_{ki}(x_1,\mu_{\rm F}^2)\Gamma^{-1}_{lj}(x_2,\mu_{\rm F}^2)\,\mathrm{d}\hat{\sigma}^{(0)}_{kl}(x_1\xi_1 P_A, x_2\xi_2 P_B). \tag{3.57}$$

If we expand the bare partonic cross section, $\mathrm{d}\hat{\sigma}^{(0)}_{ab}$, and the inverse mass factorization kernels, Γ^{-1}_{ki}, in the strong coupling constant and collect terms of the same perturbative order we obtain,

$$\mathrm{d}\hat{\sigma}_{ij,LO}(\xi_1 P_A,\xi_2 P_B) = \mathrm{d}\hat{\sigma}^{(0)}_{ij,LO}(\xi_1 P_A,\xi_2 P_B), \tag{3.58}$$

$$\mathrm{d}\hat{\sigma}_{ij,NLO}(\xi_1 P_A, \xi_2 P_B) = \mathrm{d}\hat{\sigma}^{(0)}_{ij,NLO}(\xi_1 P_A, \xi_2 P_B) + \mathrm{d}\hat{\sigma}^{MF}_{ij,NLO}(\xi_1 P_A, \xi_2 P_B), \quad (3.59)$$

$$\mathrm{d}\hat{\sigma}_{ij,NNLO}(\xi_1 P_A, \xi_2 P_B) = \mathrm{d}\hat{\sigma}^{(0)}_{ij,NNLO}(\xi_1 P_A, \xi_2 P_B) + \mathrm{d}\hat{\sigma}^{MF}_{ij,NNLO}(\xi_1 P_A, \xi_2 P_B). \quad (3.60)$$

The mass factorization contributions to the cross section at the respective perturbative order, also known as collinear counterterms, are given by

$$\mathrm{d}\hat{\sigma}^{MF}_{ij,NLO}(\xi_1 P_A, \xi_2 P_B) = -\int \frac{\mathrm{d}x_1}{x_1}\frac{\mathrm{d}x_2}{x_2}\Gamma^{(1)}_{ij,kl}(x_1, x_2)\mathrm{d}\hat{\sigma}_{kl,LO}(x_1\xi_1 P_A, x_2\xi_2 P_B) \quad (3.61)$$

$$\begin{aligned}\mathrm{d}\hat{\sigma}^{MF}_{ij,NNLO}(\xi_1 P_A, \xi_2 P_B) = &-\int \frac{\mathrm{d}x_1}{x_1}\frac{\mathrm{d}x_2}{x_2}\Gamma^{(2)}_{ij,kl}(x_1, x_2)\mathrm{d}\hat{\sigma}_{kl,LO}(x_1\xi_1 P_A, x_2\xi_2 P_B) \\ &-\int \frac{\mathrm{d}x_1}{x_1}\frac{\mathrm{d}x_2}{x_2}\Gamma^{(1)}_{ij,kl}(x_1, x_2)\mathrm{d}\hat{\sigma}_{kl,NLO}(x_1\xi_1 P_A, x_2\xi_2 P_B), \end{aligned} \quad (3.62)$$

where we have used the notation,

$$\Gamma^{(1)}_{ij,kl}(z_1, z_2) = \delta(1-z_2)\delta_{lj}\Gamma^{(1)}_{ki}(z_1) + \delta(1-z_1)\delta_{ki}\Gamma^{(1)}_{lj}(z_2), \quad (3.63)$$

$$\Gamma^{(2)}_{ij;kl}(z_1, z_2) = \delta(1-z_2)\delta_{lj}\Gamma^{(2)}_{ki}(z_1) + \delta(1-z_1)\delta_{ki}\Gamma^{(2)}_{lj}(z_2) + \Gamma^{(1)}_{ki}(z_1)\Gamma^{(1)}_{lj}(z_2). \quad (3.64)$$

Chapter 4

Antenna subtraction

4.1 The subtraction method

The calculation of higher-order corrections in massless gauge theories generally includes individually IR-divergent contributions. However, for sufficiently inclusive observables the Kinoshita–Lee–Nauenberg (KLN) theorem [97, 98] and factorization theorems [99] guarantee a finite result at a given order of perturbation theory. Applied to a calculation at next-to-leading order in perturbation theory with respect to a given LO process including n partons in the final state these theorems guarantee that all IR divergences cancel between the real contribution, $\mathrm{d}\hat{\sigma}^{\mathrm{R}}_{\mathrm{NLO}}$, including the radiation of an additional massless parton, the virtual contribution, $\mathrm{d}\hat{\sigma}^{\mathrm{V}}_{\mathrm{NLO}}$, including 1-loop corrections, and the mass factorization term, $\mathrm{d}\hat{\sigma}^{\mathrm{MF}}_{\mathrm{NLO}}$, introduced in Section 3.3,

$$\int \mathrm{d}\hat{\sigma}_{\mathrm{NLO}} = \int_{n+1} \mathrm{d}\hat{\sigma}^{\mathrm{R}}_{\mathrm{NLO}} + \int_{n} \left(\mathrm{d}\hat{\sigma}^{\mathrm{V}}_{\mathrm{NLO}} + \mathrm{d}\hat{\sigma}^{\mathrm{MF}}_{\mathrm{NLO}}\right). \tag{4.1}$$

The definition of specific observables is implicitly included in the three contributions on the right-hand side of (4.1) and the observables are parametrized by the introduction of so-called jet functions, $J^{(N)}_n$, where n is the number of resolved particles (jets) in an N-parton final state. To make the dependence on observables more apparent we consider the term corresponding to the real contribution in (4.1) on the level of the corresponding matrix element $\mathcal{M}^{\mathrm{R}}_{n+1}$,

$$\mathrm{d}\hat{\sigma}^{\mathrm{R}}_{\mathrm{NLO}} = \mathrm{d}\Phi_{n+1}(\{p_i\}^{n+1}_{i=1}; p_a, p_b)|\mathcal{M}^{\mathrm{R}}_{n+1}(\{p_i\}^{n+1}_{i=1}; p_a, p_b)|^2 J^{(n+1)}_n(\{p_i\}^{n+1}_{i=1}), \tag{4.2}$$

where $\mathrm{d}\Phi_n$ is the $2 \to n$ particle phase space and we used the shorthand notation $\{p_i\}^{n+1}_{i=1} = \{p_1, \ldots, p_{n+1}\}$ for the set of all momenta. In order to guarantee the cancellation of IR divergences between real and virtual contributions according to the KLN theorem, the jet functions have to be chosen from the class of so-called IR-safe observables which are insensitive to soft emissions and collinear splittings,

$$\begin{aligned} J^{(n+1)}_n(\ldots, p_i, p_j, p_k, \ldots; p_a) &\xrightarrow{p_j \to 0} && J^{(n)}_n(\ldots, p_i, p_k, \ldots; p_a), \\ &\xrightarrow{p_j \cdot p_i \to 0} && J^{(n)}_n(\ldots, p_i + p_j, p_k, \ldots; p_a), \\ &\xrightarrow{p_j \to (1-x)p_a} && J^{(n)}_n(\ldots, p_i, p_k, \ldots; xp_a). \end{aligned} \tag{4.3}$$

The appearance of jet functions in (4.1) make an analytic evaluation of the PS integrals unfeasible and instead numerical integration is more suitable. However, since the real and virtual contributions are not integrated over the same phase space and are both individually IR divergent, a naive integration of the real and virtual part is not possible. One solution to this problem is the introduction of so-called subtraction terms where one adds terms of the form

$$0 = -\int_{n+1} \mathrm{d}\hat{\sigma}^{\mathrm{S}}_{\mathrm{NLO}} + \int_n \int_1 \mathrm{d}\hat{\sigma}^{\mathrm{S}}_{\mathrm{NLO}} \tag{4.4}$$

to the NLO cross section calculation in (4.1), where the first term in (4.4) is combined with the real radiation contribution and the second part with the virtual contribution,

$$\int \mathrm{d}\hat{\sigma}_{\mathrm{NLO}} = \int_{n+1} \left[\mathrm{d}\hat{\sigma}^{\mathrm{R}}_{\mathrm{NLO}} - \mathrm{d}\hat{\sigma}^{\mathrm{S}}_{\mathrm{NLO}}\right] + \int_n \left(\mathrm{d}\hat{\sigma}^{\mathrm{V}}_{\mathrm{NLO}} + \mathrm{d}\hat{\sigma}^{\mathrm{MF}}_{\mathrm{NLO}} + \int_1 \mathrm{d}\hat{\sigma}^{\mathrm{S}}_{\mathrm{NLO}}\right). \tag{4.5}$$

The subtraction term is constructed in such a way that it has the same asymptotic behaviour as the real correction in the limit of soft or collinear partons. The first part in square brackets in (4.5) is therefore IR finite and can be numerically integrated over the $(n+1)$ particle phase space without any further regulator. By factoring the $(n+1)$-particle phase space in (4.4) into an n-particle phase space and the one-particle phase space of the radiated parton, the virtual correction to the cross section and the subtraction term integrated over the one-particle phase space can be combined under the same n-particle phase space integral. Therefore, apart from the correct asymptotic behaviour in unresolved limits the subtraction term must also be simple enough to be integrated analytically over the one-particle phase space of the radiated particle. The analytic integration of the subtraction term over the one-particle phase space leads to the integrated subtraction term which contains explicit IR poles that cancel against the poles in the virtual cross section correction and the mass factorization term by virtue of the KLN theorem and factorization.

Motivated by the factorization properties of amplitudes in single- and double-unresolved limits shown in Section 3.2 the structure of subtraction terms used in the framework of antenna subtraction is given by the product of a singular factor and the squared matrix element of the underlying leading-order process,

$$\begin{aligned}\mathrm{d}\hat{\sigma}^{\mathrm{S}}_{\mathrm{NLO}} = {} & \mathrm{d}\Phi_{n+1}(\{p_i\}_{i=1}^{n+1}; p_a, p_b) X_3^0(p_i, p_j, p_k) \\ & \times |\mathcal{M}_n^{\mathrm{LO}}(p_1, \ldots, p_I, p_K, \ldots, p_{n+1}; p_a, p_b)|^2 J_n^{(n)}(\ldots, p_I, p_K, \ldots),\end{aligned} \tag{4.6}$$

where the function $X_3^0(p_i, p_j, p_k)$ is a so-called antenna function that becomes singular if parton j becomes unresolved with respect to the partons i and k. We will also use the notation $X^m_{i,jk} \equiv X_3^m(p_i, p_j, p_k)$, where m indicates the number of loops and the indices before (after) the comma in the subscript indicate the initial-state (final-state) partons involved in the antenna. The LO matrix element in (4.6) depends on the momenta of the factorized n-particle phase space obtained after factoring out the one-particle phase space of the radiated particle from the full $(n+1)$-particle phase space. The particles that carry the momenta p_i and p_k are referred to as radiator partons of the potentially unresolved parton with momentum p_j. In order to obtain a proper factorization of the $(n+1)$-particle

phase space so-called antenna mappings are used which have to be constructed such that the mapped momenta have the correct behaviour in unresolved limits. Furthermore, the mapped momenta respect momentum conservation and all mass-shell conditions. It is important to note that the jet function in (4.6) can only depend on the mapped momenta and not on the momentum of the radiated particle in order to guarantee the analytic integrability of the subtraction term over the one-particle phase space associated to the radiated particle.

The NNLO correction to the cross section is obtained by including two additional potentially unresolved radiative particles with respect to the LO process. The nature of both additional particles can be of real or virtual kind leading to three types of NNLO corrections. Double real corrections, $\mathrm{d}\hat{\sigma}^{\mathrm{RR}}_{\mathrm{NNLO}}$, involve two additional real particles with an $(n+2)$-particle final state and zero loops, real–virtual corrections, $\mathrm{d}\hat{\sigma}^{\mathrm{RV}}_{\mathrm{NNLO}}$, are characterized by a final state with $(n+1)$ particles including an one-loop correction, and double virtual corrections include two-loop corrections with no real radiation. The full NNLO correction to the cross section reads

$$\begin{aligned}\int \mathrm{d}\hat{\sigma}_{\mathrm{NNLO}} = &\int_{n+2} \mathrm{d}\hat{\sigma}^{\mathrm{RR}}_{\mathrm{NNLO}} + \int_{n+1} \left(\mathrm{d}\hat{\sigma}^{\mathrm{RV}}_{\mathrm{NNLO}} + \mathrm{d}\hat{\sigma}^{\mathrm{MF,1}}_{\mathrm{NNLO}}\right) \\ &+ \int_{n} \left(\mathrm{d}\hat{\sigma}^{\mathrm{VV}}_{\mathrm{NNLO}} + \mathrm{d}\hat{\sigma}^{\mathrm{MF,2}}_{\mathrm{NNLO}}\right),\end{aligned} \tag{4.7}$$

where the mass factorization terms are given in (4.110) and (4.111). Similar to the case at NLO the individual contributions to the NNLO correction are IR divergent and a naive numerical integration fails. Also at NNLO it is possible to include subtraction terms which then have to be added back in an integrated form to a contribution with a different particle multiplicity of final-state partons. In the antenna method a double real, $\mathrm{d}\hat{\sigma}^{\mathrm{S}}_{\mathrm{NNLO}}$, and a real–virtual, $\mathrm{d}\hat{\sigma}^{\mathrm{VS}}_{\mathrm{NNLO}}$, subtraction term are introduced to cancel the implicit IR divergences in the double real and real–virtual contributions, respectively. The integrated double real subtraction term is split into two parts contributing to both the $(n+1)$- and the n-particle final-state contribution of the NNLO correction,

$$\int_{n+2} \mathrm{d}\hat{\sigma}^{\mathrm{S}}_{\mathrm{NNLO}} = \int_{n+1} \int_{1} \mathrm{d}\hat{\sigma}^{\mathrm{S,1}}_{\mathrm{NNLO}} + \int_{n} \int_{2} \mathrm{d}\hat{\sigma}^{\mathrm{S,2}}_{\mathrm{NNLO}}, \tag{4.8}$$

where the first part, $\mathrm{d}\hat{\sigma}^{\mathrm{S,1}}_{\mathrm{NNLO}}$, integrated over the one-particle phase space, associated to one of the potentially unresolved partons, is used to cancel the explicit poles in the real–virtual contribution. The second part, $\mathrm{d}\hat{\sigma}^{\mathrm{S,2}}_{\mathrm{NNLO}}$, integrated over the two-particle phase space of the radiated particles combined with the integrated real–virtual subtraction term, $\mathrm{d}\hat{\sigma}^{\mathrm{VS}}_{\mathrm{NNLO}}$, is used to cancel the explicit poles of the double-virtual correction to the cross section. The subtraction terms are constructed such that the contributions contained in square brackets are individually free from explicit and implicit IR divergences,

$$\begin{aligned}\int \mathrm{d}\hat{\sigma}_{\mathrm{NNLO}} = &\int_{n+2} \left[\mathrm{d}\hat{\sigma}^{\mathrm{RR}}_{\mathrm{NNLO}} - \mathrm{d}\hat{\sigma}^{\mathrm{S}}_{\mathrm{NNLO}}\right] \\ &+ \int_{n+1} \left[\mathrm{d}\hat{\sigma}^{\mathrm{RV}}_{\mathrm{NNLO}} - \mathrm{d}\hat{\sigma}^{\mathrm{T}}_{\mathrm{NNLO}}\right] \\ &+ \int_{n} \left[\mathrm{d}\hat{\sigma}^{\mathrm{VV}}_{\mathrm{NNLO}} - \mathrm{d}\hat{\sigma}^{\mathrm{U}}_{\mathrm{NNLO}}\right],\end{aligned} \tag{4.9}$$

where

$$\mathrm{d}\hat{\sigma}^{\mathrm{T}}_{\mathrm{NNLO}} = \mathrm{d}\hat{\sigma}^{\mathrm{VS}}_{\mathrm{NNLO}} - \int_1 \mathrm{d}\hat{\sigma}^{\mathrm{S},1}_{\mathrm{NNLO}} - \mathrm{d}\hat{\sigma}^{\mathrm{MF},1}_{\mathrm{NNLO}}, \tag{4.10}$$

$$\mathrm{d}\hat{\sigma}^{\mathrm{U}}_{\mathrm{NNLO}} = -\int_1 \mathrm{d}\hat{\sigma}^{\mathrm{VS}}_{\mathrm{NNLO}} - \int_2 \mathrm{d}\hat{\sigma}^{\mathrm{S},2}_{\mathrm{NNLO}} - \mathrm{d}\hat{\sigma}^{\mathrm{MF},2}_{\mathrm{NNLO}}. \tag{4.11}$$

We can summarize the introduced subtraction terms and their integrated counterparts in the following way,

$$\begin{aligned} 0 = &-\int_{n+2} \mathrm{d}\hat{\sigma}^{\mathrm{S}}_{\mathrm{NNLO}} \\ &+ \int_{n+1} \left(-\mathrm{d}\hat{\sigma}^{\mathrm{VS}}_{\mathrm{NNLO}} + \int_1 \mathrm{d}\hat{\sigma}^{\mathrm{S},1}_{\mathrm{NNLO}} \right) \\ &+ \int_n \left(\int_1 \mathrm{d}\hat{\sigma}^{\mathrm{VS}}_{\mathrm{NNLO}} + \int_2 \mathrm{d}\hat{\sigma}^{\mathrm{S},2}_{\mathrm{NNLO}} \right). \end{aligned} \tag{4.12}$$

4.2 Phase-space factorization and mappings

In the previous section we saw that it is necessary to factorize one- and two-particle phase spaces from an original $(n+2)$-particle phase space in order to construct the integrated subtraction terms used in antenna subtraction. In this section we discuss mappings that allow us to write the phase space as a direct product of a phase space of lower dimension than the original phase space constructed from mapped momenta and an antenna phase space that only depends on momenta independent of the mapped momenta and is used in the antenna function.

There are three different scenarios that we have to consider and each of them requires different mappings. They are determined by the locations of the two radiator partons emitting the potentially unresolved parton into the final state: The radiating partons are contained in the final state (final–final case), one radiating parton is in the final and the other in the initial state (initial–final case), and finally the case where both radiating partons are initial-state partons (initial–initial case). The mappings used in the three different scenarios all fulfill general constraints in order to be applicable in the context of antenna subtraction. Momentum conservation and on-shellness of mapped momenta are needed in order to be able to combine the integrated subtraction term with virtual or real–virtual contributions. In order to properly subtract implicit IR singularities from real corrections it is necessary that the mapped momenta reduce to the original momenta in singular limits and do not introduce any spurious singularities.

Final–final case

To factorize the $(n+1)$-particle phase space we use a mapping [100] where the momenta of all particles remain unchanged except for the three momenta p_i, p_j, and p_k involved in the antenna function $X_3(i,j,k)$. In order to obtain the reduced n-particle phase space, the antenna momenta p_i, p_j, and p_k are mapped to two composite momenta $\tilde{p}_I = \widetilde{(ij)}$ and

$\tilde{p}_K = \widetilde{(jk)}$. The two composite momenta

$$\tilde{p}_I = xp_i + rp_j + zp_k, \quad \tilde{p}_K = (1-x)p_i + (1-r)p_j + (1-z)p_k \tag{4.13}$$

are constructed in terms of the factors x, z, and r which are defined by

$$\begin{aligned} x =& \frac{1}{2(s_{ij}+s_{ik})}\Big[(1+\rho)\, s_{ijk} - 2\, r\, s_{jk}\Big], \\ z =& \frac{1}{2(s_{jk}+s_{ik})}\Big[(1-\rho)\, s_{ijk} - 2\, r\, s_{ij}\Big], \\ \rho^2 =& 1 + \frac{4\, r(1-r)\, s_{ij}s_{jk}}{s_{ijk}s_{ik}}, \\ r =& \frac{s_{jk}}{s_{ij}+s_{jk}}. \end{aligned} \tag{4.14}$$

The parametrization of the $(n+1)$-particle phase space in terms of the new momenta allows for the factorization of the phase space into a mapped reduced n-particle phase space and an antenna phase space,

$$\begin{aligned} &\mathrm{d}\Phi_{n+1}(p_1, \cdots, p_i, p_j, p_k, \cdots, p_{n+1}; p_a, p_b) \\ &= \mathrm{d}\Phi_n(p_1, \cdots, p_I, p_K, \cdots, p_{n+1}; p_a, p_b) \cdot \mathrm{d}\Phi_{X_{ijk}}(p_i, p_j, p_k; p_I + p_K). \end{aligned} \tag{4.15}$$

Using the last equation in the case of $n = 2$ we see that the three-parton antenna phase space is proportional to the three-particle phase space,

$$\mathrm{d}\Phi_3 = P_2\, \mathrm{d}\Phi_{X_{ijk}}, \tag{4.16}$$

where we have used that the two-particle phase space is a constant for massless final-state particles [84],

$$P_2 = \int \mathrm{d}\Phi_2 = 2^{-3+2\epsilon}\pi^{-1+\epsilon}\frac{\Gamma(1-\epsilon)}{\Gamma(2-2\epsilon)}(q^2)^{-\epsilon}. \tag{4.17}$$

From the explicit form of the final–final mapping (4.13) and (4.14) it is obvious that the mapping respects momentum conservation and it can be shown that the constructed momenta have the desired behaviour in singular limits [82]:

$$\begin{aligned} &\tilde{p}_I \to p_i, && \tilde{p}_K \to p_k, && \text{for } j \to 0, \\ &\tilde{p}_I \to p_i + p_j, && \tilde{p}_K \to p_k, && \text{for } j||i, \\ &\tilde{p}_I \to p_i, && \tilde{p}_K \to p_j + p_k, && \text{for } j||k. \end{aligned} \tag{4.18}$$

For two potentially unresolved partons with momenta p_j and p_k, and two radiator partons with momenta p_i and p_l, the NLO final–final mapping can be generalized to an NNLO mapping [101], where the composite momenta,

$$\tilde{p}_I \equiv \widetilde{(ijk)}\ ,\ \tilde{p}_J \equiv \widetilde{(jkl)}\ , \tag{4.19}$$

are given by

$$\begin{aligned}\tilde{p}_I &= x\,p_i + r_1\,p_j + r_2\,p_k + z\,p_l,\\ \tilde{p}_J &= (1-x)\,p_i + (1-r_1)\,p_j + (1-r_2)\,p_k + (1-z)\,p_l\ ,\end{aligned} \tag{4.20}$$

with

$$\begin{aligned}
r_1 &= \frac{s_{jk}+s_{jl}}{s_{ij}+s_{jk}+s_{jl}},\\
r_2 &= \frac{s_{kl}}{s_{ik}+s_{jk}+s_{kl}},\\
x &= \frac{1}{2(s_{ij}+s_{ik}+s_{il})}\Big[(1+\rho)\,s_{ijkl} - r_1\,(s_{jk}+2\,s_{jl}) - r_2\,(s_{jk}+2\,s_{kl})\\
&\qquad + (r_1-r_2)\frac{s_{ij}s_{kl}-s_{ik}s_{jl}}{s_{il}}\Big],\\
z &= \frac{1}{2(s_{il}+s_{jl}+s_{kl})}\Big[(1-\rho)\,s_{ijkl} - r_1\,(s_{jk}+2\,s_{ij}) - r_2\,(s_{jk}+2\,s_{ik})\\
&\qquad - (r_1-r_2)\frac{s_{ij}s_{kl}-s_{ik}s_{jl}}{s_{il}}\Big],\\
\rho^2 &= 1 + \frac{(r_1-r_2)^2}{s_{il}^2\,s_{ijkl}^2}\,\lambda(s_{ij}\,s_{kl}, s_{il}\,s_{jk}, s_{ik}\,s_{jl})\\
&\quad + \frac{1}{s_{il}\,s_{ijkl}}\Big\{2\,\big(r_1\,(1-r_2) + r_2(1-r_1)\big)\big(s_{ij}s_{kl} + s_{ik}s_{jl} - s_{jk}s_{il}\big)\\
&\qquad + 4\,r_1\,(1-r_1)\,s_{ij}s_{jl} + 4\,r_2\,(1-r_2)\,s_{ik}s_{kl}\Big\},\\
\lambda(u,v,w) &= u^2+v^2+w^2-2(uv+uw+vw)\ .
\end{aligned} \tag{4.21}$$

In terms of the mapped momenta the $(n+2)$-particle phase space can be again factorized into a reduced n-particle phase space including the mapped composite momenta and an antenna phase space that only depends on the antenna momenta p_i, p_j, p_k, and p_l, and does not depend on the mapped momenta,

$$\begin{aligned}
&\mathrm{d}\Phi_{n+2}(p_1,\ldots,p_i,p_j,p_k,p_l,\ldots,p_{n+2};p_a,p_b)\\
&= \mathrm{d}\Phi_n(p_1,\ldots,p_I,p_J,\cdots,p_{n+2};p_a,p_b)\cdot \mathrm{d}\Phi_{X_{ijkl}}(p_i,p_j,p_k,p_l;p_I+p_J).
\end{aligned} \tag{4.22}$$

Again, for $n=2$ we see that the four-parton antenna phase space is proportional to the four-particle phase space,

$$\mathrm{d}\Phi_4 = P_2\ \mathrm{d}\Phi_{X_{ijkl}}, \tag{4.23}$$

with P_2 given in (4.17). In order to construct subtraction terms it is important to note that the NNLO finial–final $4\to 2$ map reduces to an NLO $3\to 2$ map in all single unresolved limits [102]. This means that single unresolved limits of the four-parton antenna can be subtracted by terms that are build from products of two three-parton antennae. This behaviour is essential in order to avoid over-subtraction of singularities when constructing subtraction terms. We will discuss this in more detail for initial–final and initial–initial mappings as they are the phase-space mappings that we will use to construct subtraction terms relevant for this work.

Initial–final case

If one of the radiator partons is in the initial state with momentum p_a and the other is a final state parton with momentum p_k the application of a momentum mapping similar to the one in the final–final case leads to a non-factorizable phase space as it will in general bend the momentum of the initial-state radiator away from the beam axis [103]. If the mapping is chosen such that the momentum of the radiator in the initial state is just a rescaling, the $(n+1)$-parton phase space indeed factorizes [103] into an n-parton phase space convoluted with a two parton phase space. In detail, the momenta p_a, p_i, and p_j are mapped to $\bar{a} = \bar{p}_a$ and $\widetilde{(ij)} = p_I$,

$$\bar{p}_a = \hat{x} p_a, \qquad p_I = p_i + p_j - (1-\hat{x}) p_a. \tag{4.24}$$

Momentum conservation of the mapped momenta immediately follows from the definition, and the constraint of on-shellness of the mapped momenta fixes the free parameter $\hat{x}$ to

$$\hat{x} = \frac{s_{aj} + s_{ai} - s_{ij}}{s_{aj} + s_{ai}}. \tag{4.25}$$

In terms of the new momenta one obtains the $(n+1)$-particle phase space as a convolution of a reduced n-particle phase space and a two-particle phase space,

$$\begin{aligned} &\mathrm{d}\Phi_{n+1}(p_1, \cdots, p_i, p_j, \cdots, p_{n+1}; p_a, p_b) \\ &= \frac{Q^2}{2\pi} \frac{\mathrm{d}x}{x} \delta(x - \hat{x}) \mathrm{d}\Phi_n(p_1, \cdots, p_I, \cdots, p_{n+1}; x p_a, p_b) \cdot \mathrm{d}\Phi_2(p_i, p_j; p_a, q(x)), \end{aligned} \tag{4.26}$$

where

$$q(x) = p_i + p_j - p_a = p_I - \bar{p}_a \tag{4.27}$$

dictates the scale $Q^2 = -q^2$, p_a is the momentum assigned to the initial-state parton involved in the initial–final antenna function and the delta distribution including $\hat{x}$ ensures the on-shellness of the mapped momentum p_I.

It can be shown [103] that the mapping given above has the required behaviour in single unresolved limits of parton j,

$$\begin{aligned} &\bar{p}_a \to p_a, && p_I \to p_i; && \text{for } j \to 0, \\ &\bar{p}_a \to p_a, && p_I \to p_i + p_j, && \text{for } j || i, \\ &\bar{p}_a \to p_a - p_j, && p_I \to p_i, && \text{for } j || a. \end{aligned} \tag{4.28}$$

The generalization of the mapping defined in (4.24) and (4.25) to the case with two unresolved partons j, k, an initial-state radiator a, and a final-state radiator parton i is given by

$$\begin{aligned} \hat{x} &= \frac{s_{aj} + s_{ak} + s_{ai} - s_{jk} - s_{ji} - s_{ki}}{s_{aj} + s_{ak} + s_{ai}}, \\ p_I &= p_i + p_j + p_k - (1-\hat{x}) p_a. \end{aligned} \tag{4.29}$$

Reparametrizing the phase space in this way one obtains again a factorized phase space, but this time with an additional convolution,

$$\begin{aligned}&\mathrm{d}\Phi_{n+2}(p_1,\cdots,p_i,p_j,p_k,\cdots,p_{n+2};p_a,p_b)\\&=\frac{Q^2}{2\pi}\frac{\mathrm{d}x}{x}\delta(x-\hat{x})\mathrm{d}\Phi_n(p_1,\cdots,p_I,\cdots,p_{n+2};xp_a,p_b)\cdot\mathrm{d}\Phi_3(p_i,p_j,p_k;p_a,q(x)).\end{aligned}\tag{4.30}$$

The NNLO initial–final phase space mapping reduces to NLO phase-space mappings in all single unresolved limits [103]. As in the finial–final case, this allows for the subtraction of singularities of the four-parton antenna $X_{a,jki}$ in single unresolved limits by products of two three-parton antenna functions [102]. If parton k becomes unresolved the potential singularities of $X_{a,jki}$ occur when k is soft or collinear to one of the other final-state partons i,j. There is no singularity if k becomes collinear to the initial-state radiator a due to the colour ordering used in the construction of the antenna. To subtract the singularities of the four-parton antenna in the kinematic regions where only k is unresolved we therefore need the product of a finial–final and a initial–final antenna $X_{jki}\cdot X_{a,JI}$. The The NNLO initial–final phase space mapping also reflects this behaviour and (4.29) reduces to

$$\begin{aligned}
&p_k\to 0: && \hat{x}\to\frac{s_{aj}+s_{ai}-s_{ij}}{s_{aj}+s_{ai}}, && p_I\to p_i+p_j-(1-\hat{x})p_a,\\
&p_k||p_j,p_j+p_k=p_K: && \hat{x}\to\frac{s_{aK}+s_{ai}-s_{iK}}{s_{aK}+s_{ai}}, && p_I\to p_i+p_K-(1-\hat{x})p_a,\\
&p_k||p_i,p_i+p_k=p_K: && \hat{x}\to\frac{s_{aK}+s_{aj}-s_{jK}}{s_{aK}+s_{aj}}, && p_I\to p_j+p_K-(1-\hat{x})p_a,
\end{aligned}\tag{4.31}$$

i.e. the NNLO initial–final mapping reduces to an NLO initial–final mapping from (4.24) and $\hat{x}$ as in (4.25), where the momenta p_i,p_j, and p_K that appear in the NLO initial–final mapping are the result of the NLO final–final mapping (4.14) in the limit where k is unresolved. Therefore, the NNLO initial–final mapping reduces to the product of an NLO final–final and an NLO initial–final phase space mapping which is in line with the behaviour we found for the corresponding four-parton initial–final antenna.

On the other hand, if parton j becomes unresolved, $X_{a,jki}$ becomes singular if j is soft or collinear to either the initial-state radiator a or the final-state parton k. Again, there is no singularity if j becomes collinear to i. The appropriate product of three-parton antennae to subtract single unresolved limits in this case is given by $X_{a,jk}\cdot X_{\bar{a},Ki}$. One can see that the relevant phase-space mapping for this limit of the NNLO initial–final phase-space mapping is given by the product of two NLO initial–final mappings similar to the case with a product of an NLO finial–final and an NLO initial–final mapping discussed above.

Initial–initial case

When both radiator partons a and b are in the initial state we use a phase-space mapping where the corresponding momenta are rescaled according to

$$\bar{p}_a=\hat{x}_a p_a,\qquad \bar{p}_b=\hat{x}_b p_b,\tag{4.32}$$

so that the sum of the rescaled radiator momenta,

$$\tilde{q} = \bar{p}_a + \bar{p}_b, \tag{4.33}$$

is parallel to the beam axis, which avoids the introduction of a transverse component that would spoil any phase-space factorization [103]. In order to maintain momentum conservation one has to apply a mapping λ to all other momenta, since the sum of the remaining final-state momenta $q = p_a + p_b - p_i$ is in general not parallel to the beam axis given by $p_a - p_b$. As the remaining mapped momenta are required to stay on their mass shell, the mapping λ must be a Lorentz transformation. The required limiting behaviour of the phase-space mapping in unresolved limits of the radiated parton i has to be

$$\begin{aligned}
&\bar{p}_a \to p_a, && \bar{p}_b \to p_b, && \tilde{p}_j \to p_j && \text{for } i \to 0,\\
&\bar{p}_a \to p_a - p_i, && \bar{p}_b \to p_b, && \tilde{p}_j \to p_j && \text{for } i||a,\\
&\bar{p}_a \to p_a, && \bar{p}_b \to p_b - p_i, && \tilde{p}_j \to p_j && \text{for } i||b,
\end{aligned} \tag{4.34}$$

which means that when q is already parallel to the the beam axis (i.e. p_i is unresolved with respect to parton a or b) the Lorentz transformation λ has to reduce to $\mathbb{1}$, because in this case $\tilde{q} = q$ due to (4.34). A possible boost that fulfills this requirement and maps q onto $\tilde{q}$ is given by

$$\lambda^{\mu}{}_{\nu}(q, \tilde{q}) = g^{\mu}{}_{\nu} - \frac{2(q+\tilde{q})^{\mu}(q+\tilde{q})_{\nu}}{(q+\tilde{q})^2} + \frac{2\tilde{q}^{\mu} q_{\nu}}{q^2}. \tag{4.35}$$

It is now possible to obtain the two factors x_a and x_b from the on shell condition $q^2 = \tilde{q}^2$ and properties of the chosen boost [103] leading to

$$\begin{aligned}
\hat{x}_a &= \left(\frac{s_{ab} - s_{bi}}{s_{ab}} \, \frac{s_{ab} - s_{ai} - s_{bi}}{s_{ab} - s_{ai}} \right)^{\frac{1}{2}},\\
\hat{x}_b &= \left(\frac{s_{ab} - s_{ai}}{s_{ab}} \, \frac{s_{ab} - s_{ai} - s_{bi}}{s_{ab} - s_{bi}} \right)^{\frac{1}{2}}.
\end{aligned} \tag{4.36}$$

The reparametrization of momenta using the mapping described above leads to a phase space in a factorized form including two convolutions,

$$\mathrm{d}\Phi_{n+1}(\{p_k\}_{k=1}^{n+1}; p_a, p_b) = \mathrm{d}\Phi_n(\{\tilde{p}_k\}_{k=1}^{n+1} \setminus \{\tilde{p}_i\}; \bar{p}_a, \bar{p}_b)[\mathrm{d}p_i] \, \mathrm{d}x_a \mathrm{d}x_b \, \delta(x_a - \hat{x}_a)\delta(x_b - \hat{x}_b). \tag{4.37}$$

In order to generalize the mapping to NNLO one simply needs to adjust the vector q to the case of two potentially unresolved partons i and j. Therefore, it now includes p_i and p_j, $q = p_a + p_b - p_i - p_j$, instead of just p_i. The rescaling factors of the initial-state momenta are in this case given by

$$\hat{x}_a = \left(\frac{s_{ab} - s_{ib} - s_{jb}}{s_{ab}} \, \frac{s_{ab} - s_{ai} - s_{aj} - s_{ib} - s_{jb} + s_{ij}}{s_{ab} - s_{ia} - s_{ja}} \right)^{\frac{1}{2}}, \tag{4.38}$$

$$\hat{x}_b = \left(\frac{s_{ab} - s_{ia} - s_{ja}}{s_{ab}} \, \frac{s_{ab} - s_{ai} - s_{aj} - s_{ib} - s_{jb} + s_{ij}}{s_{ab} - s_{ib} - s_{jb}} \right)^{\frac{1}{2}}, \tag{4.39}$$

and the boost applied to the final-state momenta is the same as the one used for the NLO mapping. The phase-space factorization generalizes to,

$$\mathrm{d}\Phi_{n+2}(\{p_k\}_{k=1}^{n+2}; p_a, p_b) = \mathrm{d}\Phi_n(\{\tilde{p}_k\}_{k=1}^{n+2} \setminus \{\tilde{p}_i, \tilde{p}_j\}; \bar{p}_a, \bar{p}_b)[\mathrm{d}p_i][\mathrm{d}p_j]\,\mathrm{d}x_a \mathrm{d}x_b\,\delta(x_a - \hat{x}_a)\delta(x_b - \hat{x}_b). \tag{4.40}$$

Also in this case the NNLO initial–initial map reduces to a product of NLO mappings in single unresolved limits [103], so that single unresolved limits of four-parton antennae $X_{ab,ij}$ can be subtracted by products of three-parton antennae. If parton i becomes unresolved with respect to a initial-state radiator a and a final-state radiator j the NNLO initial–initial map reduces to an NLO initial–initial map as a function of momenta that are the result of a NLO initial–final map in the limit where i is unresolved. This means that in order to subtract this single unresolved limit from the four-parton antenna the proper product of three-parton antennae is given by the product of an initial–final and an initial–initial antenna, $X_{a,ij}X_{\bar{a}b,J}$. In the case where i becomes unresolved to two initial-state radiator partons a and b the corresponding subtraction term in order to subtract this single unresolved limit from the four-parton antenna $X_{ab,ij}$ is given by the product of two initial–initial three-parton antennae $X_{ab,i}X_{\bar{a}\bar{b},\tilde{j}}$.

4.3 Construction of antenna functions

The antenna functions introduced in (4.6) are the key ingredients in the construction of antenna subtraction terms. They are constructed such that they mimic the asymptotic behaviour of the real matrix element in all IR-singular limits and are simple enough to be integrated analytically over all phase-space regions that contain singular configurations of the real matrix element. At NLO, three-parton colour-ordered tree-level matrix elements naturally have the correct singular behaviour and are also integrable over the relevant phase-space regions. The idea of antenna subtraction is to use these physical matrix elements for the construction of subtraction functions. Hence, the three-parton tree-level antenna functions are defined as the ratio of the colour-ordered three-parton tree-level squared matrix element and the squared matrix element of the underlying two-parton born process,

$$X_3^0(i,j,k) = S_{ijk,IK}\frac{|\mathcal{M}_{ijk}^0|^2}{|\mathcal{M}_{IK}^0|^2}, \tag{4.41}$$

where the symmetry factor S takes identical particles symmetries and degeneracies in the definition of the antenna into account. At NNLO the construction of antenna functions is based on renormalized one-loop three-parton and tree-level four-parton matrix elements, where the tree-level four-parton antenna is defined as

$$X_4^0(i,j,k,l) = S_{ijkl,IK}\frac{|\mathcal{M}_{ijkl}^0|^2}{|\mathcal{M}_{IL}^0|^2}, \tag{4.42}$$

and the one-loop three-parton antenna is given by

$$X_3^1(i,j,k) = S_{ijk,IK}\frac{|\mathcal{M}_{ijk}^1|^2}{|\mathcal{M}_{IK}^0|^2} - X_3^0(i,j,k)\frac{|\mathcal{M}_{IK}^1|^2}{|\mathcal{M}_{IK}^0|^2}. \tag{4.43}$$

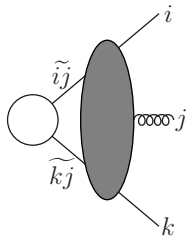

(a) $A_3^0, A_3^1, \tilde{A}_3^1, \hat{A}_3^1$

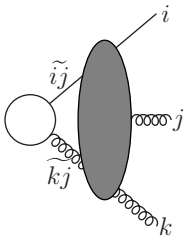

(b) $D_3^0, D_3^1, \hat{D}_3^1$

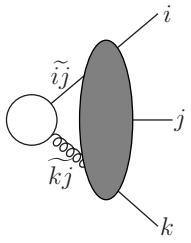

(c) $E_3^0, E_3^1, \tilde{E}_3^1, \hat{E}_3^1$

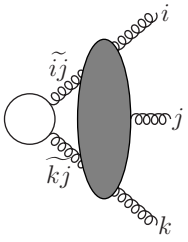

(d) $F_3^0, F_3^1, \hat{F}_3^1$

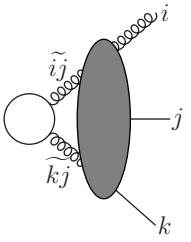

(e) $G_3^0, G_3^1, \tilde{G}_3^1, \hat{G}_3^1$

Figure 4.1: Tree-level and one-loop three-parton antenna functions. White blobs represent tree structres with one incoming particle being either a photon, a neutralino, or a Higgs boson depending on the respective antenna function. Grey blobs represent tree structures in QCD for tree-level antennae X_3^0 and one-loop QCD corrections for one-loop antenna functions X_3^1. The partons i and k are the hard radiators, and $\widetilde{ij}$ and $\widetilde{kj}$ represent the partons the antenna collapses to in unresolved limits of parton j.

As we have seen in Section 3.2, one-loop amplitudes behave in implicit singular limits as (tree×loop)+(loop×tree), where the first factor in the two products describes the perturbative order of the antenna function (tree or loop level), and the second factor describes the order of the multiplied squared matrix element. The one-loop three-parton antenna X_3^1 is used to construct the (loop×tree) part and, therefore, the second part on the right-hand side of (4.43) is used to remove the (tree×loop) part from the definition of the one-loop three-parton antenna.

Antenna functions can be determined by their external partons and by the radiator partons, which are the partons with corresponding hard momenta in IR-singular limits of the antenna. In Table 4.1 we show the different antennae, where we classify them according to their radiator partons leading to three different groups: the quark–antiquark antenna functions ($X = A, B, C$), the quark–gluon antenna functions ($X = D, E$), and the gluon–gluon antenna functions ($X = F, G, H$). The physical matrix elements used to calculate the quark–antiquark antenna functions are obtained from $\gamma^* \to q\bar{q} +$ (partons) [104], quark–gluon antennae from neutralino decays $\tilde{\chi} \to \tilde{g} +$ (partons) [105] and gluon–gluon antennae from $H \to$ (partons) [106]. All antenna functions are listed in Table 4.1 and depicted in Figs. 4.1 and 4.2.

Radiator	External partons	Antennae
$q\bar{q}$	$qg\bar{q}$	$A_3^0(q,g,\bar{q}), A_3^1(q,g,\bar{q}), \tilde{A}_3^1(q,g,\bar{q}), \hat{A}_3^1(q,g,\bar{q})$
	$qgg\bar{q}$	$A_4^0(q,g,g,\bar{q}), \tilde{A}_4^0(q,g,g,\bar{q})$
	$qq'\bar{q}'\bar{q}$	$B_4^0(q,q',\bar{q}',\bar{q})$
	$qq\bar{q}\bar{q}$	$C_4^0(q,q,\bar{q},\bar{q})$
qg	qgg	$D_3^0(q,g,g), D_3^1(q,g,g), \hat{D}_3^1(q,g,g)$
	$qggg$	$D_4^0(q,g,g,g)$
	$qq'\bar{q}'$	$E_3^0(q,q',\bar{q}'), E_3^1(q,q',\bar{q}'), \tilde{E}_3^1(q,q',\bar{q}'), \hat{E}_3^1(q,q',\bar{q}')$
	$qq'\bar{q}'g$	$E_4^0(q,q',\bar{q}',g), \tilde{E}_4^0(q,q',\bar{q}',g)$
gg	ggg	$F_3^0(g,g,g), F_3^1(g,g,g), \hat{F}_3^1(g,g,g)$
	$gggg$	$F_4^0(g,g,g,g)$
	$gq\bar{q}$	$G_3^0(g,q,\bar{q}), G_3^1(g,q,\bar{q}), \tilde{G}_3^1(g,q,\bar{q}), \hat{G}_3^1(g,q,\bar{q})$
	$gq\bar{q}g$	$G_4^0(g,q,\bar{q},g), \tilde{G}_4^0(g,q,\bar{q},g)$
	$q\bar{q}q'\bar{q}'$	$H_4^0(q,\bar{q},q',\bar{q}')$

Table 4.1: Antenna functions classified according to their radiator partons. Subleading colour contributions are indicated by a tilde and antennae that include corrections that depend on the number of fermion flavours are indicated with a hat.

Integration of antennae

The physical processes used to construct antenna functions are chosen such that the antennae defined in the previous section can be integrated over the its singular phase-space regions analytically. The use of unitarity relations allows the phase-space integrals to be rewritten in terms of loop integrals with cut propagators [94, 107–109] which were then reduced to a set of master integrals using integration-by-parts (IBP) relations obtained with Laporta's algorithm. The obtained master integrals were then calculated via the differential-equations technique leading to the analytical results for the integrated antennae presented in [107–110]. Using this procedure, the integrated final–final three-parton tree-level and one-loop antenna functions are obtained by integrating the corresponding final–final antennae over the reduced three-particle antenna phase space introduced in (4.16),

$$\mathcal{X}_{ijk}^n(s_{ijk}) = \frac{1}{C(\epsilon)} \int \mathrm{d}\Phi_{X_{ijk}} X_{ijk}^n(i,j,k), \quad n = 0, 1, \tag{4.44}$$

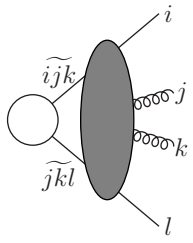

(a) $A_4^0, \tilde{A}_4^0$

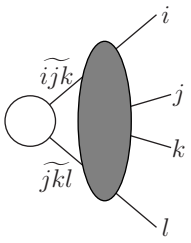

(b) B_4^0, C_4^0

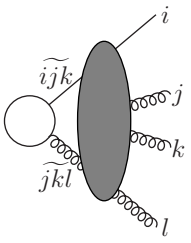

(c) D_4^0

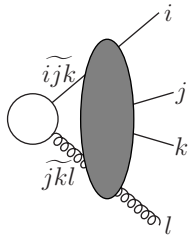

(d) $E_4^0, \tilde{E}_4^0$

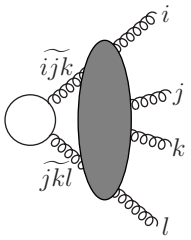

(e) F_4^0

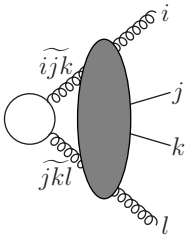

(f) $G_4^0, \tilde{G}_4^0$

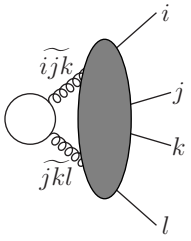

(g) H_4^0

Figure 4.2: Tree-level four-parton antenna functions. As in Fig. 4.1, white blobs represent tree structures with one incoming particle being either a photon, a neutralino, or a Higgs boson depending on the respective antenna function, and grey blobs represent tree structures in QCD. The partons i and l are the hard radiators, and $\widetilde{ijk}$ and $\widetilde{jkl}$ represent the partons the antenna collapses to in unresolved limits of partons j and k.

where the factor

$$C(\epsilon) = \frac{(4\pi)^\epsilon e^{-\gamma\epsilon}}{8\pi^2} \tag{4.45}$$

is included to account for the normalization of the renormalized strong coupling constant [84]. Similarly, the integrated final–final four-parton antenna functions are obtained by integration over the four-parton antenna phase space (4.23),

$$\mathcal{X}_{ijkl}^0(s_{ijkl}) = \frac{1}{C(\epsilon)^2} \int \mathrm{d}\Phi_{X_{ijkl}} X_{ijkl}^0(i,j,k,l). \tag{4.46}$$

Considering the different phase-space factorization in the initial–final case (4.26) compared to the final–final case the three-parton initial–final integrated antenna functions are defined as

$$\mathcal{X}_{a,ij}^n(s_{aij}; x_a) = \frac{1}{C(\epsilon)} \int \mathrm{d}\Phi_2 \frac{Q^2}{2\pi} \delta(x_a - \hat{x}_a) X_{a,ij}^n(a,i,j), \quad n = 0, 1. \tag{4.47}$$

The four-parton integrated initial–final antennae are obtained via

$$\mathcal{X}^0_{a,ijk}(s_{aijk};x_a) = \frac{1}{C(\epsilon)^2}\int \mathrm{d}\Phi_3 \frac{Q^2}{2\pi}\delta(x_a-\hat{x}_a)X^0_{a,ijk}(a,i,j,k), \tag{4.48}$$

in line with the phase-space factorization in (4.30). The initial–initial integrated antenna functions follow from the integration over the reduced phase space given in (4.37),

$$\mathcal{X}^n_{ab,i}(s_{abi};x_a,x_b) = \frac{1}{C(\epsilon)}\int [\mathrm{d}k_i]x_a x_b \delta(x_a-\hat{x}_a)\delta(x_b-\hat{x}_b)X^n_{ab,i}(a,b,i), \quad n=0,1, \tag{4.49}$$

and at NNLO from the integration over the reduced phase space in (4.40),

$$\mathcal{X}^0_{ab,ij}(s_{abij};x_a,x_b) = \frac{1}{C(\epsilon)^2}\int [\mathrm{d}k_i][\mathrm{d}k_j]x_a x_b \delta(x_a-\hat{x}_a)\delta(x_b-\hat{x}_b)X^0_{ab,ij}(a,b,i,j). \tag{4.50}$$

Angular terms

In Section 4.2 we saw that NNLO phase-space mappings are constructed such that they reduce to NLO mappings in single unresolved limits. This allows for the subtraction of singularities in single unresolved limits of the four-parton antenna functions, e.g. $X_{ab,ij}$, by products of two three-parton antenna functions, e.g. $X_{a,ij}X_{\bar{a}b,J}$. This behaviour of antenna functions is vital to avoid over-subtraction in single unresolved limits when constructing subtraction terms that approach the full matrix element in all unresolved limits before any integration (see Section 4.5). However, there are four-parton antenna functions that do not reduce to a product of unpolarized splitting functions and spin-averaged three-parton antenna functions in single unresolved limits but instead include spin-dependent splitting functions $P^{\mu\nu}$ and tensorial three-parton antenna functions $(X^0_3)_{\mu\nu}$. The four-parton antenna functions that show this behaviour are the ones that include collinear singularities arising from gluon splittings and have the following factorization properties in the corresponding singular limits:

$$\begin{aligned}
A^0_4(1,3,4,2) &\xrightarrow{3_g\|4_g} \frac{1}{s_{34}}P^{\mu\nu}_{gg\to G}(z)(A^0_3)_{\mu\nu}(1,(34),2),\\
B^0_4(1,3,4,2) &\xrightarrow{3_q\|4_{\bar{q}}} \frac{1}{s_{34}}P^{\mu\nu}_{q\bar{q}\to G}(z)(A^0_3)_{\mu\nu}(1,(34),2),\\
D^0_4(1,3,4,5) &\xrightarrow{3_g\|4_g} \frac{1}{s_{34}}P^{\mu\nu}_{gg\to G}(z)(D^0_3)_{\mu\nu}(1,(34),5),\\
D^0_4(1,3,4,5) &\xrightarrow{4_g\|5_g} \frac{1}{s_{45}}P^{\mu\nu}_{gg\to G}(z)(D^0_3)_{\mu\nu}(1,3,(45)),\\
E^0_4(1,3,4,5) &\xrightarrow{3_q\|4_{\bar{q}}} \frac{1}{s_{34}}P^{\mu\nu}_{q\bar{q}\to G}(z)(D^0_3)_{\mu\nu}(1,(34),5),\\
F^0_4(1,2,3,4) &\xrightarrow{i_g\|j_g} \frac{1}{s_{ij}}P^{\mu\nu}_{gg\to G}(z)(F^0_3)_{\mu\nu}((ij),k,l),\\
G^0_4(1,3,4,2) &\xrightarrow{1_g\|2_g} \frac{1}{s_{12}}P^{\mu\nu}_{gg\to G}(z)(G^0_3)_{\mu\nu}((12),3,4),\\
G^0_4(1,3,4,2) &\xrightarrow{3_q\|4_{\bar{q}}} \frac{1}{s_{34}}P^{\mu\nu}_{q\bar{q}\to G}(z)(F^0_3)_{\mu\nu}(1,(34),2),
\end{aligned}$$

$$H_4^0(1,2,3,4) \overset{1_q||2_{\bar{q}}}{\longrightarrow} \frac{1}{s_{12}} P^{\mu\nu}_{q\bar{q}\to G}(z)(G_3^0)_{\mu\nu}((12),3,4),$$
$$H_4^0(1,2,3,4) \overset{3_q||4_{\bar{q}}}{\longrightarrow} \frac{1}{s_{34}} P^{\mu\nu}_{q\bar{q}\to G}(z)(G_3^0)_{\mu\nu}((34),1,2). \tag{4.51}$$

As a result of this factorization behaviour it is not possible to subtract single unresolved limits of the four-parton antennae in (4.51) in the respective collinear limits by a product of spin-averaged three-parton antennae. There are two ways to construct a fully local subtraction term and therefore circumvent this problem. The first method modifies the four-parton antenna functions in (4.51) by a local counterterm,

$$X_4^0(1,i,j,2) \to X_4^0(1,i,j,2) - \Theta_{X_3^0}(i,j,z,k_\perp), \tag{4.52}$$

that integrates to zero over the unresolved phase space and is constructed such that the modified antennae have the desired asymptotic behaviour in unresolved limits. The variables $k_\perp$ and z in (4.52) are used to parametrize the collinear limit of the two potentially collinear partons. In detail, the collinear limit of two partons p_1 and p_2 can be parametrized by

$$p_1^\mu = zP^\mu + k_\perp^\mu - \frac{k_\perp^2}{z}\frac{n^\mu}{2P\cdot n}, \tag{4.53}$$
$$p_2^\mu = (1-z)P^\mu - k_\perp^\mu - \frac{k_\perp^2}{1-z}\frac{n^\mu}{2P\cdot n}, \tag{4.54}$$

where P^μ denotes the collinear direction. We can now define the local counterterm as [84]

$$\Theta_{X_3^0}(i,j,z,k_\perp) = \frac{1}{s_{ij}} P^{\mu\nu}_{ij\to(ij)}(z,k_\perp)(X_3^0)_{\mu\nu}(1,(ij),2) - \frac{1}{s_{ij}} P_{ij\to(ij)}(z) X_3^0(1,(ij),2). \tag{4.55}$$

That this definition leads to the desired asymptotic behaviour is obvious. Note that the phase space integral involves an integration over the azimuthal angle ϕ parametrizing the angle of $k_\perp$ in the perpendicular plane to the collinear direction P. In order to show that the local counterterm integrates to zero when integrating over the final-state phase space we now analyze the Lorentz decomposition of a scalar function $f(k_\perp^2)$ multiplied by $k_\perp^\mu k_\perp^\nu$ integrated over ϕ, starting with the following ansatz for the integral

$$I^{\mu\nu} \equiv \frac{1}{2\pi}\int_0^{2\pi} \mathrm{d}\phi\, k_\perp^\mu k_\perp^\nu f(k_\perp^2) = A\cdot g^{\mu\nu} + B\cdot G^{\mu\nu}, \quad G^{\mu\nu} = P^\mu n^\nu + P^\nu n^\mu. \tag{4.56}$$

Contracting the ansatz with $G_{\mu\nu}$ and the metric tensor fixes the prefactors in the Lorentz decomposition of $I^{\mu\nu}$ and leads to

$$I^{\mu\nu} = \frac{k_\perp^2 f(k_\perp^2)}{D-2}\cdot d_{\mu\nu}, \tag{4.57}$$

where

$$d_{\mu\nu} = g_{\mu\nu} - \frac{G_{\mu\nu}}{P\cdot n}. \tag{4.58}$$

Using that the spin-dependent splitting functions $P^{\mu\nu}_{ij\to(ij)}$ have the structure

$$P^{\mu\nu}_{ij\to(ij)} = P_g \cdot g^{\mu\nu} + P_{k_\perp} \cdot k^\mu_\perp k^\nu_\perp, \tag{4.59}$$

we can now show that the integration over the phase space of the local counterterm (4.55) reduces to zero,

$$\frac{1}{2\pi}\int_0^{2\pi} \mathrm{d}\phi\, P^{\mu\nu}_{ij\to(ij)}(z,k_\perp)(X^0_3)_{\mu\nu}(1,(ij),2) \tag{4.60}$$

$$= \frac{1}{2\pi}\int_0^{2\pi} \mathrm{d}\phi \left((P_g \cdot \{ \underbrace{g^{\mu\nu} - \frac{G^{\mu\nu}}{P\cdot n}}_{d_{\mu\nu}} + \frac{G^{\mu\nu}}{P\cdot n}\} + P_{k_\perp}\cdot k^\mu_\perp k^\nu_\perp \right)(X^0_3)_{\mu\nu}(1,(ij),2) \tag{4.61}$$

$$= \underbrace{\left(P_g + P_{k_\perp}\frac{k^2_\perp}{D-2}\right)}_{=P_{ij\to(ij)}} d^{\mu\nu} X^0_{3,\mu\nu}(1,(ij),2) + \underbrace{P_g \frac{G^{\mu\nu}X^0_{3,\mu\nu}(1,(ij),2)}{P\cdot n}}_{=0} \tag{4.62}$$

$$= P_{ij\to(ij)}(z,k_\perp)(X^0_3)(1,(ij),2). \tag{4.63}$$

In the first step we have applied (4.57) to the tensorial part of the local counterterm in (4.55) and used that the mapped momenta in the tensorial antenna do not depend on $k_\perp$. In the second step we have identified the spin-averaged splitting and antenna functions and used the Ward identity for the radiator gluon,

$$P^\mu X^0_{3,\mu\nu}(1,(ij),2) = 0. \tag{4.64}$$

This, indeed, leads us to the conclusion that the local counterterm (4.55) integrated over ϕ vanishes. The second method is also based on the possibility of constructing a local counterterm as (4.55), but here two phase-space points at a time are combined so that it is not necessary to explicitly use local counterterms. In more detail, the collinear limit of antennae in (4.51) can be written as

$$X^0_4(1,i,j,2) \xrightarrow{i\|j} \frac{1}{s_{ij}} P^{\mu\nu}_{ij\to G}(z)(X^0_3)_{\mu\nu}(1,(ij),2) \tag{4.65}$$

$$= \frac{1}{s_{ij}} P_{ij\to G}(z)(X^0_3)(1,(ij),2) + \text{ang.}, \tag{4.66}$$

where the angular terms "ang." in the last equation are given by the local counterterm $\Theta_{X^0_3}(i,j,z,k_\perp)$ and contain ϕ-dependent terms being proportional to $\cos(2\phi+\alpha)$ [111]. Therefore, by combining two phase-space points that are related by a rotation around the collinear axis by $\Delta\phi = \frac{\pi}{2}$ the angular terms drop out in the sum. In this way one can avoid the explicit use of the local counterterm when implementing subtraction terms that include antennae in (4.51).

As we have seen in Section 3.1, the subleading colour part is relevant in order to extract the part of loop amplitudes with abelian gluons. Therefore, in order to calculate $\mathcal{O}(\alpha_s\alpha)$ corrections we only need subleading colour parts of antenna functions. Since only leading colour antenna functions are present in (4.51) angular terms are not relevant for $\mathcal{O}(\alpha_s\alpha)$ corrections.

4.4 Antenna subtraction at NLO

Here we discuss the construction of real and virtual subtraction terms and their combination with mass factorization kernels at NLO. We limit our discussion to subtraction terms relevant for this work. An extensive review of all subtraction terms at NLO can be found in [82, 96]. In principle, colour ordering of amplitudes is required in order to construct antenna subtraction terms. However, as described in Section 3.1 we can extend the construction of antenna subtraction terms from leading colour also to subleading colour by rewriting these contributions in terms of squared matrix elements with abelian gluons (which is possible for up to five coloured particles [96]). Therefore, antenna subtraction can also be applied to $\mathcal{O}(\alpha_s\alpha)$ corrections, keeping in mind that for higher multiplicities than five coloured particles modifications are needed. In the following, however, we will restrict the discussion to leading colour contributions and always assume that squared matrix elements have been reduced to the sum of colour-ordered squared subamplitudes.

4.4.1 Mass factorization term at NLO

As discussed in Section 3.3, at NLO, the mass factorization term is given by

$$\begin{aligned} \mathrm{d}\hat{\sigma}^{MF}_{ij,NLO} = -C(\epsilon) \int \frac{\mathrm{d}z_a}{z_a}\frac{\mathrm{d}z_b}{z_b}\mathrm{d}\Phi_n(\{p_i\}_{i=1}^n; z_a p_a, z_b p_b)\frac{1}{S_n} \\ \times \Gamma^{(1)}_{ij,kl}(z_a, z_b)|\mathcal{M}^0_n(p_1, \ldots, p_n; z_a p_a, z_b p_b)|^2 J^{(n)}_n(p_1, \ldots, p_n), \end{aligned} \tag{4.67}$$

where

$$\Gamma^{(1)}_{ij,kl}(z_a, z_b) = \delta(1-z_b)\delta_{lj}\Gamma^{(1)}_{ki}(z_a) + \delta(1-z_a)\delta_{ki}\Gamma^{(1)}_{lj}(z_b) \tag{4.68}$$

with $\Gamma^{(1)}_{ij}$ given in (3.50). In antenna subtraction the mass factorization kernels are combined with integrated antenna functions to form antenna strings used to cancel the explicit poles in the virtual correction included in an NLO calculation. In the next section this is explained in more detail.

4.4.2 Real and virtual subtraction terms

We are now able to construct subtraction terms $\mathrm{d}\hat{\sigma}^{\mathrm{S}}_{\mathrm{NLO}}$ that mimic the real NLO correction, $\mathrm{d}\hat{\sigma}^{\mathrm{R}}_{\mathrm{NLO}}$, in all single unresolved limits and therefore allow for a numerical integration of their combination in four space-time dimensions,

$$\int_{n+1} \left[\mathrm{d}\hat{\sigma}^{\mathrm{R}}_{\mathrm{NLO}} - \mathrm{d}\hat{\sigma}^{\mathrm{S}}_{\mathrm{NLO}}\right]. \tag{4.69}$$

The two basic properties that govern the structure of the subtraction terms are the factorization of the $(n+1)$-particle phase space and the factorization of squared matrix elements in unresolved limits. These properties were used in order to construct the phase-space mappings and antenna functions discussed in the previous sections. On the one hand, the factorization of squared matrix elements into an antenna function and an underlying

squared n-parton matrix element is the key ingredient that motivates the shape of the real subtraction term. On the other hand, the phase-space mappings allow for the factorization of the $(n+1)$-parton phase space into a n-particle phase space of composite momenta and an antenna phase space, which is used to define integrated antennae that cancel explicit divergences in the virtual NLO correction, $\mathrm{d}\hat{\sigma}^{\mathrm{V}}_{\mathrm{NLO}}$.

We start with the construction of the real subtraction term for the final–final case,

$$\begin{aligned}\mathrm{d}\hat{\sigma}^{\mathrm{S},ff}_{\mathrm{NLO}} =& \mathcal{N}_{\mathcal{C}}\mathcal{N}^{R}_{\mathrm{NLO}} \sum_{j} \mathrm{d}\Phi_{n+1}(\{p_i\}_{i=1}^{n+1}; p_a, p_b)\frac{1}{S_{n+1}} \\ &\times X_3^0(p_i,p_j,p_k)|\mathcal{M}_n^0(p_1,\dots,p_I,p_K,\dots,p_n;p_a,p_b)|^2 J_n^{(n)}(\dots,p_I,p_K,\dots),\end{aligned} \tag{4.70}$$

which reflects the factorization properties of the real squared matrix element. The sum over j includes all possibly unresolved partons in the final state, and we introduced the constants,

$$\bar{C}(\epsilon) = (4\pi)^{\epsilon} e^{-\epsilon\gamma}, \tag{4.71}$$

$$\mathcal{N}^{R}_{NLO} = \frac{\alpha_{\mathrm{s}}}{2\pi}\frac{\bar{C}(\epsilon)}{C(\epsilon)}. \tag{4.72}$$

with $C(\epsilon)$ defined in (4.45). As we have to distinguish between electroweak and QCD corrections in later chapters we also introduce the notation

$$\mathcal{N}^{R_{\mathrm{s}}}_{NLO} = \frac{\alpha_{\mathrm{s}}}{2\pi}\frac{\bar{C}(\epsilon)}{C(\epsilon)}, \qquad \mathcal{N}^{R_{\mathrm{ew}}}_{NLO} = \frac{\alpha}{2\pi}\frac{\bar{C}(\epsilon)}{C(\epsilon)}. \tag{4.73}$$

The reduced matrix element $\mathcal{M}_n^0$ and the jet function $J_n^{(n)}$ include momenta mapped by the finial–final phase-space mapping, p_I, p_K. Furthermore, $\mathcal{N}_{\mathcal{C}} = \mathcal{C}\,\mathcal{N}_{\mathcal{C},ij}$, $ij = q\bar{q}, qg$, is the product of a process dependent colour factor $\mathcal{C}$ and an additional channel dependent factor,

$$\mathcal{N}_{\mathcal{C},q\bar{q}} = 1, \qquad \mathcal{N}_{\mathcal{C},qg} = \frac{N}{N^2-1}, \tag{4.74}$$

which adjusts the colour normalization of the reduced matrix element. In principle, in d dimensions also the normalization factor for the helicity degrees of freedom has to be adjusted leading to a ε-dependent factor $\mathcal{N}^{\varepsilon}_{\mathcal{C}}$. As IR singularities in integrated subtraction terms are regularized dimensionally this factor $\mathcal{N}^{\varepsilon}_{\mathcal{C}}$ has to be used there and is explicitly given in (4.86). However, in four spacetime dimensions $\mathcal{N}^{\varepsilon}_{\mathcal{C}} = \mathcal{N}_{\mathcal{C}} + \mathcal{O}(\varepsilon)$, since quarks and gluons have the same number of helicity degrees of freedom for $d = 4$. For quark–antiquark-induced processes the normalization of the original and the reduced matrix element are equal and therefore no adaptation is needed. However, in case of (anti)quark–gluon-induced processes the reduced matrix element is quark–antiquark induced and has the corresponding colour normalization. Therefore, the normalization has to be adapted to be the one of (anti)quark-gluon induced processes by including $\mathcal{N}_{\mathcal{C},qg}$.

In cases with one radiator parton in the initial state and one radiator in the final state the corresponding subtraction term is given by

$$\mathrm{d}\hat{\sigma}^{\mathrm{S},if}_{\mathrm{NLO}} = \mathcal{N}_{\mathcal{C}}\mathcal{N}^{R}_{NLO} \sum_{j} \sum_{\substack{i=a,b \\ l\in\{a,b\}\setminus i}} \mathrm{d}\Phi_{n+1}(\{p_r\}_{r=1}^{n+1}; p_a, p_b)\frac{1}{S_{n+1}} \tag{4.75}$$

$$\times X^0_{i,jk}(p_i,p_j,p_k)|\mathcal{M}^0_n(p_1,\dots,p_J,\dots,p_n;x_ip_i,p_l)|^2 J^{(n)}_n(\dots,p_J,\dots),$$

where the initial–final phase-space mapping is used to construct the composite momenta that appear in the reduced matrix element and the jet function. In cases where only one radiating parton is contained in the initial state, say parton a, the sum over $i=a,b$ has to be replace by the term $i=a$ only.

Similar to the final–final and initial–final cases, the initial–initial subtraction term is given by

$$\begin{aligned}\mathrm{d}\hat{\sigma}^{\mathrm{S},ii}_{\mathrm{NLO}} =&\mathcal{N}_{\mathcal{C}}\mathcal{N}^R_{NLO}\sum_j \mathrm{d}\Phi_{n+1}(\{p_i\}^{n+1}_{i=1};p_a,p_b)\frac{1}{S_{n+1}} \\ &\times X^0_{ab,j}(p_a,p_j,p_b)|\mathcal{M}^0_n(\tilde{p}_1,\dots,\tilde{p}_n;x_ap_a,x_bp_b)|^2 J^{(n)}_n(\tilde{p}_1,\dots,\tilde{p}_{n+1}).\end{aligned} \tag{4.76}$$

After reparametrizing the $(n+1)$-particle phase space in the finial–final, initial–final, and initial–initial NLO subtraction functions in terms of the corresponding mapped momenta one can integrate analytically over the factorized antenna phase space, since the reduced matrix elements and jet functions depend only on the mapped momenta but not on antenna momenta. This leads to integrated subtraction terms for the finial–final, the initial–final, and the initial–initial case. Explicitly, integrated finial–final NLO subtraction terms are given by

$$\begin{aligned}\mathrm{d}\hat{\sigma}^{T,ff}_{NLO} =& -\frac{\mathcal{N}_{\mathcal{C}}\mathcal{N}^V_{NLO}}{S_{n+1}}\sum_{i,k}\int\frac{\mathrm{d}z_a}{z_a}\frac{\mathrm{d}z_b}{z_b}\mathrm{d}\Phi_n(\{p_i\}^n_{i=1};z_ap_a,z_bp_b) \\ &\times \boldsymbol{\mathcal{J}}^{(1)}_{2,ff}(i,k)|\mathcal{M}^0_n(p_1,\dots,p_n;z_ap_a,z_bp_b)|^2\, J^{(n)}_n(\{p_i\}^n_{i=1}),\end{aligned} \tag{4.77}$$

where

$$\mathcal{N}^V_{NLO}=\frac{\alpha_{\mathrm{s}}}{2\pi}\bar{C}(\epsilon),\qquad \mathcal{N}^{V_{\mathrm{s}}}_{NLO}=\frac{\alpha_{\mathrm{s}}}{2\pi}\bar{C}(\epsilon),\qquad \mathcal{N}^{V_{\mathrm{ew}}}_{NLO}=\frac{\alpha}{2\pi}\bar{C}(\epsilon), \tag{4.78}$$

and the integrated final–final antenna string $\boldsymbol{\mathcal{J}}^{(1)}_{2,ff}$ is given by the integrated three-parton antenna functions (4.44),

$$\boldsymbol{\mathcal{J}}^{(1)}_{2,ff}(I,K)=\delta(1-z_a)\delta(1-z_b)\mathcal{X}^0_{ijk}(s_{IK}). \tag{4.79}$$

Similar, the integrated initial–final NLO subtraction term

$$\begin{aligned}\mathrm{d}\hat{\sigma}^{T,if}_{NLO} =& -\frac{\mathcal{N}^{\varepsilon}_{\mathcal{C}}\mathcal{N}^V_{NLO}}{S_{n+1}}\sum_k\sum_{\substack{j=a,b\\ l\in\{a,b\}\setminus j}}\int\frac{\mathrm{d}z_a}{z_a}\frac{\mathrm{d}z_b}{z_b}\mathrm{d}\Phi_n(\{p_r\}^n_{r=1};z_ap_a,z_bp_b) \\ &\times \boldsymbol{\mathcal{J}}^{(1)}_{2,if}(j,k;z_j,z_l)|\mathcal{M}^0_n(p_1,\dots,p_n;z_ap_a,z_bp_b)|^2\, J^{(n)}_n(\{p_i\}^n_{i=1})\end{aligned} \tag{4.80}$$

depends on NLO initial–final antenna strings $\boldsymbol{\mathcal{J}}^{(1)}_{2,if}$ that include mass factorization kernels $\Gamma^{(1)}_{ki}$ in order to cancel all explicit IR singularities in the virtual contribution. The only NLO initial–final antenna string, $\boldsymbol{\mathcal{J}}^{(1)}_{2,if}$, relevant for this work is given by

$$\boldsymbol{\mathcal{J}}^{(1)}_{2,if}(\hat{\bar{a}}_q,J_{\bar{q}};x_a,x_b)=\mathcal{A}^0_{q,gq}(s_{\bar{a}J},x_a)\delta(1-x_b)-\Gamma^{(1)}_{qq}(x_a)\delta(1-x_b). \tag{4.81}$$

This antenna string is relevant for cases with a potentially unresolved gluon radiated from an initial- and a final-state quark. We have also introduced the factor $\mathcal{N}_{\mathcal{C}}^{\varepsilon}$ which is given in (4.86) below. In the initial–final case one of the radiator partons is in the initial state and therefore one convolution is included in (4.80). In case of two initial-state radiators the corresponding subtraction term includes two convolutions,

$$\begin{aligned}\mathrm{d}\hat{\sigma}_{NLO}^{T,ii} = &-\frac{\mathcal{N}_{\mathcal{C}}^{\varepsilon}\mathcal{N}_{NLO}^{V}}{S_{n+1}}\sum_{j,k}\int\frac{\mathrm{d}z_a}{z_a}\frac{\mathrm{d}z_b}{z_b}\mathrm{d}\Phi_n(\{p_i\}_{i=1}^n; z_a p_a, z_b p_b)\\ &\times \boldsymbol{\mathcal{J}}_{2,ii}^{(1)}(j,k,z_a,z_b)|\mathcal{M}_n^0(p_1,\ldots,p_n; z_a p_a, z_b p_b)|^2\, J_n^{(n)}(\{p_i\}_{i=1}^n).\end{aligned} \tag{4.82}$$

Again, the integrated antenna strings include mass factorization kernels, and the integrated single unresolved antennae strings, $\boldsymbol{\mathcal{J}}_2^{(1)}$, relevant for this work are given by

$$\begin{aligned}\boldsymbol{\mathcal{J}}_{2,ii}^{(1)}(\hat{\tilde{a}}_q,\hat{\tilde{b}}_{\bar{q}};x_a,x_b) &= \mathcal{A}_{qq,g}^0(s_{\bar{a}\bar{b}},x_a,x_b) - \Gamma_{qq}^{(1)}(x_a)\delta_{x_b} - \Gamma_{qq}^{(1)}(x_b)\delta_{x_a},\\ \boldsymbol{\mathcal{J}}_{2,ii}^{(1),g\to q}(\hat{\tilde{a}}_q,\hat{\tilde{b}}_{\bar{q}};x_a,x_b) &= \mathcal{A}_{qg,q}^0(s_{\bar{a}\bar{b}},x_a,x_b) - \Gamma_{qg}^{(1)}(x_b)\delta_{x_a}.\end{aligned} \tag{4.83}$$

If a potentially unresolved gluon is radiated off an initial-state quark pair, then the unintegrated antenna function corresponding to the first antenna string, $\boldsymbol{\mathcal{J}}_{2,ii}^{(1)}$, mimics the singular behaviour in this situation. The second integrated antenna string corresponds to cases where a quark is radiated off an initial-state quark and an initial-state gluon.

In order to obtain corrections to hadronic cross sections one has to include convolutions with parton distribution functions. By shifting the convolution over the energy fraction, $1-z_i$, of the potentially unresolved particle to the parton distribution functions (see App. F), the stability of the corresponding numerically evaluated integrals can be improved. In case of initial–initial corrections to hadronic cross sections one obtains,

$$\begin{aligned}\mathrm{d}\sigma_{NLO}^{T,ii} = &-\mathcal{N}_{\mathcal{C}}^{\varepsilon}\mathcal{N}_{NLO}^{R}\bar{C}(\epsilon)\int\frac{\mathrm{d}\zeta_a}{\zeta_a}\frac{\mathrm{d}\zeta_b}{\zeta_b}\int_{\zeta_a}^1\frac{\mathrm{d}z_a}{z_b}\int_{\zeta_b}^1\frac{\mathrm{d}z_b}{z_b}\frac{S_n}{S_{n+1}}f_a\left(\frac{\zeta_a}{z_a}\right)f_b\left(\frac{\zeta_b}{z_b}\right)\\ &\times\sum_{j,k}\boldsymbol{\mathcal{J}}_{2,ii}^{(1)}(j,k,z_a,z_b)\,\mathrm{d}\hat{\sigma}^{\mathrm{LO}}(\zeta_a P_a,\zeta_b P_b).\end{aligned} \tag{4.84}$$

For initial–final corrections the corresponding modification leads to

$$\begin{aligned}\mathrm{d}\sigma_{NLO}^{T,if} = &-\mathcal{N}_{\mathcal{C}}^{\varepsilon}\mathcal{N}_{NLO}^{R}\bar{C}(\epsilon)\int\frac{\mathrm{d}\zeta_a}{\zeta_a}\frac{\mathrm{d}\zeta_b}{\zeta_b}\int_{\zeta_a}^1\frac{\mathrm{d}z_a}{z_b}\int_{\zeta_b}^1\frac{\mathrm{d}z_b}{z_b}\frac{S_n}{S_{n+1}}f_a\left(\frac{\zeta_a}{z_a}\right)f_b\left(\frac{\zeta_b}{z_b}\right)\\ &\times\sum_{k}\sum_{\substack{j=a,b\\ l\in\{a,b\}\setminus j}}\delta(1-z_l)\boldsymbol{\mathcal{J}}_{2,if}^{(1)}(j,k,z_j,z_l)\,\mathrm{d}\hat{\sigma}^{\mathrm{LO}}(\zeta_a P_a,\zeta_b P_b).\end{aligned} \tag{4.85}$$

Finally, we have to discuss the proper inclusion of the factor $\mathcal{N}_{\mathcal{C}}^{\varepsilon}$ which takes care of the correct normalization of subtraction terms. For quark–antiquark induced processes this factor is just 1, but for (anti)quark–gluon-induced processes it is given by

$$\mathcal{N}_{\mathcal{C},qg}^{\varepsilon} = \mathcal{N}_{\mathcal{C},qg}\frac{1}{S_{g\to q}}, \tag{4.86}$$

where

$$S_{g\to q} = \frac{\#\text{helicities}_{\text{gluons}}}{\#\text{helicities}_{\text{quarks}}} = \frac{d-2}{2} = 1-\varepsilon. \tag{4.87}$$

However, since we use the $\overline{\text{MS}}$ scheme the mass factorization kernels only include a $1/\varepsilon$ contribution and a generic finite part, but no further finite contributions. This means that we do not include any finite terms that would be produced when $\mathcal{N}^{\varepsilon}_{\mathcal{C},qg}$ is multiplied with a mass factorization kernel, so that $\mathcal{N}^{\varepsilon}_{\mathcal{C},qg}$ has to be used in the following way,

$$\mathcal{N}^{\varepsilon}_{\mathcal{C},qg}\boldsymbol{\mathcal{J}}^{(1)}_2 = \mathcal{N}^{\varepsilon}_{\mathcal{C},qg}\mathcal{X}^0_3 + \mathcal{N}_{\mathcal{C},qg}\Gamma^{(1)}, \tag{4.88}$$

and additional finite terms are only produced in the combination of the integrated antenna function $\mathcal{X}^0_3$ and $\mathcal{N}^{\varepsilon}_{\mathcal{C},qg}$, but not in combination with the mass factorization kernel. This prescription is equivalent to

$$\mathcal{N}^{\varepsilon}_{\mathcal{C},qg}\boldsymbol{\mathcal{J}}^{(1)}_2 = \mathcal{N}_{\mathcal{C},qg}\mathcal{X}^0_3 + \mathcal{N}_{\mathcal{C},qg}S_{g\to q}\Gamma^{(1)}, \tag{4.89}$$

leading to the same additional finite terms as the ones produced in (4.88).

4.5 Antenna subtraction at NNLO

We now proceed by extending the description of the antenna formalism to NNLO calculations. At this perturbative order four-parton tree-level antenna functions and their integrated counterparts are introduced in order to handle singularities in matrix elements due to double-soft and triple-collinear configurations. Since the various antenna functions, needed to construct the NNLO antenna subtraction terms described in the following sections, are spread over various papers we give a short overview of potential sources without any claim of completeness. For scenarios with hadronic initial-state radiators at NLO all needed antennae and in particular the integrated antennae are constructed in [103]. The relevant antennae for radiator partons of type final–final at NLO and NNLO can be found in [84]. Antenna functions for the double-real case with hadronic initial states at NNLO can be obtained via crossing of the antenna functions constructed for the case with two final–final radiator partons. The integrated versions of them including integrated four-parton tree antennae, integrated three-parton one loop antenna functions, and integrated three-parton tree-level antennae including terms in the Laurent expansion in ϵ up to ϵ^2 are reported in [108–110, 112].

4.5.1 Double-real subtraction term

We again assume that squared matrix elements have been written in terms of a sum of colour-ordered squared subamplitudes which allows for the identification of four pieces contributing to the double-real NNLO subtraction term,

$$\mathrm{d}\hat{\sigma}^{S}_{\text{NNLO}} = \mathrm{d}\hat{\sigma}^{S,a}_{\text{NNLO}} + \mathrm{d}\hat{\sigma}^{S,b}_{\text{NNLO}} + \mathrm{d}\hat{\sigma}^{S,c}_{\text{NNLO}} + \mathrm{d}\hat{\sigma}^{S,d}_{\text{NNLO}}, \tag{4.90}$$

(a) Partons j and k are colour connected.

(b) Partons j and l are almost colour connected.

(c) Partons j and o are colour disconnected.

Figure 4.3: Different colour connections relevant for the construction of subtraction terms within the antenna subtraction method.

categorized according to their colour structure. The first double-real subtraction term, $\mathrm{d}\hat{\sigma}^{S,a}_{\mathrm{NNLO}}$, subtracts singular limits where only one parton in the final state becomes unresolved. The second, $\mathrm{d}\hat{\sigma}^{S,b}_{\mathrm{NNLO}}$, is used to cancel singular limits where two colour-connected partons become unresolved. It can be further split into a part that involves the four-parton tree-level antenna functions, $\mathrm{d}\hat{\sigma}^{S,b_1}_{\mathrm{NNLO}}$, subtracting the colour-connected limit, and a part including the product of two three-parton tree-level antennae, $\mathrm{d}\hat{\sigma}^{S,b_2}_{\mathrm{NNLO}}$, that subtracts spurious singularities of $\mathrm{d}\hat{\sigma}^{S,b_1}_{\mathrm{NNLO}}$ in single unresolved limits,

$$\mathrm{d}\hat{\sigma}^{S,b}_{\mathrm{NNLO}} = \mathrm{d}\hat{\sigma}^{S,b_1}_{\mathrm{NNLO}} + \mathrm{d}\hat{\sigma}^{S,b_2}_{\mathrm{NNLO}}. \tag{4.91}$$

The third contribution to the full double-real NNLO subtraction term, $\mathrm{d}\hat{\sigma}^{S,c}_{\mathrm{NNLO}}$, is used to cancel oversubtractions caused by $\mathrm{d}\hat{\sigma}^{S,a}_{\mathrm{NNLO}}$ and $\mathrm{d}\hat{\sigma}^{S,b_2}_{\mathrm{NNLO}}$ in limits where two almost colour-connected partons become unresolved, where the different kinds of colour connections between partons are depicted in Fig. 4.3. This subtraction term also receives contributions from terms that cancel oversubtractions in wide-angle soft gluon radiation configurations. This subtraction term is only relevant for processes that involve more than five partons with three resolved jets in the double-real contribution. The last ingredient in the construction of the double-real subtraction term, $\mathrm{d}\hat{\sigma}^{S,d}_{\mathrm{NNLO}}$, compensates oversubtractions caused by $\mathrm{d}\hat{\sigma}^{S,a}_{\mathrm{NNLO}}$ in double-unresolved colour-unconnected limits. For processes with less than six external partons in the double-real contribution this subtraction term is not needed.

4.5.1.1 Subtraction term for single-unresolved partons, $\mathrm{d}\hat{\sigma}^{\mathbf{S,a}}_{\mathrm{NNLO}}$

For single-unresolved limits we already constructed an appropriate subtraction term, $\mathrm{d}\hat{\sigma}^{\mathrm{S}}_{\mathrm{NLO}}$, in the discussion of antenna subtraction at NLO. The subtraction term used at NLO can be extended to NNLO by a modification of the number of external partons used by the jet function to form n jets, i.e. $J^{(n)}_n \to J^{(n+1)}_n$. This leads to the following NNLO subtraction term,

$$\begin{aligned}\mathrm{d}\hat{\sigma}^{\mathrm{S},a}_{\mathrm{NNLO}} =& \frac{\mathcal{N}_{\mathcal{C}}\,\mathcal{N}^{RR}_{NNLO}}{S_{n+2}} \sum_j \mathrm{d}\Phi_{n+2}(\{p_i\}^{n+2}_{i=1}; p_a, p_b) \\ & \times X^0_3(p_i, p_j, p_k) |\mathcal{M}^0_{n+1}(\{\tilde{p}_i\}^{n+2}_{i=1} \setminus \{\tilde{p}_j\}; \bar{p}_a, \bar{p}_b)|^2 J^{(n+1)}_n(\{\tilde{p}_i\}^{n+2}_{i=1} \setminus \{\tilde{p}_j\}),\end{aligned} \tag{4.92}$$

where the mapping used to produce the composite momenta $\tilde{p}_i, \bar{p}_a, \bar{p}_b$ depends on the type of the radiator partons i and k involved in the antenna function. For two-loop QCD corrections the prefactor $\mathcal{N}^{RR}_{NNLO}$ is given by

$$\mathcal{N}^{RR}_{NNLO} = (\mathcal{N}^{R}_{NLO})^2. \tag{4.93}$$

In the case of NNLO $\mathcal{O}(\alpha_s\alpha)$ corrections we have

$$\mathcal{N}^{R_s R_{ew}}_{NNLO} = \mathcal{N}^{R_s}_{NLO}\mathcal{N}^{R_{ew}}_{NLO}. \tag{4.94}$$

After integration over the antenna phase space parametrized by the momenta p_i, p_j, p_k (the momenta involved in the antenna) the subtraction term for single-unresolved partons $\mathrm{d}\hat{\sigma}^{\mathrm{S},a}_{\mathrm{NNLO}}$ is reintroduced in the real–virtual part in order to cancel explicit singularities.

4.5.1.2 Subtraction term for two unresolved colour-connected partons, $\mathrm{d}\hat{\sigma}^{\mathbf{S,b}}_{\mathrm{NNLO}}$

The subtraction term for configurations with two colour-connected unresolved partons is split into two parts,

$$\mathrm{d}\hat{\sigma}^{S,b}_{\mathrm{NNLO}} = \mathrm{d}\hat{\sigma}^{S,b_1}_{\mathrm{NNLO}} + \mathrm{d}\hat{\sigma}^{S,b_2}_{\mathrm{NNLO}}, \tag{4.95}$$

where the first part, $\mathrm{d}\hat{\sigma}^{S,b_1}_{\mathrm{NNLO}}$, contains four-parton tree-level antenna functions which are genuinely new ingredients at NNLO. This part is subtracting the singularities in double-unresolved limits. However, it also introduces spurious singularities in single-unresolved limits leading to the introduction of the second part, $\mathrm{d}\hat{\sigma}^{S,b_2}_{\mathrm{NNLO}}$, in order to cancel them. In this way, $\mathrm{d}\hat{\sigma}^{S,b}_{\mathrm{NNLO}}$ contains singularities only in double-unresolved limits. Explicitly, the subtraction term for configurations with colour-connected double-unresolved partons reads

$$\begin{aligned}\mathrm{d}\hat{\sigma}^{\mathrm{S},b_1}_{\mathrm{NNLO}} =& \frac{\mathcal{N}_{\mathcal{C}}\,\mathcal{N}^{RR}_{NNLO}}{S_{n+2}} \sum_{j,k} \mathrm{d}\Phi_{n+2}(\{p_i\}_{i=1}^{n+2}; p_a, p_b) \\ &\times X^0_4(p_i, p_j, p_k, p_l)|\mathcal{M}^0_n(\{\tilde{p}_i\}_{i=1}^{n+2}\setminus\{\tilde{p}_j,\tilde{p}_k\}; \bar{p}_a, \bar{p}_b)|^2 J^{(n)}_n(\{\tilde{p}_i\}_{i=1}^{n+2}\setminus\{\tilde{p}_j,\tilde{p}_k\}),\end{aligned} \tag{4.96}$$

where the $(n+2) \to n$ phase-space mapping used to obtain the composite momenta $\tilde{p}_i$ has to be adjusted according to the type (initial–initial, initial–final, or finial–final) of the involved antenna.

In singular unresolved limits four-parton tree-level antennae reduce to a product of two three-parton tree-level antenna functions. Therefore, spurious singularities in single-unresolved limits can be removed from $\mathrm{d}\hat{\sigma}^{\mathrm{S},b_1}_{\mathrm{NNLO}}$ with

$$\begin{aligned}\mathrm{d}\hat{\sigma}^{\mathrm{S},b_2}_{\mathrm{NNLO}} =& -\frac{\mathcal{N}_{\mathcal{C}}\,\mathcal{N}^{RR}_{NNLO}}{S_{n+2}} \sum_{j} \mathrm{d}\Phi_{n+2}(\{p_i\}_{i=1}^{n+2}; p_a, p_b) \\ &\times X^0_3(p_i, p_j, p_k) X^0_3(\tilde{p}_i, \tilde{p}_k, \tilde{p}_l)|\mathcal{M}^0_n(\{\tilde{\tilde{p}}_i\}_{i=1}^{n+2}\setminus\{\tilde{\tilde{p}}_j,\tilde{\tilde{p}}_k\}; \bar{p}_a, \bar{p}_b)|^2 \\ &\times J^{(n)}_n(\{\tilde{\tilde{p}}_i\}_{i=1}^{n+2}\setminus\{\tilde{\tilde{p}}_j,\tilde{\tilde{p}}_k\}).\end{aligned} \tag{4.97}$$

After integration over the single-unresolved antenna phase space, $\mathrm{d}\hat{\sigma}^{\mathrm{S},b_2}_{\mathrm{NNLO}}$ is reintroduced in the real–virtual subtraction term in order to remove explicit divergences in

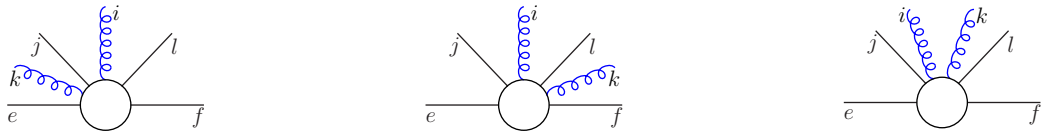

Figure 4.4: The three emission patterns of the potentially unresolved gluons i and k between the hard radiators e, j, l, and f that lead to an over-subtraction of singularities in $\mathrm{d}\hat{\sigma}^{\mathrm{S},a}_{\mathrm{NNLO}}$ and $\mathrm{d}\hat{\sigma}^{\mathrm{S},b_2}_{\mathrm{NNLO}}$.

the loop×tree subtraction term, $\mathrm{d}\hat{\sigma}^{\mathrm{T},b_2}_{\mathrm{NNLO}}$, relevant for the cancellation of implicit singularities of real–virtual amplitudes. In contrast to $\mathrm{d}\hat{\sigma}^{\mathrm{S},b_2}_{\mathrm{NNLO}}$, $\mathrm{d}\hat{\sigma}^{\mathrm{S},b_1}_{\mathrm{NNLO}}$ is integrated over the double-unresolved antenna phase space and reintroduced in the double-virtual subtraction term.

4.5.1.3 Subtraction term for almost colour-connected partons, $\mathrm{d}\hat{\sigma}^{\mathbf{S,c}}_{\mathrm{NNLO}}$

The subtraction term $\mathrm{d}\hat{\sigma}^{S,c}_{\mathrm{NNLO}}$ for singularities originating from the emission of almost colour-connected partons is only relevant for processes with more than four external partons. This subtraction term accounts for oversubtracted singularities in $\mathrm{d}\hat{\sigma}^{\mathrm{S},a}_{\mathrm{NNLO}}$ and $\mathrm{d}\hat{\sigma}^{\mathrm{S},b}_{\mathrm{NNLO}}$ that appear due to unordered emissions of unresolved partons in the subleading colour contribution. As the unordered emission of partons is only present in the subleading colour contribution $\mathrm{d}\hat{\sigma}^{S,c}_{\mathrm{NNLO}}$ does not contribute to the leading colour part. Even though processes relevant for this work never reach multiplicities of external partons large enough to produce spurious singularities associated to $\mathrm{d}\hat{\sigma}^{S,c}_{\mathrm{NNLO}}$, we still discuss this contribution in the following in order to obtain a full description of all ingredients relevant for constructing subtraction terms within the framework of antenna subtraction at NNLO.

In case of two almost-colour-connected unresolved partons the subtraction function $\mathrm{d}\hat{\sigma}^{\mathrm{S},a}_{\mathrm{NNLO}}$ is twice as big as it should be compared to the matrix element. Moreover, at subleading colour the subtraction term $\mathrm{d}\hat{\sigma}^{\mathrm{S},b}_{\mathrm{NNLO}}$ potentially oversubtracts implicit singularities from the subleading colour antennae X^0_4. The purpose of the subtraction term $\mathrm{d}\hat{\sigma}^{\mathrm{S},c}_{\mathrm{NNLO}}$ is to correct for both of these over-subtractions originating either from $\mathrm{d}\hat{\sigma}^{\mathrm{S},a}_{\mathrm{NNLO}}$ or $\mathrm{d}\hat{\sigma}^{\mathrm{S},b}_{\mathrm{NNLO}}$.

We follow [96] and discuss the final–final case; a similar construction is also possible for the two other cases. The subleading colour subtraction term $\mathrm{d}\hat{\sigma}^{\mathrm{S},b_1}_{\mathrm{NNLO}}$ relevant for two unresolved colour-connected limits involves four-parton antenna functions $\tilde{X}^0_4$, where each of them leads to a corresponding block in $\mathrm{d}\hat{\sigma}^{\mathrm{S},c}_{\mathrm{NNLO}}$. Consider two potentially unresolved partons i, k each emitted between two of the four hard radiators e, j, l, f. First, parton k is emitted between $(e, j), (j, l)$, or (l, f). Second, the potentially unresolved parton i is always emitted between the pair (j, l), as depicted in Fig. 4.4. We also have to include the reversed order where first parton i is emitted and then parton k.

We first consider the subtraction function $\mathrm{d}\hat{\sigma}^{\mathrm{S},a}_{\mathrm{NNLO}}$ which includes contributions of the form

$$S^a_{eij} \equiv X^0_{3,eij}|\mathcal{M}^0_{n+1}(\dots,\tilde{p}_e,\tilde{p}_j,\dots)|^2,$$
$$S^a_{ekj} \equiv X^0_{3,ekj}|\mathcal{M}^0_{n+1}(\dots,\tilde{p}_e,\tilde{p}_j,\dots)|^2$$

leading to over-subtraction of singular limits where both partons i and k become unresolved. The corresponding block in $\mathrm{d}\hat{\sigma}^{\mathrm{S},c}_{\mathrm{NNLO}}$ to cancel half of S^a_{eij} and S^a_{ekj} in the limit where i and k are unresolved is of the form

$$-\frac{1}{2}\sum_{\substack{s=i,k\\ s'\in\{i,k\}\setminus s}} X_3^0(e,s,j)\; X_3^0(\widetilde{(js)},s',l)\;|\mathcal{M}_n^0(\ldots,\widetilde{(es)},\widetilde{((js)s')},\widetilde{(s'l)},f,\ldots)|^2,$$

and a similar contribution for the emission pattern that corresponds to the terms S^a_{lif} and S^a_{lkf}. Additionally, also $\mathrm{d}\hat{\sigma}^{\mathrm{S},b_2}_{\mathrm{NNLO}}$ leads to over-subtractions in limits where partons i,k become unresolved with respect to parton j due to terms like

$$\begin{aligned}&- X_3^0(j,i,k)X_3^0(\widetilde{(ij)},\widetilde{(ik)},l) - X_3^0(j,k,i)X_3^0(\widetilde{(jk)},\widetilde{(ki)},l)\\ &\overset{i\|k\|j}{\sim} -2X_3^0(j,i,k)X_3^0(j,k,l),\end{aligned} \tag{4.98}$$

present in $\mathrm{d}\hat{\sigma}^{\mathrm{S},b_2}_{\mathrm{NNLO}}$. The same applies to situations where partons i and k become unresolved with respect to parton l. The term in $\mathrm{d}\hat{\sigma}^{\mathrm{S},c}_{\mathrm{NNLO}}$ that cures this potential over-subtraction for i and k becoming unresolved with respect to j is schematically given by

$$\sum_{\substack{s=i,k\\ s'\in\{i,k\}\setminus s}}\frac{1}{2}\; X_3^0(j,s,l)\; X_3^0(\widetilde{(js)},s',\widetilde{(sl)})\;|\mathcal{M}_n^0(\ldots,e,\widetilde{((js)s')},\widetilde{(s'(sl))},f,\ldots)|^2. \tag{4.99}$$

Therefore, the subtraction term $\mathrm{d}\hat{\sigma}^{\mathrm{S},c}_{\mathrm{NNLO}}$ consists of blocks of the following form,

$$\begin{aligned}\mathrm{d}\hat{\sigma}^{\mathrm{S},c}_{\mathrm{NNLO}} &= \frac{\mathcal{N}_{\mathcal{C}}\,\mathcal{N}^{RR}_{NNLO}}{S_{n+2}}\sum_{s,s'}\mathrm{d}\Phi_{n+2}(\{p_i\}_{i=1}^{n+2};p_a,p_b)\\ &\times\Big\{\frac{1}{2}\; X_3^0(j,s,l)\; X_3^0(\widetilde{(js)},s',\widetilde{(sl)})\;\Big[|\mathcal{M}_n^0|^2J_n^{(n)}\Big](\ldots,e,\widetilde{((js)s')},\widetilde{(s'(sl))},f,\ldots)\\ &-\frac{1}{2}\; X_3^0(e,s,j)\; X_3^0(\widetilde{(js)},s',l)\;\Big[|\mathcal{M}_n^0|^2J_n^{(n)}\Big](\ldots,\widetilde{(es)},\widetilde{((js)s')},\widetilde{(s'l)},f,\ldots)\\ &-\frac{1}{2}\; X_3^0(l,s,f)\; X_3^0(j,s',\widetilde{(ls)})\;\Big[|\mathcal{M}_n^0|^2J_n^{(n)}\Big](\ldots,e,\widetilde{(js')},\widetilde{(s'(ls)},\widetilde{(fs)},\ldots)\Big\}.\end{aligned} \tag{4.100}$$

In [113] it has been first noticed that the sum of the differential cross section $\mathrm{d}\hat{\sigma}^{(0)}_5$ used to calculate three-jet observables in e^+e^- collisions and the double-real NNLO subtraction term $\mathrm{d}\hat{\sigma}^{S}_{\mathrm{NNLO}}$,

$$\mathrm{d}\hat{\sigma}^{(0)}_5 - \mathrm{d}\hat{\sigma}^{S,a}_{\mathrm{NNLO}} - \mathrm{d}\hat{\sigma}^{S,b}_{\mathrm{NNLO}} - \mathrm{d}\hat{\sigma}^{S,c}_{\mathrm{NNLO}} - \mathrm{d}\hat{\sigma}^{S,d}_{\mathrm{NNLO}}, \tag{4.101}$$

still contains soft poles noticeable as a logarithmic dependence on a slicing parameter that corresponds to a cut in the corresponding soft phase-space region. These soft poles were attributed to phase-space regions where the soft parton is emitted with a large polar angle with respect to one of the hard radiators in the center-of-mass frame of the reduced momenta (i.e. the momenta obtained after the application of a final-state phase-space mapping) of the two hard radiator partons. Therefore, an additional subtraction term

$\mathrm{d}\hat{\sigma}^{\mathrm{soft}}$ has to be introduced in order to cancel this large-angle soft radiation. It can be shown [96] that the large-angle soft terms corresponding to the three constituents included in $\mathrm{d}\hat{\sigma}^{\mathrm{S},c}_{\mathrm{NNLO}}$ in (4.100) can be chosen as

$$-\frac{1}{2}\,\left[S_{\alpha s\beta}-S_{ASB}\,\right]\cdot X_3^0(\widetilde{(sj)},s',\widetilde{(sl)})\;|\mathcal{M}_n^0(\ldots,e,\widetilde{(\widetilde{(sj)}s')},\widetilde{(s'\widetilde{(sl)})},f,\ldots)|^2, \tag{4.102}$$

with

$$\begin{aligned}(\alpha,\beta)&=\big\{\big(e,\widetilde{(sj)}\big),\big(\widetilde{(sj)},\widetilde{(sl)}\big),\big(\widetilde{(sl)},f\big)\big\},\\ (A,B)&=\big\{\big(e,\widetilde{(\widetilde{(sj)}s')}\big),\big(\widetilde{(\widetilde{(sj)}s')},\widetilde{(s'\widetilde{(il)})}\big),\big(\widetilde{(s'\widetilde{(sl)})},f\big)\big\}.\end{aligned} \tag{4.103}$$

The complete subtraction term $\mathrm{d}\hat{\sigma}^{\mathrm{S},c}_{\mathrm{NNLO}}$, taking care of the over-subtractions due to the $\mathrm{d}\hat{\sigma}^{\mathrm{S},a}_{\mathrm{NNLO}}$ and $\mathrm{d}\hat{\sigma}^{\mathrm{S},b_2}_{\mathrm{NNLO}}$ and including also the large-angle soft subtraction term $\mathrm{d}\hat{\sigma}^{\mathrm{soft}}$, is now given by

$$\begin{aligned}\mathrm{d}\hat{\sigma}^{\mathrm{S},c}_{\mathrm{NNLO}}=&\frac{\mathcal{N}_{\mathcal{C}}\,\mathcal{N}^{RR}_{NNLO}}{S_{n+2}}\sum_{s,s'}\mathrm{d}\Phi_{n+2}(\{p_i\}_{i=1}^{n+2};p_a,p_b)\\ &\times\Bigg\{\frac{1}{2}\;X_3^0(j,s,l)\;X_3^0(\widetilde{(js)},s',\widetilde{(sl)})\;\Big[|\mathcal{M}_n^0|^2J_n^{(n)}\Big](\ldots,e,\widetilde{(\widetilde{(js)}s')},\widetilde{(s'\widetilde{(sl)})},f,\ldots)\\ &-\frac{1}{2}\;X_3^0(e,s,j)\;X_3^0(\widetilde{(js)},s',l)\;\Big[|\mathcal{M}_n^0|^2J_n^{(n)}\Big](\ldots,\widetilde{(es)},\widetilde{(\widetilde{(js)}s')},\widetilde{(s'l)},f,\ldots)\\ &-\frac{1}{2}\;X_3^0(l,s,f)\;X_3^0(j,s',\widetilde{(ls)})\;\Big[|\mathcal{M}_n^0|^2J_n^{(n)}\Big](\ldots,e,\widetilde{(js')},\widetilde{(s'\widetilde{(ls)}},\widetilde{(fs)}\ldots)\\ &+\frac{1}{2}\Big[\big(S_{\widetilde{(sj)},s,\widetilde{(sl)}}-S_{\widetilde{(\widetilde{(sj)}s')s(s'\widetilde{(sl)})}}\big)-\;\big(S_{es\widetilde{(sj)}}-S_{es\widetilde{(\widetilde{(sj)}s')}}\big)-\big(S_{fs\widetilde{(sl)}}-S_{fs\widetilde{((sl)s')}}\big)\Big]\\ &X_3^0(\widetilde{(sj)},s',\widetilde{(sl)})\;\Big[|\mathcal{M}_n^0|^2J_n^{(n)}\Big](\ldots,e,\widetilde{(\widetilde{(sj)}s')},\widetilde{(s'\widetilde{(sl)})},f,\ldots)\Bigg\}\,.\end{aligned} \tag{4.104}$$

4.5.1.4 Colour-disconnected subtraction term, $\mathrm{d}\hat{\sigma}^{\mathbf{S,d}}_{\mathrm{NNLO}}$

Colour-disconnected double-unresolved singularities occur in configurations where two unresolved partons are separated by more than one hard radiator and therefore are only present in processes with more than five coloured particles. The subtraction term for single-unresolved limits, $\mathrm{d}\hat{\sigma}^{S,a}_{\mathrm{NNLO}}$, over-subtracts singularities in colour disconnected limits. The reason for this over-subtraciton is that for each term in $\mathrm{d}\hat{\sigma}^{S,a}_{\mathrm{NNLO}}$ where a parton j is part of the antenna and parton m is part of the reduced matrix element there is also a subtraction term in $\mathrm{d}\hat{\sigma}^{S,a}_{\mathrm{NNLO}}$ where j and m change their role. Both of these configurations lead, however, to the same singular limit in double-unresolved colour-disconnected configurations leading to twice the result needed to cancel the singularities present in the double-real matrix element. The over-subtraction can be fixed by introducing subtraction terms like

$$\mathrm{d}\hat{\sigma}^{\mathrm{S},d}_{\mathrm{NNLO}}=\frac{\mathcal{N}_{\mathcal{C}}\,\mathcal{N}^{RR}_{NNLO}}{S_{n+2}}\sum_{j,m}\mathrm{d}\Phi_{n+2}(\{p_i\}_{i=1}^{n+2};p_a,p_b) \tag{4.105}$$

$$\times X_3^0(p_i,p_j,p_k)X_3^0(p_l,p_m,p_n)|\mathcal{M}_n^0(\{\tilde{p}_i\}_{i=1}^{n+2}\setminus\{\tilde{p}_j,\tilde{p}_m\};\bar{p}_a,\bar{p}_b)|^2$$
$$\times J_n^{(n)}(\{\tilde{p}_i\}_{i=1}^{n+2}\setminus\{\tilde{p}_j,\tilde{p}_m\}).$$

As the two unresolved partons are colour disconnected it is possible to integrate $\mathrm{d}\hat{\sigma}^{\mathrm{S},d}_{\mathrm{NNLO}}$ analytically over the two corresponding disconnected three-parton antenna phase spaces. The integrated subtraction term is reintroduced in the double-virtual subtraction term.

4.5.2 Real–virtual subtraction term

Real–virtual corrections to squared matrix elements include one-loop corrections and the radiation of one potentially unresolved parton. Both characteristics lead to singularities of different kind that have to be accounted for in the corresponding real–virtual subtraction terms. Loop corrections lead to explicit poles originating from the one-loop integration whereas the radiated, potentially unresolved parton leads to implicit divergences when integrating over the phase space. The subtraction term used to cancel these singularities also reflects these two characteristic properties of real–virtual corrections by being split into different parts,

$$\mathrm{d}\hat{\sigma}^{T}_{\mathrm{NNLO}} = \mathrm{d}\hat{\sigma}^{T,a}_{\mathrm{NNLO}} + \mathrm{d}\hat{\sigma}^{T,b}_{\mathrm{NNLO}} + \mathrm{d}\hat{\sigma}^{T,c}_{\mathrm{NNLO}}, \tag{4.106}$$

where each of the first two contributions to $\mathrm{d}\hat{\sigma}^{T}_{\mathrm{NNLO}}$ is used for the cancellation of one of the different kinds of singularity types, respectively. $\mathrm{d}\hat{\sigma}^{T,a}_{\mathrm{NNLO}}$ contains terms proportional to integrated antennae $\mathcal{X}_3^0$ used to cancel explicit poles and is the integrated counterpart to $\mathrm{d}\hat{\sigma}^{S,a}_{\mathrm{NNLO}}$, whereas $\mathrm{d}\hat{\sigma}^{T,b}_{\mathrm{NNLO}}$ is constructed such that it cancels the implicit singularities of the potentially unresolved parton in real–virtual corrections. This contribution is split further into three parts,

$$\mathrm{d}\hat{\sigma}^{T,b}_{\mathrm{NNLO}} = \mathrm{d}\hat{\sigma}^{T,b_1}_{\mathrm{NNLO}} + \mathrm{d}\hat{\sigma}^{T,b_2}_{\mathrm{NNLO}} + \mathrm{d}\hat{\sigma}^{T,b_3}_{\mathrm{NNLO}}, \tag{4.107}$$

where the first two contributions are motivated by the behaviour of one-loop matrix elements in implicit IR-singular limits and the third contribution is needed to adapt the renormalization scale used in the renormalization of one-loop antenna functions to the renormalization scale of other contributions within a certain calculation. The last contribution to the real–virtual subtraction term, $\mathrm{d}\hat{\sigma}^{T,c}_{\mathrm{NNLO}}$, is the integrated version of the almost colour-connected subtraction term $\mathrm{d}\hat{\sigma}^{S,c}_{\mathrm{NNLO}}$ introduced in the previous section and contains contributions of the form $\mathcal{X}_3^0 X_3^0$.

4.5.2.1 Mass factorization terms at NNLO: Real–virtual contribution

In Section 3.3 we discussed mass factorization kernels needed to cancel all explicit IR singularities that remain after adding all virtual and real corrections because of the lack of inclusiveness with respect to initial-state partons in NNLO calculations and classified them according to the number of final-state partons involved in the appearing matrix elements. We can use the definition of the NLO correction to the cross section within the framework of antenna subtraction,

$$\int_{n+1}\mathrm{d}\hat{\sigma}_{ij,NLO} = \int_{n+1}\left(\mathrm{d}\hat{\sigma}^{R}_{ij,NLO} - \mathrm{d}\hat{\sigma}^{S}_{ij,NLO}\right) + \int_{n}\left(\int_{1}\mathrm{d}\hat{\sigma}^{S}_{ij,NLO} + \mathrm{d}\hat{\sigma}^{V}_{ij,NLO} + \mathrm{d}\hat{\sigma}^{MF}_{ij,NLO}\right), \tag{4.108}$$

in order to rewrite the NNLO mass factorization kernel in (3.62) as a sum of two contributions,

$$\mathrm{d}\hat{\sigma}^{MF}_{ij,NNLO}(\xi_1 P_A, \xi_2 P_B) = \mathrm{d}\hat{\sigma}^{MF,1}_{ij,NNLO}(\xi_1 P_A, \xi_2 P_B) + \mathrm{d}\hat{\sigma}^{MF,2}_{ij,NNLO}(\xi_1 P_A, \xi_2 P_B), \tag{4.109}$$

where

$$\begin{aligned}
\mathrm{d}\hat{\sigma}^{MF,1}_{ij,NNLO}(\xi_1 P_A, \xi_2 P_B) &= -\int \frac{\mathrm{d}z_1}{z_1}\frac{\mathrm{d}z_2}{z_2} \\
&\times \frac{\alpha_s N}{2\pi}\,\bar{C}(\epsilon)\,\Gamma^{(1)}_{ij;kl}(z_1,z_2)\Big(\mathrm{d}\hat{\sigma}^{R}_{kl,NLO} - \mathrm{d}\hat{\sigma}^{S}_{kl,NLO}\Big)(z_1\xi_1 P_A, z_2\xi_2 P_B), \qquad (4.110)\\
\mathrm{d}\hat{\sigma}^{MF,2}_{ij,NNLO}(\xi_1 P_A, \xi_2 P_B) &= -\int \frac{\mathrm{d}z_1}{z_1}\frac{\mathrm{d}z_2}{z_2}\Bigg\{ \\
&\left(\frac{\alpha_s N}{2\pi}\right)^2 \bar{C}(\epsilon)^2\,\Gamma^{(2)}_{ij;kl}(z_1,z_2)\mathrm{d}\hat{\sigma}_{kl,LO}(z_1\xi_1 P_A, z_2\xi_2 P_B) \qquad (4.111)\\
&+ \frac{\alpha_s N}{2\pi}\,\bar{C}(\epsilon)\,\Gamma^{(1)}_{ij;kl}(z_1,z_2)\Big(\mathrm{d}\hat{\sigma}^{V}_{kl,NLO} - \mathrm{d}\hat{\sigma}^{T}_{kl,NLO} + \mathrm{d}\hat{\sigma}^{MF}_{kl,NLO}\Big)(z_1\xi_1 P_A, z_2\xi_2 P_B)\Bigg\},
\end{aligned}$$

and

$$\Gamma^{(2)}_{ij;kl}(z_1,z_2) = \delta(1-z_2)\delta_{lj}\Gamma^{(2)}_{ki}(z_1) + \delta(1-z_1)\delta_{ki}\Gamma^{(2)}_{lj}(z_2) + \Gamma^{(1)}_{ki}(z_1)\Gamma^{(1)}_{lj}(z_2). \tag{4.112}$$

The second mass factorization term in (4.109) will be used to cancel collinear singularities in the double-virtual contribution while the NNLO mass factorization term in (4.110) involving $(n+1)$ final-state partons is used to cancel collinear singularities in real–virtual contributions and can be further split into two pieces,

$$\mathrm{d}\hat{\sigma}^{MF,1}_{ij,\mathrm{NNLO}} = \mathrm{d}\hat{\sigma}^{MF,1,a}_{ij,\mathrm{NNLO}} + \mathrm{d}\hat{\sigma}^{MF,1,b}_{ij,\mathrm{NNLO}}. \tag{4.113}$$

The first part contains the NLO real cross section,

$$\begin{aligned}
\mathrm{d}\hat{\sigma}^{MF,1,a}_{ij,\mathrm{NNLO}}(\xi_a P_a, \xi_b P_b) &= -\int \frac{\mathrm{d}z_a}{z_a}\frac{\mathrm{d}z_b}{z_b} \qquad (4.114)\\
&\times \frac{\alpha_s N}{2\pi}\,\bar{C}(\epsilon)\,\Gamma^{(1)}_{ij;kl}(z_a,z_b)\;\mathrm{d}\hat{\sigma}^{R}_{kl,\mathrm{NLO}}(z_a\xi_a P_a, z_b\xi_b P_b),
\end{aligned}$$

and the second part includes the corresponding real NLO subtraction term,

$$\begin{aligned}
\mathrm{d}\hat{\sigma}^{MF,1,b}_{ij,\mathrm{NNLO}}(\xi_a P_a, \xi_b P_b) &= \int \frac{\mathrm{d}z_a}{z_a}\frac{\mathrm{d}z_b}{z_b} \qquad (4.115)\\
&\times \frac{\alpha_s N}{2\pi}\,\bar{C}(\epsilon)\,\Gamma^{(1)}_{ij;kl}(z_a,z_b)\;\mathrm{d}\hat{\sigma}^{S}_{kl,\mathrm{NLO}}(z_a\xi_a P_a, z_b\xi_b P_b).
\end{aligned}$$

In order to connect to the different parts of the subtraction term in (4.107) the mass factorization terms including the NLO subtraction term is rewritten as

$$\mathrm{d}\hat{\sigma}^{MF,1,b}_{ij,\mathrm{NNLO}} = \mathrm{d}\hat{\sigma}^{MF,1,b_1}_{ij,\mathrm{NNLO}} + \mathrm{d}\hat{\sigma}^{MF,1,b_2}_{ij,\mathrm{NNLO}} + \mathrm{d}\hat{\sigma}^{MF,1,b_3}_{ij,\mathrm{NNLO}}, \tag{4.116}$$

where

$$\mathrm{d}\hat{\sigma}^{MF,1,b_2}_{ij,\mathrm{NNLO}}(\xi_a P_a, \xi_b P_2) = \mathrm{d}\hat{\sigma}^{MF,1,b}_{ij,\mathrm{NNLO}}(\xi_a P_a, \xi_b P_b), \tag{4.117}$$

$$\begin{aligned}\mathrm{d}\hat{\sigma}^{MF,1,b_1}_{ij,\mathrm{NNLO}}(\xi_a P_a, \xi_b P_b) = &\int \frac{\mathrm{d}z_a}{z_a}\frac{\mathrm{d}z_b}{z_b} \\ &\times \frac{\alpha_s N}{2\pi}\,\bar{C}(\epsilon)\,\Gamma^{(1)}_{cd;cd}(z_a, z_b)\;\mathrm{d}\hat{\sigma}^{S}_{ij,\mathrm{NLO}}(z_a\xi_a P_a, z_b\xi_b P_b),\end{aligned} \tag{4.118}$$

$$= -\,\mathrm{d}\hat{\sigma}^{MF,1,b_3}_{ij,\mathrm{NNLO}}(\xi_a P_a, \xi_b P_b). \tag{4.119}$$

Note that c and d in the last equation are given by $c = i$ and $d = j$ for processes where unresolved limits do not change the initial-state partons. Otherwise, they are given by the species of the initial-state partons involved in the reduced matrix element in the NLO real subtraction term. For further details and a specific example see [96].

The NNLO real–virtual mass factorization contribution including the NLO real cross section, $\mathrm{d}\hat{\sigma}^{MF,1,a}_{ij,\mathrm{NNLO}}$, is part of the integrated antenna string used in $\mathrm{d}\hat{\sigma}^{T,a}_{\mathrm{NNLO}}$. The mass factorization contribution $\mathrm{d}\hat{\sigma}^{MF,b_1}_{ij,\mathrm{NNLO}}$ is included in $\mathrm{d}\hat{\sigma}^{T,b_1}_{\mathrm{NNLO}}$. The remaining real–virtual mass factorization contributions are part of antenna strings included in $\mathrm{d}\hat{\sigma}^{T,b_2}_{\mathrm{NNLO}}$.

4.5.2.2 Subtraction terms to cancel explicit poles, $\mathrm{d}\hat{\sigma}^{\mathbf{T,a}}_{\mathrm{NNLO}}$

At NLO the real subtraction term, $\mathrm{d}\hat{\sigma}^{S}_{\mathrm{NLO}}$, discussed in Section 4.4 canceled all implicit IR singularities of real $n+1$ parton squared matrix elements. Integrated over the one-parton unresolved antenna phase space $\mathrm{d}\hat{\sigma}^{S}_{\mathrm{NLO}}$ was sufficient to cancel all explicit poles in the one-loop correction to n parton squared matrix elements (when including mass factorization kernels). To cancel single unresolved singularities at NNLO we generalized $\mathrm{d}\hat{\sigma}^{S}_{\mathrm{NLO}}$ from $(n+1)$ to $(n+2)$ final state partons and obtained $\mathrm{d}\hat{\sigma}^{S,a}_{\mathrm{NNLO}}$. Therefore, $\mathrm{d}\hat{\sigma}^{S,a}_{\mathrm{NNLO}}$, being the generalization of $\mathrm{d}\hat{\sigma}^{S}_{\mathrm{NLO}}$ to NNLO, integrated over the unresolved one-parton antenna phase space will now subtract all explicit poles from the one-loop correction to $(n+1)$ parton squared amplitudes when including proper mass factorization kernels.

The integrated version of the subtraction term $\mathrm{d}\hat{\sigma}^{S,a}_{\mathrm{NNLO}}$ and also the mass factorization cross section, $\mathrm{d}\hat{\sigma}^{MF,1,a}_{ij,\mathrm{NNLO}}$, involve $(n+1)$-parton tree squared matrix elements. The sum of the integrated subtraction term and the mass factorization contribution leads to exactly the same integrated antenna string as the ones that we already encountered at NLO in (4.82) and (4.83),

$$\begin{aligned}\mathrm{d}\hat{\sigma}^{T,a}_{\mathrm{NNLO}} &= -\int_1 \mathrm{d}\hat{\sigma}^{S,a}_{\mathrm{NNLO}} - \mathrm{d}\hat{\sigma}^{MF,1,a}_{ij,\mathrm{NNLO}} \\ &= -\frac{\mathcal{N}^{\varepsilon}_{\mathcal{C}}\,\mathcal{N}^{RV}_{\mathrm{NNLO}}}{S_{n+1}}\sum_{j,k}\int \frac{\mathrm{d}z_a}{z_a}\frac{\mathrm{d}z_b}{z_b}\mathrm{d}\Phi_{n+1}(\{p_i\}^{n+1}_{i=1}; z_a p_a, z_b p_b) \\ &\quad\times \boldsymbol{\mathcal{J}}^{(1)}_2(j,k,z_a,z_b)|\mathcal{M}^0_{n+1}(\{p_i\}^{n+1}_{i=1}; z_a p_a, z_b p_b)|^2\; J^{(n+1)}_n(\{p_i\}^{n+1}_{i=1}),\end{aligned} \tag{4.120}$$

with the prefactor

$$\mathcal{N}^{RV}_{\mathrm{NNLO}} = C(\epsilon)\mathcal{N}^{RR}_{\mathrm{NNLO}}, \tag{4.121}$$

relevant for real–virtual corrections.

4.5.2.3 Subtraction term to cancel implicit poles, $\mathrm{d}\hat{\sigma}^{\mathbf{T,b}}_{\mathrm{NNLO}}$

To construct a subtraction term for implicit singularities in real–virtual corrections it is useful to introduce two terms,

$$\mathrm{d}\hat{\sigma}^{T,b}_{\mathrm{NNLO}} = \mathrm{d}\hat{\sigma}^{T,b_1}_{\mathrm{NNLO}} + \mathrm{d}\hat{\sigma}^{T,b_2}_{\mathrm{NNLO}}, \tag{4.122}$$

where each of them mimics one of the structures that are present in the factorization behaviour of one-loop amplitudes in single unresolved limits [96] that we observed in (3.39),

$$\text{1-loop} \;\to \underbrace{(\text{tree} \times \text{loop})}_{\mathrm{d}\hat{\sigma}^{T,b_1}_{\mathrm{NNLO}}} + \underbrace{(\text{loop} \times \text{tree})}_{\mathrm{d}\hat{\sigma}^{T,b_2}_{\mathrm{NNLO}}}.$$

The first part of the subtraction term, $\mathrm{d}\hat{\sigma}^{T,b_1}_{\mathrm{NNLO}}$, includes a tree-level three-parton antenna function multiplied with an n-parton one-loop reduced matrix element whereas the second part, $\mathrm{d}\hat{\sigma}^{T,b_2}_{\mathrm{NNLO}}$, involves a one-loop three-parton antenna function multiplied with a tree-level n-parton reduced matrix element. However, as both contributions contain explicit poles and to avoid the introduction of them as spurious explicit IR poles—the explicit poles of the real–virtual squared matrix element are already canceled by $\mathrm{d}\hat{\sigma}^{T,a}_{\mathrm{NNLO}}$—additional terms have to be included in both contributions. The explicit poles in $\mathrm{d}\hat{\sigma}^{T,b_1}_{\mathrm{NNLO}}$ are present in the one-loop matrix element and can be removed by an integrated antenna string familiar already from NLO. This leads to the first part of the subtraction term,

$$\begin{aligned}\mathrm{d}\hat{\sigma}^{T,b_1}_{\mathrm{NNLO}} =& \frac{\mathcal{N}_C^{\varepsilon}\,\mathcal{N}^{RV}_{\mathrm{NNLO}}}{S_{n+1}} \int \frac{\mathrm{d}z_a}{z_a}\frac{\mathrm{d}z_b}{z_b}\mathrm{d}\Phi_{n+1}(\{p_i\}_{i=1}^{n+1}; z_a p_a, z_b p_b) \\ &\times \sum_j X_3^0(i,j,k)\Big\{\delta(1-z_a)\delta(1-z_b)\; M_n^1(\{\tilde{p}_i\}_{i=1}^{n+1}\setminus\{\tilde{p}_j\}; z_a p_a, z_b p_b) \\ &+ c_J \boldsymbol{\mathcal{J}}_n^{(1)}(\{\tilde{p}_i\}_{i=1}^{n+1}\setminus\{\tilde{p}_j\})|\mathcal{M}_n^0(\{\tilde{p}_i\}_{i=1}^{n+1}\setminus\{\tilde{p}_j\}; z_a p_a, z_b p_b)|^2\Big\}\; J_n^{(n)}(\{\tilde{p}_i\}_{i=1}^{n+1}\setminus\{\tilde{p}_j\}),\end{aligned} \tag{4.123}$$

where we abbreviate the sum of antenna strings by

$$\begin{aligned}\boldsymbol{\mathcal{J}}_n^{(1)}(\hat{\tilde{1}}_q, i_g, j_g, \cdots, k_g, l_g, \hat{\tilde{2}}_{\bar{q}}) =& \boldsymbol{\mathcal{J}}_2^{(1)}(\hat{\tilde{1}}_q, i_g) + \boldsymbol{\mathcal{J}}_2^{(1)}(i_g, j_g) + \cdots \\ &+ \boldsymbol{\mathcal{J}}_2^{(1)}(k_g, l_g) + \boldsymbol{\mathcal{J}}_2^{(1)}(\hat{\tilde{2}}_q, l_g),\end{aligned} \tag{4.124}$$

and write the contribution of the one-loop matrix element to the squared matrix element as,

$$M_n^1 = 2\mathrm{Re}\{(\mathcal{M}_n^0)^*\mathcal{M}_n^1\}. \tag{4.125}$$

The constant c_J equals one in all cases relevant for this thesis but is in general given by

$$c_J = \begin{cases} 2 & n = 2 \text{ and all particles are gluons,} \\ 1 & \text{otherwise.}\end{cases} \tag{4.126}$$

Integrated over the unresolved antenna phase space, $\mathrm{d}\hat{\sigma}^{T,b_1}_{\mathrm{NNLO}}$ reappears as part of the double-virtual subtraction term.

The (loop×tree) contribution to the subtraction term also includes explicit IR poles that need to be canceled by adding additional terms. Including the additional terms needed to cancel all spurious explicit poles the complete subtraction term is given by,

$$\begin{aligned}\mathrm{d}\hat{\sigma}^{T,b_2}_{\mathrm{NNLO}} =& \frac{\mathcal{N}^{\varepsilon}_{\mathcal{C}}\,\mathcal{N}^{RV}_{\mathrm{NNLO}}}{S_{n+1}} \int \frac{\mathrm{d}z_a}{z_a}\frac{\mathrm{d}z_b}{z_b}\mathrm{d}\Phi_{n+1}(\{p_i\}^{n+1}_{i=1}; z_a p_a, z_b p_b) \\ &\times \sum_j \Big[X^1_3(i,j,k)\delta(1-z_a)\delta(1-z_b) + \boldsymbol{\mathcal{J}}^{(1)}_X(i,j,k) X^0_3(i,j,k) \\ &\qquad - M_X X^0_3(i,j,k)\boldsymbol{\mathcal{J}}^{(1)}_2(\tilde{p}_i,\tilde{p}_k)\Big] \\ &\times |\mathcal{M}^0_n(\{\tilde{p}_i\}^{n+1}_{i=1}\setminus\{\tilde{p}_j\}; z_a p_a, z_b p_b)|^2 J^{(n)}_n(\{\tilde{p}_i\}^{n+1}_{i=1}\setminus\{\tilde{p}_j\}),\end{aligned} \tag{4.127}$$

where

$$\boldsymbol{\mathcal{J}}^{(1)}_X = \sum_{(i,j)=1}^{N_X} \boldsymbol{\mathcal{J}}^{(1)}_2(i,j). \tag{4.128}$$

The constants N_X is the number of colour-connected parton pairs (i,j) within X^1_3 and both N_X and M_X are equal to 1 in all cases relevant for this work. However, in general they differ from one [96] and have to be adapted depending on the type of one-loop antenna X^1_3 in (4.127). The structure of the additional terms in (4.127) used to remove explicit poles is determined by X^1_3 defined in (4.43),

$$X^1_3(i,j,k) = S_{ijk,IK}\frac{|\mathcal{M}^1_{ijk}|^2}{|\mathcal{M}^0_{IK}|^2} - X^0_3(i,j,k)\frac{|\mathcal{M}^1_{IK}|^2}{|\mathcal{M}^0_{IK}|^2}. \tag{4.129}$$

The part proportional to $\boldsymbol{\mathcal{J}}^{(1)}_X X^0_3$ cancels the poles of the one-loop three-parton contribution to X^1_3, while the part including $X^0_3\boldsymbol{\mathcal{J}}^{(1)}_2$ cancels the explicit poles in the two-parton one-loop contribution.

The integrated version of the two terms that include X^1_3 and $X^0_3\boldsymbol{\mathcal{J}}^{(1)}_2$ are reintroduced in the double-virtual subtraction term, whereas the term including $\boldsymbol{\mathcal{J}}^{(1)}_X X^0_3$ is the integrated version of the double-real subtraction term $\mathrm{d}\hat{\sigma}^{\mathrm{S},b_2}_{\mathrm{NNLO}}$.

4.5.2.4 Renormalization subtraction term, $\mathrm{d}\hat{\sigma}^{\mathbf{T},\mathbf{b_3}}_{\mathrm{NNLO}}$

In the calculation of one-loop three-parton antenna functions the renormalization scale is fixed to s_{ijk}. However, to ensure a cancellation of explicit IR poles it is necessary to change the renormalization scale of the one-loop antennae to different values dictated by the renormalization scale choice used in other one-loop quantities present in the calculation such as M^1_n in (4.123). The renormalization scale used in the one-loop antennae (4.43) can be adapted by using the transformation rule

$$X^1_{3,ijk} \to X^1_{3,ijk} + \frac{\beta_0}{\epsilon}\, X^0_{3,ijk}\left(|s_{ijk}|^{-\epsilon} - (\mu^2)^{-\epsilon}\right). \tag{4.130}$$

The coefficient in the QCD β function β_0 is given by

$$\beta_0 = b_0 N + b_{0,F} N_F, \tag{4.131}$$

where $b_0 = 11/6$ and $b_{0,F} = -1/3$. In order to understand this structure we split the discussion into antennae constructed from photons and the Higgs boson, and antennae constructed from neutralino decays. In cases where the processes photon $\to q\bar{q}$ and Higgs $\to$ partons are used to construct the corresponding antennae the tree-level $1 \to 2$ matrix elements included in $X^1_{3,ijk}$ involve no strong coupling constant and are therefore not affected by QCD renormalization transformations if we choose to renormalize only the coupling of the theory. The respective $1 \to 3$ tree-level processes, however, are proportional to the strong coupling constant and therefore lead to a counterterm diagram that is proportional to the renormalization constant δZ_{α_s} of the strong coupling constant. As this counterterm diagram is sufficient to cancel all UV poles of the one-loop correction to the $1 \to 3$ processes included in (4.43), this allows us to identify the UV pole structure of the one-loop three-parton antennae calculated from photon and Higgs decays

$$X^1_{3,ijk}\Big|_{\text{UV-Poles}} = S_{ijk,IK} \frac{|\mathcal{M}^1_{ijk}|^2}{|\mathcal{M}^0_{IK}|^2}\Big|_{\text{UV-Poles}} = \delta Z_{\alpha_s} X^0_{3,ijk}, \tag{4.132}$$

where we used that the one-loop $1 \to 2$ part is free of UV poles (or to be more precise, they cancel against IR poles with the opposite sign), as argued above. In case of the neutralino decay the $1 \to 2$ decay matrix element is proportional to the effective coupling η which is affected by QCD renormalization transformations and therefore also the $1 \to 2$ part in (4.43) contributes to the UV pole structure (see [105] for the Feynman rules of the relevant neutralino decays),

$$\begin{aligned} X^1_{3,ijk}\Big|_{\text{UV-Poles}} &= S_{ijk,IK} \frac{|\mathcal{M}^1_{ijk}|^2}{|\mathcal{M}^0_{IK}|^2}\Big|_{\text{UV-Poles}} - X^0_{3,ijk} \frac{|\mathcal{M}^1_{IK}|^2}{|\mathcal{M}^0_{IK}|^2}\Big|_{\text{UV-Poles}} \\ &= (\delta Z_{\alpha_s} + \delta Z_\eta) X^0_{3,ijk} - \delta Z_\eta X^0_{3,ijk} \end{aligned} \tag{4.133}$$

Therefore, for all antennae independent of their specific type we obtain

$$X^1_{3,ijk}\Big|_{\text{UV-Poles}} = \delta Z_{\alpha_s} X^0_{3,ijk} = \mu^{2\epsilon} \frac{\beta_0}{\epsilon} \frac{\alpha_s}{2\pi} X^0_{3,ijk}, \tag{4.134}$$

leading to the result in (4.130). Note that in (4.130) the factor $\alpha_s/(2\pi)$ is not included as it is part of $\mathcal{N}^{RV}_{\text{NNLO}}$ included in the complete subtraction term,

$$\begin{aligned} \mathrm{d}\hat{\sigma}^{T,b_3}_{\text{NNLO}} =& \frac{\mathcal{N}^{\varepsilon}_{\mathcal{C}} \mathcal{N}^{RV}_{\text{NNLO}}}{S_{n+1}} \int \frac{\mathrm{d}z_a}{z_a} \frac{\mathrm{d}z_b}{z_b} \mathrm{d}\Phi_{n+1}(\{p_i\}^{n+1}_{i=1}; z_a p_a, z_b p_b) \\ &\times \sum_j \frac{\beta_0}{\epsilon} \left(\left(\frac{\mu^2}{|s_{ijk}|} \right)^{\epsilon} - 1 \right) X^0_3(i,j,k) \delta(1-z_a) \delta(1-z_b) \\ &\times |\mathcal{M}^0_n(\{\tilde{p}_i\}^{n+1}_{i=1} \setminus \{\tilde{p}_j\}; z_a p_a, z_b p_b)|^2 J^{(n)}_n(\{\tilde{p}_i\}^{n+1}_{i=1} \setminus \{\tilde{p}_j\}), \end{aligned} \tag{4.135}$$

which adjusts the renormalization scale used to calculate the one-loop three-parton antennae to the one used in a calculation where antenna subtraction is applied. The colour decomposition of β_0 in (4.131) allows for the identification of terms that are needed in a certain part of a calculation organized by colour decomposition. More explicitly, we can read off that there is no subleading colour contribution to the antenna subtraction term $\mathrm{d}\hat{\sigma}^{T,b_3}_{\text{NNLO}}$.

4.5.2.5 Real–virtual almost-colour-connected subtraction term, $\mathrm{d}\hat{\sigma}^{\mathbf{T,c}}_{\mathrm{NNLO}}$

The last ingredient of the real–virtual subtraction term is obtained by integrating the double-real subtraction term for almost-colour-connected configurations, $\mathrm{d}\hat{\sigma}^{S,c}_{\mathrm{NNLO}}$, over the single unresolved antenna phase space,

$$\begin{aligned}
\mathrm{d}\hat{\sigma}^{T,c}_{NNLO} = &-\frac{\mathcal{N}^{\varepsilon}_{\mathcal{C}}\mathcal{N}^{RV}_{\mathrm{NNLO}}}{S_{n+1}}\int\frac{\mathrm{d}z_a}{z_a}\frac{\mathrm{d}z_b}{z_b}\mathrm{d}\Phi_{n+1}(\{p_i\}_{i=1}^{n+1};z_ap_a,z_bp_b) \\
&\times\Bigg\{\frac{1}{2}\sum_j\Bigg[\ \big(\mathcal{X}_3^0(s_{ik})-\mathcal{X}_3^0(s_{(ij)(jk)})\big) \\
&-\ \big(\mathcal{X}_3^0(s_{ai})-\mathcal{X}_3^0(s_{a(ij)})\big)-\ \big(\mathcal{X}_3^0(s_{kb})-\mathcal{X}_3^0(s_{(kj)b})\big) \\
&-\Bigg(\big(\mathcal{S}(s_{ik},s_{ik},1)-\mathcal{S}(s_{(ij)(jk)},s_{ik},x_{(ij)(jk),ik})\big) \\
&-\big(\mathcal{S}(s_{ai},s_{ik},x_{ai,ik})-\mathcal{S}(s_{a(ij)},s_{ik},x_{a(ij),ik})\big) \\
&-\big(\mathcal{S}(s_{kb},s_{ik},x_{kb,ik})-\mathcal{S}(s_{(jk)b},s_{ik},x_{(jk)b,ik})\big)\Bigg)\delta(1-z_a)\delta(1-z_b)\Bigg]\Bigg\} \\
&\times X_3^0(i,j,k)|\mathcal{M}_n^0(\{\tilde{p}_i\}_{i=1}^{n+1}\setminus\{\tilde{p}_j\};z_ap_a,z_bp_b)|^2J_n^{(n)}(\{\tilde{p}_i\}_{i=1}^{n+1}\setminus\{\tilde{p}_j\}),
\end{aligned} \tag{4.136}$$

where

$$\mathcal{S}(s_{ac},s_{IK},x_{ac,IK})=\frac{1}{C(\epsilon)}\int\mathrm{d}\Phi_{X_{ijk}}S_{ajc}. \tag{4.137}$$

The terms in (4.136) involving integrated antenna functions with mapped momenta, $\mathcal{X}_3^0(s_{(ij)(jk)})$, $\mathcal{X}_3^0(s_{a(ij)})$, and $\mathcal{X}_3^0(s_{(kj)b})$, are introduced in order to ensure IR finiteness of the subtraction term. They have to be canceled in the double-virtual subtraction term. The result for the soft functions $\mathcal{S}$ is given by [95],

$$\mathcal{S}(s_{ac},s_{ik},x_{ac,ik})=\left(\frac{s_{ik}}{\mu^2}\right)^{-\epsilon}\left[\frac{1}{\epsilon^2}-\frac{1}{\epsilon}\ln\left(x_{ac,ik}\right)-\mathrm{Li}_2\left(-\frac{1-x_{ac,ik}}{x_{ac,ik}}\right)-\frac{7\pi^2}{12}+\mathcal{O}(\epsilon)\right], \tag{4.138}$$

and $x_{ac,ik}$ is defined as

$$x_{ac,ik}=\frac{s_{ac}s_{ik}}{(s_{ai}+s_{ak})(s_{ci}+s_{ck})}\,. \tag{4.139}$$

4.5.3 Double-virtual subtraction term

In the double-virtual subtraction term no new subtraction terms can be introduced and only integrated versions of contributions present in the double-real or real–virtual subtraction terms that have not yet been canceled are included. However, according to the KLN theorem this has to be sufficient to cancel all explicit IR singularities present in double-virtual corrections to underlying tree-level squared matrix elements when including mass factorization kernels to account for hadronic collinear singularities. The double-virtual subtraction term $\mathrm{d}\hat{\sigma}^{U}_{\mathrm{NNLO}}$ receives contributions that contain a product of a integrated

three-parton antenna function and a one-loop n-parton matrix element, $\mathrm{d}\hat{\sigma}^{U,A}_{\mathrm{NNLO}}$, contributions that include a convolution of two integrated three-parton antennae, $\mathrm{d}\hat{\sigma}^{U,B}_{\mathrm{NNLO}}$, and a last ingredient, $\mathrm{d}\hat{\sigma}^{U,C}_{\mathrm{NNLO}}$, that contains integrated four-parton antenna functions,

$$\mathrm{d}\hat{\sigma}^{U}_{\mathrm{NNLO}} = \mathrm{d}\hat{\sigma}^{U,A}_{\mathrm{NNLO}} + \mathrm{d}\hat{\sigma}^{U,B}_{\mathrm{NNLO}} + \mathrm{d}\hat{\sigma}^{U,C}_{\mathrm{NNLO}}. \tag{4.140}$$

All of the three contributions include parts of the NLO mass factorization kernel relevant for double-virtual corrections (4.111). The distribution of different contributions to the mass factorization kernel amongst the ingredients of the double-virtual subtraction function is subject of the next section.

4.5.3.1 Mass factorization term for double virtual corrections, $\mathrm{d}\hat{\sigma}^{\mathbf{MF,2}}_{\mathrm{NNLO}}$

We introduced the NNLO mass factorization contribution relevant for the NNLO double-virtual correction in (4.111). It is again useful to split $\mathrm{d}\hat{\sigma}^{MF,2}_{ij,NNLO}$ into three parts,

$$\mathrm{d}\hat{\sigma}^{MF,2}_{ij,NNLO} = \mathrm{d}\hat{\sigma}^{MF,2,A}_{ij,NNLO} + \mathrm{d}\hat{\sigma}^{MF,2,B}_{ij,NNLO} + \mathrm{d}\hat{\sigma}^{MF,C}_{ij,NNLO}, \tag{4.141}$$

where each of the terms $\mathrm{d}\hat{\sigma}^{MF,2,i}_{ij,NNLO}$ is combined with $\mathrm{d}\hat{\sigma}^{U,i}_{\mathrm{NNLO}}$ in the construction of the double-virtual subtraction terms. Explicitly, the individual contributions of the mass factorization terms to the subtraction terms read,

$$\mathrm{d}\hat{\sigma}^{MF,2,A}_{ij,NNLO} = -\int \frac{\mathrm{d}z_a}{z_a}\frac{\mathrm{d}z_b}{z_b} \left(\frac{\alpha_s N}{2\pi}\right) \bar{C}(\epsilon)\, \Gamma^{(1)}_{ij;kl}\left(\mathrm{d}\hat{\sigma}^{V}_{kl,NLO} - \frac{\beta_0}{\epsilon}\mathrm{d}\hat{\sigma}_{kl,LO}\right), \tag{4.142}$$

$$\begin{aligned}\mathrm{d}\hat{\sigma}^{MF,2,B}_{ij,NNLO} = &+\int \frac{\mathrm{d}z_a}{z_a}\frac{\mathrm{d}z_b}{z_b} \left(\frac{\alpha_s N}{2\pi}\right) \bar{C}(\epsilon)\, \Gamma^{(1)}_{ij;kl}\mathrm{d}\hat{\sigma}^{T}_{kl,NLO} \\ &-\int \frac{\mathrm{d}z_a}{z_a}\frac{\mathrm{d}z_b}{z_b} \left(\frac{\alpha_s N}{2\pi}\right)^2 \bar{C}(\epsilon)^2\, \frac{1}{2}\big[\Gamma^{(1)}_{ij;ab}\otimes\Gamma^{(1)}_{ab;kl}\big]\mathrm{d}\hat{\sigma}_{kl,LO},\end{aligned} \tag{4.143}$$

$$\mathrm{d}\hat{\sigma}^{MF,2,C}_{ij,NNLO} = -\int \frac{\mathrm{d}z_a}{z_a}\frac{\mathrm{d}z_b}{z_b} \left(\frac{\alpha_s N}{2\pi}\right)^2 \bar{C}(\epsilon)^2\, \overline{\Gamma}^{(2)}_{ij;kl}\ \mathrm{d}\hat{\sigma}_{kl,LO}, \tag{4.144}$$

where we have introduced the convolution of two functions $f(x_a, x_b)$ and $g(x_a, x_b)$,

$$\big[f\otimes g\big](z_1,z_2) \equiv \int \mathrm{d}x_1\mathrm{d}x_2\mathrm{d}y_1\mathrm{d}y_2 f(x_1,x_2)g(y_1,y_2)\delta(z_1-x_1y_1)\delta(z_2-x_2y_2). \tag{4.145}$$

We also used the decomposition of the genuine NNLO mass factorization kernel,

$$\Gamma^{(2)}_{ij;kl}(z_1,z_2) = \overline{\Gamma}^{(2)}_{ij;kl}(z_1,z_2) - \frac{\beta_0}{\epsilon}\Gamma^{(1)}_{ij;kl}(z_1,z_2) + \frac{1}{2}\big[\Gamma^{(1)}_{ij;ab}\otimes\Gamma^{(1)}_{ab;kl}\big](z_1,z_2), \tag{4.146}$$

where $\overline{\Gamma}^{(2)}_{ij;kl}$ fulfills the relation

$$\overline{\Gamma}^{(2)}_{ij;kl}(z_1,z_2) = \overline{\Gamma}^{(2)}_{ik}(z_1)\delta_{jl}\delta(1-z_2) + \overline{\Gamma}^{(2)}_{jl}(z_2)\delta_{ik}\delta(1-z_1) \tag{4.147}$$

and is given by,

$$\overline{\Gamma}^{(2)}_{ij}(z) = -\frac{1}{2\epsilon}\left(p^1_{ij}(z) + \frac{\beta_0}{\epsilon}p^0_{ij}(z)\right). \tag{4.148}$$

Note that in (4.143) we have two different contributions, one including a convolution and another including just a normal product of a mass factorization kernel and the integrated NLO subtraction term. In order to combine both contributions with the NNLO subtraction term $\mathrm{d}\hat{\sigma}^{U,B}_{\mathrm{NNLO}}$, which is proportional to convolutions of integrated three-parton antennae, it is useful to write (4.143) purely in terms of convolutions as well. We can achieve this by inserting the explicit expression for $\mathrm{d}\hat{\sigma}^{T}_{kl,NLO}$ (not including potential mass factorization kernels present at NLO) which schematically leads to

$$\begin{aligned}\mathrm{d}\hat{\sigma}^{MF,2,B}_{ij,NNLO} = &-\left(\frac{\alpha_s N}{2\pi}\right)^2 \bar{C}(\epsilon)^2 \int \frac{\mathrm{d}z_a}{z_a}\frac{\mathrm{d}z_b}{z_b}\int \frac{\mathrm{d}x_a}{x_a}\frac{\mathrm{d}x_b}{x_b} \\ &\times \Gamma^{(1)}_{ij;kl}(z_a,z_b)\mathcal{X}^0_3(x_a,x_b)\ \mathrm{d}\hat{\sigma}_{kl,LO}(p_1,\ldots,p_n;x_a z_a p_a, x_b z_b p_b) \\ &-\int \frac{\mathrm{d}z_a}{z_a}\frac{\mathrm{d}z_b}{z_b}\ \left(\frac{\alpha_s N}{2\pi}\right)^2 \bar{C}(\epsilon)^2 \frac{1}{2}\big[\Gamma^{(1)}_{ij;ab}\otimes\Gamma^{(1)}_{ab;kl}\big]\mathrm{d}\hat{\sigma}_{kl,LO}.\end{aligned}$$

If we now insert two additional integrals $1 = \prod_{i=a,b}\int \mathrm{d}y_i\ \delta(y_i - x_i z_i)$ we obtain the desired form of $\mathrm{d}\hat{\sigma}^{MF,2,B}_{ij,NNLO}$ purely in terms of convolutions using (4.145),

$$\begin{aligned}\mathrm{d}\hat{\sigma}^{MF,2,B}_{ij,NNLO} = &-\int \frac{\mathrm{d}z_a}{z_a}\frac{\mathrm{d}z_b}{z_b}\ \left(\frac{\alpha_s N}{2\pi}\right)^2 \bar{C}(\epsilon)^2 \\ &\times\left\{\big[\Gamma^{(1)}_{ij;kl}\otimes\mathcal{X}^0_3\big] + \frac{1}{2}\big[\Gamma^{(1)}_{ij;ab}\otimes\Gamma^{(1)}_{ab;kl}\big]\right\}\mathrm{d}\hat{\sigma}_{kl,LO}.\end{aligned} \tag{4.149}$$

4.5.3.2 Double-virtual subtraction term, $\mathrm{d}\hat{\sigma}^{\mathbf{U,A}}_{\mathrm{NNLO}}$

The double-virtual subtraction term $\mathrm{d}\hat{\sigma}^{U,A}_{\mathrm{NNLO}}$ receives contributions from parts of real–virtual subtraction terms integrated over the single unresolved antenna phase space and one part of the NNLO mass factorization contribution,

$$\mathrm{d}\hat{\sigma}^{U,A}_{ij,\mathrm{NNLO}} = \int_1 \mathrm{d}\hat{\sigma}^{T,b_1}_{ij,NNLO}\Big|_{\propto M^{(1)}_n} + \int_1 \mathrm{d}\hat{\sigma}^{T,b_3}_{ij,NNLO}\Big|_{\mu^2=0} + \mathrm{d}\hat{\sigma}^{MF,2,A}_{ij,NNLO}, \tag{4.150}$$

where the first part is the integrated version of the (tree×loop) real–virtual subtraction term, $\mathrm{d}\hat{\sigma}^{T,b_1}_{ij,NNLO}$, including only the part proportional to the one-loop n-parton matrix element and not the one proportional to the integrated three-parton antenna string. The second contribution is given by the real–virtual one-loop renormalization subtraction term (4.135) including only the contribution that is not proportional to $(\mu^2/|s_{ijk}|)^\epsilon$ integrated over the single-unresolved antenna phase space. The complete subtraction term can be written as

$$\begin{aligned}\mathrm{d}\hat{\sigma}^{U,A}_{ij,NNLO} = &-\frac{\mathcal{N}^{\varepsilon}_{\mathcal{C}}\mathcal{N}^{VV}_{\mathrm{NNLO}}}{S_n}\int \frac{\mathrm{d}z_a}{z_a}\frac{\mathrm{d}z_b}{z_b}\mathrm{d}\Phi_n(\{p_i\}^n_{i=1};z_a p_a, z_b p_b) \\ &\times \boldsymbol{\mathcal{J}}^{(1)}_n(\{p_i\}^n_{i=1};z_a p_a, z_b p_b)\Big(\big[M^1_n\, J^{(n)}_n\big](\{p_i\}^n_{i=1};z_a p_a, z_b p_b) \\ &-\frac{\beta_0}{\epsilon}\big[|\mathcal{M}^0_n|^2\, J^{(n)}_n\big](\{p_i\}^n_{i=1};z_a p_a, z_b p_b)\Big),\end{aligned} \tag{4.151}$$

where we have introduced

$$\mathcal{N}^{VV}_{\text{NNLO}} = C(\epsilon)\mathcal{N}^{RV}_{\text{NNLO}}. \tag{4.152}$$

Note that the term proportional to β_0 does not give any contribution at subleading colour which can be seen by considering the colour decomposition of β_0 in (4.131).

4.5.3.3 Double-virtual subtraction term, $\mathrm{d}\hat{\sigma}^{\mathbf{U,B}}_{\text{NNLO}}$

This subtraction term is generated by the integrated version of the remaining part of $\mathrm{d}\hat{\sigma}^{T,b_1}_{ij,NNLO}$ which has not been included in $\mathrm{d}\hat{\sigma}^{U,A}_{\text{NNLO}}$, some of the terms additionally introduced in $\mathrm{d}\hat{\sigma}^{T,c}_{ij,NNLO}$ integrated over the single-unresolved antenna phase space, the integral of $\mathrm{d}\hat{\sigma}^{T,d}_{ij,NNLO}$, and the corresponding mass factorization term. In terms of convolutions of integrated antenna strings the complete subtraction term reads

$$\begin{aligned}\mathrm{d}\hat{\sigma}^{U,B}_{ij,NNLO} = &- \frac{\mathcal{N}^{\varepsilon}_{\mathcal{C}}\,\mathcal{N}^{VV}_{\text{NNLO}}}{S_n}\int \frac{\mathrm{d}z_a}{z_a}\frac{\mathrm{d}z_b}{z_b}\mathrm{d}\Phi_n(\{p_i\}^n_{i=1}; z_a p_a, z_b p_b)\\ &\times \frac{1}{2}\big[\boldsymbol{\mathcal{J}}^{(1)}_n(1,\dots,n)\otimes\boldsymbol{\mathcal{J}}^{(1)}_n(1,\dots,n)\big](z_a,z_b)\\ &\times \big[|\mathcal{M}^0_n|^2\, J^{(n)}_n\big](\{p_i\}^n_{i=1}; z_a p_a, z_b p_b).\end{aligned} \tag{4.153}$$

To our best knowledge, not all of the needed convolutions of integrated antenna strings are publicly available, in particular not the ones that are needed for this work. The analytic calculation of these convolutions is part of this work and details of this calculation are given when they become first relevant in Section 6. Partial analytic results for the convolutions are given in App. E. For completeness we mention that in [114] the relevant convolutions for gluon scattering at NNLO are explicitly given in the appendices.

4.5.3.4 Double-virtual subtraction term, $\mathrm{d}\hat{\sigma}^{\mathbf{U,C}}_{\text{NNLO}}$

The last double-virtual subtraction term is generated by all contributions from the double-real and real–virtual subtraction term that so far have no integrated counterparts and the appropriate double-virtual mass factorization term. In terms of the NNLO antenna string $\boldsymbol{\mathcal{J}}^{(2)}_2$ it is given by

$$\begin{aligned}\mathrm{d}\hat{\sigma}^{U,C}_{NNLO} = &- \frac{\mathcal{N}^{\varepsilon}_{\mathcal{C}}\,\mathcal{N}^{VV}_{\text{NNLO}}}{S_n}\sum_{i,j}\int \frac{\mathrm{d}z_a}{z_a}\frac{\mathrm{d}z_b}{z_b}\mathrm{d}\Phi_n(\{p_i\}^n_{i=1}; z_a p_a, z_b p_b)\\ &\times \boldsymbol{\mathcal{J}}^{(2)}_2(i,j)\ \big[|\mathcal{M}^0_n|^2\, J^{(n)}_n\big](\{p_i\}^n_{i=1}; z_a p_a, z_b p_b).\end{aligned} \tag{4.154}$$

The initial–initial antenna string is given by

$$\begin{aligned}\boldsymbol{\mathcal{J}}^{(2)}_2(\bar{p}_a,\bar{p}_b) =& c_1^{II}\mathcal{X}^0_4(s_{\bar{a}\bar{b}}) + c_2^{II}\tilde{\mathcal{X}}^0_4(s_{\bar{a}\bar{b}}) + c_3^{II}\mathcal{X}^1_3(s_{\bar{a}\bar{b}}) + \frac{\beta_0}{\epsilon}\left(\frac{|s_{\bar{a}\bar{b}}|}{\mu^2}\right)^{-\epsilon} c_4^{II}\mathcal{X}^0_3(s_{\bar{a}\bar{b}})\\ &+ c_5^{II}\mathcal{X}^0_3(s_{\bar{a}\bar{b}})\otimes\mathcal{X}^0_3(s_{\bar{a}\bar{b}}) - \overline{\Gamma}^{(2)}_{ij;kl}(z_a,z_b),\end{aligned} \tag{4.155}$$

including also the mass factorization contribution where the labels i,j specify the initial state partons of the cross section whereas k,l denote the initial state partons of the matrix element. Note that similar terms can be constructed for the final–final and initial–final case and are given in [96].

Chapter 5

QCD×electroweak $\mathcal{O}(N_f\alpha_s\alpha)$ corrections to single-W/Z production

Physics beyond the SM might show up in the tails of invariant-mass or transverse-momentum distributions outside the resonance regions of the DY-like produced intermediate W/Z bosons. Therefore, it is important to provide information about the size of $\mathcal{O}(\alpha_s\alpha)$ corrections in off-shell regions of phase space. This chapter is devoted to the description of $\mathcal{O}(N_f\alpha_s\alpha)$ corrections to DY-like W/Z-boson production and their fully differential calculation in the complete phase space. As the number of fermion flavours, N_f, is a free paramter of the theory they form a gauge-invariant part of the full set of $\mathcal{O}(\alpha_s\alpha)$ corrections. The restriction to NNLO QCD×electroweak corrections that are enhanced by the number of fermion families demands that all relevant diagrams include closed fermionic loops and therefore reduces the relevant diagrams describing $\mathcal{O}(\alpha_s\alpha)$ corrections considerably.

We start by establishing some basic facts about DY processes at leading order and proceed by describing the relevant ingredients contributing to $\mathcal{O}(N_f\alpha_s\alpha)$ corrections to the squared matrix element in Section 5.2.1. Radiative corrections introduce IR and UV divergences, which in principle require the use of complicated subtraction schemes at NNLO. However, the restriction to corrections that are N_f enhanced reduces not only the number of relevant diagrams but also the complexity of IR singularities. As there are no double-real N_f enhanced corrections, NLO antenna subtraction terms are sufficient to cancel all IR singularities at $\mathcal{O}(N_f\alpha_s\alpha)$ (relevant subtraction terms are discussed in Section 5.2.2). The renormalization procedure used to cancel local UV divergences and also UV subdivergences is discussed in Section 5.2.3. In this context we also discuss the extension of the complex-mass scheme to $\mathcal{O}(N_f\alpha_s\alpha)$ enabling us to treat the W/Z resonances in a gauge-invariant way. Finally, in Section 5.3 we study the effect of $\mathcal{O}(N_f\alpha_s\alpha)$ corrections on the (transverse) invariant-mass and transverse-momentum spectra of the W and Z boson, respectively. The results discussed in this chapter have been published in [115].

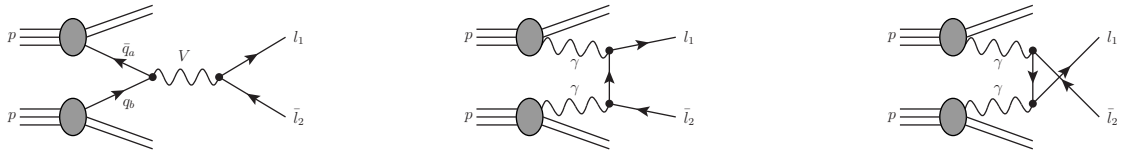

Figure 5.1: LO Feynman diagrams of DY processes, where $V = \gamma, Z, W^{\pm}$. The first diagram contributes to both the NC and the CC DY processes, whereas the second and third diagram only contributes to the NC DY processes.

5.1 The leading-order DY cross section

The DY-like pp scattering processes can be classified by the charge of the intermediate vector bosons,

$$\mathrm{pp} \to \mathrm{W}^{\pm} \to \ell^+\nu_\ell/\bar{\nu}_\ell\ell^- + X, \tag{5.1}$$

$$\mathrm{pp} \to \gamma/\mathrm{Z} \to \ell^+\ell^- + X, \tag{5.2}$$

where the former is the so-called charged-current (CC) process involving the charged intermediate W boson, and the latter the neutral-current (NC) process including the neutral intermediate photon or Z boson. The charged leptons $\ell^{\pm}$ in the final state are either $\mathrm{e}^{\pm}$ or $\mu^{\pm}$. While the CC process at leading order receives contributions solely from $q\bar{q}'$ annihilation, the NC process includes the production via $q\bar{q}$ annihilation and $\gamma\gamma$ scattering. As has been shown in [26, 28–30, 116], the $\gamma\gamma$ channel delivers only a small fraction to the NC cross section. Furthermore, it does not develop a Z-boson resonance due to the t-channel structure depicted in Fig. 5.1. In our calculation of $\mathcal{O}(N_f\alpha_s\alpha)$ corrections we do not include the $\gamma\gamma$ channel in the following and restrict our calculation to $q\bar{q}^{(\prime)}$ annihilation. This procedure is justified by the fact that already at NLO the EW corrections to the $\gamma\gamma$ channel turn out to be phenomenologically negligible [29].

In our calculations we use the five-flavour scheme with $q = u, d, c, s, b$ as potential massless incoming quarks. However, in the following sections in the context of the calculation of $\mathcal{O}(N_f\alpha_s\alpha)$ corrections, when the bottom quark shows up as virtual particle in closed fermionic loops we might also assign a non-vanishing mass to it while keeping all external fermions (including external bottom quarks) massless.

In terms of the Mandelstam variables

$$\hat{s} = (p_a + p_b)^2, \quad \hat{t} = (p_a - p_{\ell_1})^2, \quad \hat{u} = (p_a - p_{\ell_2})^2, \tag{5.3}$$

we can write the LO matrix element of the polarized generic amplitude, which describes the partonic scattering process involved in the hadronic processes (5.1) and (5.2), as

$$\mathrm{i}\mathcal{M}^{\bar{q}_a q_b \to \ell_1 \bar{\ell}_2}_{\mathrm{LO},V,\tau_q\tau_\ell} = \frac{\mathrm{i}e^2}{\hat{s} - \mu_V^2} C^{\tau_q}_{V\bar{q}_a q_b} C^{\tau_l}_{V\bar{\ell}_1\ell_2} \mathcal{A}^{\tau_q\tau_l}_{\mathrm{LO}}. \tag{5.4}$$

Due to the simple kinematics of the LO process the so-called strandard matrix elements $\mathcal{A}^{\tau_q\tau_l}_{\mathrm{LO}}$ reduce to

$$\mathcal{A}^{\pm\pm}_{\mathrm{LO}} = 2\hat{u}, \qquad \mathcal{A}^{\pm\mp}_{\mathrm{LO}} = 2\hat{t}. \tag{5.5}$$

The chiral couplings in (5.4) are given by

$$\begin{aligned} C^{+}_{Z\bar{f}f} =& \frac{s_w}{c_w} C^{\pm}_{\gamma\bar{f}f} = g^{+}_{f} = -\frac{s_w}{c_w} Q_f = g^{-}_{f} - \frac{I^3_{w,f}}{s_w c_w}, & C^{-}_{Z\bar{f}f} &= g^{-}_{f}, \\ C^{-}_{W^+u_i d_j} =& V_{ij}\, C^{-}_{W^+\bar{\nu}_l l} = V_{ij}\, C^{-}_{W^-\bar{l}\nu_l} = \frac{V_{ij}}{\sqrt{2}s_w}, & C^{-}_{W^-d_i u_j} &= \frac{V^*_{ji}}{\sqrt{2}s_w}. \end{aligned} \tag{5.6}$$

By the sign τ_f appearing in the chiral coupling $C^{\tau_f}_{V\bar{f}f}$ we can determine the helicity of an incoming (anti-)fermion to be $+\tau_f/2$ $(-\tau_f/2)$ and for an outgoing (anti-)fermion $-\tau_f/2$ $(+\tau_f/2)$. Therefore, only the helicity configurations $\sigma_{q_b} = -\sigma_{q_a} = \tau_q/2$ and $\sigma_{l_2} = -\sigma_{l_1} = \tau_q/2$ are non vanishing. The spin- and colour-averaged amplitude is obtained as

$$\langle|\mathcal{M}^{\bar{q}_a q_b\to\ell_1\bar{\ell}_2}_{\mathrm{LO},V}|^2\rangle = \frac{1}{N_C^2}\frac{1}{2^2}\sum_{\mathcal{C}_a,\mathcal{C}_b=1}^{N_C}\sum_{\tau_q,\tau_\ell=\pm}\delta_{\mathcal{C}_a\mathcal{C}_b}|\mathcal{M}^{\bar{q}_a q_b\to\ell_1\bar{\ell}_2}_{\mathrm{LO},V,\tau_q\tau_\ell}|^2, \tag{5.7}$$

which is needed in order to calculate the $2\to 2$ partonic cross section given in (A.37). The hadronic cross section (3.56) is calculated by convoluting the partonic cross section of partons a and b with the respective parton distribution functions,

$$\sigma^{\mathrm{LO}}(P_A,P_B) = \sum_{a,b}\int_0^1\frac{\mathrm{d}\xi_1}{\xi_1}\int_0^1\frac{\mathrm{d}\xi_2}{\xi_2}\, f_a(\xi_1,\mu_F^2) f_b(\xi_2,\mu_F^2)\,\mathrm{d}\hat{\sigma}^{\mathrm{LO}}_{ab}(\xi_1 P_A,\xi_2 P_B), \tag{5.8}$$

where $\mathrm{d}\hat{\sigma}^{\mathrm{LO}}_{ab}$ is normalized to the hadronic flux factor. Using (B.12), this equation can also be rewritten in terms of the Mandelstam variable $\hat{s}$ and the rapidity y,

$$\begin{aligned} \sigma^{\mathrm{LO}}(P_A,P_B) = \sum_{a,b}\int_0^1\mathrm{d}\hat{s}\int_0^1\mathrm{d}y\;& \frac{f_a(\xi_1(\hat{s},y),\mu_F^2)}{\xi_1(\hat{s},y)}\frac{f_b(\xi_2(\hat{s},y),\mu_F^2)}{\xi_2(\hat{s},y)} \\ &\times\frac{\partial(\xi_1,\xi_2)}{\partial(y,\hat{s})}\,\mathrm{d}\hat{\sigma}^{\mathrm{LO}}_{ab}(\xi_1(\hat{s},y)P_A,\xi_2(\hat{s},y)P_B). \end{aligned} \tag{5.9}$$

This shows that differential rapidity distributions

$$\begin{aligned} \frac{\mathrm{d}\sigma^{\mathrm{LO}}}{\mathrm{d}y}(y) = \sum_{a,b}\int_0^1\mathrm{d}\hat{s}\;& \frac{f_a(\xi_1(\hat{s},y),\mu_F^2)}{\xi_1(\hat{s},y)}\frac{f_b(\xi_2(\hat{s},y),\mu_F^2)}{\xi_2(\hat{s},y)} \\ &\times\frac{\partial(\xi_1,\xi_2)}{\partial(y,\hat{s})}\,\mathrm{d}\hat{\sigma}^{\mathrm{LO}}_{ab}(\xi_1(\hat{s},y)P_A,\xi_2(\hat{s},y)P_B) \end{aligned} \tag{5.10}$$

are dominated by the resonance region of the intermediate vector boson $V = W/Z$, as the dominant contribution from the partonic cross section $\mathrm{d}\hat{\sigma}^{\mathrm{LO}}_{ab}$ to the integral over $\hat{s}$ is coming from exactly this region.

5.2 Corrections of $\mathcal{O}(N_f\alpha_s\alpha)$ to single-W/Z production

5.2.1 Corrections of $\mathcal{O}(N_f\alpha_s\alpha)$ to the squared amplitude

A complete off-shell calculation of $\mathcal{O}(\alpha_s\alpha)$ corrections to DY processes is a very challenging task. To tackle the problem and proceed towards a full off-shell calculation one can select

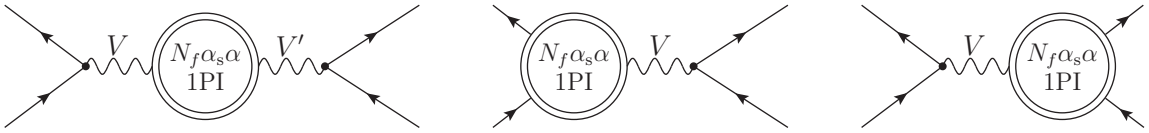

Figure 5.2: One-particle-irreducible virtual–virtual (vv-1PI) two-loop contributions to DY-like processes at $\mathcal{O}(N_f\alpha_s\alpha)$. In the first diagram the two-loop $\mathcal{O}(N_f\alpha_s\alpha)$ self-energy insertions are shown, whereas the second and third diagrams represent the finite gauge-boson–fermion counterterms described in Section 5.2.3.1.

gauge-invariant pieces and calculate them individually. In the following we choose the set of $\mathcal{O}(\alpha_s\alpha)$ corrections that is enhanced by the number of fermion flavours N_f in the SM. The enhancement factor N_f requires the contributing diagrams to include a closed fermion loop and therefore restricts the set of diagrams describing $\mathcal{O}(\alpha_s\alpha)$ corrections to DY-like W/Z production that have to be considered.

Due to colour conservation there are no genuine $\mathcal{O}(N_f\alpha_s\alpha)$ vertex corrections by closed fermion loops. As these closed fermionic loops are required for the N_f enhancement, genuine two-loop $\mathcal{O}(N_f\alpha_s\alpha)$ corrections show up in gauge-boson self-energies only. The possible double-virtual one-particle-irreducible (vv-1PI) diagrams are depicted in Fig. 5.2, where the shown vertex corrections are solely due to vertex counterterms that we will discuss below. The vv-1PI self-energy insertions can only be produced by closed quarks loops at $\mathcal{O}(N_f\alpha_s\alpha)$, as a gluon has to couple the fermions running in the loop.
Apart from the vv-1PI $\mathcal{O}(N_f\alpha_s\alpha)$ corrections there are also reducible double-virtual corrections (vv-red) of the form (one-loop)×(one-loop), which combine the insertion of the closed fermion loops in the EW gauge-boson propagators with the NLO QCD loop diagrams in all possible ways. The relevant diagrams of this kind are depicted in Fig. 5.3. In contrast to the vv-1PI corrections in the vv-red corrections the closed fermion loops can be produced by quarks and leptons as the involved gluon of the QCD correction is contained in a separate loop.
As shown in Fig. 5.4, similar to the vv-red contributions the real–virtual (rv) corrections combine NLO real QCD corrections with closed quark and lepton loops in the EW gauge-boson propagators. Note that we do not depict the qg induced scattering processes for brevity.
In general, radiative corrections at NNLO also include double-real corrections. At $\mathcal{O}(N_f\alpha_s\alpha)$ these corrections to the squared amplitude arise from interference contributions of amplitudes of the process $\bar{q}_a q_b \to Z/\gamma/W + \bar{q}'q'$ once with a intermediate photon and once with a gluon (see Fig. 6.2a and Fig. 6.3 for a pictorial representation of such amplitudes with $q_a = q_b = q'$). Therefore, there are no double-real contributions that have to be considered in case of $\mathcal{O}(N_f\alpha_s\alpha)$ NNLO corrections as they combine a g $\to q\bar{q}$ and $\gamma/\mathrm{Z} \to f\bar{f}$ splitting within a single spinor chain, and therefore vanish due to colour conservation. If we considered $\mathcal{O}(N_f\alpha_s^2)$ or $\mathcal{O}(N_f\alpha^2)$ corrections, such double-real corrections would lead to a non-vanishing contribution.

As discussed above, the only relevant vv-1PI two-loop building blocks at $\mathcal{O}(N_f\alpha_s\alpha)$ are given by the EW gauge-boson self-energies. For the relation between the two-point vertex functions $\Gamma^{V'V}$ and the self-energies $\Sigma^{V'V}$ in the 't Hooft-Feynman we use the conventions

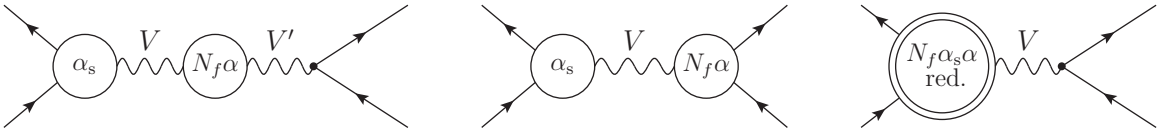

(a) Reducible virtual–virtual contributions within one diagram

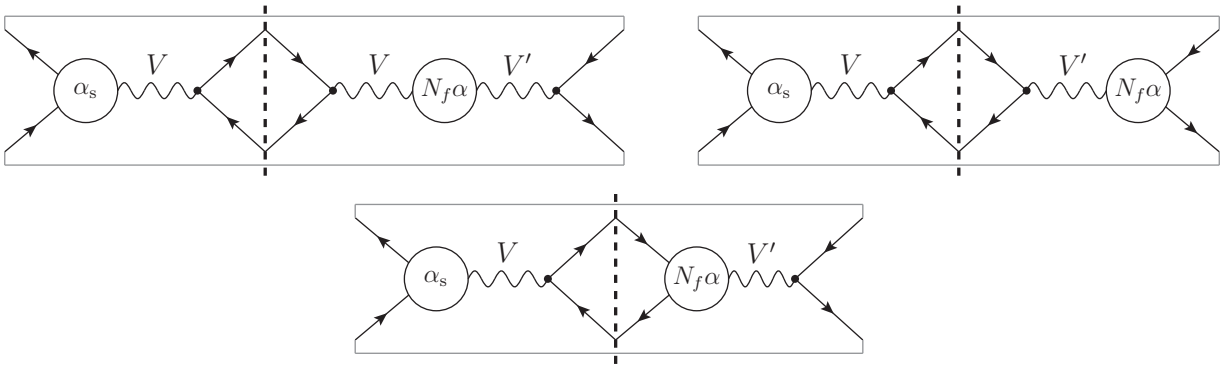

(b) Interference diagrams of type reducible virtual–virtual

Figure 5.3: Different types of reducible virtual–virtual (vv-red) diagrams contributing at $\mathcal{O}(N_f\alpha_s\alpha)$ to DY-like processes, where the relative orders of the loop corrections are indicated in the vertex blobs.

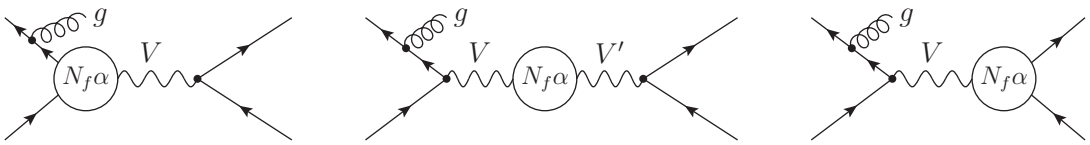

Figure 5.4: Different types of real–virtual (rv) diagrams contributing at $\mathcal{O}(N_f\alpha_s\alpha)$ to DY-like processes, where the relative orders of the loop corrections are indicated in the vertex blobs.

introduced before in (2.56) (identifying $\Sigma^{WW} \equiv \Sigma^{W}$),

$$\Gamma^{V'V}_{\mu\nu}(-k,k) = -\mathrm{i}g_{\mu\nu}(k^2 - M_V^2)\delta_{V'V} - \mathrm{i}\Sigma^{V'V}_{\mu\nu}(k^2), \tag{5.11}$$

with

$$\Sigma^{V'V}_{\mu\nu}(k^2) = \left(g_{\mu\nu} - \frac{k_\mu k_\nu}{k^2}\right)\Sigma^{V'V}_{\mathrm{T}}(k^2) + \frac{k_\mu k_\nu}{k^2}\Sigma^{V'V}_{\mathrm{L}}(k^2), \tag{5.12}$$

where $V'V = \gamma\gamma, \gamma\mathrm{Z}, \mathrm{ZZ}, \mathrm{WW}$, and k^2 denotes the virtuality of the gauge bosons V, V'. Including the $\mathcal{O}(N_f\alpha_s\alpha)$ EW gauge-boson self-energy contribution $\Sigma^{V'V}_{\mathrm{T},(\alpha_s\alpha)}$ in the amplitude of the leading-order DY process we obtain

$$\mathrm{i}\mathcal{M}^{q_a\bar{q}_b\to\ell_1\bar{\ell}_2}_{\Sigma_{\alpha_s\alpha},VV',\tau_q\tau_l} = \quad = -\frac{C^{\tau_l}_{V'\ell_1\bar{\ell}_2}}{C^{\tau_l}_{V\bar{\ell}_1\ell_2}}\frac{\Sigma^{V'V}_{\mathrm{T},(\alpha_s\alpha)}(p^2)}{p^2-\mu^2_{V'}}\mathrm{i}\mathcal{M}^{q_a\bar{q}_b\to\ell_1\bar{\ell}_2}_{\mathrm{LO},V,\tau_q\tau_\ell}, \tag{5.13}$$

where the expression for the LO amplitude is given in (5.4). The longitudinal part of the self-energy drops out in (5.13), as the momenta contained in its prefactors in (5.12) are contracted with the $Vq_a\bar{q}_b$- or $V'\ell_1\bar{\ell}_2$-vector current, which, using the Dirac equation

for massless fermions, $\not{p}_a u(p_a) = \bar{v}(p_b)\not{p}_b = 0$, leads to zero. Therefore, we only have to consider the transverse self-energy parts $\Sigma_{\mathrm{T}}^{V'V}$ in the following. Equation (5.13) is obtained by dressing the gauge-boson self-energy diagram with a propagator on each side and reducing the expression to the tree-level expression of the propagator,

$$\frac{\mathrm{i}g^{\mu\nu}}{p^2-\mu_V^2}\Sigma_{\nu\rho}^{V'V}(p^2)\frac{\mathrm{i}g^{\rho\eta}}{p^2-\mu_{V'}^2} = -\frac{\Sigma_{\mathrm{T}}^{V'V}(p^2)}{p^2-\mu_{V'}^2}\underbrace{\frac{\mathrm{i}g^{\mu\eta}}{p^2-\mu_V^2}}_{\to\mathcal{M}_{\mathrm{LO},V}^{q_a\bar{q}_b\to\ell_1\bar{\ell}_2}} + \ldots, \tag{5.14}$$

where the remaining terms that are not explicitly shown on the r.h.s. of the last equation vanish when contracted with the initial- or final-state vector current, as argued before.

Apart from the insertion of the gauge-boson self-energy we also need the counterterm contributions at the respective order in perturbation theory, as illustrated in Fig. 5.2. By the replacement

$$C_{V\bar{f}f}^{\sigma} \to C_{V\bar{f}f}^{\sigma}\delta_{V\bar{f}f,(\alpha_s\alpha)}^{\mathrm{ct},\sigma} \tag{5.15}$$

to one of the vertices in $\mathcal{M}_{\mathrm{LO},V,\tau_q\tau_\ell}^{q_a\bar{q}_b\to\ell_1\bar{\ell}_2}$ we obtain double-virtual vv-1PI diagrams including $\mathcal{O}(N_f\alpha_s\alpha)$ vertex counterterms. The double-virtual matrix elements including $\mathcal{O}(N_f\alpha_s\alpha)$ vertex counterterms are given by

$$\mathrm{i}\mathcal{M}_{\delta_{(\alpha_s\alpha)}^{\mathrm{ct}},V,\tau_q\tau_l}^{\bar{q}_a q_b\to\ell_1\bar{\ell}_2} = \mathrm{i}\big(\delta_{V\bar{q}_a q_b,(\alpha_s\alpha)}^{\mathrm{ct},\tau_q} + \delta_{V\bar{\ell}_1\ell_2,(\alpha_s\alpha)}^{\mathrm{ct},\tau_\ell}\big)\mathcal{M}_{\mathrm{LO},V,\tau_q\tau_\ell}^{q_a\bar{q}_b\to\ell_1\bar{\ell}_2}. \tag{5.16}$$

The relevant vertex counterterms $\delta_{V\bar{f}f,(\alpha_s\alpha)}^{\mathrm{ct},\sigma}$ are given in (5.49), (5.50), and (5.51). To calculate contributions to the squared matrix element we first add the matrix elements in (5.13) and (5.16),

$$\mathrm{i}\mathcal{M}_{\text{vv-1PI},VV',\tau_q\tau_l}^{\bar{q}_a q_b\to\ell_1\bar{\ell}_2} \equiv \mathrm{i}\mathcal{M}_{\Sigma_{\alpha_s\alpha},VV',\tau_q\tau_l}^{q_a\bar{q}_b\to\ell_1\bar{\ell}_2} + \mathrm{i}\,\delta_{VV'}\mathcal{M}_{\delta_{(\alpha_s\alpha)}^{\mathrm{ct}},V,\tau_q\tau_l}^{\bar{q}_a q_b\to\ell_1\bar{\ell}_2}. \tag{5.17}$$

The contribution of the double-virtual 1PI amplitudes to the squared amplitude at order $\mathcal{O}(N_f\alpha_s\alpha)$ is then obtained by projecting onto the LO amplitude and summing all relevant contributions,

$$M_{\text{vv-1PI},\tau_q\tau_\ell}^{q_a\bar{q}_b\to\ell_1\bar{\ell}_2} \equiv \begin{cases} \sum_{V,V',\tilde{V}=\gamma,Z} 2\mathrm{Re}\Big[\big(\mathcal{M}_{\mathrm{LO},\tilde{V},\tau_q\tau_\ell}^{q_a\bar{q}_b\to\ell_1\bar{\ell}_2}\big)^*\,\mathcal{M}_{\text{vv-1PI},VV',\tau_q\tau_l}^{q_a\bar{q}_b\to\ell_1\bar{\ell}_2}\Big], & \text{for NC,} \\ 2\mathrm{Re}\Big[\big(\mathcal{M}_{\mathrm{LO},WW,\tau_q\tau_\ell}^{q_a\bar{q}_b\to\ell_1\bar{\ell}_2}\big)^*\,\mathcal{M}_{\text{vv-1PI},WW,\tau_q\tau_l}^{q_a\bar{q}_b\to\ell_1\bar{\ell}_2}\Big], & \text{for CC.} \end{cases} \tag{5.18}$$

To calculate reducible diagrams, which contain a one-loop QCD vertex correction and a $\mathcal{O}(N_f\alpha)$ correction as shown in Fig. 5.3a, we use that the virtual QCD correction, given by

$$\delta_{\mathrm{V_s}}^{Z\bar{q}q}(s_{ab}) = \frac{\alpha_s}{2\pi}C_F\left[2\,I_{q\bar{q}}^{(1)}\Big(\epsilon,\frac{s_{ab}}{\mu^2}\Big) - 4\right], \tag{5.19}$$

factorizes from the matrix element. Therefore, all amplitudes of this form can be obtained by changing the perturbative order of the gauge-boson self-energies and vertex counterterms in (5.17) from $\mathcal{O}(N_f\alpha_s\alpha)$ to $\mathcal{O}(N_f\alpha)$ and multiplying by $\delta^{Z\bar{q}q}_{\mathrm{V_s}}$. In the last equation we used the $I^{(1)}_{q\bar{q}}$ operator, which was introduced in (3.19). The needed $\mathcal{O}(N_f\alpha)$ vertex counterterms can be found in e.g. [60] by taking only fermionic corrections to gauge-boson self-energies into account. The contribution of corrections that combine a virtual QCD correction with a $\mathcal{O}(N_f\alpha)$ correction within one diagram to the squared matrix element, can be combined with the interference contribution to the squared amplitude, obtained from an amplitude including a one-loop QCD correction combined with an amplitude that includes a $\mathcal{O}(N_f\alpha)$ correction. This leads to the following contribution to the squared amplitude,

$$\begin{aligned}
&2\,\mathrm{Re}\Big[\big(\delta_{VV'}\mathcal{M}^{\bar{q}_a q_b\to\ell_1\bar{\ell}_2}_{\mathrm{V_s}\otimes\delta^{\mathrm{ct}}_{(\alpha)},V,\tau_q\tau_l}+\mathcal{M}^{q_a\bar{q}_b\to\ell_1\bar{\ell}_2}_{\mathrm{V_s}\otimes\Sigma_\alpha,VV',\tau_q\tau_l}\big)^*\cdot\mathcal{M}^{q_a\bar{q}_b\to\ell_1\bar{\ell}_2}_{\mathrm{LO},\tilde{V},\tau_q\tau_\ell}\\
&\qquad+\big(\delta_{VV'}\mathcal{M}^{\bar{q}_a q_b\to\ell_1\bar{\ell}_2}_{\delta^{\mathrm{ct}}_{(\alpha)},V,\tau_q\tau_l}+\mathcal{M}^{q_a\bar{q}_b\to\ell_1\bar{\ell}_2}_{\Sigma_\alpha,VV',\tau_q\tau_l}\big)^*\cdot\mathcal{M}^{\bar{q}_a q_b\to\ell_1\bar{\ell}_2 g}_{\mathrm{V_s},V,\tau_q\tau_l}\Big]\\
=&2\,\mathrm{Re}\Big[\Big(\delta^{Z\bar{q}q}_{\mathrm{V_s}}+\big(\delta^{Z\bar{q}q}_{\mathrm{V_s}}\big)^*\Big)\cdot\big(\delta_{VV'}\mathcal{M}^{\bar{q}_a q_b\to\ell_1\bar{\ell}_2}_{\delta^{\mathrm{ct}}_{(\alpha)},V,\tau_q\tau_l}+\mathcal{M}^{q_a\bar{q}_b\to\ell_1\bar{\ell}_2}_{\Sigma_\alpha,VV',\tau_q\tau_l}\big)^*\cdot\mathcal{M}^{q_a\bar{q}_b\to\ell_1\bar{\ell}_2}_{\mathrm{LO},\tilde{V},\tau_q\tau_\ell}\Big]\\
=&4\,\mathrm{Re}\big(\delta^{Z\bar{q}q}_{\mathrm{V_s}}\big)\,\mathrm{Re}\Big(\big(\delta_{VV'}\mathcal{M}^{\bar{q}_a q_b\to\ell_1\bar{\ell}_2}_{\delta^{\mathrm{ct}}_{(\alpha)},V,\tau_q\tau_l}+\mathcal{M}^{q_a\bar{q}_b\to\ell_1\bar{\ell}_2}_{\Sigma_\alpha,VV',\tau_q\tau_l}\big)^*\cdot\mathcal{M}^{q_a\bar{q}_b\to\ell_1\bar{\ell}_2}_{\mathrm{LO},\tilde{V},\tau_q\tau_\ell}\Big).
\end{aligned}\tag{5.20}$$

The amplitudes corresponding to the rv contribution at $\mathcal{O}(N_f\alpha_s\alpha)$ are slight modifications of the real NLO QCD corrections. Therefore, it is instructive to first discuss the real QCD corrections and afterwards modify them to obtain the rv $\mathcal{O}(N_f\alpha_s\alpha)$ corrections. The amplitudes corresponding to the NLO real QCD corrections are

$$\mathrm{i}\mathcal{M}^{\bar{q}_a q_b\to\ell_1\bar{\ell}_2 g}_{\mathrm{R_s},V,\tau_q\tau_l\lambda_g}=2\sqrt{2}\,\mathrm{i}e^2g_s C^{\tau_q}_{V\bar{q}_a q_b}C^{\tau_l}_{V\bar{\ell}_1\ell_2}\mathrm{M}^{\tau_q\tau_l\lambda_g}_{\mathrm{R_s}}(\{k_g,a\},\{p_i,c_i\}_{i\in\mathcal{S}}),\tag{5.21}$$

where $\mathcal{S}=\{a,b,\ell_1,\ell_2\}$ and the first entry of a tuple $\{p,c\}$ describes the momentum and the second the colour of a particle. Due to the symmetries of the partial amplitudes,

$$\begin{aligned}
\mathrm{M}^{-\tau_q\tau_l\lambda_g}_{\mathrm{R_s}}(\{k_g,a\},\{p_i,c_i\}_{i\in\mathcal{S}})&=\mathrm{M}^{\tau_q\tau_l\lambda_g}_{\mathrm{R_s}}(\{k_g,a\},\{p_i,c_i\}_{i\in\mathcal{S}})\Big|_{\{p_a,c_a\}\leftrightarrow\{p_b,c_b\}},\\
\mathrm{M}^{\tau_q-\tau_l\lambda_g}_{\mathrm{R_s}}(\{k_g,a\},\{p_i,c_i\}_{i\in\mathcal{S}})&=\mathrm{M}^{\tau_q\tau_l\lambda_g}_{\mathrm{R_s}}(\{k_g,a\},\{p_i,c_i\}_{i\in\mathcal{S}})\Big|_{\{p_{\ell_1}\}\leftrightarrow\{p_{\ell_2}\}},\\
\mathrm{M}^{\tau_q\tau_l-\lambda_g}_{\mathrm{R_s}}(\{k_g,a\},\{p_i,c_i\}_{i\in\mathcal{S}})&=\big[\mathrm{M}^{-\tau_q-\tau_l\lambda_g}_{\mathrm{R_s}}(\{k_g,a\},\{p_i,c_i\}_{i\in\mathcal{S}})\big]^*,
\end{aligned}\tag{5.22}$$

it is sufficient to calculate only one helicity configuration, where we choose

$$\mathrm{M}^{---}_{\mathrm{R_s}}(\{k_g,a\},\{p_i,c_i\}_{i\in\mathcal{S}})=t^a_{c_a c_b}\frac{\langle p_{\ell_1}|p_{\ell_2}\rangle\,(\langle p_a|p_{\ell_2}\rangle^*)^2}{\langle p_a|k_g\rangle^*\,\langle p_b|k_g\rangle^*\,(p_V^2-\mu_V^2)}.\tag{5.23}$$

Diagrams of type rv including $\mathcal{O}(N_f\alpha)$ vertex counterterms, depicted in Fig. 5.4, are obtained by the application of the following replacement,

$$C^{\sigma}_{V\bar{f}f}\to C^{\sigma}_{V\bar{f}f}\delta^{\mathrm{ct},\sigma}_{V\bar{f}f,(\alpha)},\tag{5.24}$$

to one of the vertices in $\mathrm{M}_{\mathrm{R_s}}^{-\tau_q\tau_l\lambda_g}$ leading to

$$\mathrm{i}\mathcal{M}^{\bar{q}_a q_b\to\ell_1\bar{\ell}_2 g}_{\mathrm{R_s}\otimes\delta^{\mathrm{ct}}_{(\alpha)},V,\tau_q\tau_l\lambda_g} = \mathrm{i}\big(\delta^{\mathrm{ct},\tau_q}_{V\bar{q}_a q_b,(\alpha)} + \delta^{\mathrm{ct},\tau_\ell}_{V\bar{\ell}_1\ell_2,(\alpha)}\big)\mathcal{M}^{\bar{q}_a q_b\to\ell_1\bar{\ell}_2 g}_{\mathrm{R_s},V,\tau_q\tau_l\lambda_g} \tag{5.25}$$

for the rv matrix elements including $\mathcal{O}(N_f\alpha)$ vertex counterterms. The rv contribution in Fig. 5.4 that we have not yet discussed is the one that receives a one-loop $\mathcal{O}(N_f\alpha)$ gauge-boson self-energy correction. The amplitude for this kind of rv correction is given by,

$$\mathrm{i}\mathcal{M}^{\bar{q}_a q_b\to\ell_1\bar{\ell}_2 g}_{\mathrm{R_s}\otimes\Sigma_\alpha,VV',\tau_q\tau_l\lambda_g} = -\frac{C^{\tau_l}_{V'\ell_1\bar{\ell}_2}}{C^{\tau_l}_{V\bar{\ell}_1\ell_2}}\frac{\Sigma^{V'V}_{\mathrm{T}}(p^2)}{p^2-\mu^2_{V'}}\mathrm{i}\mathcal{M}^{\bar{q}_a q_b\to\ell_1\bar{\ell}_2 g}_{\mathrm{R_s},V,\tau_q\tau_l\lambda_g}, \tag{5.26}$$

which follows from the same arguments we used to motivate (5.13). By projecting onto the matrix element of the real QCD correction, (5.21), we obtain the contribution to the squared matrix element, similar to the case of the genuine two-loop gauge-boson self-energy insertion described in (5.18).

5.2.2 IR singularities and antenna subtraction terms

In this section we list the antenna subtraction terms needed to cancel all implicit and explicit IR divergences present in $\mathcal{O}(N_f\alpha_s\alpha)$ corrections to single W/Z-production. The only source of explicit IR divergences is found in vv-red contributions to the squared matrix element given in (5.20). Accordingly, only the rv-red contributions to squared matrix element contain implicit IR divergences. In combination with the fact that there are no double-real contributions and that the vv-1PI corrections do not involve IR singularities this means that the subtraction terms relevant for the cancellation of IR divergences in $\mathcal{O}(N_f\alpha_s\alpha)$ are of NLO complexity. Therefore, NLO antenna subtraction terms, discussed in detail in Section 4.4, are sufficient to cancel all IR divergences and we only list the explicit real and virtual subtraction terms in the following.

Quark–antiquark initial state:

The real–virtual antenna subtraction term of NLO complexity for the $q\bar{q}$ induced partonic channel is given by

$$\begin{aligned}\mathrm{d}\hat{\sigma}^{\mathrm{S},ii,q\bar{q}}_{\mathrm{NNLO}} =& 2C_F\,\mathcal{N}_{\mathcal{C},q\bar{q}}\mathcal{N}^R_{\mathrm{NLO}}\,\mathrm{d}\Phi_3(\{p_i\}^3_{i=1};p_a,p_b)\\ &\times A^0_3(p_a,p_3,p_b)\langle M^{q_a\bar{q}_b\to\ell_1\bar{\ell}_2}_{\text{v-1PI}}(\tilde{p}_1,\tilde{p}_2;x_a p_a,x_b p_b)\rangle J^{(2)}_2(\tilde{p}_1,\tilde{p}_2),\end{aligned} \tag{5.27}$$

where the one-loop correction to the squared amplitude, $M^{q_a\bar{q}_b\to\ell_1\bar{\ell}_2}_{\text{v-1PI}}$, can be calculated in the same way as $M^{q_a\bar{q}_b\to\ell_1\bar{\ell}_2}_{\text{vv-1PI}}$ in (5.18), but taking into account only one-loop $\mathcal{O}(N_f\alpha)$ gauge-boson self-energy corrections instead of $\mathcal{O}(N_f\alpha_s\alpha)$ corrections. As in (5.7), the brackets $\langle.\rangle$ indicate spin and colour averaging. The factors $\mathcal{N}_{\mathcal{C},q\bar{q}}$ and $\mathcal{N}^R_{\mathrm{NLO}}$ were introduced in (4.74) and (4.72). The corresponding integrated subtraction term, which is combined with the vv-red contribution to the squared matrix element (5.20), is given by

$$\mathrm{d}\hat{\sigma}^{T,ii,q\bar{q}}_{\mathrm{NNLO}} = -\,2C_F\,\mathcal{N}^{\varepsilon}_{\mathcal{C},q\bar{q}}\mathcal{N}^V_{NLO}\int\frac{\mathrm{d}z_a}{z_a}\frac{\mathrm{d}z_b}{z_b}\mathrm{d}\Phi_2(\{p_i\}^2_{i=1};z_a p_a,z_b p_b)$$

$$\times \boldsymbol{\mathcal{J}}^{(1)}_{2,ii}(a,b,z_a,z_b)\langle M^{q_a\bar{q}_b\to\ell_1\bar{\ell}_2}_{\text{v-1PI}}(p_1,p_2;z_ap_a,z_bp_b)\rangle\, J^{(2)}_2(p_1,p_2), \tag{5.28}$$

with $\mathcal{N}^V_{NLO}$ given in (4.78).

Quark–gluon initial state:

The real–virtual antenna subtraction term and its integrated counterpart for the qg induced partonic channel (and similar for the $\bar{q}g$ channel) are given by

$$\begin{aligned}\mathrm{d}\hat{\sigma}^{\mathrm{S},ii,qg}_{\mathrm{NNLO}} =& 2C_F\,\mathcal{N}_{\mathcal{C},qg}\mathcal{N}^R_{\mathrm{NLO}}\,\mathrm{d}\Phi_3(\{p_i\}^3_{i=1};p_a,p_b)\\ &\times A^0_{3,qg\to qq}(p_g,p_a,p_b)\langle M^{q_a\bar{q}_b\to\ell_1\bar{\ell}_2}_{\text{v-1PI}}(\tilde{p}_1,\tilde{p}_2;x_ap_a,x_bp_b)\rangle J^{(2)}_2(\tilde{p}_1,\tilde{p}_2)\end{aligned} \tag{5.29}$$

and

$$\begin{aligned}\mathrm{d}\hat{\sigma}^{T,ii,qg}_{\mathrm{NNLO}} =& -2C_F\,\mathcal{N}^{\varepsilon}_{\mathcal{C},qg}\,\mathcal{N}^V_{NLO}\int\frac{\mathrm{d}z_a}{z_a}\frac{\mathrm{d}z_b}{z_b}\mathrm{d}\Phi_2(\{p_i\}^2_{i=1};z_ap_a,z_bp_b)\\ &\times \boldsymbol{\mathcal{J}}^{(1),g\to q}_{2,ii}(a,b,z_a,z_b)\langle M^{q_a\bar{q}_b\to\ell_1\bar{\ell}_2}_{\text{v-1PI}}(p_1,p_2;z_ap_a,z_bp_b)\rangle\, J^{(2)}_2(p_1,p_2).\end{aligned} \tag{5.30}$$

5.2.3 Renormalization at $\mathcal{O}(N_f\alpha_s\alpha)$

In this section we discuss the renormalization procedure that we apply at $\mathcal{O}(N_f\alpha_s\alpha)$. The renormalization of vv-red and rv contributions is of NLO complexity as they only involve one-loop subdiagrams. However, the renormalization of the vv-1PI gauge-boson self-energy insertions requires an extension of the renormalization prescription to $\mathcal{O}(N_f\alpha_s\alpha)$. In addition, the renormalization constants determined in the process of extending the NLO prescription to NNLO also lead to vertex counterterms of the gauge-boson–fermion vertices at $\mathcal{O}(N_f\alpha_s\alpha)$.

The extension of multiplicative renormalization transformations in the electroweak sector to all orders in perturbation theory is discussed in [117]. The beginning of this section essentially follows the line of thought presented there, as we apply some of the results of [117] to the case of $\mathcal{O}(N_f\alpha_s\alpha)$ corrections. Further, we apply the "parameter-renormalized tadpole scheme" (PRTS) as defined in Refs. [60, 69]. Therefore, our results for $\Sigma^{V'V}_{\mathrm{T}}$ do not include tadpole contributions. In the following we only discuss the renormalization of the photon/Z-boson sector. However, the results can also be extended to the renormalization of processes that involve the W boson by removing terms that originate from the photon-Z mixing and by replacing the mass of the Z boson by the mass of the W boson.

To expand our renormalization prescription to NNLO we start by considering the renormalized two-point functions $\hat{\Gamma}^{\mathrm{V'V}}_{\mu\nu}$. Their relation to the unrenormalized two-point functions $\Gamma^{\mathrm{V_1V_2}}_{\mu\nu}$ is given by

$$\hat{\Gamma}^{\mathrm{V'V}}_{\mu\nu}(-k,k) = \sum_{V_1,V_2=A,Z} Z^{1/2}_{\mathrm{V_1V'}}Z^{1/2}_{\mathrm{V_2V}}\Gamma^{\mathrm{V_1V_2}}_{\mu\nu}(-k,k). \tag{5.31}$$

As the OS renormalization conditions in (2.54) and (2.58) involve projections onto the physical degrees of freedom using the polarization vectors, only the transversal parts of $\hat{\Gamma}^{\mathrm{VA}}_{\mu\nu}$ are relevant for the renormalization procedure and the longitudinal parts drop out.

To make the structure of renormalized two-point functions and their dependence on renormalization constants explicit, we again rewrite them in terms of self-energy contributions,

$$\hat{\Gamma}_{\mathrm{T}}^{\mathrm{V'V}}(k^2) = -\delta_{\mathrm{V'V}}\,(k^2 - \delta_{\mathrm{VZ}}\,M_{\mathrm{Z}}^2) - \hat{\Sigma}_{\mathrm{T}}^{\mathrm{V'V}}(k^2, \{c_i\}). \tag{5.32}$$

The introduction of the renormalized parameters $\{c_i\}$ in the self-energies is used to keep track of their parameter dependence which will become relevant later in Section 5.2.3.2. The bare parameters $c_{i,0}$ are labeled with an additional subscript to distinguish them from the renormalized parameters $\{c_i\}$. By the application of multiplicative renormalization transformations to the fields in the free Lagrangian and the mass of the Z boson one can also obtain

$$\hat{\Gamma}_{\mathrm{T}}^{\mathrm{V'V}}(k^2) = -Z_{\mathrm{AV'}}^{1/2} Z_{\mathrm{AV}}^{1/2} k^2 - Z_{\mathrm{ZV'}}^{1/2} Z_{\mathrm{ZV}}^{1/2}(k^2 - M_{\mathrm{Z}}^2 - \delta M_{\mathrm{Z}}^2) - \Sigma_{\mathrm{SR,T}}^{\mathrm{V'V}}(k^2, \{c_i\}), \tag{5.33}$$

where the subgraph-renormalized (SR) self-energies $\Sigma_{\mathrm{SR,T}}^{\mathrm{V'V}}$ include all diagrams with loops and counterterm insertions in loops, but no counterterm diagrams without loop parts, as these parts are already part of the two-loop Z factors. The inclusion of diagrams with one-loop counterterms in loops ensures that all UV subdivergences, i.e. UV divergences that are proportional to non-polynomial functions in k^2, are cancelled in $\Sigma_{\mathrm{SR,T}}^{\mathrm{V'V}}$, even though local UV divergences that are proportional to k^2 and cancel against genuine counterterm diagrams, might be still contained in $\Sigma_{\mathrm{SR,T}}^{\mathrm{V'V}}$. We can combine (5.32) and (5.33) to obtain the renormalized self-energies in terms of SR self-energies and renormalization constants,

$$\begin{aligned}\hat{\Sigma}_{\mathrm{T}}^{\mathrm{V'V}}(k^2, \{c_i\}) = \Sigma_{\mathrm{SR,T}}^{\mathrm{V'V}}(k^2, \{c_i\}) &+ \left(Z_{\mathrm{AV'}}^{1/2} Z_{\mathrm{AV}}^{1/2} + Z_{\mathrm{ZV'}}^{1/2} Z_{\mathrm{ZV}}^{1/2} - \delta_{\mathrm{V'V}}\right) k^2 \\ &- \left(Z_{\mathrm{ZV'}}^{1/2} Z_{\mathrm{ZV}}^{1/2} - \delta_{\mathrm{V'Z}}\,\delta_{\mathrm{VZ}}\right) M_{\mathrm{Z}}^2 - Z_{\mathrm{ZV'}}^{1/2} Z_{\mathrm{ZV}}^{1/2}\,\delta M_{\mathrm{Z}}^2.\end{aligned} \tag{5.34}$$

A perturbative expansion of products of renormalization constants present in the last equation up to $\mathcal{O}(\alpha_s\alpha)$ contains in principle also products of one-loop wave-function renormalization constants such as

$$\begin{aligned}Z_{\mathrm{AV'}}^{1/2} Z_{\mathrm{AV}}^{1/2} =& \delta_{\mathrm{AV'}}\delta_{\mathrm{AV}} + \frac{\delta_{\mathrm{AV'}}\delta Z_{\mathrm{AV}}^{(\alpha)}}{2} + \frac{\delta_{\mathrm{AV}}\delta Z_{\mathrm{AV'}}^{(\alpha)}}{2} \\ &+ \frac{\delta_{\mathrm{AV'}}\delta Z_{\mathrm{AV}}^{(\alpha_s)}}{2} + \frac{\delta_{\mathrm{AV}}\delta Z_{\mathrm{AV'}}^{(\alpha_s)}}{2} + \frac{\delta_{\mathrm{AV'}}\delta Z_{\mathrm{AV}}^{(\alpha_s\alpha)}}{2} + \frac{\delta_{\mathrm{AV}}\delta Z_{\mathrm{AV'}}^{(\alpha_s\alpha)}}{2} \\ &- \frac{\delta_{\mathrm{AV'}}\delta Z_{\mathrm{AV}}^{(\alpha)}\delta Z_{\mathrm{AV}}^{(\alpha_s)}}{4} + \frac{\delta Z_{\mathrm{AV}}^{(\alpha)}\delta Z_{\mathrm{AV'}}^{(\alpha_s)}}{4} + \frac{\delta Z_{\mathrm{AV}}^{(\alpha_s)}\delta Z_{\mathrm{AV'}}^{(\alpha)}}{4} - \frac{\delta_{\mathrm{AV}}\delta Z_{\mathrm{AV'}}^{(\alpha)}\delta Z_{\mathrm{AV'}}^{(\alpha_s)}}{4}.\end{aligned} \tag{5.35}$$

However, as there are no one-loop QCD contributions to $Z_{VV'}$, i.e. $\delta Z_{\mathrm{AV}}^{(\alpha_s)} = 0$, the last expression simplifies to

$$Z_{\mathrm{AV'}}^{1/2} Z_{\mathrm{AV}}^{1/2} = \delta_{\mathrm{AV'}}\delta_{\mathrm{AV}} + \frac{\delta_{\mathrm{AV'}}\delta Z_{\mathrm{AV}}^{(\alpha)}}{2} + \frac{\delta_{\mathrm{AV}}\delta Z_{\mathrm{AV'}}^{(\alpha)}}{2} + \frac{\delta_{\mathrm{AV'}}\delta Z_{\mathrm{AV}}^{(\alpha_s\alpha)}}{2} + \frac{\delta_{\mathrm{AV}}\delta Z_{\mathrm{AV'}}^{(\alpha_s\alpha)}}{2}, \tag{5.36}$$

where the superscript dressing the renormalization constants in the last equation indicates the perturbative order. Therefore, for the renormalized self-energies (5.34) in terms of the SR self-energies at order $\mathcal{O}(\alpha_s\alpha)$ we obtain

$$\hat{\Sigma}_{\mathrm{T},(\alpha_s\alpha)}^{\mathrm{V'V}}(k^2, \{c_i\}) = \Sigma_{\mathrm{SR,T},(\alpha_s\alpha)}^{\mathrm{V'V}}(k^2, \{c_i\})$$

$$+\frac{1}{2}\left(\delta_{\mathrm{AV}'}\delta Z^{(\alpha_s\alpha)}_{\mathrm{AV}}+\delta_{\mathrm{AV}}\delta Z^{(\alpha_s\alpha)}_{\mathrm{AV}'}+\delta_{\mathrm{ZV}'}\delta Z^{(\alpha_s\alpha)}_{\mathrm{ZV}}+\delta_{\mathrm{ZV}}\delta Z^{(\alpha_s\alpha)}_{\mathrm{ZV}'}\right)k^2$$
$$-\frac{1}{2}\left(\delta_{\mathrm{ZV}'}\delta Z^{(\alpha_s\alpha)}_{\mathrm{ZV}}+\delta_{\mathrm{ZV}}\delta Z^{(\alpha_s\alpha)}_{\mathrm{ZV}'}\right)M^2_{\mathrm{Z}}-\delta_{\mathrm{ZV}'}\delta_{\mathrm{ZV}}\,\delta M^2_{\mathrm{Z},(\alpha_s\alpha)}. \tag{5.37}$$

This equation has the same structure as the corresponding ones at NLO $\mathcal{O}(\alpha)$, given in (2.111). The only difference is that at $\mathcal{O}(\alpha_s\alpha)$ the SR self-energy appears, whereas at NLO the unrenormalized self-energy appears (which is, actually, equal to the SR self-energy at NLO). We therefore conclude that if we apply the same renormalization conditions to $\hat{\Sigma}^{\mathrm{V}'\mathrm{V}}_{\mathrm{T},(\alpha_s\alpha)}(k^2,\{c_i\})$ as we applied to $\hat{\Sigma}^{\mathrm{V}'\mathrm{V}}_{\mathrm{T},(\alpha)}(k^2,\{c_i\})$ at NLO in (2.112), we will obtain the same relation between the $\mathcal{O}(\alpha_s\alpha)$ SR self-energy and the $\mathcal{O}(\alpha_s\alpha)$ renormalization constants as we have in (5.42) between the NLO unrenormalized self-energy and the NLO renormalization constants.

Using, (2.52) and (5.31), the SR self-energies are related to unrenormalized self-energies according to

$$\Sigma^{\mathrm{V}'\mathrm{V}}_{\mathrm{SR,T}}(k^2,\{c_i\})=\sum_{V_1,V_2=A,Z}Z^{1/2}_{\mathrm{V_1V}'}Z^{1/2}_{\mathrm{V_2V}}\,\Sigma^{\mathrm{V_1V_2}}_{\mathrm{T}}(k^2,\{c_{i,0}\}), \tag{5.38}$$

which, in case of $\mathcal{O}(\alpha_s\alpha)$ corrections, reduces to

$$\Sigma^{\mathrm{V}'\mathrm{V}}_{\mathrm{SR,T},(\alpha_s\alpha)}(k^2,\{c_i\})=\sum_{V_1,V_2=A,Z}\delta_{\mathrm{V_1V}'}\delta_{\mathrm{V_2V}}\,\Sigma^{\mathrm{V_1V_2}}_{\mathrm{T},(\alpha_s\alpha)}(k^2,\{c_{i,0}\})=\Sigma^{\mathrm{V}'\mathrm{V}}_{\mathrm{T},(\alpha_s\alpha)}(k^2,\{c_{i,0}\}), \tag{5.39}$$

as there is no NLO $\mathcal{O}(\alpha_s)$ contribution to the self-energy $\Sigma^{\mathrm{V_1V_2}}_{\mathrm{T}}$, and therefore also not to the renormalization constants $Z_{\mathrm{VV}'}$. This means that at $\mathcal{O}(\alpha_s\alpha)$ the SR self-energies are given by the unrenormalized self-energies that depend on the bare parameters. However, it is important to note the SR self-energies contain one-loop renormalization constants δc_i so that all UV subdivergences are cancelled in $\Sigma^{\mathrm{V}'\mathrm{V}}_{\mathrm{SR,T},(\alpha_s\alpha)}$,

$$\Sigma^{\mathrm{V}'\mathrm{V}}_{\mathrm{SR,T},(\alpha_s\alpha)}(k^2,\{c_i\})=\Sigma^{\mathrm{V}'\mathrm{V}}_{\mathrm{T},(\alpha_s\alpha)}(k^2,\{c_{i,0}\})=\Sigma^{\mathrm{V}'\mathrm{V}}_{\mathrm{T},(\alpha_s\alpha)}(k^2,\{c_i\})+\delta c_i\text{-terms}. \tag{5.40}$$

In the following sections we denote the SR self-energies by

$$\Sigma^{\mathrm{V}'\mathrm{V}}_{\mathrm{T},(\alpha_s\alpha)}(k^2)\equiv\Sigma^{\mathrm{V}'\mathrm{V}}_{\mathrm{T},(\alpha_s\alpha)}(k^2,\{c_{i,0}\})\equiv\Sigma^{\mathrm{V}'\mathrm{V}}_{\mathrm{SR,T},(\alpha_s\alpha)}(k^2,\{c_i\}), \tag{5.41}$$

suppressing the parameters $\{c_i\}$ when not explicitly needed, keeping in mind that the SR self-energies and therefore also $\Sigma^{\mathrm{V}'\mathrm{V}}_{\mathrm{T},(\alpha_s\alpha)}(k^2)$ contain one-loop renormalization constants to cancel UV subdivergences as in (5.40).

5.2.3.1 Complex-mass scheme at $\mathcal{O}(N_f\alpha_s\alpha)$

We now proceed to discuss the extension of the complex-mass scheme introduced in Section 2.4.2 to $\mathcal{O}(\alpha_s\alpha)$. As absorptive parts of W/Z propagators must contain closed fermion loops at this order of perturbation theory, $\mathcal{O}(N_f\alpha_s\alpha)$ corrections are already sufficient to fully describe the extension to $\mathcal{O}(\alpha_s\alpha)$. As we have seen in the last section, the complex renormalization constants at $\mathcal{O}(N_f\alpha_s\alpha)$ can be obtained in the same way as at NLO replacing only the unrenormalized self-energies by the SR self-energies,

$$\delta\mu^2_{\mathrm{W},(\alpha_s\alpha)}=\Sigma^{W}_{\mathrm{T},(\alpha_s\alpha)}(\mu^2_{\mathrm{W}}),\qquad\qquad\delta\mu^2_{\mathrm{Z},(\alpha_s\alpha)}=\Sigma^{ZZ}_{\mathrm{T},(\alpha_s\alpha)}(\mu^2_{\mathrm{Z}}), \tag{5.42}$$

$$\begin{aligned}
\delta\mathcal{Z}_{W,(\alpha_s\alpha)} &= -\Sigma'^{W}_{\mathrm{T},(\alpha_s\alpha)}(\mu_\mathrm{W}^2), \\
\delta\mathcal{Z}_{ZA,(\alpha_s\alpha)} &= \frac{2}{\mu_\mathrm{Z}^2}\Sigma^{AZ}_{\mathrm{T},(\alpha_s\alpha)}(0), \qquad \delta\mathcal{Z}_{AZ,(\alpha_s\alpha)} = -\frac{2}{\mu_\mathrm{Z}^2}\Sigma^{AZ}_{\mathrm{T},(\alpha_s\alpha)}(\mu_\mathrm{Z}^2), \\
\delta\mathcal{Z}_{ZZ,(\alpha_s\alpha)} &= -\Sigma'^{ZZ}_{\mathrm{T},(\alpha_s\alpha)}(\mu_\mathrm{Z}^2), \qquad \delta\mathcal{Z}_{AA,(\alpha_s\alpha)} = -\Sigma'^{AA}_{\mathrm{T},(\alpha_s\alpha)}(0),
\end{aligned} \tag{5.43}$$

where $\Sigma'^{V'V}(k^2) \equiv (\partial\Sigma^{V'V}/\partial k^2)(k^2)$. Note that we write $(\alpha_s\alpha)$ as subscript when there is no distinction between between $\mathcal{O}(N_f\alpha_s\alpha)$ and $\mathcal{O}(\alpha_s\alpha)$ corrections to certain quantities.

In Section 2.4.2 we already discussed that the evaluation of the self-energies with complex k^2 on the second Riemann sheet can be circumvented by expanding them about the real part M_V^2 of μ_V^2 up to the relevant order. This leads to

$$\begin{aligned}
\delta\mu^2_{\mathrm{W},(\alpha_s\alpha)} &= \Sigma^{W}_{\mathrm{T},(\alpha_s\alpha)}(M_\mathrm{W}^2) + (\mu_\mathrm{W}^2 - M_\mathrm{W}^2)\Sigma'^{W}_{\mathrm{T},(\alpha_s\alpha)}(M_\mathrm{W}^2), \\
\delta\mu^2_{\mathrm{Z},(\alpha_s\alpha)} &= \Sigma^{ZZ}_{\mathrm{T},(\alpha_s\alpha)}(M_\mathrm{Z}^2) + (\mu_\mathrm{Z}^2 - M_\mathrm{Z}^2)\Sigma'^{ZZ}_{\mathrm{T},(\alpha_s\alpha)}(M_\mathrm{Z}^2),
\end{aligned} \tag{5.44}$$

$$\begin{aligned}
\delta\mathcal{Z}_{W,(\alpha_s\alpha)} &= -\Sigma'^{W}_{\mathrm{T},(\alpha_s\alpha)}(M_\mathrm{W}^2), \qquad \delta\mathcal{Z}_{ZA,(\alpha_s\alpha)} = \frac{2}{\mu_\mathrm{Z}^2}\Sigma^{AZ}_{\mathrm{T},(\alpha_s\alpha)}(0), \\
\delta\mathcal{Z}_{AZ,(\alpha_s\alpha)} &= -\frac{2}{M_\mathrm{Z}^2}\Sigma^{AZ}_{\mathrm{T},(\alpha_s\alpha)}(M_\mathrm{Z}^2) + \left(\frac{\mu_\mathrm{Z}^2}{M_\mathrm{Z}^2} - 1\right)\delta\mathcal{Z}_{ZA,(\alpha_s\alpha)}, \\
\delta\mathcal{Z}_{ZZ,(\alpha_s\alpha)} &= -\Sigma'^{ZZ}_{\mathrm{T},(\alpha_s\alpha)}(M_\mathrm{Z}^2).
\end{aligned} \tag{5.45}$$

As at NLO the expansion of the wave-function renormalization constants is truncated at $(\mu_V^2 - M_V^2)^0$, since they are always multiplied by $(k^2 - \mu_V^2) = \mathcal{O}(\alpha)$, for $k^2 \approx M_V^2$, in the renormalized self-energies (5.34). In comparison to (2.117) we do not need to include a term like c_T^W—which originates from diagrams including photon exchange in W-boson self-energies leading to a branch point at $k^2 = M_\mathrm{W}^2$—as the self-energies $\Sigma^{V'V}_{\mathrm{T},(\alpha_s\alpha)}$ do not involve IR singularities and are therefore analytic at $k^2 = \mu_\mathrm{W}^2$. We also used the fact that there are no $\mathcal{O}(\alpha_s)$ corrections to $\Sigma_\mathrm{T}^{V'V}$ at NLO, which means that no further terms have to be considered above.

The renormalization constants corresponding to the cosine and sine of the weak mixing angle, δc_w and δs_w, and also the result for the charge renormalization constant δZ_e are determined analogously to the NLO case described in (2.120) and (2.121). However, as a consequence of Slavnov–Taylor (ST) identities we have

$$\Sigma^{AZ}_{\mathrm{T},(\alpha_s\alpha)}(0) \equiv 0, \tag{5.46}$$

which simplifies the expression of the charge renormalization constant to

$$\delta Z_{e,(\alpha_s\alpha)} = \frac{1}{2}\Sigma'^{AA}_{\mathrm{T},(\alpha_s\alpha)}(0). \tag{5.47}$$

The renormalization constants defined above are not only part of the renormalized gauge-boson self-energies

$$\begin{aligned}
\hat{\Sigma}^{V'V}_{\mathrm{T},(\alpha_s\alpha)}(k^2) = \Sigma^{V'V}_{\mathrm{T},(\alpha_s\alpha)}(k^2) &+ \frac{1}{2}(k^2 - \mu_V^2)\delta\mathcal{Z}_{VV',(\alpha_s\alpha)} + \frac{1}{2}(k^2 - \mu_{V'}^2)\delta\mathcal{Z}_{V'V,(\alpha_s\alpha)} \\
&- \delta_{V'V}\delta\mu^2_{V,(\alpha_s\alpha)},
\end{aligned} \tag{5.48}$$

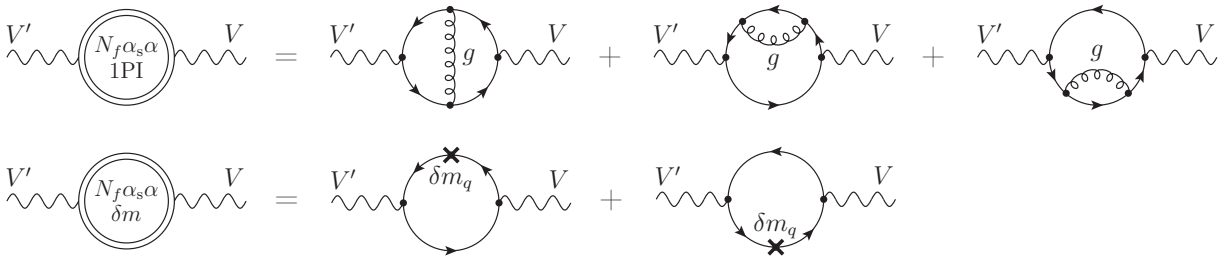

Figure 5.5: Diagrams contributing to the EW gauge-boson self-energies $\Sigma_{\mathrm{T}}^{V'V}$ at $\mathcal{O}(N_f\alpha_s\alpha)$, which all involve closed quark loops. In the first line the contributions to $\Sigma_{\mathrm{T,1PI}}^{V'V}$ and in the second line the contributions to $\Sigma_{\mathrm{T},\delta m}^{V'V}$ are shown.

with $\mu_A = 0$, but also contribute to the vertex counterterms

$$\delta^{\mathrm{ct},\sigma}_{W\bar{f}f',(N_f\alpha_s\alpha)} = \delta Z_{e,(\alpha_s\alpha)} - \frac{\delta s_{\mathrm{w},(\alpha_s\alpha)}}{s_{\mathrm{w}}} + \frac{1}{2}\delta\mathcal{Z}_{W,(\alpha_s\alpha)}, \tag{5.49}$$

$$\delta^{\mathrm{ct},\sigma}_{Z\bar{f}f,(N_f\alpha_s\alpha)} = \frac{\delta C^{\sigma}_{Z\bar{f}f,(\alpha_s\alpha)}}{C^{\sigma}_{Z\bar{f}f}} + \frac{1}{2}\delta\mathcal{Z}_{ZZ,(\alpha_s\alpha)} - \frac{Q_f}{2C^{\sigma}_{Z\bar{f}f}}\delta\mathcal{Z}_{AZ,(\alpha_s\alpha)}, \tag{5.50}$$

$$\delta^{\mathrm{ct},\sigma}_{A\bar{f}f,(N_f\alpha_s\alpha)} = \delta Z_{e,(\alpha_s\alpha)} + \frac{1}{2}\delta\mathcal{Z}_{AA,(\alpha_s\alpha)} - \frac{C^{\sigma}_{Z\bar{f}f}}{2Q_f}\delta\mathcal{Z}_{ZA,(\alpha_s\alpha)}, \tag{5.51}$$

which lead to the UV-finite vertex corrections, described in (5.16), by modifying the LO coupling factors as in (5.15). In the last expressions the renormalization constants of the LO couplings (5.6) are given by

$$\delta C^{\sigma}_{Z\bar{f}f,(\alpha_s\alpha)} = C^{\sigma}_{Z\bar{f}f}\left(\delta Z_{e,(\alpha_s\alpha)} + \frac{1}{c_{\mathrm{w}}^2}\frac{\delta s_{\mathrm{w},(\alpha_s\alpha)}}{s_{\mathrm{w}}}\right) - \frac{2I^3_{\mathrm{w},f}}{s_{\mathrm{w}}c_{\mathrm{w}}}\frac{\delta s_{\mathrm{w},(\alpha_s\alpha)}}{s_{\mathrm{w}}}\,\delta_{\sigma-}. \tag{5.52}$$

5.2.3.2 Cancellation of UV subdivergences

We have seen in (5.39) that at $\mathcal{O}(\alpha_s\alpha)$ the SR self-energies are given by the unrenormalized self-energies

$$\Sigma^{\mathrm{V'V}}_{\mathrm{SR,T}}(k^2,\{c_i\}) = \Sigma^{\mathrm{V'V}}_{\mathrm{T}}(k^2,\{c_{i,0}\}), \tag{5.53}$$

To obtain the diagrams needed to cancel subdivergences present in the EW gauge-boson self-energies at $\mathcal{O}(N_f\alpha_s\alpha)$ we apply parameter renormalization in the unrenormalized $\mathcal{O}(N_f\alpha_s\alpha)$ self-energies. This means, that we replace the bare parameters $c_{i,0}$ appearing as arguments on the r.h.s. of the last equation by

$$c_{i,0} = c_i + \delta c_i. \tag{5.54}$$

We split the contributions to the unrenormalized self-energy $\Sigma^{\mathrm{V'V}}_{\mathrm{T}}(k^2,\{c_{i,0}\})$ into the part $\Sigma^{\mathrm{V'V}}_{\mathrm{T}}(k^2,\{c_i\})$, where the $c_{i,0}$ are simply renamed into c_i, and a remainder part $\Sigma^{\mathrm{V'V}}_{\mathrm{T},\delta c}(k^2,\{c_i\})$ that absorbs all effects of the renormalization constants δc_i,

$$\Sigma^{\mathrm{V'V}}_{\mathrm{T}}(k^2,\{c_{i,0}\}) = \Sigma^{\mathrm{V'V}}_{\mathrm{T,1PI}}(k^2,\{c_i\}) + \Sigma^{\mathrm{V'V}}_{\mathrm{T},\delta c}(k^2,\{c_i\}). \tag{5.55}$$

In principle also tadpole contributions have to be considered in the last equation. However, in the PRTS they are always exactly cancelled by tadpole counterterms. Furthermore, for the class of gauge-boson self-energy diagrams at this perturbative order, the only relevant parameter renormalization transformation is given by

$$m_{q,0} = m_q + \delta m_q^{(\alpha_s)}, \tag{5.56}$$

so that (5.55) reduces to

$$\Sigma^{V'V}_{\mathrm{T},(\alpha_s\alpha)}(k^2) = \Sigma^{V'V}_{\mathrm{T},(\alpha_s\alpha),\mathrm{1PI}}(k^2) + \Sigma^{V'V}_{\mathrm{T},(\alpha_s\alpha),\delta m}(k^2), \tag{5.57}$$

where $\Sigma^{V'V}_{\mathrm{T},(\alpha_s\alpha),\mathrm{1PI}}$ comprises all one-particle irreducible (1PI) two-loop diagrams, as shown in Fig. 5.5, and $\Sigma^{V'V}_{\mathrm{T},(\alpha_s\alpha),\delta m}$ represents all fermion loops with insertions of the QCD quark-mass counterterms. In principle, also the quark-field renormalization constants of $\mathcal{O}(\alpha_s)$ have to be considered. However, their contributions to $\Sigma^{V'V}_{\mathrm{T},(\alpha_s\alpha)}$ fully cancels. This is equivalent to showing

(5.58)

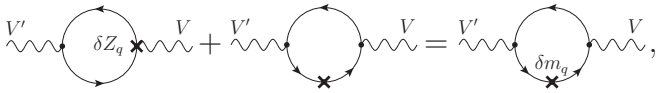

(5.59)

which can be easily seen by simply writing down the corresponding loop integrals,

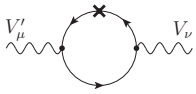

$$= -\int \frac{\mathrm{d}^d q}{(2\pi)^d} \mathrm{Tr}\Big[g_\pm \omega^\pm \gamma_\mu \frac{(\not{q}+m)}{q^2-m^2} \big((\not{q}-m)\delta Z_q^{(\alpha_s)} + \delta m_q^{(\alpha_s)} \big) \cdot \frac{(\not{q}+m)}{q^2-m^2} g_\pm \omega^\pm \gamma_\nu \frac{(\not{p}-\not{q}+m)}{(p-q)^2-m^2} \Big], \tag{5.60}$$

and

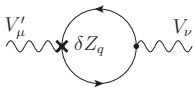

$$= \int \frac{\mathrm{d}^d q}{(2\pi)^d} \mathrm{Tr}\Big[g_\pm \omega^\pm \gamma_\mu \delta Z_q^{(\alpha_s)} \frac{(\not{q}+m)}{q^2-m^2} g_\pm \omega^\pm \gamma_\nu \frac{(\not{p}-\not{q}+m)}{(p-q)^2-m^2} \Big]. \tag{5.61}$$

By expanding the bracket containing the one-loop renormalization constants and using $(\not{q}+m)(\not{q}-m) = q^2-m^2$ in (5.60) one obtains (5.58). The cancellation of the one-loop wave function renormalization constant of the quark in (5.59) follows analogously.

By definition the SR self-energies are free of UV subdivergences such that the UV divergences present in the combination of $\Sigma^{V'V}_{\mathrm{T},(\alpha_s\alpha),\mathrm{1PI}}$ and $\Sigma^{V'V}_{\mathrm{T},(\alpha_s\alpha),\delta m}$ are of polynomial structure and can be removed by a local counterterm of the form

$$= \mathrm{i} g_{\mu\nu} [c_1\, p^2\, \delta Z^{(\alpha_s\alpha)}_{V_1V_2} + c_2\, \delta Z^{(\alpha_s\alpha)}_{V_1V_2} + c_3\, \delta Z^{(\alpha_s\alpha)}_{M^2_{V_i}}].$$

Therefore, the combination of $\Sigma^{V'V}_{\mathrm{T},(\alpha_s\alpha),\mathrm{1PI}}$, $\Sigma^{V'V}_{\mathrm{T},(\alpha_s\alpha),\delta m}$, and a local counterterm is a UV-finite quantity,

$\hat{\Sigma}^{V'V}_{(\alpha_s\alpha)} =$

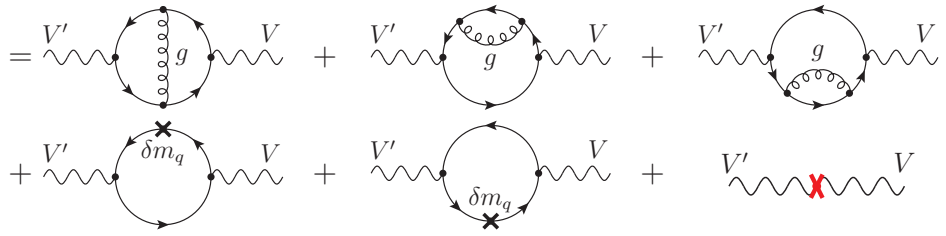

(5.62)

In the on-shell scheme using dimensional regularization the mass renormalization constants $\delta m_q = \delta m_q^{(\alpha_s)}$ (see Fig. 5.5) is given by [118]

$$\delta m_q^{(\alpha_s)} = -m_q \frac{C_F \alpha_s}{4\pi} \frac{3-2\epsilon}{1-2\epsilon} \left(\frac{4\pi\mu^2}{m_q^2}\right)^{\epsilon} \frac{\Gamma(1+\epsilon)}{\epsilon}, \tag{5.63}$$

where $C_F = \frac{4}{3}$ denotes the quadratic Casimir factor of the fundamental representation of colour $SU(3)$. The diagrams involving δm_q contribute to $\Sigma^{V'V}_{T,\delta m}$ and their calculation can be simplified using the following relation [118],

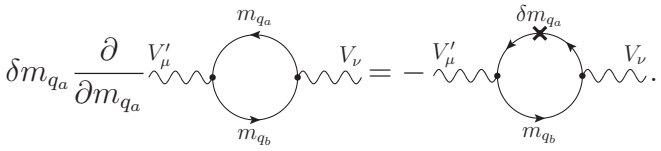

(5.64)

By applying the derivative with respect to m_{q_a} on the one-loop VV' self-energy we obtain,

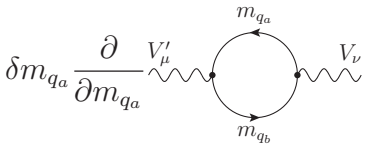

$$\begin{aligned}
&= \delta m_{q_a} \int \frac{\mathrm{d}^d q}{(2\pi)^d} \mathrm{Tr}\Big[g_\pm \omega^\pm \gamma_\mu \frac{q^2 - m_{q_a}^2 + 2m_{q_a}(\not{q} + m_{q_a})}{(q^2 - m_{q_a}^2)^2} g_\pm \omega^\pm \gamma_\nu \frac{(\not{p} - \not{q} + m_{q_b})}{(p-q)^2 - m_{q_b}^2} \Big] \\
&= \int \frac{\mathrm{d}^d q}{(2\pi)^d} \mathrm{Tr}\Big[g_\pm \omega^\pm \gamma_\mu \frac{(\not{q} + m_{q_a})}{(q^2 - m_{q_a}^2)} \delta m_{q_a} \frac{(\not{q} + m_{q_a})}{(q^2 - m_{q_a}^2)} g_\pm \omega^\pm \gamma_\nu \frac{(\not{p} - \not{q} + m_{q_b})}{(p-q)^2 - m_{q_b}^2} \Big],
\end{aligned}$$

which is equivalent to (5.60) with $\delta Z_q^{(\alpha_s)}$ set to zero. In the last step we have used $q^2 - m_{q_a}^2 + 2m_{q_a}(\not{q} + m_{q_a}) = (\not{q} + m_{q_a})^2$. With this short calculation we have checked the validity of relation (5.64) for the case $m_{q_b} \neq m_{q_a}$, where a generalization to $m_{q_b} = m_{q_a}$ is straight-forward and leads to an additional mixed loop-counterterm diagram on the right-hand side of (5.64), with a counterterm on the fermionic line corresponding to m_{q_b}.

5.2.4 Results for electroweak gauge-boson self-energies at $\mathcal{O}(\alpha_s\alpha)$

In the following we discuss our results [115] for the electroweak gauge-boson self-energies at $\mathcal{O}(\alpha_s\alpha)$. As we have seen in the previous sections, the longitudinal parts of self-energies are not relevant for our calculation and we only consider the transverse part of self-energies

$$\Sigma^{AA}_{T,(\alpha_s\alpha),1PI}(s) = \frac{\alpha_s\alpha}{\pi^2} \frac{N_c^2 - 1}{2} \sum_q Q_q^2 \, s \, f_1(s, m_q^2), \tag{5.65}$$

$$\Sigma^{AZ}_{\mathrm{T},(\alpha_s\alpha),\mathrm{1PI}}(s) = \frac{\alpha_s\alpha}{\pi^2}\frac{N_c^2-1}{2}\sum_q(-Q_q)v_q\, s\, f_1(s,m_q^2), \tag{5.66}$$

$$\Sigma^{ZZ}_{\mathrm{T},(\alpha_s\alpha),\mathrm{1PI}}(s) = \frac{\alpha_s\alpha}{\pi^2}\frac{N_c^2-1}{2}\sum_q\left[(v_q^2+a_q^2)\, s\, f_1(s,m_q^2) + a_q^2\, m_q^2\, f_2(s,m_q^2)\right], \tag{5.67}$$

$$\Sigma^{AA}_{\mathrm{T},(\alpha_s\alpha),\delta m}(s) = \frac{\alpha_s\alpha}{\pi^2}\frac{N_c^2-1}{2}\sum_q Q_q^2\, m_q^2\, f_3(s,m_q^2), \tag{5.68}$$

$$\Sigma^{AZ}_{\mathrm{T},(\alpha_s\alpha),\delta m}(s) = \frac{\alpha_s\alpha}{\pi^2}\frac{N_c^2-1}{2}\sum_q(-Q_q)v_q\, m_q^2\, f_3(s,m_q^2), \tag{5.69}$$

$$\Sigma^{ZZ}_{\mathrm{T},(\alpha_s\alpha),\delta m}(s) = \frac{\alpha_s\alpha}{\pi^2}\frac{N_c^2-1}{2}\sum_q m_q^2\left[(v_q^2+a_q^2)\, f_3(s,m_q^2) + a_q^2\, f_4(s,m_q^2)\right], \tag{5.70}$$

where $(N_c^2-1)/2 = N_cC_F = 4$ originates from the SU(N_c) colour algebra with $N_c = 3$ and the sums $\sum_q$ extend over all quark flavours $q \in \{u, d, c, s, t, b\}$ with corresponding electric charges Q_q and third components $I^3_{w,q} = \pm\frac{1}{2}$ of the weak isospin. In terms of the couplings defined in (5.6) the vector and axial-vector couplings of quark q to the Z boson are given by,

$$v_q = \frac{1}{2}(C^-_{Z\bar{q}q} + C^+_{Z\bar{q}q}), \qquad a_q = \frac{1}{2}(C^-_{Z\bar{q}q} - C^+_{Z\bar{q}q}). \tag{5.71}$$

The explicit form of the auxiliary functions $f_i(s,m_q^2)$ $(i = 1,\ldots,8)$ is given in App. D and depends on a set of 2-loop master integrals defined in (D.1). The explicit analytical results of these master integrals which can be found in [115], are expressed in terms of Goncharov Polylogarithms (GPLs) [119,120] up to weight three. To produce the numerical results presented in Section 5.3 the GPLs contained in the genuine two-loop $\mathcal{O}(N_f\alpha_s\alpha)$ corrections were evaluated using the C++ library GiNaC [121] and in a second independent calculation [115] using CHAPLIN [122]. Apart from the $\mathcal{O}(\alpha_s\alpha)$ corrections to gauge-boson self-energies present in the NC-DY process we also need the corresponding corrections in case of the CC process,

$$\Sigma^{W}_{\mathrm{T},(\alpha_s\alpha),\mathrm{1PI}}(s) = \frac{\alpha_s\alpha}{2\pi^2 s_w^2}\frac{N_c^2-1}{2}\sum_{j=1}^{3}\left[s f_5(s,m_{d_j}^2,m_{u_j}^2) + (m_{d_j}\leftrightarrow m_{u_j})\right], \tag{5.72}$$

$$\Sigma^{W}_{\mathrm{T},(\alpha_s\alpha),\delta m}(s) = \frac{\alpha_s\alpha}{2\pi^2 s_w^2}\frac{N_c^2-1}{2}\sum_{j=1}^{3}\left[m_{u_j}^2 f_6(s,m_{d_j}^2,m_{u_j}^2) + (m_{d_j}\leftrightarrow m_{u_j})\right], \tag{5.73}$$

where the sums $\sum_j$ extend over the three generations of up-type and down-type quarks u_j and d_j, respectively.

In the G_μ input-parameter scheme discussed in the following section we need the W-boson self-energy at zero-momentum transfer. The limit $s \to 0$ to obtain $\Sigma^W_{\mathrm{T},(\alpha_s\alpha)}(0)$ requires some care as can be seen by looking at the explicit expressions for the auxiliary functions $f_5(s,m_{d_j}^2,m_{u_j}^2)$ given in (D.7). The master integrals contained in this auxiliary function contain coefficients proportional to $\frac{1}{s^2}$ such that the combination $s f_5(s,m_{d_j}^2,m_{u_j}^2)$

in (5.72) contains master integrals multiplied by $\frac{1}{s}$. Therefore, the limit $s \to 0$ leads to derivatives with respect to s taken of master integrals in $f_5(s, m_{d_j}^2, m_{u_j}^2)$, that have prefactors proportional to $\frac{1}{s^2}$.
To calculate the derivatives of the master integrals $S_{10110}, S_{11101}, S_{01102}, S_{00220}$, and $S_{S_{00202}}$ (see (D.1) for the definition of the two-point two-loop integrals S_{abcde}) we first relate the genuine two-loop master integrals S_{10110}, S_{11110}, and S_{11101}, given in [115], to the dotted sunset integral with two different masses, S_{10220}, S_{20120}, and S_{20210}, via a change of basis using the reduction program KIRA [123, 124]. The vector of integrals

$$\vec{F} = (S_{00220}, S_{10220}, S_{20120}, S_{20210}) \tag{5.74}$$

fulfills the differential equation

$$\frac{\partial}{\partial s}\vec{F}(s) = -A_{-s}\vec{F}(s). \tag{5.75}$$

The matrix A_{-s} can be found in the appendix of [125] and its entries have at most simple poles in s such that

$$(A_{-s})_{ij} \underset{s\to 0}{\sim} \frac{B_{ij}}{s} + C_{ij}, \tag{5.76}$$

where B_{ij} and C_{ij} are constants which can also be zero for some combinations of i and j. The derivative at $s = 0$ is therefore given by,

$$\begin{aligned}
\frac{\partial}{\partial s}F_i(s=0) &\overset{(5.75)}{=} -\sum_{i,j}\lim_{s\to 0}(A_{-s})_{ij}F_j(s) \\
&\overset{(5.76)}{=} -\sum_{i,j}\lim_{s\to 0}\Big(\frac{B_{ij}}{s} + C_{ij}\Big)F_j(s) \\
&= -\sum_{i,j}\lim_{s\to 0} B_{ij}\frac{F_j(0) + F_j'(0)s + \mathcal{O}(s^2)}{s} - \sum_{i,j} C_{ij}F_j(0) \\
&= -\sum_{i,j}\lim_{s\to 0} B_{ij}\frac{F_j(0)}{s} - \sum_{i,j} B_{ij}F_j'(0) - \sum_{i,j} C_{ij}F_j(0).
\end{aligned} \tag{5.77}$$

By explicit calculation, using the specific form of A_{-s}, we obtain $B\vec{F}(0) = 0$. This leads to

$$\frac{\mathrm{d}}{\mathrm{d}s}F_i(s=0) = -\sum_{i,j} B_{ij}\frac{\mathrm{d}F_j}{\mathrm{d}s}(0) - \sum_{i,j} C_{ij}F_j(0), \tag{5.78}$$

which is a system of linear equations in the derivatives of the master integrals contained in the vector $\vec{F}$. By solving this system we obtain the derivative of $\vec{F}$ with respect to s at $s = 0$.
Some of the master integrals are the square of one-loop two-point functions (e.g. S_{01111}) and their derivatives with respect to s are given by

$$\frac{\mathrm{d}}{\mathrm{d}s}(I_{\mathrm{2p}}^{(1)}(s))^2 = 2I_{\mathrm{2p}}^{(1)}(s)\,\frac{\mathrm{d}}{\mathrm{d}s}I_{\mathrm{2p}}^{(1)}(s). \tag{5.79}$$

There are also master integrals which are the product of a one-loop two-point function and a one-loop tadpole (e.g. S_{01102}) with derivative

$$\frac{\mathrm{d}}{\mathrm{d}s}(I^{(1)}_{1\mathrm{p}}\, I^{(1)}_{2\mathrm{p}}(s)) = I^{(1)}_{1\mathrm{p}}\, \frac{\mathrm{d}}{\mathrm{d}s} I^{(1)}_{2\mathrm{p}}(s). \tag{5.80}$$

Using the corresponding differential equation for the one-loop integrals, the calculation of the derivative at $s = 0$ of the appearing one-loop two-point functions follows along the same lines as for the two-loop sunset integrals described above.

The limit $s \to 0$ of the master integrals was used as boundary condition in the calculation of the masters and, therefore, the corresponding integrals in this limit are known. The knowledge about the derivative with respect to s of the master integrals in $f_5(s, m^2_{d_j}, m^2_{u_j})$ at $s = 0$ and about the boundary condition fulfilled by the masters at $s = 0$ allows us now to calculate the limit $s \to 0$ of the transverse part of the W-boson self-energy. The result of the procedure leads to,

$$\Sigma^W_{\mathrm{T},(\alpha_s\alpha),1\mathrm{PI}}(0) = \frac{\alpha_s\alpha}{2\pi^2 s^2_{\mathrm{w}}} \frac{N_c^2-1}{2} \sum_{j=1}^{3} \Big[f_7(m^2_{d_j}, m^2_{u_j}) + (m_{d_j} \leftrightarrow m_{u_j}) \Big], \tag{5.81}$$

$$\Sigma^W_{\mathrm{T},(\alpha_s\alpha),\delta m}(0) = \frac{\alpha_s\alpha}{2\pi^2 s^2_{\mathrm{w}}} \frac{N_c^2-1}{2} \sum_{j=1}^{3} \Big[m^2_{u_j} f_8(m^2_{d_j}, m^2_{u_j}) + (m_{d_j} \leftrightarrow m_{u_j}) \Big]. \tag{5.82}$$

The $\mathcal{O}(N_f\alpha_s\alpha)$ corrections to the EW gauge-boson self-energies had already been calculated some time ago in Refs. [118, 126–130]. We have compared our results with the ones given in Ref. [118] and find full analytical agreement in the case of vanishing quark masses. For non-vanishing quark masses we find numerical agreement for $\Sigma^{V'V}_{\mathrm{T},(\alpha_s\alpha)}(k^2)$ with those results after fixing a mistake in the results of Ref. [118][1].

5.2.5 Electroweak input-parameter scheme at $\mathcal{O}(\alpha_s\alpha)$

In the following, we work in the G_μ-scheme which was introduced in Section 2.3 for NLO calculations. Formally, we derive the following value for α from G_μ,

$$\alpha_{G_\mu} = \frac{\sqrt{2} G_\mu M^2_{\mathrm{W}}}{\pi} \left(1 - \frac{M^2_{\mathrm{W}}}{M^2_{\mathrm{Z}}}\right), \tag{5.83}$$

i.e. we take α_{G_μ} as a real quantity which deserves some justification. In principle, the imaginary part of the renormalized coupling e is given by the imaginary part of the

[1] For $s < 0$, our results agree with the ones in Ref. [118] without modification. In order to get numerical agreement also in the region $s > 0$ we had to modify the functions $F(x)$ and $G(x)$ in Eq. (4.5) of Ref. [118] when evaluating them with squared arguments $F(x_a x_b)$, $G(x_a x_b)$ in Eq. (4.3) and likewise $F(x^2)$, $G(x^2)$ in Eq. (5.1). The modifications leading to a correct analytic continuation of the results in Ref. [118] to the region $s > 0$ explicitly read

$$F(x_a x_b) = 6\,\mathrm{Li}_3(x_a x_b) - 4\,\mathrm{Li}_2(x_a x_b)\,[\ln(x_a) + \ln(x_b)] - [\ln(x_a) + \ln(x_b)]^2\, \ln(1 - x_a x_b),$$
$$G(x_a x_b) = 2\,\mathrm{Li}_2(x_a x_b) + 2[\ln(x_a) + \ln(x_b)]\, \ln(1 - x_a x_b) + \frac{x_a x_b}{1 - x_a x_b}\, [\ln(x_a) + \ln(x_b)]^2.$$

charge renormalization constant, which in turn, is a consequence of the application of the CMS. The charge renormalization constant is determined only from self-energies at zero momentum transfer, which means, that it does not develop imaginary parts for real internal masses, as these only build up if internal particles running inside the loop of the self-energies could be produced on-shell, i.e. at the threshold (and zero momentum transfer is obviously not at the threshold of any massive particle). Therefore, the imaginary parts of the coupling e are only spurious terms, that are of formal two-loop order $\mathcal{O}(\alpha^2)$ and therefore not relevant at $\mathcal{O}(\alpha_s\alpha)$. This can be seen by a Taylor expansion of the complex masses appearing in self-energies that contribute to the charge renormalization constant around the real masses,

$$\begin{aligned}\Sigma_{\mathrm{T}}^{AA}(k^2=0,\{\mu_{\mathrm{W}},\dots\}) = \Sigma_{\mathrm{T}}^{AA}(k^2=0,\{M_{\mathrm{W}},\dots\}) \\ + \underbrace{(\mu_{\mathrm{W}}^2 - M_{\mathrm{W}}^2)}_{\mathcal{O}(\alpha)} \underbrace{\Sigma_{\mathrm{T}}'^{AA}(k^2=0,\{M_{\mathrm{W}},\dots\})}_{=\mathcal{O}(\alpha)} + \mathcal{O}(\alpha^3) + \mathcal{O}(\alpha_s\alpha^2),\end{aligned} \tag{5.84}$$

where we made the dependence of the self-energy on complex masses explicit and used that there are no one-loop QCD corrections to the electroweak gauge-boson self-energies, similar to the case in (2.115) and (5.44).

As at NLO we also need to adapt the charge renormalization constant when changing to the G_μ-scheme,

$$\delta Z_{e,(\alpha_s\alpha)}\big|_{G_\mu} = \delta Z_{e,(\alpha_s\alpha)} - \frac{1}{2}\Delta r_{(\alpha_s\alpha)}. \tag{5.85}$$

To obtain the expression of Δr at $\mathcal{O}(\alpha_s\alpha)$ we note that for its calculation only closed fermion-loop contributions to the gauge-boson self-energies are relevant at this perturbative order. Thus, we can obtain the expression for $\Delta r_{(\alpha_s\alpha)}$ from the $\mathcal{O}(\alpha)$ result for Δr (2.87) by substituting the NLO self-energies with the corresponding $\mathcal{O}(\alpha_s\alpha)$ quantities,

$$\begin{aligned}\Delta r_{(\alpha_s\alpha)} = \Sigma_{\mathrm{T},(\alpha_s\alpha)}'^{AA}(0) - \frac{c_{\mathrm{w}}^2}{s_{\mathrm{w}}^2}\left(\frac{\Sigma_{\mathrm{T},(\alpha_s\alpha)}^{ZZ}(M_{\mathrm{Z}}^2)}{M_{\mathrm{Z}}^2} - \frac{\Sigma_{\mathrm{T},(\alpha_s\alpha)}^{W}(M_{\mathrm{W}}^2)}{M_{\mathrm{W}}^2}\right) \\ + \frac{\Sigma_{\mathrm{T},(\alpha_s\alpha)}^{W}(0) - \Sigma_{\mathrm{T},(\alpha_s\alpha)}^{W}(M_{\mathrm{W}}^2)}{M_{\mathrm{W}}^2},\end{aligned} \tag{5.86}$$

where we have used (5.46).

5.3 Numerical results

5.3.1 Input parameters and event selection

The setup for the calculation is taken over from our publication [115] containing the results presented in the following sections. We choose the input parameters as [131],

$$\begin{aligned} M_{\mathrm{W,OS}} &= 80.385\,\mathrm{GeV}, & \Gamma_{\mathrm{W,OS}} &= 2.085\,\mathrm{GeV}, \\ M_{\mathrm{Z,OS}} &= 91.1876\,\mathrm{GeV}, & \Gamma_{\mathrm{Z,OS}} &= 2.4952\,\mathrm{GeV}, \\ M_{\mathrm{H}} &= 125.9\,\mathrm{GeV}, & m_{\mathrm{t}} &= 173.07\,\mathrm{GeV}, \\ G_\mu &= 1.1663787\times10^{-5}\,\mathrm{GeV}^{-2}, & m_{\mathrm{b}} &= 4.78\,\mathrm{GeV}. \end{aligned} \tag{5.87}$$

For the widths of the W- and Z-boson we use experimental values as input parameters instead of determining them by calculating their decay widths at the relevant order, which is a valid procedure in the complex-mass scheme as discussed in Section 2.4.2. The on-shell masses and widths of the vector bosons are converted to the corresponding pole masses according to (2.105). The masses of the light quark flavours (u,d,c,s) and of the leptons are neglected throughout. The masses for the top and bottom quark in (5.87) are their respective pole masses. The CKM matrix is chosen diagonal in the third generation, and the mixing between the first two generations is parametrized by the following values for the entries of the quark-mixing matrix,

$$|V_{\mathrm{ud}}| = |V_{\mathrm{cs}}| = 0.974, \qquad |V_{\mathrm{cd}}| = |V_{\mathrm{us}}| = 0.227. \tag{5.88}$$

While b-quarks appearing in closed fermion loops have the mass m_{b} given in Eq. (5.87), external b-quarks are taken as massless. The electromagnetic coupling constant is determined in the G_μ scheme, as described in the previous section.

In the OS scheme diagrams that contain the gauge-boson–fermion renormalization constants in Tab. 5.1 dictate the size of the vv-1PI $\mathcal{O}(N_f\alpha_s\alpha)$ corrections close to the resonance of the amplitude. Therefore, to estimate the size of corrections in the resonance region, in Tab. 5.1 we give numerical values for the gauge-boson–fermion renormalization constants $\delta^{\mathrm{ct},\sigma}_{V\bar{f}f',(\alpha_s\alpha)}$ defined in Eqs. (5.49) and (5.50) for $V = W, Z$. Due the smallness of $\delta^{\mathrm{ct},\sigma}_{V\bar{f}f',(\alpha_s\alpha)}$, the size of the vv-1PI $\mathcal{O}(N_f\alpha_s\alpha)$ corrections is at the permille level in the resonance regions.
Since in DY-like photon production the intermediate photon is off its mass shell in the region of the W/Z resonance, the photon–fermion renormalization constants do not enter the corrections to the resonant parts of the cross sections and we do not give values for the photon–fermion renormalization constants $\delta^{\mathrm{ct},\sigma}_{A\bar{f}f,(\alpha_s\alpha)}$. Moreover, light quarks are running in the closed fermionic loop leading to collinear singularities as the configuration for the photon-photon self-energy including these loops at zero momentum transfer (which is part of $\delta^{\mathrm{ct},\sigma}_{A\bar{f}f,(\alpha_s\alpha)}$ in the G_μ-scheme) fulfills the Landau equations depicted in Fig. 3.2. Even though present at intermediate steps, in the complete calculation those IR singularities cancel against the photon wave function renormalization constant contained in the photon self-energy correction, when the $\mathcal{O}(N_f\alpha_s\alpha)$ vertex corrections are combined with the corrections of the gauge-boson self-energy insertion, as e.g. in (5.17).

σ	$-$	$+$
$\delta^{\mathrm{ct},\sigma}_{W\bar{d}u,(\alpha_s\alpha)}/10^{-3}$	$0.0843967704 + 0.0026086585\,\mathrm{i}$	
$\delta^{\mathrm{ct},\sigma}_{W\bar{\nu}_\ell\ell,(\alpha_s\alpha)}/10^{-3}$	$0.0843967704 + 0.0026086585\,\mathrm{i}$	
$\delta^{\mathrm{ct},\sigma}_{Z\bar{u}u,(\alpha_s\alpha)}/10^{-3}$	$1.3246636238 - 0.2506548513\,\mathrm{i}$	$-4.4427625269 + 0.552219570\,\mathrm{i}$
$\delta^{\mathrm{ct},\sigma}_{Z\bar{d}d,(\alpha_s\alpha)}/10^{-3}$	$0.3190294259 - 0.1046758916\,\mathrm{i}$	$-4.4427625269 + 0.552219570\,\mathrm{i}$
$\delta^{\mathrm{ct},\sigma}_{Z\bar{\ell}\ell,(\alpha_s\alpha)}/10^{-3}$	$2.8687295153 - 0.4797272589\,\mathrm{i}$	$-4.4427625269 + 0.552219570\,\mathrm{i}$

Table 5.1: Numerical values for gauge-boson–fermion renormalization constants for the input values of Eq. (5.87) and $\alpha_s = 0.119$.

The numerical values are calculated using the complex-mass scheme and the G_μ input-parameter scheme, as described above, using the input values of Eq. (5.87) and $\alpha_s = 0.119$. For the PDFs we consistently use the NNPDF2.3 set [132], i.e. the NLO and NNLO QCD–EW corrections are evaluated using the NNPDF31_nlo_as_0118_luxqed set [133], which also includes $\mathcal{O}(\alpha)$ corrections. The value of the strong coupling $\alpha_s(M_Z) = 0.118$, which is used in the evaluation of the pp cross section, is dictated by the choice of these PDF sets. The renormalization and factorization scales are both set to a fixed value given by the respective gauge-boson mass,

$$\mu_R = \mu_F = M_V, \tag{5.89}$$

with $V = W, Z$ for W and Z production, respectively.

Phase-space cuts

For the experimental identification of the DY process we impose the following transverse momentum and rapidity cuts on the charged leptons,

$$p_{T,\ell^\pm} > 25\,\mathrm{GeV}, \qquad |y_{\ell^\pm}| < 2.5, \tag{5.90}$$

and, in case of the charged-current process, also an additional cut on the missing transverse energy (see (B.13) for a definition),

$$E_T^{\mathrm{miss}} > 25\,\mathrm{GeV}. \tag{5.91}$$

For the neutral-current process, we require a cut on the invariant mass $M_{\ell\ell}$ of the lepton pair,

$$M_{\ell\ell} = \sqrt{(p_{\ell_1} + p_{\ell_2})^2} > 50\,\mathrm{GeV}, \tag{5.92}$$

in order to avoid the photon pole at $M_{\ell\ell} \to 0$.

Since there is no photon emission involved in corrections of $\mathcal{O}(N_f\alpha_s\alpha)$, the issue of dressed leptons and photon recombination is of minor importance for the calculated corrections. The photon-recombination algorithm used in the calculation of $\mathcal{O}(\alpha_s\alpha)$ corrections to the neutral-current Drell–Yan process in PA is discussed later in Section 6.4.

5.3.2 Corrections to differential distributions

In the following, we present numerical results for corrections to the neutral- and charged-current Drell–Yan process at the LHC for a centre-of-mass energy of 14 TeV, in particular corrections of $\mathcal{O}(N_f\alpha_s\alpha)$. In case of W production the observables we consider are the transverse momentum of the positively charged lepton, the rapidity distribution of the W boson, and the transverse mass distribution, which is defined as (see also (B.15))

$$M_{\mathrm{T},\ell\nu} = \sqrt{2p_{\mathrm{T},\ell}E_{\mathrm{T,miss}}(1-\cos\phi_{\ell\nu})}. \tag{5.93}$$

For Z/γ production we study the transverse-momentum distribution of the positively charged lepton, the rapidity distribution of the final-state lepton-system, and the invariant-mass distribution of the leptons.

For on-shell DY-like W/Z production, in the rest frame of the intermediate on-shell W/Z bosons the final-state leptons are produced back-to-back with each of them having the energy $M_V/2$. This leads to the well-known Jacobian peak at $k_{\mathrm{T},\ell} = M_V/2$ clearly visible in the black graph in the upper plots of Fig. 5.6, representing the transverse-momentum distribution of the positively charge lepton for the LO cross section. Apart from the LO result Fig. 5.6 also shows the sum of the LO distribution and the NLO QCD $\mathrm{d}\sigma_{(\alpha_s)}$ corrections

$$\mathrm{d}\sigma_{\mathrm{NLOQCD}} = \mathrm{d}\sigma_{\mathrm{LO}} + \mathrm{d}\sigma_{(\alpha_s)}. \tag{5.94}$$

Furthermore, the sum of LO, NLO QCD corrections, and $\mathcal{O}(N_f\alpha_s\alpha)$ corrections

$$\mathrm{d}\sigma_{\mathrm{NNLO}} = \mathrm{d}\sigma_{\mathrm{LO}} + \mathrm{d}\sigma_{(\alpha_s)} + \mathrm{d}\sigma_{(N_f\alpha_s\alpha)} \tag{5.95}$$

is depicted. Due to jet-recoil effects (see Section B.2 for more information), where the intermediate W/Z boson recoils against initial-state QCD radiation, corrections to the transverse-momentum sprectrum can become very large, even larger than the LO contribution itself, which can be seen in Fig. 5.6. In this case, the LO prediction is obviously not a good approximation for observables that are sensitive to these jet-recoil effects. This is why we do not only consider relative $\mathcal{O}(N_f\alpha_s\alpha)$ corrections normalized to LO,

$$\delta = \frac{\mathrm{d}\sigma_{(N_f\alpha_s\alpha)}}{\mathrm{d}\sigma_{\mathrm{LO}}}, \tag{5.96}$$

but also a second variant where we normalize to the sum of LO and NLO QCD,

$$\delta' = \frac{\mathrm{d}\sigma_{(N_f\alpha_s\alpha)}}{\mathrm{d}\sigma_{\mathrm{NLOQCD}}}. \tag{5.97}$$

The ratio δ' quantifies the size of EW $\mathcal{O}(N_f\alpha)$ corrections to the cross section corrected at NLO QCD. As NLO EW corrections are relatively small compared to the NLO QCD corrections we do not include them in the second normalization version of relative corrections. However, we note in passing that due to final-state photon radiation they still lead to significant distortions of distributions and shifts therein. They can e.g. be found

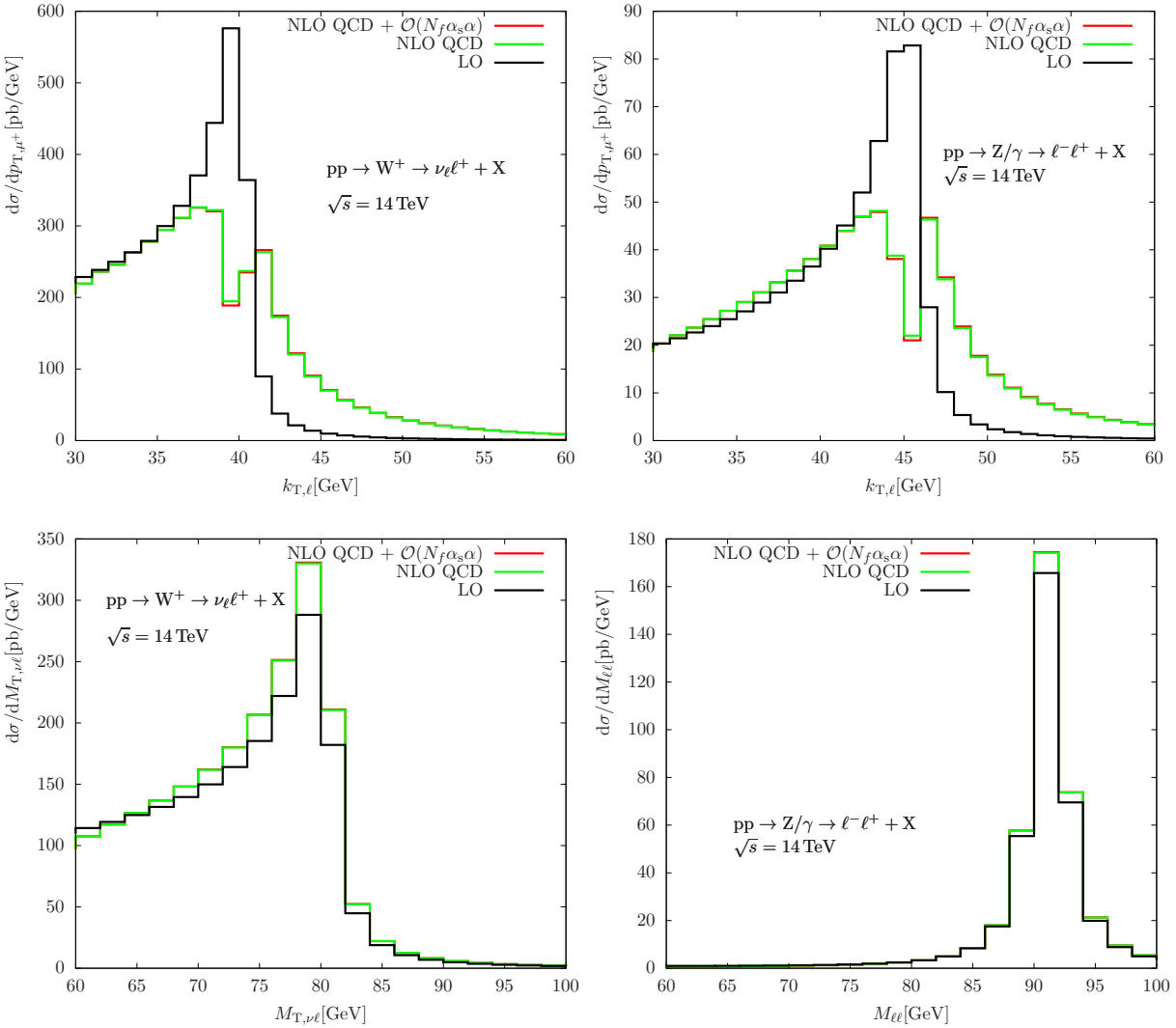

Figure 5.6: In the upper plots we show absolute distributions in the transverse-lepton-momentum for W production (left) and Z/γ production (right), whereas the lower plots show the transverse invariant-mass distribution for W production (left) and the invariant-mass distribution for Z/γ production (right).

in [21, 29]. In Fig. 5.6 we show the regions of low and high transverse momentum, as well as the region of low and high $M_{\ell\ell}$ and $M_{\mathrm{T},\ell\nu}$ individually. As we do not include longitudinal components of four-momenta in the calculation of the transverse mass (B.15), the W boson can still be on shell for $M_{\mathrm{T},\ell\nu} < M_{\mathrm{W}}$ by having a non-vanishing longitudinal component in the four-momentum. Therefore, in the charged-current case the absolute distribution in the low-mass plot is dominated by on-shell W bosons for $M_{\mathrm{T},\ell\nu} \lesssim M_{\mathrm{W}}$. In the neutral-current case the resonance of the Z boson only shows up for $M_{\ell\ell} \sim M_{\mathrm{Z}}$, visible in the lower plots of Fig. 5.6. The same reasoning also applies to the transverse-momentum distributions (as discussed in detail in Section B.1), i.e. as in the case of the transverse-mass distribution of the W boson, the W/Z boson can still be on shell when the k_{T} of the positively charged lepton is smaller than M_{V} ($V = W/Z$), and therefore, this region is dominated by the on-shell W/Z boson. This explains why the upper two

distribution and the lower one on the left in Fig. 5.6 are still relatively large below the resonance region, whereas the invariant-mass distribution of the two leptons is large only in the vicinity of the Z resonance.

In Fig. 5.7 we show the relative correction δ of $\mathcal{O}(N_f\alpha_s\alpha)$ to the distributions in the transverse mass of the final-state leptons $\nu_\ell\ell^+$ ($\ell = \mathrm{e}, \mu$) for the charged-current process and in the invariant mass of $\ell^+\ell^-$ for the neutral-current process. To get a better understanding of the size of individual contributions to the full $\mathcal{O}(N_f\alpha_s\alpha)$ and to probe possible approximations we do not only show the full $\mathcal{O}(N_f\alpha_s\alpha)$ (red curves) corrections but also corrections that include only the first two fermion generations (blue curves), neglecting the third generation that contains the in our setup massive top and bottom quarks. Furthermore, the corrections induced by reducible diagrams only (green curves) are depicted.
As discussed above, the region $M_{\mathrm{T},\ell\nu} \lesssim M_\mathrm{W}$ is dominated by the on-shell W boson, and as the absolute distribution peaks in the resonance region, the size of corrections in the low-mass plot in the charged-current case for $M_{\mathrm{T},\ell\nu} \lesssim M_\mathrm{W}$ is fully dictated by the size of the corrections in the region of on-shell W bosons. The size of corrections in the region of on-shell W bosons, in turn, can already be estimated from the renormalization constants given in Tab. 5.1, leading to the permille corrections in the low-mass plots.
In regions above the resonances, depicted in the high-mass plots on the r.h.s., the corrections grow up to 2% making them relevant in searches for new physics such as effects of W' or Z' bosons. The reducible contributions contribute the bulk of the corrections in the high-mass region, depicted on the r.h.s. of Fig. 5.7 in the green curve. However, it is also important to note that the effect of the irreducible corrections, given by the difference of the red and the green curves, is not negligible compared to the reducible corrections. Furthermore, we can clearly see that the contribution of the third fermion generation including the massive quarks is not suppressed compared to the impact of the first two generations. Comparing the red and the blue curves we can conclude that neither setting the masses of the quarks in the third generation to zero nor neglecting the third generation is a good approximation of the full $\mathcal{O}(N_f\alpha_s\alpha)$ corrections. As can be seen in the lower plots of Fig. 5.6, the NLO QCD corrections to the (transverse) invariant-mass distributions are of the order of 10%. Therefore, using the NLO QCD corrections in the normalization of the relative corrections instead of the LO distribution does not lead to large changes of the relative corrections. Qualitatively, the relative corrections δ' in Fig. 5.8 therefore show the same behaviour as the relative corrections δ normalized to LO. We note that in the lower right plots of Fig. 5.7 and Fig. 5.8 the $\mathrm{t\bar{t}}$ threshold is visible at $M_{\ell\ell} \sim 2m_\mathrm{t} \approx 346$ GeV in the full $\mathcal{O}(N_f\alpha_s\alpha)$ corrections (red curve) and the reducible part (green curve).

In Fig. 5.9 we show relative $\mathcal{O}(N_f\alpha_s\alpha)$ correction δ to the transverse-momentum distribution of the positively charged lepton in the low- (left) and high-k_T (right) region. As we have already discussed above, jet-recoil effects lead to the enhancement of NLO QCD corrections in the region above the resonance of the W/Z boson. The real initial-state radiation of a gluon or (anti)quark, the W/Z boson recoils against, is also present in $\mathcal{O}(N_f\alpha_s\alpha)$ corrections. Therefore, they are also enhanced above the resonance of the W/Z boson and grow up to 15%. As the real radiation is only present in the reducible but not in the irreducible $\mathcal{O}(N_f\alpha_s\alpha)$ corrections, the reducible corrections completely dominate in

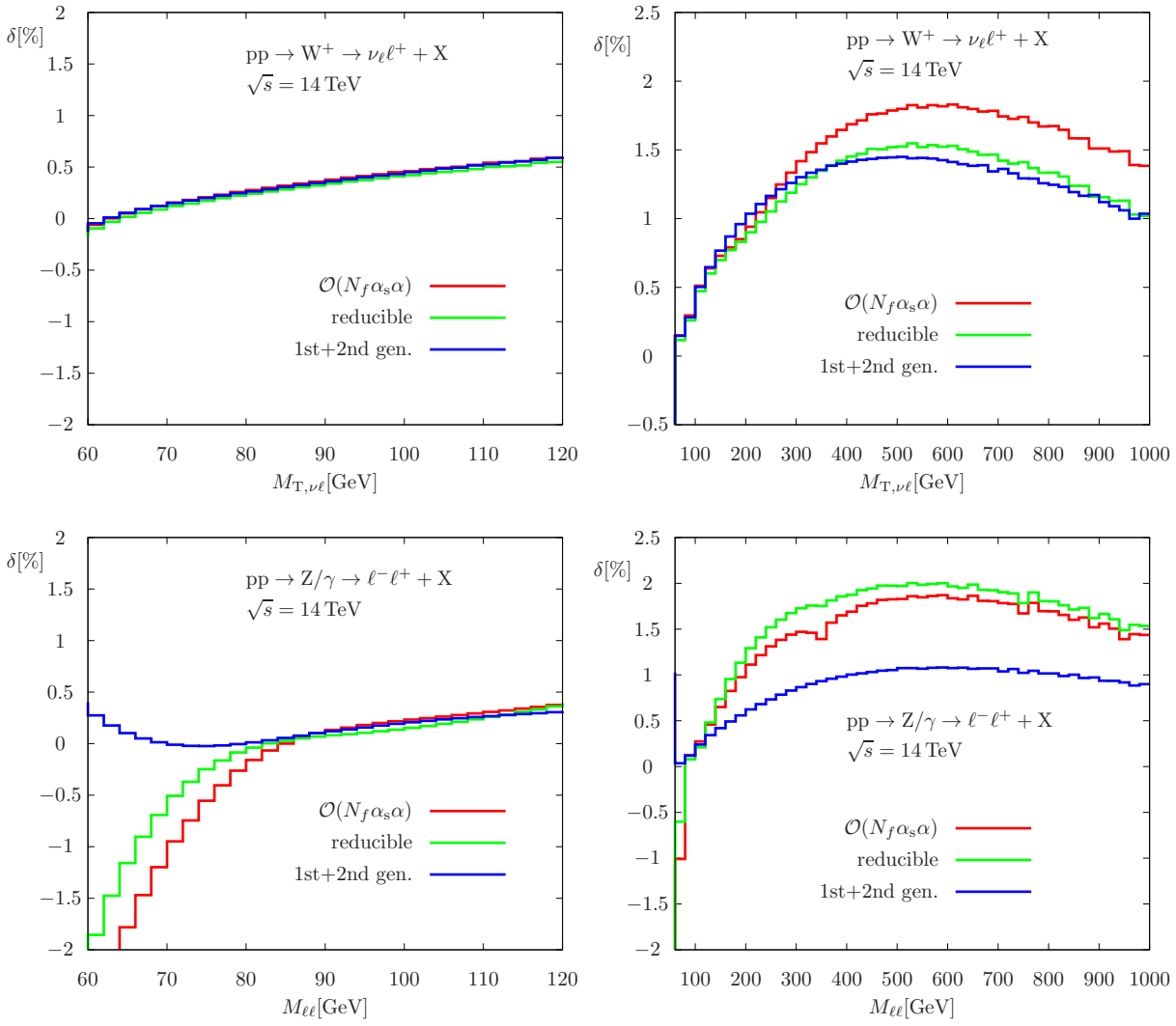

Figure 5.7: Relative $\mathcal{O}(N_f\alpha_s\alpha)$ corrections δ (normalized to the LO cross section) to distributions in the transverse invariant mass of the W bosons (upper plots) and in the invariant mass of the Z boson (lower plots), where the complete $\mathcal{O}(N_f\alpha_s\alpha)$ corrections are compared to the contribution originating from reducible graphs and to the contribution delivered by the first two fermion generations.

contrast to the situation already observed in the (transverse) invariant mass spectra. In Fig. 5.10 we show the corrections δ' to the transverse-momentum distributions normalized to the NLO QCD correction. In these distributions we find the expected size of $\mathcal{O}(\alpha_s\alpha)$ corrections as the enhancing recoil effects are now present not only in the numerator but also in the denominator of the relative correction and therefore cancel out.
The fact that the corrections δ' reach several percent on the resonance at $k_{T,\ell} \sim M_V/2$ is in fact induced by the choice of normalization. As can be seen in Fig. 5.6, the NLO QCD corrections $d\sigma_{(\alpha_s)}$ are large and negative in the vicinity of the resonance in the chosen setup leading to a local minimum of the denominator $d\sigma_{\text{NLOQCD}}$ in (5.97) and therefore enhancing δ' in this region.

Figure 5.11 shows the relative correction δ of $\mathcal{O}(N_f\alpha_s\alpha)$ to the rapidity distribution of

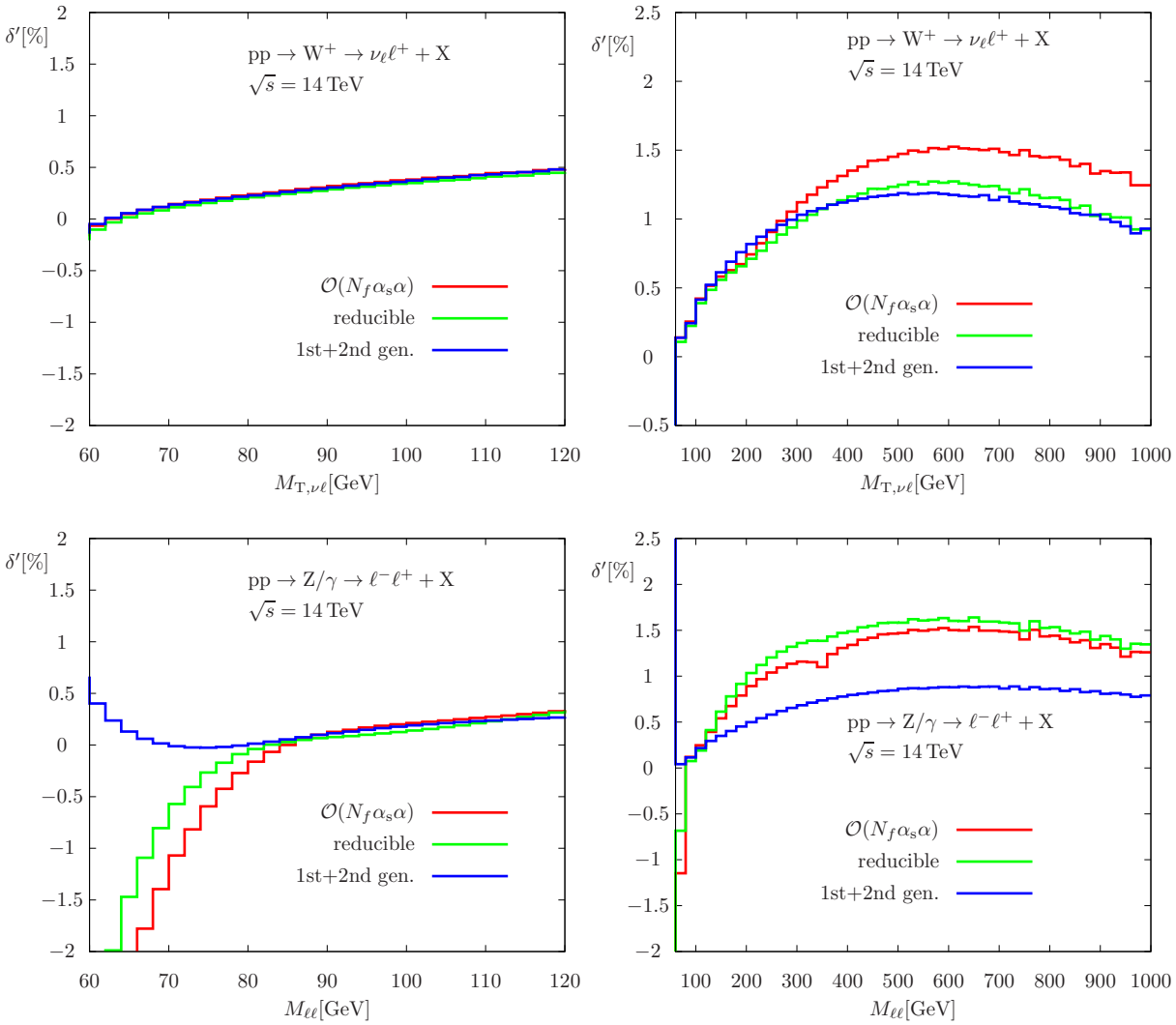

Figure 5.8: Relative $\mathcal{O}(N_f\alpha_s\alpha)$ corrections δ' (normalized to the NLO QCD cross section) to distributions in the transverse invariant mass of the W bosons (upper plots) and in the invariant mass of the Z boson (lower plots), where the complete $\mathcal{O}(N_f\alpha_s\alpha)$ corrections are compared to the contribution originating from reducible graphs and to the contribution delivered by the first two fermion generations.

the final-state leptons $\nu_\ell\ell^+$ in the charged-current process and $\ell^+\ell^-$ in the neutral-current process. Equation (5.10) in the beginning of this chapter led us to the conclusion that corrections to rapidity distributions are dominated by the size of the corrections in the resonance region. As discussed above, $\mathcal{O}(N_f\alpha_s\alpha)$ corrections are at the permille level in the vicinity of the resonance setting also the size of corrections to rapidity distributions to this magnitude, which is clearly visible in Fig. 5.11.

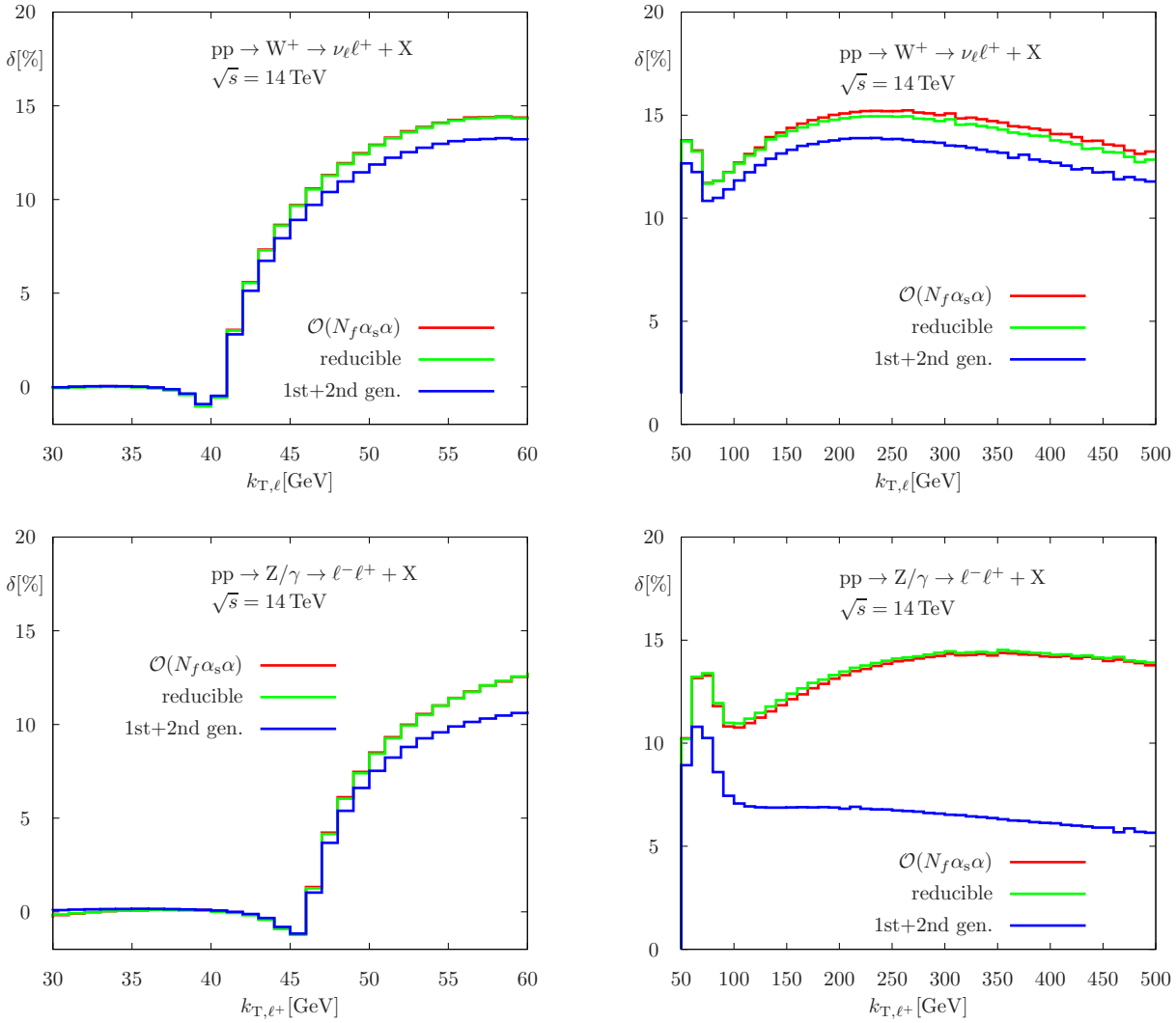

Figure 5.9: Relative $\mathcal{O}(N_f\alpha_s\alpha)$ corrections δ (normalized to the LO cross section) to transverse-momentum distributions for W-boson (upper plots) and Z-boson production (lower plots), again with a comparison of full $\mathcal{O}(N_f\alpha_s\alpha)$ corrections to its reducible parts and to the contribution of the first two fermion generations.

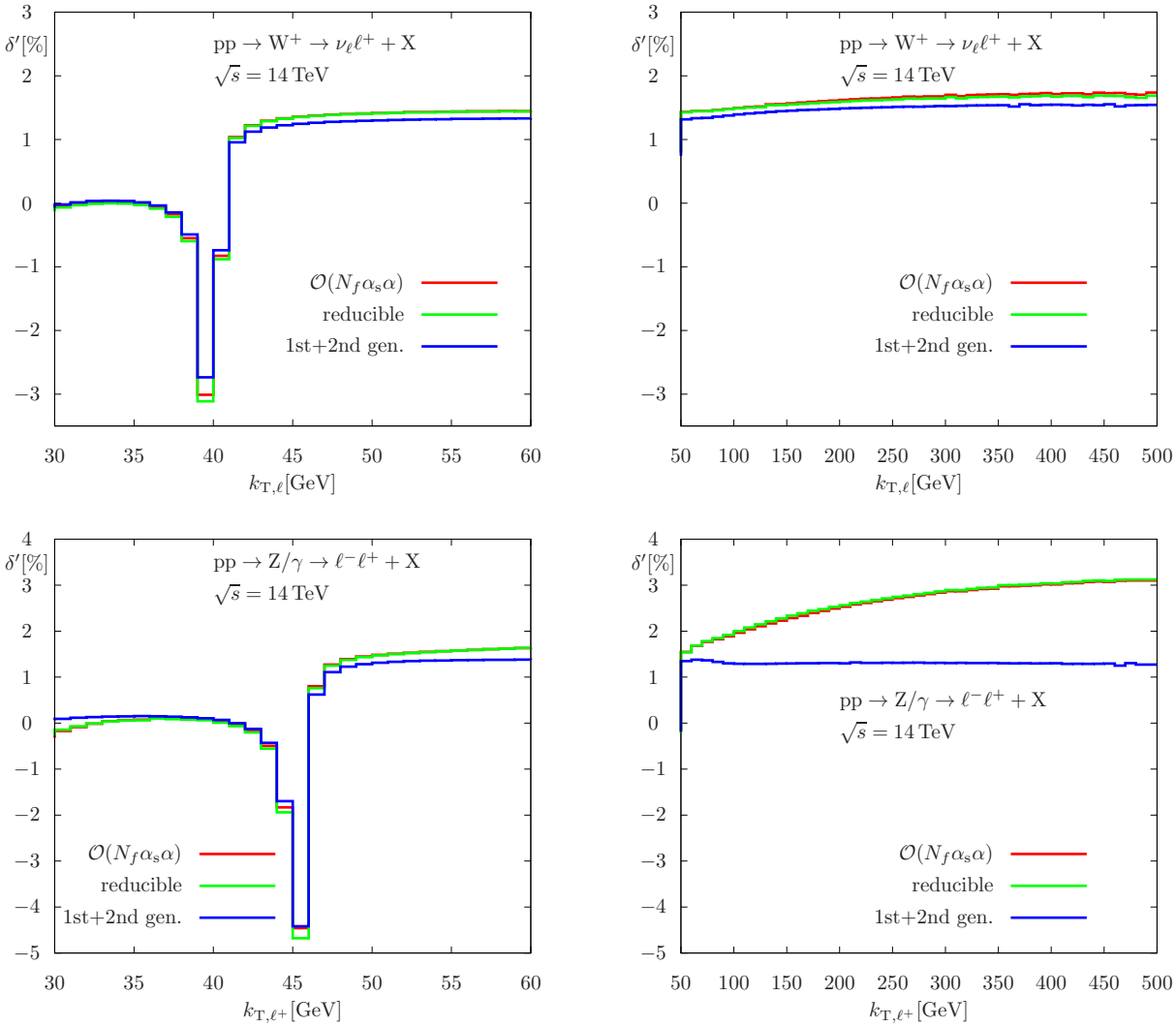

Figure 5.10: Relative $\mathcal{O}(N_f\alpha_s\alpha)$ corrections δ' (normalized to the NLO QCD cross section) to transverse-momentum distributions for W-boson (upper plots) and Z-boson production (lower plots), again with a comparison of full $\mathcal{O}(N_f\alpha_s\alpha)$ corrections to its reducible parts and to the contribution of the first two fermion generations.

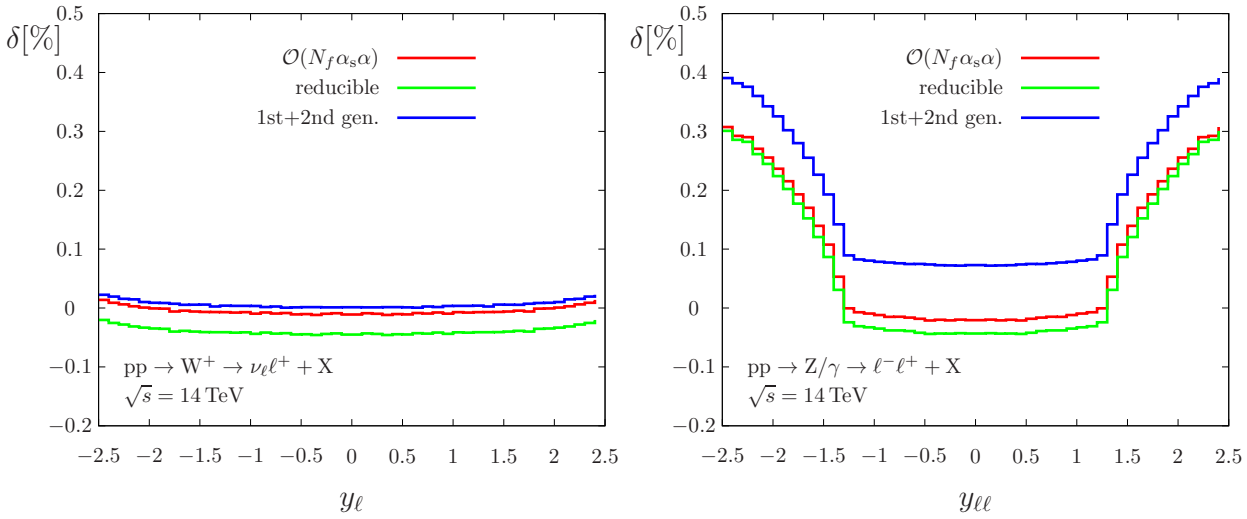

Figure 5.11: Relative $\mathcal{O}(N_f\alpha_s\alpha)$ corrections δ (normalized to the LO cross section) to distributions in rapidity distribution of the W bosons (left) and the Z boson (right), where the complete $\mathcal{O}(N_f\alpha_s\alpha)$ corrections are compared to the contribution originating from reducible graphs and to the contribution delivered by the first two fermion generations.

Chapter 6

QCD×electroweak corrections to single-Z production in pole approximation

In this section we describe the calculation of $\mathcal{O}(\alpha_s\alpha)$ corrections to the neutral-current Drell–Yan process in pole approximation (PA). We start by introducing the pole scheme for processes with a single resonance and use this as the starting point for the definition of the PA. The PA for the DY-like Z production is obtained by neglecting non-resonant parts and taking into account only the leading term of amplitudes in the expansion around the resonance of the Z boson. The neglect of non-resonant terms leads to an intrinsic uncertainty of the PA given by the width of the Z boson over its mass. The NLO contributions are therefore calculated without any approximation as the intrinsic uncertainty of the PA at NLO is of the same order as $\mathcal{O}(\Gamma_Z/M_Z)\cdot\mathcal{O}(\alpha) = \mathcal{O}(\alpha^2)$, which is roughly of the order of the NNLO corrections we are going to calculate (ignoring that α_s is larger than α for this estimate).

The application of the PA to corrections of $\mathcal{O}(\alpha_s\alpha)$ to DY-like Z production gives rise to separately gauge-invariant building blocks, which are discussed in Section 6.2. Corrections of "initial–initial" (II) type—i.e. corrections of $\mathcal{O}(\alpha_s\alpha)$ with both a QCD and a EW correction to the production of the Z boson—are the last missing piece to complete the calculation of $\mathcal{O}(\alpha_s\alpha)$ corrections to DY-like Z boson production in PA presented in [55, 56]; their calculation is discussed in Sect. 6.3. The results of this chapter are going to be published in [134].

6.1 Pole approximation for DY processes

We start with the observation that we can schematically write the transition amplitude for a process with a single resonance in the following form,

$$\mathcal{M} = \frac{W(p_V^2)}{p_V^2 - M_V^2 + \hat{\Sigma}(p_V^2)} + N(p_V^2), \tag{6.1}$$

where instability effects of the massive gauge boson V are included using the Dyson-summed propagator (2.97). The function $W(p_V^2)$ describes resonant, and $N(p_V^2)$ non-resonant parts that arise, e.g., by the connection of the initial and final state only by a

photon, i.e. $V = \gamma$. Using the gauge-invariant location of the propagator pole [76, 78, 135] given in (2.100) as the expansion point to rewrite the denominator,

$$p_V^2 - M_V^2 + \hat{\Sigma}(p_V^2) = (p_V^2 - \mu_V^2)\left(1 + \hat{\Sigma}'(\mu_V^2)\right) + \mathcal{O}\left((p_V^2 - \mu_V^2)^2\right), \tag{6.2}$$

one can isolate the resonant part of the amplitude in the following way [55, 56, 60],

$$\mathcal{M} = \underbrace{\frac{W(\mu_V^2)}{p_V^2 - \mu_V^2}\,\frac{1}{1+\hat{\Sigma}'(\mu_V^2)}}_{\text{“factorizable”}} + \underbrace{\left[\frac{W(p_V^2)}{p_V^2 - M_V^2 + \hat{\Sigma}(p_V^2)} - \frac{W(\mu_V^2)}{p_V^2 - \mu_V^2}\,\frac{1}{1+\hat{\Sigma}'(\mu_V^2)}\right]}_{\text{“non-factorizable”}} + \underbrace{N(p_V^2)}_{\text{neglected in PA}}. \tag{6.3}$$

The last equation defines the so-called pole scheme which has been applied to e.g. Z production in [29]. The PA [77, 136, 137] is obtained from the pole scheme by neglecting the non-resonant parts $N(p_V^2)$, and performing an expansion in p_V^2 around $p_V^2 = \mu_V^2$ of the term in the square brackets and keeping only the leading term of the expansion. The first term on the r.h.s. defines the so-called factorizable corrections which include the corrections to on-shell production and decay of the boson V connected by an off-shell propagator. The resonant contributions originating from the second term on the r.h.s. define the non-factorizable corrections which include contributions where the on-shell production and decay of the vector boson V is connected by a soft photon in addition to the connection by the vector boson V itself. It can be shown by power counting [138] that the combination of an on-shell V boson and a soft photon results in a single pole, i.e. a resonance enhancement. Therefore, these contributions have to be included in a resonance expansion.

Note that if we use the real OS renormalization scheme the derivative of the renormalized self-energy evaluated at M_V^2 is purely imaginary, and therefore the relevant part of the correction factor for the residue reduces to 1. To see this we first expand the correction factor for the residue

$$\frac{1}{1+\hat{\Sigma}'(\mu_V^2)} = \frac{1}{1 + \underbrace{\hat{\Sigma}'(M_V^2)}_{=\mathrm{i}\,\mathrm{Im}\left(\frac{\mathrm{d}}{\mathrm{d}p^2}\hat{\Sigma}(p^2)\big|_{p^2=M_V^2}\right)=\mathcal{O}(\Gamma_V/M_V)} + \mathcal{O}\left(M_V\Gamma_V\cdot\alpha\right)} = 1 + \mathrm{i}\,\mathcal{O}\left(\frac{\Gamma_V}{M_V}\right), \tag{6.4}$$

where we used that the renormalized self-energy $\hat{\Sigma}(p^2)$ scales as $\mathrm{i}M_V\Gamma_V$ for $p^2 \approx M_V^2$ and that $\frac{\mathrm{d}}{\mathrm{d}p^2}$ scales as $\frac{1}{M_V^2}$ to obtain the right-hand side of (6.4). Further, we note that the contribution of (6.3) to the squared amplitude is obtained by interfering $\mathcal{M}$ with the LO amplitude and afterwards taking the real part which eliminates the imaginary part on the right-hand side of (6.4). Therefore, the relevant part of the correction factor for the residue to obtain the contribution to the squared amplitude is just 1.
For corrections of $\mathcal{O}(\alpha_s\alpha)$ in the resonance region, the replacement of the complex masses μ_V^2 by M_V^2 in the numerator of the factorizable part in (6.3) also leads to an error of the same size as the intrinsic uncertainty $\mathcal{O}(\alpha_s\alpha/\pi^2 \times \Gamma_V/M_V)$ of the PA. Therefore, we can

avoid the evaluation with complex masses and replace them by their real part. This result can be obtained with a similar expansion as in (6.4)

$$\begin{aligned}
\mathcal{M}(\mu_V^2) &= \mathcal{M}(M_V^2) + (\mu_V^2 - M_V^2)\mathcal{M}'(M_V^2) + \mathcal{O}((\mu_V^2 - M_V^2)^2) \\
&= \mathcal{M}(M_V^2)\left(1 + \mathrm{i}\Gamma_V M_V \underbrace{\frac{\mathcal{M}'(M_V^2)}{\mathcal{M}(M_V^2)}}_{=\mathcal{O}(1/M_V^2)} + \mathcal{O}\left(\frac{\Gamma_V^2}{M_V^2}\right)\right) \\
&= \mathcal{M}(M_V^2) + \mathcal{O}\left(\frac{\Gamma_V}{M_V}\right) \underbrace{\mathcal{O}\big(\mathcal{M}(M_V^2)\big)}_{=\mathcal{O}(\frac{\alpha_\mathrm{s}\alpha}{\pi^2})} \\
&= \mathcal{M}(M_V^2) + \mathcal{O}\Big(\frac{\alpha_\mathrm{s}\alpha}{\pi^2} \times \frac{\Gamma_V}{M_V}\Big).
\end{aligned} \tag{6.5}$$

The on-shell evaluation of the numerator is accomplished by the application of an on-shell projection of the kinematics. The definition of the projection involves some freedom and the difference of results obtained from different projections is again of the order of the intrinsic uncertainty of the PA at the respective order in perturbation theory if the PA is only applied to the "highest" perturbative order considered in the calculation.

6.2 Survey of $\mathcal{O}(\alpha_\mathrm{s}\alpha)$ corrections to single-Z production in pole approximation

The application of the PA to neutral-current Drell–Yan processes [21, 55, 56, 77, 86, 139] allows the identification and classification of corrections to DY processes into separately gauge-invariant parts that are enhanced in the vicinity of the resonance of the intermediate Z boson. At NLO different versions of the PA have been compared to full NLO calculations. For kinematic distributions dominated by the resonance region agreement was found at the permil level between the PA and the full calculations in the resonance region [21, 55, 86, 140]. In the context of $\mathcal{O}(\alpha_\mathrm{s}\alpha)$ corrections the PA has been first applied in [55] where the classification of the corrections into four different parts has been worked out. In [55, 56] it has been shown that the factorizable corrections of type "final–final" and in particular corrections of type "initial–final"—i.e. corrections of $\mathcal{O}(\alpha_\mathrm{s}\alpha)$ where either both QCD and EW corrections are combined in the Z-boson decay, or the QCD corrections are contained in the production and the EW corrections in the Z-boson decay—are numerically dominant compared to the phenomenologically negligible non-factorizable corrections where production and decay of the intermediate Z boson are linked by a soft photon. The four types of corrections can be further classified into double-real, real–virtual, and double-virtual corrections. We show the separation of corrections into the four types in the case of double-virtual corrections in Fig. 6.1.

The expansion of the full NNLO $\mathcal{O}(\alpha_\mathrm{s}\alpha)$ correction around the resonance pole at $p_Z^2 \approx M_Z^2$ leads to the following four types of corrections:

- The factorizable initial–initial $\mathcal{O}(\alpha_\mathrm{s}\alpha)$ corrections to on-shell Z production receive contributions from genuine two-loop $\mathcal{O}(\alpha_\mathrm{s}\alpha)$ diagrams, from one-loop real–virtual

and tree-level double-real diagrams. In order to stay closer to a calculation without any approximations we split the factorizable initial–initial $\mathcal{O}(\alpha_s\alpha)$ corrections into the separately gauge-invariant QCD×weak $\mathcal{O}(\alpha_s\alpha_w)$ and QCD×photonic $\mathcal{O}(Q_q^2\alpha_s\alpha_{phot})$ corrections and calculate the QCD×photonic part without on-shell approximation for the Z boson whereas in case of the QCD×weak $\mathcal{O}(\alpha_s\alpha_w)$ corrections we have to use the PA in order to preserve gauge invariance. The calculation of these corrections of type initial–initial completes the effort [55, 56] of calculating the full set of $\mathcal{O}(\alpha_s\alpha)$ corrections to Z boson production in PA.

- Factorizable initial–final $\mathcal{O}(\alpha_s\alpha)$ corrections are given by contributions that include the $\mathcal{O}(\alpha_s)$ correction to Z production combined with the $\mathcal{O}(\alpha)$ correction to the leptonic Z decay. It has been shown in [56] that this class of corrections captures the dominant effects of $\mathcal{O}(\alpha_s\alpha)$ corrections in PA due to the large corrections of real final-state photon radiation.

- The factorizable final–final corrections include only $\mathcal{O}(\alpha_s\alpha)$ counterterm contributions to the lepton–Z-vertices and contain no contributions from real radiation diagrams. In [56] an explicit calculation of these corrections showed that their impact on distributions is phenomenologically negligible.

- Non-factorizable corrections include QCD $\mathcal{O}(\alpha_s)$ corrections to the Z-boson production, combined with a soft-photon exchange between the initial-state quarks and the final-state leptons. Individually the real and virtual non-factorizable corrections for different partonic channels lead to sizeable corrections to the (transverse) invariant mass and transverse-momentum spectra of the intermediate W/Z boson. However, due to cancellation between real and virtual corrections the numerical impact of these corrections is of the sub-permil level [55] and is therefore of no relevance for phenomenology.

The details of our calculation of the corrections of type "initial–initial" are presented in the next section, where the calculation of "initial–final" and "final–final" type corrections is discussed in [56].

We only apply the PA to weak×QCD $\mathcal{O}(\alpha_s\alpha)$ initial–initial corrections and in particular not at LO, as the application of the PA at LO would lead to an uncertainty $\mathcal{O}(\Gamma_V/M_V) = \mathcal{O}(\alpha)$ which is larger than the typical order of the NNLO corrections we are interested in. Also NLO corrections are calculated without the application of the PA. The details of the OS mappings that have to be applied to the kinematics in the PA are discussed when they become first relevant below. In contrast to the weak×QCD initial–initial corrections, which are gauge-invariant only when applying a PA, the photonic×QCD $\mathcal{O}(\alpha_s\alpha)$ initial–initial corrections are gauge invariant even without a PA as they are proportional to the charge factors $Q_{q_a}Q_{q_b}$ of the initial state quarks, and we choose to evaluate them without on-shell approximation for the Z boson to stay closer to the full calculation of the $\mathcal{O}(\alpha_s\alpha)$ corrections.

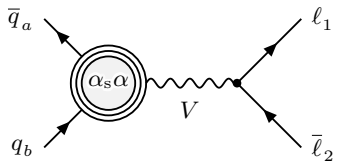

(a) Factorizable initial–initial corrections

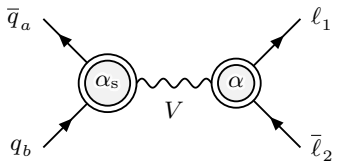

(b) Factorizable initial–final corrections

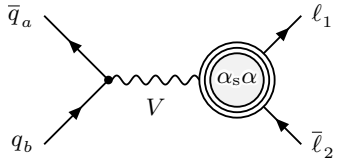

(c) Factorizable final–final corrections

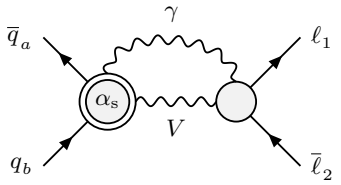

(d) Non-factorizable corrections

Figure 6.1: The four different contributions to the mixed QCD×EW corrections in PA, where simple circles represent tree structures, double circles one-loop corrections, and triple circles two-loop contributions. The pictures have been taken from [56].

6.3 Calculation of the factorizable initial–initial corrections

In this section we describe the calculation of the factorizable initial–initial corrections of $\mathcal{O}(\alpha_s\alpha)$ in detail. A pictorial representation of these corrections is shown in Fig. 6.2. As described in the last section we separate the full $\mathcal{O}(\alpha_s\alpha)$ "initial–initial" corrections into QCD×photonic $\mathcal{O}(Q_q^2\alpha_s\alpha_p)$ and QCD×weak $\mathcal{O}(\alpha_s\alpha_w)$ corrections. In order to stay closer to the full calculation of the $\mathcal{O}(\alpha_s\alpha)$ corrections we apply the PA only to the QCD×weak $\mathcal{O}(\alpha_s\alpha_w)$ part. The IR pole structure of QCD×weak initial–initial corrections is of one-loop complexity, so that one-loop subtraction schemes are sufficient to handle the IR poles. Concerning the double-real $\mathcal{O}(Q_q^2\alpha_s\alpha_p)$ initial–initial corrections there are two potentially unresolved particles in the final state demanding a proper two-loop subtraction scheme and we applied antenna subtraction. In order to construct antenna subtraction functions at $\mathcal{O}(Q_q^2\alpha_s\alpha_p)$ one can use the subleading colour parts of the known $\mathcal{O}(\alpha_s^2)$ antenna functions for the initial–final [108] and initial–initial [109, 112] cases. Apart from the subtraction terms obtained in this way we also discuss the calculation of the amplitudes relevant for $\mathcal{O}(Q_q^2\alpha_s\alpha_p)$ initial–initial corrections in the following sections. In Section 6.4 we present the corresponding numerical results.

6.3.1 Double-virtual corrections

Here we describe the calculation of the double-virtual QCD×weak $\mathcal{O}(\alpha_s\alpha_w)$ and the QCD×phot $\mathcal{O}(Q_q^2\alpha_s\alpha_p)$ initial–initial corrections to the squared $q\bar{q} \to \ell\bar{\ell}$ matrix element, where the starting point of our calculation of the $\mathcal{O}(\alpha_s\alpha_w)$ corrections is the two-loop

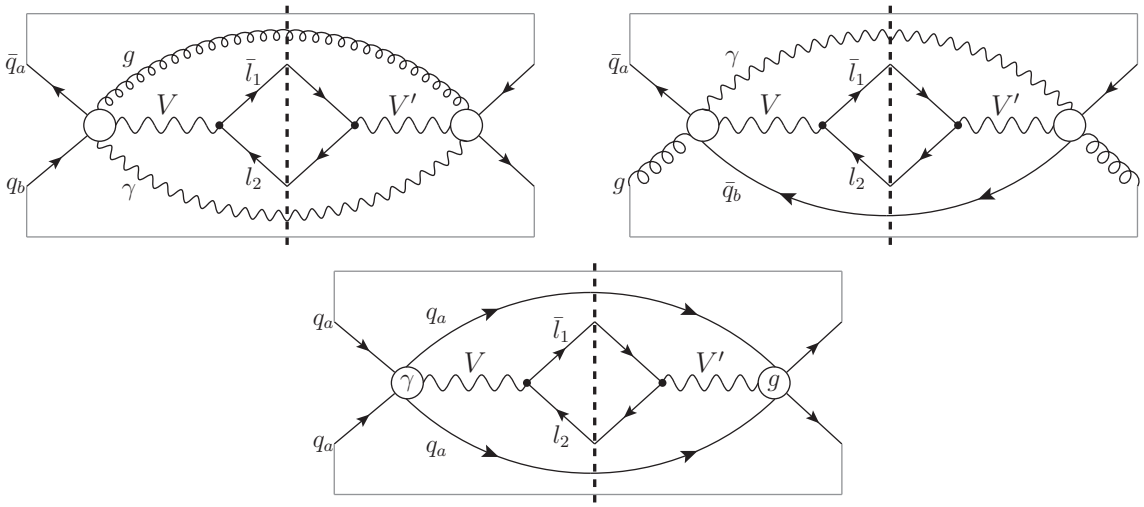

(a) Double-real $\mathcal{O}(Q_q^2\alpha_\mathrm{s}\alpha_\mathrm{p})$ initial–initial interference diagrams

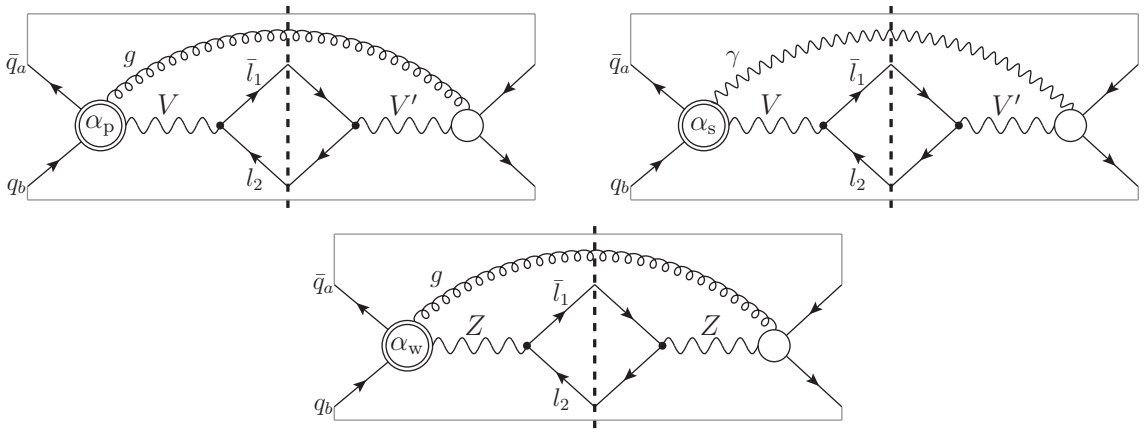

(b) Real–virtual $\mathcal{O}(Q_q^2\alpha_\mathrm{s}\alpha_\mathrm{p})$ initial–initial (first line) and factorizable $\mathcal{O}(\alpha_\mathrm{s}\alpha_\mathrm{w})$ initial–initial (second line) interference diagrams

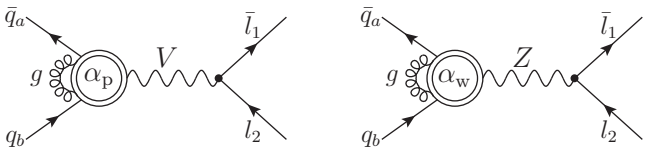

(c) Double-virtual $\mathcal{O}(Q_q^2\alpha_\mathrm{s}\alpha_\mathrm{p})$ initial–initial and factorizable $\mathcal{O}(\alpha_\mathrm{s}\alpha_\mathrm{w})$ initial–initial diagrams

Figure 6.2: Various contributions to the gauge-invariant set of $\mathcal{O}(Q_q^2\alpha_\mathrm{s}\alpha_\mathrm{p})$ and the factorizable initial–initial $\mathcal{O}(\alpha_\mathrm{s}\alpha_\mathrm{w})$ corrections, where $V, V' = Z, \gamma$. Double circles indicate one-loop corrections, simple circles indicate relevant tree structures, and simple circles with a "γ" ("g") inside represent all possible connected tree-level diagrams of the process $q_a q_a \to q_a q_a + V$ with an intermediate photon (gluon). An additional particle attached to a "one-loop blob", as e.g. in Fig. 6.2c, means that the particle has to be inserted into the corresponding one-loop diagram in all possible ways.

formfactor for light quarks,

$$F_\mu^{Z\bar{q}q}(q^2) = \mathrm{i}e\gamma_\mu \left(\frac{1+\gamma_5}{2} F_\mathrm{R}^{Z\bar{q}q}(q^2) + \frac{1-\gamma_5}{2} F_\mathrm{L}^{Z\bar{q}q}(q^2) \right). \tag{6.6}$$

The unrenormalized reducible (red) part of $\mathcal{O}(\alpha_\mathrm{w}\alpha_\mathrm{s})$ contribution to the formfactor is defined as the product of the known one-loop QCD and weak corrections to the form factor,

$$F_{\mathrm{V_s}\otimes\mathrm{V_w},\tau}^{Z\bar{q}q,\mathrm{red}}(q^2) = \delta_{\mathrm{V_s}}^{Z\bar{q}q}(q^2)\; F_{\mathrm{V_w},\tau}^{Z\bar{q}q}(q^2), \tag{6.7}$$

where the expressions for the NLO weak correction factor can be found, e.g., in [29,55] and $\delta_{\mathrm{V_s}}^{Z\bar{q}q}(q^2)$ is defined in (5.19). We define the unrenormalized irreducible (irred) contribution as the difference between the full $\mathcal{O}(\alpha_\mathrm{w}\alpha_\mathrm{s})$ formfactor and the reducible contribution,

$$F_{\mathrm{V_s}\otimes\mathrm{V_w},\tau}^{Z\bar{q}q,\mathrm{irred}}(q^2) = F_{\mathrm{V_s}\otimes\mathrm{V_w},\tau}^{Z\bar{q}q}(q^2) - F_{\mathrm{V_s}\otimes\mathrm{V_w},\tau}^{Z\bar{q}q,\mathrm{red}}(q^2), \tag{6.8}$$

which can be written in terms of two auxiliary functions ϕ_A and ϕ_NA,

$$\begin{aligned}
F_{\mathrm{V_s}\otimes\mathrm{V_w},\mathrm{R}}^{Z\bar{q}q,\mathrm{irred}}(q^2) &= C_F \frac{\alpha_s}{4\pi}\frac{\alpha}{4\pi} g_R^3\, \phi_\mathrm{A}(q^2/m_Z^2), \\
F_{\mathrm{V_s}\otimes\mathrm{V_w},\mathrm{L}}^{Z\bar{q}q,\mathrm{irred}}(q^2) &= C_F \frac{\alpha_s}{4\pi}\frac{\alpha}{4\pi} \left(g_L^3 \phi_\mathrm{A}(q^2/m_Z^2) + \frac{g_L}{2s_w^2}\phi_\mathrm{A}(q^2/m_W^2) + c_W \frac{I_3}{2s_w^3}\phi_\mathrm{NA}(q^2/m_W^2) \right),
\end{aligned} \tag{6.9}$$

where

$$g_R = -\frac{Q s_\mathrm{w}}{c_\mathrm{w}}, \qquad g_L = \frac{I_\mathrm{w}^3 - Q s_\mathrm{w}^2}{c_\mathrm{w} s_\mathrm{w}}. \tag{6.10}$$

Results for the two formfactor functions ϕ_A and ϕ_NA can be found in Ref. [141]. To evaluate the two functions ϕ_A and ϕ_NA numerically we use the Fortran library `handyG` [142].

The irreducible part of the $\mathcal{O}(\alpha_\mathrm{s}\alpha_\mathrm{w})$ formfactor $F_{\mathrm{V_s}\otimes\mathrm{V_w},\tau}^{Z\bar{q}q,\mathrm{irred}}$ is UV- and IR-finite and is not affected by the choice of a specific renormalization scheme. Therefore, in order to obtain the renormalized form factor for massless quarks $\hat{F}_{\mathrm{V_s}\otimes\mathrm{V_w},\tau}^{Z\bar{q}q}$ it is sufficient to add the Z-boson–fermion vertex counterterm to the unrenormalized weak formfactor in the reducible part of the full $\mathcal{O}(\alpha_\mathrm{s}\alpha_\mathrm{w})$ formfactor,

$$\hat{F}_{\mathrm{V_s}\otimes\mathrm{V_w},\tau}^{Z\bar{q}q}(q^2) = \hat{F}_{\mathrm{V_s}\otimes\mathrm{V_w},\tau}^{Z\bar{q}q,\mathrm{irred}}(q^2) + \delta_{\mathrm{V_s}}^{Z\bar{q}q}(q^2)(F_{\mathrm{V_w},\tau}^{Z\bar{q}q}(q^2) + \delta_{Z\bar{q}q,\mathrm{weak}}^{\mathrm{ct},\tau}), \tag{6.11}$$

where we indicate renormalized quantities by the superscript $\hat{}$ and the explicit form of the one-loop vertex counterterms in the on-shell scheme can be found in Eq. (A.44) of Ref. [60]. Note that $\delta_{\mathrm{V_s}}^{Z\bar{q}q}$ as defined in (5.19) is a UV-finite quantity and all remaining divergences in $\delta_{\mathrm{V_s}}^{Z\bar{q}q}$ are of IR origin, i.e. $\hat{\delta}_{\mathrm{V_s}}^{Z\bar{q}q} = \delta_{\mathrm{V_s}}^{Z\bar{q}q}$. This is because the quark wave-function renormalization constant $\delta Z_q^{(\alpha_\mathrm{s})}$ vanishes for massless quarks ($\delta Z_q^{(\alpha_\mathrm{s})}$ is determined from a scaleless integral and therefore vanishes in dimensional regularization) and no other renormalization constants contribute to $\delta_{\mathrm{V_s}}^{Z\bar{q}q}$.

The $\mathcal{O}(\alpha_{\rm w}\alpha_{\rm s})$ correction to the squared $q\bar{q} \to \ell\bar{\ell}$ amplitude is obtained from the interference between the genuine two-loop $\mathcal{O}(\alpha_{\rm w}\alpha_{\rm s})$ matrix element and the LO matrix element

$$\begin{aligned} M^{q\bar{q}\to\ell\bar{\ell}}_{\mathrm{V_s}\otimes\mathrm{V_w},\mathrm{II,PA}} = \quad & 2\mathrm{Re}\Big\{\mathcal{M}^{q\bar{q}\to\ell\bar{\ell}}_{\mathrm{V_s}\otimes\mathrm{V_w},\mathrm{II,PA}}\left(\mathcal{M}^{q\bar{q}\to\ell\bar{\ell}}_{\mathrm{LO},Z}\right)^*\Big\} \\ & + 2\mathrm{Re}\Big\{\mathcal{M}^{q\bar{q}\to\ell\bar{\ell}}_{\mathrm{V_s},\mathrm{I,PA}}\left(\mathcal{M}^{q\bar{q}\to\ell\bar{\ell}}_{\mathrm{V_w},\mathrm{I,PA}}\right)^*\Big\} \\ & + 2\mathrm{Re}\Big\{\mathcal{M}^{\bar{q}q\to\ell\bar{\ell}}_{\delta^{\rm ct}_{(\alpha_{\rm s}\alpha)},Z}\left(\mathcal{M}^{q\bar{q}\to\ell\bar{\ell}}_{\mathrm{LO},Z}\right)^*\Big\} \end{aligned} \tag{6.12}$$

where the second line also includes the contribution from the interference of two one-loop matrix elements, one with a $\mathcal{O}(\alpha_{\rm s})$ and the other with $\mathcal{O}(\alpha_{\rm w})$ initial-state correction. The third line includes the vertex counterterm that receives contributions from genuine two-loop $\mathcal{O}(N_f\alpha_{\rm s}\alpha)$ corrections which we obtain from (5.16) by neglecting the counterterm contributions to the Z–lepton vertex (which are part of the final–final contribution) to obtain the initial–initial part. The formfactors relevant for the calculation of the weak one-loop vertex corrections can be found in Appendix C of [143] or in [29]. In PA, the individual matrix elements in the last equation are obtained by inserting the respective on-shell form factor, $F_i^{Z\bar{q}q}(q^2 = M_Z^2)$, into

$$\mathcal{M}^{q\bar{q}\to\ell\bar{\ell}}_{i,\sigma\tau,\mathrm{PA}} = e^2\frac{\hat{F}^{Z\bar{q}q}_{i,\sigma}(M_Z^2)C^{\tau}_{Z\bar{\ell}_1\ell_2}}{q^2-\mu_Z^2}\mathcal{A}_{\sigma\tau}, \quad i = \mathrm{LO},\mathrm{V_s},\mathrm{V_w},\mathrm{V_s}\otimes\mathrm{V_w} \tag{6.13}$$

where μ_Z^2 is the gauge-invariant location of the propagator pole, the LO formfactor, $C^{\tau}_{Z\bar{\ell}_1\ell_2}$, is given in (5.6), and

$$\mathcal{A}_{\pm\pm} = 2u, \qquad \mathcal{A}_{\pm\mp} = 2t. \tag{6.14}$$

The evaluation of the amplitudes present in Eq. (6.12) with on-shell formfactors ensures the gauge invariance of $\mathcal{O}(\alpha_{\rm s}\alpha_{\rm w})$ initial–initial corrections. In principle, products of weak and QCD one-loop corrections contained in (6.12) require the evaluation of the weak one-loop factor to order $\mathcal{O}(\epsilon^2)$ to catch all finite terms. However, after the combination with integrated antenna subtraction terms, which are discussed in the next section for the double-virtual case, the additional finite terms, produced in the combination of the higher-order ϵ-terms of the weak correction with the poles of the one-loop QCD correction, drop out. This is because in the relevant terms in both the subtraction term and (6.12) there is a weak one-loop correction factor, which can be factored out when combining (6.12) with the corresponding integrated antenna subtraction term. The weak one-loop correction, after factoring it out, is multiplied with the sum of the one-loop QCD correction factor $\delta^{Z\bar{q}q}_{\mathrm{V_s}}$ and a integrated antenna, which is free of IR poles.

The $\mathcal{O}(Q_q^2\alpha_{\rm s}\alpha_{\rm p})$ initial–initial corrections form a gauge-invariant subset of the full class of $\mathcal{O}(\alpha\alpha_{\rm s})$ corrections. Therefore, we calculate them for off-shell Z-boson production not applying the PA. As for the double-virtual $\mathcal{O}(\alpha_{\rm w}\alpha_{\rm s})$ corrections the double-virtual QCD × photonic corrections contribute to the squared amplitude via an interference between two one-loop amplitudes with initial state corrections and the interference of the genuine two-loop $\mathcal{O}(\alpha_{\rm phot}\alpha_{\rm s})$ initial–initial correction to the $q\bar{q} \to \ell\bar{\ell}$ amplitude and the LO amplitude,

$$\begin{aligned} M^{q\bar{q}\to\ell\bar{\ell}}_{\mathrm{V_s}\otimes\mathrm{V_{phot}},\mathrm{II}} = \quad & 2\mathrm{Re}\Big\{\mathcal{M}^{q\bar{q}\to\ell\bar{\ell}}_{\mathrm{V_s}\otimes\mathrm{V_{phot}},\mathrm{II}}\left(\mathcal{M}^{q\bar{q}\to\ell\bar{\ell}}_{\mathrm{LO},Z/\gamma}\right)^*\Big\} \\ & + 2\mathrm{Re}\Big\{\mathcal{M}^{q\bar{q}\to\ell\bar{\ell}}_{\mathrm{V_s},\mathrm{I}}\left(\mathcal{M}^{q\bar{q}\to\ell\bar{\ell}}_{\mathrm{V_{phot}},\mathrm{I}}\right)^*\Big\}. \end{aligned} \tag{6.15}$$

The $\mathcal{O}(\alpha_\mathrm{s}\alpha_\mathrm{p})$ correction has been calculated a long time ago and can be factorized off from the LO amplitude

$$\mathcal{M}^{q\bar{q}\to\ell\bar{\ell}}_{\mathrm{V_s}\otimes\mathrm{V_{phot}},\mathrm{II}} = \delta^{Z\bar{q}q,[2\times0]}_{\mathrm{V_s}\otimes\mathrm{V_{phot}}}\mathcal{M}^{q\bar{q}\to\ell\bar{\ell}}_{\mathrm{LO},Z/\gamma}, \tag{6.16}$$

$$\mathcal{M}^{q\bar{q}\to\ell\bar{\ell}}_{\mathrm{V_s},\mathrm{I}}\left(\mathcal{M}^{q\bar{q}\to\ell\bar{\ell}}_{\mathrm{V_{phot}},\mathrm{I}}\right)^* = \delta^{Z\bar{q}q,[1\times1]}_{\mathrm{V_s}\otimes\mathrm{V_{phot}}}\mathcal{M}^{q\bar{q}\to\ell\bar{\ell}}_{\mathrm{LO},Z/\gamma}. \tag{6.17}$$

The explicit expressions for the factorized correction factors can be extracted from the subleading colour contribution of the $\mathcal{O}(\alpha_\mathrm{s}^2)$ correction to the $q\bar{q}\to\ell\bar{\ell}$ amplitude [104][1] using the method presented in Section 3.1.1. We obtain

$$\begin{aligned}
\delta^{Z\bar{q}q,[2\times0]}_{\mathrm{V_s}\otimes\mathrm{V_{phot}}}(s) =& 2Q_q^2C_F\frac{\alpha\alpha_\mathrm{s}}{\pi^2}\,\mathcal{C}_\epsilon^2\left(\frac{\mu^2}{s}\right)^{2\epsilon}\left[\frac{1}{4\epsilon^4}+\frac{3}{4\epsilon^3}+\frac{1}{\epsilon^2}\left(\frac{41}{16}-\frac{13\pi^2}{24}\right)\right.\\
&\left.+\frac{1}{\epsilon}\left(\frac{221}{32}-\frac{3\pi^2}{2}-\frac{8}{3}\zeta_3\right)+\left(\frac{1151}{64}-\frac{475\pi^2}{96}-\frac{29}{4}\zeta_3+\frac{59\pi^4}{288}\right)+\mathcal{O}(\epsilon)\right],\\
\delta^{Z\bar{q}q,[1\times1]}_{\mathrm{V_s}\otimes\mathrm{V_{phot}}}(s) =& 2Q_q^2C_F\frac{\alpha\alpha_\mathrm{s}}{\pi^2}\,\mathcal{C}_\epsilon^2\left(\frac{\mu^2}{s}\right)^{2\epsilon}\left[\frac{1}{4\epsilon^4}+\frac{3}{4\epsilon^3}+\frac{1}{\epsilon^2}\left(\frac{41}{16}-\frac{\pi^2}{24}\right)\right.\\
&\left.+\frac{1}{\epsilon}\left(7-\frac{\pi^2}{8}-\frac{7}{6}\zeta_3\right)+\left(18-\frac{41\pi^2}{96}-\frac{7}{2}\zeta_3-\frac{7\pi^4}{480}\right)+\mathcal{O}(\epsilon)\right],
\end{aligned} \tag{6.18}$$

where $\mathcal{C}_\epsilon = (4\pi)^\epsilon e^{-\epsilon\gamma}$.

6.3.1.1 Double-virtual antenna subtraction terms

We now present the subtraction terms needed to cancel the explicit IR poles in the double-virtual contribution. The double-virtual QCD×photonic corrections in (6.18) contain overlapping IR singularities of the virtual photon and gluon leading to poles in ϵ up to order four. NLO subtraction schemes therefore fail to cancel the singularities in these contributions enforcing the use of a NNLO scheme, where our method of choice is the NNLO antenna subtraction scheme. In Section 4.5.3 we presented the subtraction functions relevant for the double-virtual term,

$$\begin{aligned}
\mathrm{d}\hat{\sigma}^{U,ii,q\bar{q}}_{\mathrm{NNLO}} =& -2\,C_F\,\mathcal{N}^{\varepsilon}_{\mathcal{C},q\bar{q}}\mathcal{N}^{V_\mathrm{s}}_{NLO}\int\frac{\mathrm{d}z_a}{z_a}\frac{\mathrm{d}z_b}{z_b}\mathrm{d}\Phi_2(\{p_i\}_{i=1}^2;z_ap_a,z_bp_b)\\
&\times\left[\boldsymbol{\mathcal{J}}^{(1)}_{2,ii}(z_a,z_b)\,2\,\mathrm{Re}\left\{\mathcal{M}^{q\bar{q}\to\ell\bar{\ell}}_{V_\mathrm{phot},I}\left(\mathcal{M}^{q\bar{q}\to\ell\bar{\ell}}_{\mathrm{LO},Z/\gamma}\right)^*\right\}\right.\\
&+\frac{2\,Q_q\,\mathcal{N}^{V_\mathrm{ew}}_{NLO}}{2}\left[\boldsymbol{\mathcal{J}}^{(1)}_{2,ii}\otimes\boldsymbol{\mathcal{J}}^{(1)}_{2,ii}\right](z_a,z_b)\,|\mathcal{M}^{q\bar{q}\to\ell\bar{\ell}}_{\mathrm{LO},Z/\gamma}|^2\\
&\left.+\frac{2\,Q_q\,\mathcal{N}^{V_\mathrm{ew}}_{NLO}}{2}\widetilde{\boldsymbol{\mathcal{J}}}^{(2)}_{2,ii}(z_a,z_b)\,|\mathcal{M}^{q\bar{q}\to\ell\bar{\ell}}_{\mathrm{LO},Z/\gamma}|^2\right]J^{(2)}_2(p_1,p_2)
\end{aligned}$$

[1]Note that the coefficient of the ϵ^{-1} contribution to $\delta^{Z\bar{q}q,[1\times1]}_{\mathrm{V_s}\otimes\mathrm{V_{phot}}}$ in [104] differs from our result by a sign change of the term proportional to ζ_3.

$$+ (V_\mathrm{s} \leftrightarrow V_\mathrm{phot}), \tag{6.19}$$

where we have suppressed the arguments $z_a p_a, z_b p_b, p_1, p_2$ of the appearing matrix elements and the NLO factors have been defined in Section 4.4.2. Due to symmetries of the amplitudes and prefactors in the last equation, the exchange of factors resulting from the virtual QCD and factors originating from the virtual photonic correction, indicated in the last line, basically only leads to an additional factor of two on the r.h.s. in the very first line of the last equation. The genuine two-loop antenna string is given by

$$\widetilde{\mathcal{J}}^{(2)}_{2,ii}(z_a,z_b) = \frac{1}{2}\tilde{\mathcal{A}}^0_{4,q\bar{q}} + \tilde{\mathcal{A}}^1_{3,q\bar{q}} + 2\mathcal{C}^0_{4,q\bar{q}} + 2\mathcal{C}^0_{4,\bar{q}q} + \delta_a \tilde{\bar{\Gamma}}^{(2)}_{qq}(z_b) + \delta_b \tilde{\bar{\Gamma}}^{(2)}_{qq}(z_a) - \frac{1}{2}\left[\mathcal{A}^0_{3,q\bar{q}} \otimes \mathcal{A}^0_{3,q\bar{q}}\right], \tag{6.20}$$

where the relevant mass factorization kernels $\tilde{\bar{\Gamma}}^{(2)}_{qq}$ can be found in Appendix A of [96]. The qg-channel has no double-virtual contribution to the amplitude but instead receives only contributions from subtraction terms that are introduced in the double-real and real–virtual part. The subtraction term in this case is therefore IR finite on its own and reads

$$\begin{aligned}
\mathrm{d}\hat{\sigma}^{U,ii,qg}_\mathrm{NNLO} = &-2\,C_F\,\mathcal{N}^\varepsilon_{\mathcal{C},qg}\,\mathcal{N}^{V_\mathrm{s}}_{NLO}\int \frac{\mathrm{d}z_a}{z_a}\frac{\mathrm{d}z_b}{z_b}\mathrm{d}\Phi_2(\{p_i\}^2_{i=1}; z_a p_a, z_b p_b)\\
&\times\Bigg[\mathcal{J}^{(1),g\to q}_{2,ii}(z_a,z_b)\,2\,\mathrm{Re}\left\{\mathcal{M}^{q\bar{q}\to\ell\bar{\ell}}_{V_\mathrm{phot},I}\left(\mathcal{M}^{q\bar{q}\to\ell\bar{\ell}}_{\mathrm{LO},Z/\gamma}\right)^*\right\}\\
&\quad+\frac{2\,Q_q\,\mathcal{N}^{V_\mathrm{ew}}_{NLO}}{2}\left[\mathcal{J}^{(1)}_{2,ii}\otimes\mathcal{J}^{(1),g\to q}_{2,ii}\right](z_a,z_b)\,|\mathcal{M}^{q\bar{q}\to\ell\bar{\ell}}_{\mathrm{LO},Z/\gamma}|^2\\
&\quad+\frac{2\,Q_q\,\mathcal{N}^{V_\mathrm{ew}}_{NLO}}{2}\widetilde{\mathcal{J}}^{(2),g\to q}_{2,ii}(z_a,z_b)\,|\mathcal{M}^{q\bar{q}\to\ell\bar{\ell}}_{\mathrm{LO},Z/\gamma}|^2\Bigg]J^{(2)}_2(p_1,p_2),
\end{aligned} \tag{6.21}$$

where

$$\begin{aligned}
\mathcal{N}^\varepsilon_{\mathcal{C},qg}\,\widetilde{\mathcal{J}}^{(2),g\to q}_{2,ii}(z_a,z_b) = -\mathcal{N}_{\mathcal{C},qg}\Big\{&\tilde{\mathcal{A}}^0_{4,qg} + \tilde{\mathcal{A}}^1_{3,qg} + \delta_a S_{g\to q}\tilde{\bar{\Gamma}}^{(2)}_{qg}(z_b) + \left[\mathcal{A}^0_{3,q\bar{q}}\otimes\mathcal{A}^0_{3,qg}\right]\\
&-\left[\delta_a\Gamma^{(1)}_{qq}(z_b)\otimes\left(\mathcal{A}^0_{3,qg}+\frac{1}{2}\delta_a S_{g\to q}\Gamma^{(1)}_{qg}(z_b)\right)\right]\Big\}.
\end{aligned} \tag{6.22}$$

As in the qg-channel also the qq-channel receives only contributions from integrated subtraction terms

$$\begin{aligned}
\mathrm{d}\hat{\sigma}^{U,ii,qq}_\mathrm{NNLO} = &-4\,C_F\,Q_q\,\mathcal{N}^{V_\mathrm{ew}}_{NLO}\,\mathcal{N}^{V_\mathrm{s}}_{NLO}\int\frac{\mathrm{d}z_a}{z_a}\frac{\mathrm{d}z_b}{z_b}\mathrm{d}\Phi_2(\{p_i\}^2_{i=1}; z_a p_a, z_b p_b)\\
&\times\left[\left(\mathcal{C}^0_{4,qq}(z_a,z_b)+\tilde{\bar{\Gamma}}^{(2)}_{q\bar{q}}(z_b)\right)|\mathcal{M}^{q\bar{q}\to\ell\bar{\ell}}_{\mathrm{LO},Z/\gamma}(z_a p_a, z_b p_b, p_1, p_2)|^2 + (a\leftrightarrow b)\right]J^{(2)}_2(p_1,p_2).
\end{aligned} \tag{6.23}$$

Due to the non-vanishing mass of the weak gauge bosons the IR pole structure of weak × QCD double-virtual contributions to the matrix element are only of NLO complexity leading to simpler subtraction terms compared to the case involving photons and gluons. Using NLO antennae the subtraction term for the $q\bar{q}$ induced channel reads

$$\mathrm{d}\hat{\sigma}^{U,ii,q\bar{q}}_\mathrm{NNLO}\big|_{\alpha_\mathrm{s}\alpha_\mathrm{w}} = -\mathcal{N}^\varepsilon_{\mathcal{C},q\bar{q}}\,\mathcal{N}^V_{NLO}\int\frac{\mathrm{d}z_a}{z_a}\frac{\mathrm{d}z_b}{z_b}\mathrm{d}\Phi_2(\{p_i\}^2_{i=1}; z_a p_a, z_b p_b)$$

$$\times \boldsymbol{\mathcal{J}}^{(1)}_{2,ii}(z_a,z_b)\,2\mathrm{Re}\Big\{\mathcal{M}^{q\bar{q}\to\ell\bar{\ell}}_{\mathrm{V_w,I,PA}}\left(\mathcal{M}^{q\bar{q}\to\ell\bar{\ell}}_{\mathrm{LO},Z}\right)^*\Big\}\,J^{(2)}_2(p_1,p_2). \tag{6.24}$$

The subtraction term for the qg-channel is given by

$$\begin{aligned}\mathrm{d}\hat{\sigma}^{U,ii,qg}_{\mathrm{NNLO}}\big|_{\alpha_\mathrm{s}\alpha_\mathrm{w}} =& -\mathcal{N}^{\varepsilon}_{\mathcal{C},qg}\mathcal{N}^{V}_{NLO}\int\frac{\mathrm{d}z_a}{z_a}\frac{\mathrm{d}z_b}{z_b}\mathrm{d}\Phi_2(\{p_i\}^2_{i=1};z_ap_a,z_bp_b)\\ &\times\boldsymbol{\mathcal{J}}^{(1),g\to q}_{2,ii}(z_a,z_b)\,2\mathrm{Re}\Big\{\mathcal{M}^{q\bar{q}\to\ell\bar{\ell}}_{\mathrm{V_w,I,PA}}\left(\mathcal{M}^{q\bar{q}\to\ell\bar{\ell}}_{\mathrm{LO},Z}\right)^*\Big\}\,J^{(2)}_2(p_1,p_2).\end{aligned} \tag{6.25}$$

6.3.1.2 Convolutions of integrated three-parton antennae

The convolution of integrated antenna strings relevant for the construction of the double-virtual subtraction term $\mathrm{d}\hat{\sigma}^{U,B}_{\mathrm{NNLO}}$ in (4.153) are (to our best knowledge) only partially available in the literature [114]. In particular, the convolution of the qqb- and qg-antenna strings presented in the subtraction terms in the last section

$$\begin{aligned}\left[\boldsymbol{\mathcal{J}}^{(1)}_{2,ii}\otimes\boldsymbol{\mathcal{J}}^{(1)}_{2,ii}\right](s,s';z_a,z_b) =& \int\mathrm{d}x_1\mathrm{d}x_2\,\mathrm{d}y_1\mathrm{d}y_2\,\boldsymbol{\mathcal{J}}^{(1)}_{2,ii}(s,x_1,x_2)\,\boldsymbol{\mathcal{J}}^{(1)}_{2,ii}(s',y_1,y_2)\\ &\times\delta(z_a-x_1y_1)\delta(z_b-x_2y_2),\end{aligned} \tag{6.26}$$

are not publicly available and we discuss their calculation in the following. Similar expression for $\left[\boldsymbol{\mathcal{J}}^{(1)}_{2,ii}\otimes\boldsymbol{\mathcal{J}}^{(1),g\to q}_{2,ii}\right](s,s';z_a,z_b)$ are also relevant, where the antenna strings are defined in (4.83). It is important to note that the contributions given by the convolution of integrated three-parton antennae of the form $\left[\mathcal{X}^0_3\otimes\mathcal{X}^0_3\right](s,s';z_1,z_2)$,with $\mathcal{X}^0_3=\mathcal{A}^0_{qq,g},\mathcal{A}^0_{qg,q}$, actually drop out in the sum of $\mathrm{d}\hat{\sigma}^{U,B}_{\mathrm{NNLO}}$ and $\mathrm{d}\hat{\sigma}^{U,C}_{\mathrm{NNLO}}$ in (6.19) and (6.21). Therefore, it is not necessary to calculate these terms, which drastically simplifies the calculation. The remaining contributions to (6.26) that have to be calculated are convolutions of integrated antennae and mass-factorization kernels or convolutions of two mass-factorization kernels,

$$\left[\Gamma^{(1)}_{ki}\otimes\mathcal{X}^0_3\right]_1(s;z_1,z_2) = \int\mathrm{d}x_1\,\mathrm{d}y_1\,\Gamma^{(1)}_{ki}(x_1)\,\mathcal{X}^0_3(s,y_1,z_2)\delta(z_1-x_1y_1)\,, \tag{6.27}$$

$$\left[\Gamma^{(1)}_{ki}\otimes\mathcal{X}^0_3\right]_2(s;z_1,z_2) = \int\mathrm{d}x_2\,\mathrm{d}y_2\,\Gamma^{(1)}_{ki}(x_2)\,\mathcal{X}^0_3(s;z_1,y_2)\delta(z_2-x_2y_2)\,, \tag{6.28}$$

$$\left[\Gamma^{(1)}_{kl}\otimes\Gamma^{(1)}_{li}\right]_1(z_1,z_2) = \int\mathrm{d}x_1\,\mathrm{d}y_1\,\Gamma^{(1)}_{kl}(x_1)\,\Gamma^{(1)}_{li}(y_1)\delta(z_1-x_1y_1)\delta(1-z_2)\,, \tag{6.29}$$

$$\left[\Gamma^{(1)}_{kl}\otimes\Gamma^{(1)}_{li}\right]_2(z_1,z_2) = \int\mathrm{d}x_2\,\mathrm{d}y_2\,\Gamma^{(1)}_{kl}(x_2)\,\Gamma^{(1)}_{li}(y_2)\delta(z_2-x_2y_2)\delta(1-z_1). \tag{6.30}$$

Note that the last contribution has the symmetry

$$\left[\Gamma^{(1)}_{kl}\otimes\Gamma^{(1)}_{li}\right]_2(z_1,z_2) = \left[\Gamma^{(1)}_{kl}\otimes\Gamma^{(1)}_{li}\right]_1(z_2,z_1)\,. \tag{6.31}$$

In App. E we give explicit results for the relevant convolutions. In the calculation of the results presented in App. E we use that the convolutions of mass-factorization kernels and integrated antennae can be reduced to convolutions of simple functions, functions

combined with plus distributions, and convolutions involving only plus distributions. Convolutions that only involve plus distributions

$$[\mathcal{D}_n \otimes \mathcal{D}_m](z) = \int \mathrm{d}x\,\mathrm{d}y \left(\frac{\ln^n(1-x)}{1-x}\right)_+ \left(\frac{\ln^n(1-y)}{1-y}\right)_+ \delta(z-xy) \tag{6.32}$$

can be reduced to harmonic polylogarithms [144] (see App. A.4 for a definition) and read [114, 145]

$$\begin{aligned}
[\mathcal{D}_0 \otimes \mathcal{D}_0](z) &= -\zeta_2\delta(1-z) + 2\mathcal{D}_1(z) - \frac{\mathrm{H}(0,z)}{1-z}\,, && (6.33)\\
[\mathcal{D}_1 \otimes \mathcal{D}_0](z) &= \zeta_3\delta(1-z) - \zeta_2\mathcal{D}_0(z) + \frac{3}{2}\mathcal{D}_2(z) + \frac{\mathrm{H}(0,1,z)}{1-z} + \frac{\mathrm{H}(1,0,z)}{1-z}\,, && (6.34)\\
[\mathcal{D}_2 \otimes \mathcal{D}_0](z) &= -2\zeta_4\delta(1-z) + 2\zeta_3\mathcal{D}_0(z) - 2\zeta_2\mathcal{D}_1(z) + \frac{4}{3}\mathcal{D}_3(z) - \frac{2\mathrm{H}(0,1,1,z)}{1-z}\\
&\quad - \frac{2\mathrm{H}(1,0,1,z)}{1-z} - \frac{2\mathrm{H}(1,1,0,z)}{1-z}\,, && (6.35)\\
[\mathcal{D}_1 \otimes \mathcal{D}_1](z) &= -\frac{\zeta_4}{4}\delta(1-z) + 2\zeta_3\mathcal{D}_0(z) - 2\zeta_2\mathcal{D}_1(z) + \mathcal{D}_3(z) - \frac{2\zeta_3}{1-z} - \frac{\mathrm{H}(0,1,0,z)}{1-z}\\
&\quad - \frac{2\mathrm{H}(0,1,1,z)}{1-z} - \frac{2\mathrm{H}(1,0,1,z)}{1-z} - \frac{2\mathrm{H}(1,1,0,z)}{1-z}\,. && (6.36)
\end{aligned}$$

Analytic results of convolutions of functions $f(x,y)$ and $h(x,y)$ can be obtained using

$$\begin{aligned}
[f \otimes h](z_a, z_b) &= \int_0^1 \mathrm{d}x_1\mathrm{d}x_2\,\mathrm{d}y_1\mathrm{d}y_2\, f(x_1,x_2)\, h(y_1,y_2)\delta(z_a - x_1y_1)\delta(z_b - x_2y_2),\\
&= \int_{z_a}^1 \mathrm{d}x_1 \int_{z_b}^1 \mathrm{d}x_2\, f(x_1,x_2)\, h\left(\frac{z_a}{x_1}, \frac{z_b}{x_2}\right). \qquad (6.37)
\end{aligned}$$

Similarly, convolutions of a function $g(z)$ and a plus distribution can be obtained by using

$$[\mathcal{D}_n \otimes g](z) = \int_z^1 \mathrm{d}x \frac{\log^n(1-x)}{1-x}\left[\frac{1}{x}g\left(\frac{z}{x}\right) - g(z)\right] + \frac{g(z)\log^{n+1}(1-z)}{n+1}. \tag{6.38}$$

In App. E we prove (6.37) and (6.38) explicitly.

6.3.2 Real–virtual corrections

The factorizable real–virtual initial–initial $\mathcal{O}(\alpha_\mathrm{s}\alpha)$ corrections receive contributions from various partonic channels of Z+jet production,

$$\begin{aligned}
\bar{q}_a(p_a) + q_b(p_b) &\to Z(p_Z) + g(k_g), && (6.39)\\
\bar{q}_a(p_a) + q_b(p_b) &\to Z(p_Z) + \gamma(k_\gamma), && (6.40)\\
g(p_g) + q_b(p_b) &\to Z(p_Z) + q_a(k_a), && (6.41)\\
g(p_g) + \bar{q}_a(p_a) &\to Z(p_Z) + \bar{q}_b(k_b), && (6.42)
\end{aligned}$$

and can be split into three different types of interference diagrams. The first type is given by a interference of diagrams where one diagram contains a virtual photonic and a real QCD correction to Z production. The second contribution is given by the interference of a virtual weak and a real QCD correction, and the last type is obtained by a virtual QCD combined with a photonic real correction as shown in Fig. 6.2b. As described before, the corrections including real or virtual photonic corrections are calculated without on-shell approximation of the Z boson including also off-shell photon production whereas for the part with a virtual weak correction the PA is needed. The corresponding amplitude for the quark-induced channels including a virtual weak and real QCD correction is given by

$$\mathcal{M}^{\bar{q}_a q_b \to \ell_1 \bar{\ell}_2,\mathrm{PA}}_{\mathrm{V_w}\otimes\mathrm{R_s},Z,\mathrm{prod}\times\mathrm{prod}} = \sum_{\lambda_Z} \frac{\mathcal{M}^{\bar{q}_a q_b \to g Z}_{\mathrm{V_w}\otimes\mathrm{R_s},\mathrm{PA}}(\lambda_Z)\, \mathcal{M}^{Z\to\ell_1\bar{\ell}_2}_{0,\mathrm{PA}}(\lambda_Z)}{p_Z^2 - \mu_Z^2}. \tag{6.43}$$

The one-loop matrix elements needed for the calculation of the real–virtual corrections were generated using FeynArts [146,147], calculated with FormCalc [148] and Collier [149–152], and modified to match the right-hand side of Eq. (6.43).

In detail we apply the following procedure to obtain OS kinematics in the production matrix element $\mathcal{M}^{\bar{q}_a q_b \to g Z}_{\mathrm{V_w}\otimes\mathrm{R_s},\mathrm{PA}}(\lambda_Z)$ of the Z boson. We start with a rescaling of all external momenta

$$p_i \to \hat{p}_i = p_i \frac{M_Z}{\sqrt{2 p_\ell p_{\bar{\ell}}}}, \quad i = a, b, \ell, \bar{\ell}, g, \tag{6.44}$$

where, due to the simple structure of the mapping, we preserve on-shellness of all (lightlike) momenta and momentum conservation, and achieve

$$\hat{p}_Z^2 = 2\, \hat{p}_\ell \hat{p}_{\bar{\ell}} = M_Z^2. \tag{6.45}$$

In (6.13) we fixed the PA for $2 \to 2$ processes by inserting the on-shell form factors for a given correction and keeping the Dirac structures $\mathcal{A}_{\sigma\tau}$ off-shell. As the functions $\mathcal{A}_{\sigma\tau}$ scale under (6.44) like

$$\mathcal{A}_{\sigma\tau} \to \hat{\mathcal{A}}_{\sigma\tau} = \mathcal{A}_{\sigma\tau} \frac{M_Z^2}{2 p_\ell p_{\bar{\ell}}}, \tag{6.46}$$

the choice for the OS projection described in (6.13) for $2 \to 2$ processes can be schematically summarized in the following way,

$$\mathcal{M}^{2\to2}_{Z,\mathrm{PA}}(p_a, p_b, p_\ell, p_{\bar{\ell}}) = \frac{\left[\mathcal{M}^{2\to2}_Z \cdot (p_Z^2 - \mu_Z^2)\right]\big|_{p_i \to \hat{p}_i}}{p_Z^2 - \mu_Z^2} \cdot \frac{2\, p_\ell p_{\bar{\ell}}}{M_Z^2}. \tag{6.47}$$

The last factor on the r.h.s is used to compensate the scaling behaviour of the $\mathcal{A}_{\sigma\tau}$ in (6.46). The double-virtual corrections involve implicit IR singularities which have to be cancelled by subtraction terms that include $2 \to 2$ amplitudes as well. Therefore, the choice we made in (6.47) concering the OS mapping also determines the scaling of double-virtual subtraction terms for the QCD×weak corrections. These subtraction terms, however, are the integrated counterparts of the real–virtual subtraction terms. Therefore, to

have a consistent calculation we need to make sure that the OS mapping applied in the real–virtual subtraction terms is in line with the mapping in the integrated subtraction terms, which are part of the double-virtual correction and are fixed by (6.47). This can be used to fix the PA of the real–virtual contribution to the squared matrix element. We start with an ansatz for the PA, which is schematically of the form

$$\begin{aligned}|\mathcal{M}^{2\to3}_{Z,\mathrm{PA}}(p_a,p_b,p_\ell,p_{\bar\ell},p_g)|^2 &= \left|\frac{\left[\mathcal{M}^{2\to3}_Z\cdot(p_Z^2-\mu_Z^2)\right]\big|_{p_i\to\hat p_i}}{p_Z^2-\mu_Z^2}\right|^2\cdot\left(\frac{2\,p_\ell p_{\bar\ell}}{M_Z^2}\right)^n\\ &\equiv|\hat{\mathcal{M}}^{2\to3}_Z(\hat p_a,\hat p_b,\hat p_\ell,\hat p_{\bar\ell},\hat p_g)|^2\left(\frac{2\,p_\ell p_{\bar\ell}}{M_Z^2}\right)^n,\end{aligned}\tag{6.48}$$

where the exponent n has to be fixed by the comparison to the real–virtual subtraction term, whose PA is already fixed by the double virtual subtraction terms for the QCD×weak corrections, as argued before. The real–virtual subtraction terms for the QCD×weak correction in PA are given by the product of a three-parton antenna and a reduced squared matrix element in PA, which can be schematically written as (c.f. (4.76))

$$\begin{aligned}&A_3^0(p_a,p_g,p_b)\,|\mathcal{M}^{2\to2}_{Z,\mathrm{PA}}(x_ap_a,x_bp_b,\tilde p_\ell,\tilde p_{\bar\ell})|^2\\ &=A_3^0(p_a,p_g,p_b)\left|\frac{\left[\mathcal{M}^{2\to2}_Z\cdot(p_Z^2-\mu_Z^2)\right]\big|_{p_i\to\hat p_i}}{p_Z^2-\mu_Z^2}\right|^2\cdot\left(\frac{2\,\tilde p_\ell\tilde p_{\bar\ell}}{M_Z^2}\right)^2\\ &=\underbrace{A_3^0(\hat p_a,\hat p_g,\hat p_b)\left|\frac{\left[\mathcal{M}^{2\to2}_Z\cdot(p_Z^2-\mu_Z^2)\right]\big|_{p_i\to\hat p_i}}{p_Z^2-\mu_Z^2}\right|^2}_{\text{subtraction function for }|\hat{\mathcal{M}}^{2\to3}_Z(\hat p_a,\hat p_b,\hat p_\ell,\hat p_{\bar\ell},\hat p_g)|^2}\cdot\frac{2\,\tilde p_\ell\tilde p_{\bar\ell}}{M_Z^2}\end{aligned}\tag{6.49}$$

where we have used the explicit scaling behaviour of the three-parton antenna [84] in the last line to absorb a factor of $2\,\tilde p_\ell\tilde p_{\bar\ell}/M_Z^2$ into the antenna function. The exponent n in (6.48) can now be determined to be $n=1$ by comparing (6.49) to (6.48), keeping in mind that implicit IR divergences in (6.48) have to cancel the ones in (6.49).

The procedure to obtain OS kinematics in the $2\to3$ contributions can be summarized as follows

$$\mathcal{M}^{\bar q_a q_b\to\ell_1\bar\ell_2,\mathrm{PA}}_{\mathrm{V_w}\otimes\mathrm{R_s},Z,\mathrm{prod}\times\mathrm{prod}}=\frac{\left[\mathcal{M}^{\bar q_a q_b\to\ell_1\bar\ell_2}_{\mathrm{V_w}\otimes\mathrm{R_s},Z,\mathrm{prod}\times\mathrm{prod}}\cdot(p_Z^2-\mu_Z^2)\right]\big|_{p_i\to\hat p_i}}{p_Z^2-\mu_Z^2}\cdot\sqrt{\frac{2\,p_\ell p_{\bar\ell}}{M_Z^2}}.\tag{6.50}$$

Note that the choice we made for the OS projection is not unique and different choices are possible, e.g. we could have chosen to keep also the Dirac structures in (6.47) on-shell. Different versions for the OS projection lead to results that differ at the order of the intrinsic uncertainty of the PA in the vicinity of the Z resonance. The guiding principle that we used to construct the on-shell projection was self-consistency, i.e. once we fixed the OS projection for $2\to2$ processes we were able to determine also the OS projection of all $2\to3$ processes that enter our calculation. In principle, it is possible to deviate from this strategy and choose an OS projection where the projections applied to the $2\to2$ and $2\to3$ contributions are not related by self-consistency arguments. Even though such

choices lead to results that differ from our strategy at the order of the intrinsic uncertainty in the vicinity of the resonance of the Z boson, it is important to note that a procedure that does not apply OS projections to $2 \to 2$ and $2 \to 3$ contributions in a consistent way might lead to large artificial effects in the off-shell region of distributions (such as the invariant-mass distribution of the Z boson).

6.3.2.1 Real–virtual antenna subtraction terms

We now present the real–virtual subtraction terms for both the QCD×weak and QCD × photonic corrections, where the former involve only NLO complexity as already discussed when constructing the double-virtual subtraction terms. The real–virtual antenna subtraction term for the $q\bar{q}$-induced channel in the QCD×photonic case reads

$$\begin{aligned}
\mathrm{d}\hat{\sigma}^{T,ii,q\bar{q}}_{\mathrm{NNLO}} =& \mathcal{N}^{\varepsilon}_{\mathcal{C},q\bar{q}} \int \frac{\mathrm{d}z_a}{z_a}\frac{\mathrm{d}z_b}{z_b}\, \mathrm{d}\Phi_3(\{p_i\}_{i=1}^3; \bar{p}_a, \bar{p}_b) \\
&\times \Bigg[-2\,Q_q\,\mathcal{N}^{V_{\mathrm{ew}}}_{NLO}\,\boldsymbol{\mathcal{J}}^{(1)}_{2,ii}(s_{ab})\,\left|\mathcal{M}^{q\bar{q}\to\ell\bar{\ell}g}_{R_{\mathrm{s}},Z/\gamma}(\{\Phi_3\})\right|^2 J_2^{(3)}(p_1,p_2,p_3) \\
&\quad + 2\,C_F\,\mathcal{N}^{R_{\mathrm{s}}}_{NLO} A_3^0(\bar{p}_a,p_3,\bar{p}_b)\Bigg(2\mathrm{Re}\Big\{\mathcal{M}^{q\bar{q}\to\ell\bar{\ell}}_{\mathrm{V_{phot}},\mathrm{I}}\left(\mathcal{M}^{q\bar{q}\to\ell\bar{\ell}}_{\mathrm{LO},Z/\gamma}\right)^*\Big\}(\{\widetilde{\Phi}_3\}_{ii})\delta_{z_a}\delta_{z_b} \\
&\qquad - 2\,Q_q\,\mathcal{N}^{R_{\mathrm{ew}}}_{NLO}\boldsymbol{\mathcal{J}}^{(1)}_{2,ii}(s_{\overline{ab}})\,\left|\mathcal{M}^{q\bar{q}\to\ell\bar{\ell}}_{\mathrm{LO},Z/\gamma}(\{\widetilde{\Phi}_3\}_{ii})\right|^2\Bigg) J_2^{(2)}(\tilde{p}_1,\tilde{p}_2) \\
&\quad + 4\,C_F\,Q_q\,\mathcal{N}^{R_{\mathrm{s}}}_{NLO}\mathcal{N}^{R_{\mathrm{ew}}}_{NLO}\Bigg(\tilde{A}_3^1(\bar{p}_a,p_3,\bar{p}_b)\delta_{z_a}\delta_{z_b} \\
&\qquad + \Big(\boldsymbol{\mathcal{J}}^{(1)}_{2,ii}(s_{ab}) - \boldsymbol{\mathcal{J}}^{(1)}_{2,ii}(s_{\overline{ab}})\Big) A_3^0(\bar{p}_a,p_3,\bar{p}_b)\Bigg)\,\left|\mathcal{M}^{q\bar{q}\to\ell\bar{\ell}}_{\mathrm{LO},Z/\gamma}(\{\widetilde{\Phi}_3\}_{ii})\right|^2 J_2^{(2)}(\tilde{p}_1,\tilde{p}_2)\Bigg] \\
&\quad + (R_{\mathrm{s}} \to R_{\mathrm{phot}}, V_{\mathrm{phot}} \to V_{\mathrm{s}}),
\end{aligned} \tag{6.51}$$

where the real emission amplitude is given in (5.21) and we used $\delta_{z_i} = \delta(1-z_i)$. We also introduced the shorthand notation $\{\Phi_n\} = \{\bar{p}_a, \bar{p}_b, \{p_i\}_{i=1}^n\}$, $\{\widetilde{\Phi}_n\}_{ii} = \{\bar{\bar{p}}_a, \bar{\bar{p}}_b, \{\tilde{p}_i\}_{i=1}^{n-1}\}$, where the subscript in the second set of momenta indicates the applied initial–initial phase-space mapping

$$\begin{aligned}
&\bar{p}_a = z_a p_a, \qquad \bar{p}_b = z_b p_b, \qquad s_{ab} = (\bar{p}_a + \bar{p}_b)^2, \qquad \tilde{p}_i = \lambda(q,\tilde{q})p_i, \qquad i = 1,2, \\
&\bar{\bar{p}}_a = x_a z_a p_a, \qquad \bar{\bar{p}}_b = x_b z_b p_b, \qquad s_{\overline{ab}} = (\bar{\bar{p}}_a + \bar{\bar{p}}_b)^2.
\end{aligned} \tag{6.52}$$

The Lorentz transformation $\lambda(q,\tilde{q})$ is given in (4.35). Similarly, the cancellation of implicit and explicit divergences in the real–virtual correction to the squared matrix element for the qg-channel can be cancelled by the subtraction term

$$\begin{aligned}
\mathrm{d}\hat{\sigma}^{T,ii,qg}_{\mathrm{NNLO}} =& \mathcal{N}^{\varepsilon}_{\mathcal{C},qg} \int \frac{\mathrm{d}z_a}{z_a}\frac{\mathrm{d}z_b}{z_b}\, \mathrm{d}\Phi_3(\{p_i\}_{i=1}^3; \bar{p}_a, \bar{p}_b) \\
&\times \Bigg[-2\,Q_q\,\mathcal{N}^{V_{\mathrm{ew}}}_{NLO}\,\boldsymbol{\mathcal{J}}^{(1),g\to q}_{2,ii}(s_{ab})\,\left|\mathcal{M}^{q\bar{q}\to\ell\bar{\ell}g}_{R_{\mathrm{s}},Z/\gamma}(\{\Phi_3\})\right|^2 J_2^{(3)}(p_1,p_2,p_3) \\
&\quad - 2\,Q_q\,\mathcal{N}^{V_{\mathrm{ew}}}_{NLO}\,\boldsymbol{\mathcal{J}}^{(1)}_{2,if}(s_{a3})\,\left|\mathcal{M}^{qg\to\ell\bar{\ell}q}_{R_{\mathrm{s}},Z/\gamma}(\{\Phi_3\})\right|^2 J_2^{(3)}(p_1,p_2,p_3)
\end{aligned} \tag{6.53}$$

$$
\begin{aligned}
&- 2\,C_F\,\mathcal{N}^{R_\mathrm{s}}_{NLO} A^0_{3,g\to q}(\bar{p}_a,\bar{p}_b,p_3)\Bigg(2\mathrm{Re}\Big\{\mathcal{M}^{q\bar{q}\to\ell\bar{\ell}}_{\mathrm{V_{phot}},\mathrm{I}}\left(\mathcal{M}^{q\bar{q}\to\ell\bar{\ell}}_{\mathrm{LO},Z/\gamma}\right)^*\Big\}\big(\{\widetilde{\Phi}_3\}_{ii}\big)\delta_{z_a}\delta_{z_b}\\
&\qquad - 2\,Q_q\,\mathcal{N}^{R_\mathrm{ew}}_{NLO}\boldsymbol{\mathcal{J}}^{(1)}_{2,ii}(s_{\overline{ab}})\,\Big|\mathcal{M}^{q\bar{q}\to\ell\bar{\ell}}_{\mathrm{LO},Z/\gamma}\big(\{\widetilde{\Phi}_3\}_{ii}\big)\Big|^2\Bigg)J_2^{(2)}(\tilde{p}_1,\tilde{p}_2)\\
&- 4\,C_F\,Q_q\,\mathcal{N}^{R_\mathrm{s}}_{NLO}\mathcal{N}^{R_\mathrm{ew}}_{NLO}\,\boldsymbol{\mathcal{J}}^{(1),g\to q}_{2,ii}(s_{ab})\,A^0_3(\bar{p}_a,p_3,\bar{p}_b)\\
&\qquad\times\Big|\mathcal{M}^{q\bar{q}\to\ell\bar{\ell}}_{\mathrm{LO},Z/\gamma}\big(\{\widetilde{\Phi}_3\}_{ii}\big)\Big|^2 J_2^{(2)}(\tilde{p}_1,\tilde{p}_2)\\
&- 4\,C_F\,Q_q\,\mathcal{N}^{R_\mathrm{s}}_{NLO}\mathcal{N}^{R_\mathrm{ew}}_{NLO}\Bigg(\tilde{A}^1_{3,g\to q}(\bar{p}_a,\bar{p}_b,p_3)\delta_{z_a}\delta_{z_b}\\
&\qquad+\Big(\boldsymbol{\mathcal{J}}^{(1)}_{2,if}(s_{a3})-\boldsymbol{\mathcal{J}}^{(1)}_{2,ii}(s_{\overline{ab}})\Big)\,A^0_{3,g\to q}(\bar{p}_a,\bar{p}_b,p_3)\Bigg)\\
&\qquad\times\Big|\mathcal{M}^{q\bar{q}\to\ell\bar{\ell}}_{\mathrm{LO},Z/\gamma}\big(\{\widetilde{\Phi}_3\}_{ii}\big)\Big|^2 J_2^{(2)}(\tilde{p}_1,\tilde{p}_2)\Bigg].
\end{aligned}
$$

The subtraction terms for the weak×QCD real–virtual corrections read

$$
\begin{aligned}
\mathrm{d}\hat{\sigma}^{\mathrm{S},ii,q\bar{q}}_{\mathrm{NNLO}} =& 2C_F\,\mathcal{N}_{\mathcal{C},q\bar{q}}\mathcal{N}^R_{\mathrm{NLO}}\,\mathrm{d}\Phi_3(\{p_i\}_{i=1}^3;p_a,p_b) \\
&\times A^0_3(p_a,p_3,p_b)\,2\mathrm{Re}\Big\{\mathcal{M}^{q\bar{q}\to\ell\bar{\ell}}_{\mathrm{V_w,I,PA}}\left(\mathcal{M}^{q\bar{q}\to\ell\bar{\ell}}_{\mathrm{LO},Z}\right)^*\Big\}(\tilde{p}_1,\tilde{p}_2;x_ap_a,x_bp_b)\,J_2^{(2)}(\tilde{p}_1,\tilde{p}_2),
\end{aligned}
\tag{6.54}
$$

and

$$
\begin{aligned}
\mathrm{d}\hat{\sigma}^{\mathrm{S},ii,qg}_{\mathrm{NNLO}} =& 2C_F\,\mathcal{N}_{\mathcal{C},qg}\mathcal{N}^R_{\mathrm{NLO}}\,\mathrm{d}\Phi_3(\{p_i\}_{i=1}^3;p_a,p_b) \\
&\times A^0_{3,qg\to qq}(p_3,p_a,p_b)\,2\mathrm{Re}\Big\{\mathcal{M}^{q\bar{q}\to\ell\bar{\ell}}_{\mathrm{V_w,I,PA}}\left(\mathcal{M}^{q\bar{q}\to\ell\bar{\ell}}_{\mathrm{LO},Z}\right)^*\Big\}(\tilde{p}_1,\tilde{p}_2;x_ap_a,x_bp_b)\,J_2^{(2)}(\tilde{p}_1,\tilde{p}_2).
\end{aligned}
\tag{6.55}
$$

In line with (6.13) and (6.47) the pole approximation of the reduced matrix element multiplying the antenna function and including the virtual weak correction is obtained by evaluating the weak form factor for an on-shell Z boson, neglecting photon production and evaluating everything else (i.e. the remaining Dirac structures in (6.14)) with off-shell kinematics.

6.3.3 Double-real corrections

The double-real corrections arise only from diagrams including corrections of $\mathcal{O}(Q_q^2\alpha_\mathrm{s}\alpha_\mathrm{phot})$, and the QCD×weak corrections do not contribute here. The channels that have to be considered are

$$
\begin{aligned}
\bar{q}_a(p_a)+q_b(p_b)&\to Z(p_Z)+g(k_g)+\gamma(p_\gamma), && (6.56)\\
g(p_g)+q_b(p_b)&\to Z(p_Z)+q_a(k_a)+\gamma(p_\gamma), && (6.57)\\
g(p_g)+\bar{q}_a(p_a)&\to Z(p_Z)+\bar{q}_b(k_b)+\gamma(p_\gamma), && (6.58)\\
q_b(p_a)+q_b(p_b)&\to Z(p_Z)+q_b(k_a)+q_b(k_b), && (6.59)\\
\bar{q}_a(p_a)+\bar{q}_a(p_b)&\to Z(p_Z)+\bar{q}_a(k_a)+\bar{q}_a(k_b), && (6.60)\\
\bar{q}_a(p_a)+q_a(p_b)&\to Z(p_Z)+\bar{q}_a(k_a)+q_a(k_b), && (6.61)
\end{aligned}
$$

and are illustrated in Fig. 6.2a. The helicity amplitudes corresponding to the different partonic channels were calculated using the spinor-helicity formalism [153] and checked against helicity amplitudes calculated using FeynArts/FormCalc. Note that in Fig. 6.2a in the double-real cross-interference term of four identical quark amplitudes, once with photon and once with gluon exchange, only the contributions with one closed quark line contribute and the ones with two closed quark lines vanish owing to colour conservation.

The amplitudes corresponding to the double-real contribution can be calculated using the spinor-helicity formalism and are given by

$$\mathrm{i}\mathcal{M}^{\bar{q}q\to\ell\bar{\ell}g\gamma}_{\mathrm{R_s}\mathrm{R}_{\mathrm{phot}},Z,\tau_q\tau_l\lambda_g\lambda_\gamma} = 4\mathrm{i}e^3 g_s C^{\tau_q}_{Z\bar{q}q} C^{\tau_l}_{Z\bar{\ell}\ell} \mathrm{M}^{\tau_q\tau_l\lambda_g\lambda_\gamma}_{\mathrm{R_s}\mathrm{R}_{\mathrm{phot}}}(k_\gamma,\{k_g,a\},\{p_i,c_i\}_{i\in\mathcal{S}}), \tag{6.62}$$

where $\mathcal{S}=\{a,b,\ell_1,\ell_2\}$. Due to the symmetries of the partial amplitude,

$$\begin{aligned}
\mathrm{M}^{-\tau_q\tau_l\lambda_g\lambda_\gamma}_{\mathrm{R_s}\mathrm{R}_{\mathrm{phot}}}(k_\gamma,\{k_g,a\},\{p_i,c_i\}_{i\in\mathcal{S}}) &= \mathrm{M}^{\tau_q\tau_l\lambda_g\lambda_\gamma}_{\mathrm{R_s}\mathrm{R}_{\mathrm{phot}}}(k_\gamma,\{k_g,a\},\{p_i,c_i\}_{i\in\mathcal{S}})\Big|_{\{p_a,c_a,Q_a\}\leftrightarrow\{p_b,c_b,-Q_b\}},\\
\mathrm{M}^{\tau_q-\tau_l\lambda_g\lambda_\gamma}_{\mathrm{R_s}\mathrm{R}_{\mathrm{phot}}}(k_\gamma,\{k_g,a\},\{p_i,c_i\}_{i\in\mathcal{S}}) &= \mathrm{M}^{\tau_q\tau_l\lambda_g\lambda_\gamma}_{\mathrm{R_s}\mathrm{R}_{\mathrm{phot}}}(k_\gamma,\{k_g,a\},\{p_i,c_i\}_{i\in\mathcal{S}})\Big|_{\{p_{\ell_1}\}\leftrightarrow\{p_{\ell_2}\}},\\
\mathrm{M}^{\tau_q\tau_l-\lambda_g-\lambda_\gamma}_{\mathrm{R_s}\mathrm{R}_{\mathrm{phot}}}(k_\gamma,\{k_g,a\},\{p_i,c_i\}_{i\in\mathcal{S}}) &= \big[\mathrm{M}^{-\tau_q-\tau_l\lambda_g\lambda_\gamma}_{\mathrm{R_s}\mathrm{R}_{\mathrm{phot}}}(k_\gamma,\{k_g,a\},\{p_i,c_i\}_{i\in\mathcal{S}})\big]^*,
\end{aligned} \tag{6.63}$$

it is sufficient to calculate only two helicity configurations, where we choose

$$\begin{aligned}
\mathrm{M}^{--++}_{\mathrm{R_s}\mathrm{R}_{\mathrm{phot}}}(\{\Phi_4,\mathcal{C}\}) = {}& \frac{t^a_{c_ac_b}Q_q}{(k_g+k_\gamma-p_a)^2(p_Z^2-\mu_Z^2)\langle k_g|p_a\rangle\langle k_\gamma|p_a\rangle\langle p_b|k_g\rangle\langle p_b|k_\gamma\rangle}\\
&\times\Big(\big(\langle p_{\bar{\ell}}|k_g\rangle^*\langle p_b|k_g\rangle+\langle p_{\bar{\ell}}|k_\gamma\rangle^*\langle p_b|k_\gamma\rangle-\langle p_{\bar{\ell}}|p_a\rangle^*\langle p_b|p_a\rangle\big)\\
&\times\langle p_b|p_\ell\rangle^*\Big(\langle k_g|p_a\rangle\big(\langle k_g|k_\gamma\rangle^*\langle p_b|k_\gamma\rangle-\langle k_g|p_a\rangle^*\langle p_b|p_a\rangle\big)\\
&+\langle k_\gamma|p_a\rangle\big(\langle k_\gamma|k_g\rangle^*\langle p_b|k_g\rangle-\langle k_\gamma|p_a\rangle^*\langle p_b|p_a\rangle\big)\Big)\Big),
\end{aligned} \tag{6.64}$$

$$\begin{aligned}
\mathrm{M}^{--+-}_{\mathrm{R_s}\mathrm{R}_{\mathrm{phot}}}(\{\Phi_4,\mathcal{C}\}) = {}& \frac{t^a_{c_ac_b}Q_q}{\langle p_a|k_\gamma\rangle^*(p_Z^2-\mu_Z^2)\langle p_b|k_g\rangle}\\
&\times\Bigg[\frac{\langle p_a|k_\gamma\rangle^*\langle p_a|p_{\bar{\ell}}\rangle^*\langle p_b|k_\gamma\rangle}{\langle k_\gamma|p_b\rangle^*(k_g+k_\gamma-p_b)^2}\big(\langle k_g|k_\gamma\rangle^*\langle p_\ell|k_\gamma\rangle^*-\langle k_g|p_b\rangle^*\langle p_\ell|p_b\rangle\big)\\
&+\frac{1}{\langle k_g|p_a\rangle}\Bigg(\frac{\langle p_a|k_g\rangle^*\langle p_b|k_g\rangle\langle p_b|p_\ell\rangle^*}{(k_g+k_\gamma-p_a)^2}\big(\langle p_{\bar{\ell}}|k_g\rangle^*\langle k_\gamma|k_g\rangle-\langle p_{\bar{\ell}}|p_a\rangle^*\langle k_\gamma|p_a\rangle\big)\\
&+\frac{1}{\langle k_\gamma|p_b\rangle^*}\Big(\big(\langle p_{\bar{\ell}}|p_a\rangle^*\langle p_b|p_a\rangle-\langle p_{\bar{\ell}}|k_g\rangle^*\langle p_b|k_g\rangle\big)\\
&\times\big(\langle p_a|k_\gamma\rangle^*\langle p_\ell|k_\gamma\rangle^*-\langle p_1|p_b\rangle\langle p_\ell|p_b\rangle\big)\Big)\Bigg)\Bigg],
\end{aligned} \tag{6.65}$$

where $\{\Phi_4,\mathcal{C}\}=\{k_\gamma,\{k_g,a\},\{p_i,c_i\}_{i\in\mathcal{S}}\}$, $p_Z=p_\ell+p_{\bar{\ell}}$, and the spinor product $\langle p|k\rangle$ of two Weyl spinors p,k is defined in (A.20). The contribution to the squared amplitude

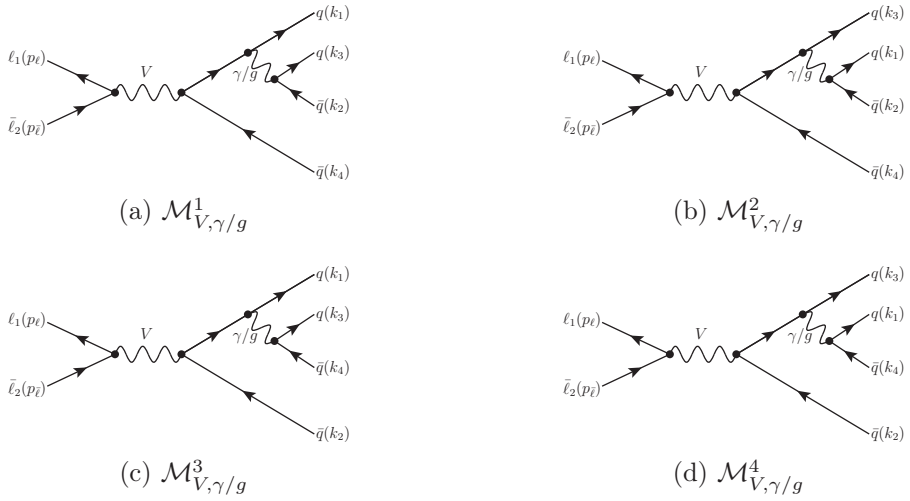

(a) $\mathcal{M}^1_{V,\gamma/g}$ (b) $\mathcal{M}^2_{V,\gamma/g}$

(c) $\mathcal{M}^3_{V,\gamma/g}$ (d) $\mathcal{M}^4_{V,\gamma/g}$

Figure 6.3: The different amplitudes that contribute to the process $\ell(p_\ell)\bar{\ell}(p_{\bar{\ell}}) \to V(p_V) \to q(k_1)\bar{q}(k_2)q(k_3)\bar{q}(k_4)$ at tree level in PA, where $V = Z$. There are also contributions where the inner quark–anti-quark pair attached to the photon/gluon is radiated from the lower leg, which are not depicted. The corresponding $\mathcal{O}(\alpha_s\alpha)$ correction to the squared matrix element is obtained by summing all possible interference diagrams, e.g. $2\mathrm{Re}\{(\mathcal{M}^1_{V,\gamma})^* \cdot \mathcal{M}^2_{V,g}\}$.

is obtained by squaring of (6.62), averaging over the initial-state helicities, and summing the final state helicities.

We now proceed with the calculation of the amplitudes for the process

$$\ell(p_\ell)\bar{\ell}(p_{\bar{\ell}}) \to Z(p_Z) \to q(k_1)\bar{q}(k_2)q(k_3)\bar{q}(k_4), \tag{6.66}$$

once involving a quark–gluon and once a quark–photon splitting, see Fig. 6.3. The amplitudes (6.59) to (6.61) can be obtained from the ones describing the process (6.66) by crossing the leptons to the final and two of the four quarks to the initial state, where it depends on the desired amplitude which final-state quarks have to be crossed to the initial state. The interference of two amplitudes describing the process (6.66), one of the amplitudes involving a quark-gluon and the other a quark-photon splitting, is an $\mathcal{O}(\alpha_s\alpha)$ correction to the process

$$\ell\bar{\ell} \to Z \to q\bar{q}. \tag{6.67}$$

Therefore, the crossed versions (with the leptons in the final state and (anti-)quarks in the initial state) of such interference contributions is a correction of $\mathcal{O}(\alpha_s\alpha)$ to the neutral-current DY process.

As there are identical particles in the final state of (6.66) we can assign the momenta in four different ways to the quark and anti-quark pairs which lead to different contributions to the complete amplitude. Note that the four different contributions to (6.66) are related by an exchange of momenta between (anti-)quark, (anti-)quark pairs but never between a quark and an anti-quark. We define the amplitude $\mathcal{M}^1_{Z,\gamma/g}$ as the sum of the diagram on the top left of Fig. 6.3 plus the diagram with the same momentum assignment but the photon/gluon radiated from the anti-quark that carries momentum k_4. Similarly $\mathcal{M}^2_{Z,\gamma/g}$

is defined from the contribution on the top right, $\mathcal{M}^3_{Z,\gamma/g}$ from the lower left, and $\mathcal{M}^4_{Z,\gamma/g}$ from the contribution on the lower right. The full amplitude is obtained as the sum of these four contributions

$$\mathcal{M}^{\ell\bar{\ell}\to q\bar{q}q}_{Z,\gamma/g} = \sum_{i=1}^{4} \mathcal{M}^i_{Z,\gamma/g}. \tag{6.68}$$

The amplitude $\mathcal{M}^1_{Z,\gamma/g}$ is given by

$$\begin{aligned}\mathrm{i}\mathcal{M}^1_{Z,\gamma/g,\sigma_\ell\sigma_{\bar{\ell}}\sigma_1\sigma_2\sigma_3\sigma_4}(p_\ell,p_{\bar{\ell}},k_1,\ldots,k_4) =& 4\,\mathrm{i}\,e^2 g\, t^q_{1,\gamma/g}\, t^q_{2,\gamma/g}\, \delta_{\sigma_\ell,-\sigma_{\bar{\ell}}}\, \delta_{\sigma_1,-\sigma_4}\, \delta_{\sigma_3,-\sigma_2} \\ &\times \frac{C^{\tau_q}_{Z\bar{q}q} C^{\tau_l}_{Z\bar{\ell}\ell} \mathrm{M}^{\sigma_\ell\sigma_1\sigma_3}_{Z,1}(p_\ell,p_{\bar{\ell}},k_1,\ldots,k_4)}{(k_1+k_2)^2\,(p_Z^2-\mu_Z^2)},\end{aligned} \tag{6.69}$$

where $t^q_{1,\gamma/g}$ and $t^q_{2,\gamma/g}$ are both either Gell-Mann matrices $t^q_{1,g} = t^a_{c_a c_b}$ and $t^q_{2,g} = t^a_{c_c c_d}$ or are given by the charge of the quarks $t^q_{1,\gamma} = t^q_{2,\gamma} = Q_q$, respectively. The other contributions to the amplitude can be obtained via the following symmetries,

$$\begin{aligned}\mathcal{M}^2_{Z,\gamma/g,\sigma_\ell\sigma_{\bar{\ell}}\sigma_1\sigma_2\sigma_3\sigma_4}(p_\ell,p_{\bar{\ell}},k_1,\ldots,k_4) &= -\mathcal{M}^1_{Z,\gamma/g,\sigma_\ell\sigma_{\bar{\ell}}\sigma_3\sigma_2\sigma_1\sigma_4}(p_\ell,p_{\bar{\ell}},k_3,k_2,k_1,k_4),\\ \mathcal{M}^3_{Z,\gamma/g,\sigma_\ell\sigma_{\bar{\ell}}\sigma_1\sigma_2\sigma_3\sigma_4}(p_\ell,p_{\bar{\ell}},k_1,\ldots,k_4) &= -\mathcal{M}^1_{Z,\gamma/g,\sigma_\ell\sigma_{\bar{\ell}}\sigma_1\sigma_4\sigma_3\sigma_2}(p_\ell,p_{\bar{\ell}},k_1,k_4,k_3,k_2),\\ \mathcal{M}^4_{Z,\gamma/g,\sigma_\ell\sigma_{\bar{\ell}}\sigma_1\sigma_2\sigma_3\sigma_4}(p_\ell,p_{\bar{\ell}},k_1,\ldots,k_4) &= \mathcal{M}^1_{Z,\gamma/g,\sigma_\ell\sigma_{\bar{\ell}}\sigma_3\sigma_4\sigma_1\sigma_2}(p_\ell,p_{\bar{\ell}},k_3,k_4,k_1,k_2),\end{aligned} \tag{6.70}$$

where the additional sign appears when one has to interchange an odd number of pairs of fermionic fields in $\mathcal{M}^1_{Z,\gamma/g}$ to obtain $\mathcal{M}^i_{Z,\gamma/g}, i = 2,3,4$, e.g. to obtain the first line of (6.70) we have to interchange k_1 and k_3 leading to an additional sign. For the different helicity configurations the partial amplitude $\mathrm{M}^{\sigma_\ell\sigma_1\sigma_3}_{Z,\gamma/g,1}$ is given by

$$\begin{aligned}\mathrm{M}^{---}_{Z,1}(p_\ell,p_{\bar{\ell}},k_1,\ldots,k_4) =& -\frac{\langle k_4|k_2\rangle^*\left(\langle p_\ell|k_2\rangle^*\langle k_3|k_2\rangle + \langle p_\ell|k_4\rangle^*\langle k_3|k_4\rangle\right)\langle p_{\bar{\ell}}|k_1\rangle}{(k_2+k_3+k_4)^2} \\ &+ \frac{\langle p_\ell|k_4\rangle^*\langle k_1|k_3\rangle\left(\langle k_2|k_1\rangle^*\langle p_{\bar{\ell}}|k_1\rangle + \langle k_2|k_3\rangle^*\langle p_{\bar{\ell}}|k_3\rangle\right)}{(k_1+k_2+k_3)^2},\end{aligned} \tag{6.71}$$

$$\begin{aligned}\mathrm{M}^{+--}_{Z,1}(p_\ell,p_{\bar{\ell}},k_1,\ldots,k_4) =& -\frac{\langle k_4|k_2\rangle^*\left(\langle p_{\bar{\ell}}|k_2\rangle^*\langle k_3|k_2\rangle + \langle p_{\bar{\ell}}|k_4\rangle^*\langle k_3|k_4\rangle\right)\langle p_\ell|k_1\rangle}{(k_2+k_3+k_4)^2} \\ &+ \frac{\langle p_{\bar{\ell}}|k_4\rangle^*\langle k_1|k_3\rangle\left(\langle k_2|k_1\rangle^*\langle p_\ell|k_1\rangle + \langle k_2|k_3\rangle^*\langle p_\ell|k_3\rangle\right)}{(k_1+k_2+k_3)^2},\end{aligned} \tag{6.72}$$

$$\begin{aligned}\mathrm{M}^{-+-}_{Z,1}(p_\ell,p_{\bar{\ell}},k_1,\ldots,k_4) =& +\frac{\langle k_1|k_2\rangle^*\left(\langle p_\ell|k_1\rangle^*\langle k_3|k_1\rangle + \langle p_\ell|k_2\rangle^*\langle k_3|k_2\rangle\right)\langle p_{\bar{\ell}}|k_4\rangle}{(k_1+k_2+k_3)^2} \\ &- \frac{\langle p_\ell|k_1\rangle^*\langle k_4|k_3\rangle\left(\langle k_2|k_3\rangle^*\langle p_{\bar{\ell}}|k_3\rangle + \langle k_2|k_4\rangle^*\langle p_{\bar{\ell}}|k_4\rangle\right)}{(k_2+k_3+k_4)^2},\end{aligned} \tag{6.73}$$

$$\begin{aligned}\mathrm{M}^{++-}_{Z,1}(p_\ell,p_{\bar{\ell}},k_1,\ldots,k_4) =& +\frac{\langle k_1|k_2\rangle^*\left(\langle p_{\bar{\ell}}|k_1\rangle^*\langle k_3|k_1\rangle + \langle p_{\bar{\ell}}|k_2\rangle^*\langle k_3|k_2\rangle\right)\langle p_\ell|k_4\rangle}{(k_1+k_2+k_3)^2} \\ &- \frac{\langle p_{\bar{\ell}}|k_1\rangle^*\langle k_4|k_3\rangle\left(\langle k_2|k_3\rangle^*\langle p_\ell|k_3\rangle + \langle k_2|k_4\rangle^*\langle p_\ell|k_4\rangle\right)}{(k_2+k_3+k_4)^2},\end{aligned} \tag{6.74}$$

$$\mathrm{M}^{--+}_{Z,1}(p_\ell,p_{\bar{\ell}},k_1,\ldots,k_4) = -\frac{\langle k_4|k_3\rangle^*\left(\langle p_\ell|k_3\rangle^*\langle k_2|k_3\rangle + \langle p_\ell|k_4\rangle^*\langle k_2|k_4\rangle\right)\langle p_{\bar{\ell}}|k_1\rangle}{(k_2+k_3+k_4)^2}$$

$$+\frac{\langle p_\ell|k_4\rangle^*\langle k_1|k_2\rangle\left(\langle k_3|k_1\rangle^*\langle p_{\bar\ell}|k_1\rangle+\langle k_3|k_2\rangle^*\langle p_{\bar\ell}|k_2\rangle\right)}{(k_1+k_2+k_3)^2}, \quad (6.75)$$

$$\mathrm{M}^{+-+}_{Z,1}(p_\ell,p_{\bar\ell},k_1,\ldots,k_4) = -\frac{\langle k_4|k_3\rangle^*\left(\langle p_{\bar\ell}|k_3\rangle^*\langle k_2|k_3\rangle+\langle p_{\bar\ell}|k_4\rangle^*\langle k_2|k_4\rangle\right)\langle p_\ell|k_1\rangle}{(k_2+k_3+k_4)^2}$$
$$+\frac{\langle p_{\bar\ell}|k_4\rangle^*\langle k_1|k_2\rangle\left(\langle k_3|k_1\rangle^*\langle p_\ell|k_1\rangle+\langle k_3|k_2\rangle^*\langle p_\ell|k_2\rangle\right)}{(k_1+k_2+k_3)^2}, \quad (6.76)$$

$$\mathrm{M}^{-++}_{Z,1}(p_\ell,p_{\bar\ell},k_1,\ldots,k_4) = +\frac{\langle k_1|k_3\rangle^*\left(\langle p_\ell|k_1\rangle^*\langle k_2|k_1\rangle+\langle p_\ell|k_3\rangle^*\langle k_2|k_3\rangle\right)\langle p_{\bar\ell}|k_4\rangle}{(k_1+k_2+k_3)^2}$$
$$-\frac{\langle p_\ell|k_1\rangle^*\langle k_4|k_2\rangle\left(\langle k_3|k_2\rangle^*\langle p_{\bar\ell}|k_2\rangle+\langle k_3|k_4\rangle^*\langle p_{\bar\ell}|k_4\rangle\right)}{(k_2+k_3+k_4)^2}, \quad (6.77)$$

$$\mathrm{M}^{+++}_{Z,1}(p_\ell,p_{\bar\ell},k_1,\ldots,k_4) = +\frac{\langle k_1|k_3\rangle^*\left(\langle p_{\bar\ell}|k_1\rangle^*\langle k_2|k_1\rangle+\langle p_{\bar\ell}|k_3\rangle^*\langle k_2|k_3\rangle\right)\langle p_\ell|k_4\rangle}{(k_1+k_2+k_3)^2}$$
$$-\frac{\langle p_{\bar\ell}|k_1\rangle^*\langle k_4|k_2\rangle\left(\langle k_3|k_2\rangle^*\langle p_\ell|k_2\rangle+\langle k_3|k_4\rangle^*\langle p_\ell|k_4\rangle\right)}{(k_2+k_3+k_4)^2}. \quad (6.78)$$

The $\mathcal{O}(\alpha_s\alpha)$ correction to the squared amplitude is obtained as

$$2\mathrm{Re}\left\{\left(\mathcal{M}^{\ell\bar\ell\to q\bar q\bar q}_{Z,\gamma}\right)^*\mathcal{M}^{\ell\bar\ell\to q\bar q\bar q}_{Z,g}\right\} = \sum_{\substack{i,j=1\\ i\neq j}}^{4} 2\mathrm{Re}\left\{\left(\mathcal{M}^{i}_{Z,\gamma}\right)^*\mathcal{M}^{j}_{Z,g}\right\}, \quad (6.79)$$

where we have suppressed the summation/averaging over the helicities on the r.h.s. and used that $\left(\mathcal{M}^{i}_{Z,\gamma}\right)^*\mathcal{M}^{i}_{Z,g}=0$, which holds due to colour conservation. Note that there are more tuples of (i,j) such that $\left(\mathcal{M}^{i}_{Z,\gamma}\right)^*\mathcal{M}^{j}_{Z,g}=0$ as a consequence of colour conservation. Therefore, (6.79) could be simplified even further. For completeness we mention that these combinations are $(i,j)\in\{(1,4),(2,3)\}$, where the order of i and j in the tuple is not relevant.

6.3.3.1 Double-real antenna subtraction terms

In this section we present the subtraction terms corresponding to the double-real QCD × photonic corrections to the squared amplitude. As there are no double-real weak×QCD corrections we only have to consider the photonic×QCD corrections which again lead to overlapping soft and collinear singularities due to the real emission of a gluon and a photon. The subtraction term that cancels these singularities in the $q\bar q$-induced channel is given by

$$\begin{aligned}\mathrm{d}\hat\sigma^{S,ii,q\bar q}_{\mathrm{NNLO}} =& \mathcal{N}_{\mathcal{C},q\bar q}\,\mathrm{d}\Phi_4(\{p_i\}_{i=1}^4;p_a,p_b) \\ &\times\Bigg[+2\,Q_q\,\mathcal{N}^{R_{\mathrm{ew}}}_{NLO}\,A^0_3(p_a,p_3,p_b)\,\left|\mathcal{M}^{q\bar q\to\ell\bar\ell g}_{R_{\mathrm{s}},Z/\gamma}\left(\{\widetilde\Phi_4\}_{ii}\right)\right|^2 J^{(3)}_2(\tilde p_1,\tilde p_2,\tilde p_4) \\ &\quad+2\,C_F\,\mathcal{N}^{R_{\mathrm{s}}}_{NLO}A^0_3(p_a,p_4,p_b)\,\left|\mathcal{M}^{q\bar q\to\ell\bar\ell\gamma}_{R_{\mathrm{phot}},Z/\gamma}\left(\{\widetilde\Phi_4\}_{ii}\right)\right|^2 J^{(3)}_2(\tilde p_1,\tilde p_2,\tilde p_3) \\ &\quad+4\,Q_q\,C_F\,\mathcal{N}^{R_{\mathrm{s}}}_{NLO}\mathcal{N}^{R_{\mathrm{ew}}}_{NLO}\,\tilde A^0_4(p_a,p_3,p_4,p_b)\,\left|\mathcal{M}^{q\bar q\to\ell\bar\ell}_{\mathrm{LO},Z/\gamma}\left(\{\widetilde\Phi^{\mathrm{NNLO}}_4\}_{ii}\right)\right|^2 J^{(2)}_2(\tilde{\tilde p}_1,\tilde{\tilde p}_2)\end{aligned} \quad (6.80)$$

$$
\begin{aligned}
&- 4\,Q_q\,C_F\,\mathcal{N}^{R_\mathrm{s}}_{NLO}\,\mathcal{N}^{R_\mathrm{ew}}_{NLO}\,\left|\mathcal{M}^{q\bar{q}\to\ell\bar{\ell}}_{\mathrm{LO},Z/\gamma}\left(\{\widetilde{\widetilde{\Phi}}_4\}_{ii,ii}\right)\right|^2 \\
&\qquad\times\left(A^0_3(p_a,p_3,p_b)\,A^0_3(\bar{p}_a,\tilde{p}_4,\bar{p}_b)+A^0_3(p_a,p_4,p_b)\,A^0_3(\bar{p}_a,\tilde{p}_3,\bar{p}_b)\right)\,J^{(2)}_2(\tilde{\tilde{p}}_1,\tilde{\tilde{p}}_2)\Bigg],
\end{aligned}
$$

using the notation $\{\widetilde{\Phi}_n\}_{ii}=\{\bar{p}_a,\bar{p}_b,\{\tilde{p}_i\}_{i=1}^{n-1}\}$, $\{\widetilde{\widetilde{\Phi}}_n\}_{ii,ii}=\{\bar{\bar{p}}_a,\bar{\bar{p}}_b,\{\tilde{\tilde{p}}_i\}_{i=1}^{n-2}\}$, where the momenta are obtained by the application of the one-fold or two-fold application of the NLO initial–initial phase-space mapping

$$
\begin{aligned}
&\bar{p}_a=z_a p_a, && \bar{p}_b=z_b p_b, && \tilde{p}_i=\lambda(q,\tilde{q})p_i, && i=1,2,\\
&\bar{\bar{p}}_a=x_a z_a p_a, && \bar{\bar{p}}_b=x_b z_b p_b, && \tilde{\tilde{p}}_i=\lambda(\tilde{q},\tilde{\tilde{q}})\tilde{p}_i, && i=1,2.
\end{aligned}
\tag{6.81}
$$

By contrast, the momenta in $\{\widetilde{\Phi}^{\mathrm{NNLO}}_n\}_{ii}=\{\bar{p}_a,\bar{p}_b,\{\tilde{p}_i\}_{i=1}^{n-2}\}$ are obtained by the application of the NNLO initial–initial mapping.

The subtraction term for the qg-induced channel is given by

$$
\begin{aligned}
\mathrm{d}\hat{\sigma}^{S,ii,qg}_{\mathrm{NNLO}} =&\mathcal{N}_{\mathcal{C},qg}\,\mathrm{d}\Phi_4(\{p_i\}_{i=1}^4;p_a,p_b) \\
&\times\Bigg[+2\,Q_q\,\mathcal{N}^{R_\mathrm{ew}}_{NLO}\,A^0_3(p_a,p_3,p_4)\,\left|\mathcal{M}^{qg\to\ell\bar{\ell}q}_{R_\mathrm{s},Z/\gamma}\left(\{\widetilde{\Phi}_4\}_{if}\right)\right|^2 J^{(3)}_2(p_1,p_2,\widetilde{(p_3p_4)}) \\
&\quad-2\,C_F\,\mathcal{N}^{R_\mathrm{s}}_{NLO}A^0_{3,g\to q}(p_a,p_b,p_4)\,\left|\mathcal{M}^{q\bar{q}\to\ell\bar{\ell}\gamma}_{R_\mathrm{phot},Z/\gamma}\left(\{\widetilde{\Phi}_4\}_{ii}\right)\right|^2 J^{(3)}_2(\tilde{p}_1,\tilde{p}_2,\tilde{p}_3) \\
&\quad+4\,Q_q\,C_F\,\mathcal{N}^{R_\mathrm{s}}_{NLO}\,\mathcal{N}^{R_\mathrm{ew}}_{NLO}\,J^{(2)}_2(\tilde{\tilde{p}}_1,\tilde{\tilde{p}}_2) \\
&\qquad\times\Bigg(-\tilde{A}^0_4(p_a,p_b,p_3,p_4)\,\left|\mathcal{M}^{q\bar{q}\to\ell\bar{\ell}}_{\mathrm{LO},Z/\gamma}\left(\{\widetilde{\Phi}^{\mathrm{NNLO}}_4\}_{ii}\right)\right|^2 \\
&\qquad\quad+A^0_3(p_a,p_3,p_4)\,A^0_{3,g\to q}(\bar{p}_a,p_b,\widetilde{(p_3p_4)})\,\left|\mathcal{M}^{q\bar{q}\to\ell\bar{\ell}}_{\mathrm{LO},Z/\gamma}\left(\{\widetilde{\widetilde{\Phi}}_4\}_{if,ii}\right)\right|^2 \\
&\qquad\quad+A^0_{3,g\to q}(p_a,p_b,p_4)\,A^0_3(\bar{p}_a,\tilde{p}_3,\bar{p}_b)\,\left|\mathcal{M}^{q\bar{q}\to\ell\bar{\ell}}_{\mathrm{LO},Z/\gamma}\left(\{\widetilde{\widetilde{\Phi}}_4\}_{ii,ii}\right)\right|^2\Bigg)\Bigg].
\end{aligned}
\tag{6.82}
$$

Note that the first line takes care of the case where the photon becomes unresolved with respect to the quark in the initial or final state (leading to an initial–final NLO mapping), whereas the second line subtracts singularities of the configuration where the quark in the final state becomes unresolved (consequently, a initial–initial NLO mapping is used). Finally, the subtraction term for the qq-channel reads

$$
\begin{aligned}
\mathrm{d}\hat{\sigma}^{S,ii,qq}_{\mathrm{NNLO}} =&\mathcal{N}_{\mathcal{C},q\bar{q}}\,\mathrm{d}\Phi_4(\{p_i\}_{i=1}^4;p_a,p_b) \\
&\times 4\,Q_q\,C_F\,\mathcal{N}^{R_\mathrm{s}}_{NLO}\,\mathcal{N}^{R_\mathrm{ew}}_{NLO}\,J^{(2)}_2(\tilde{p}_1,\tilde{p}_2) \\
&\times\left(C^0_4(p_a,p_b,p_3,p_4)\,\left|\mathcal{M}^{q\bar{q}\to\ell\bar{\ell}}_{\mathrm{LO},Z/\gamma}\left(\{\widetilde{\Phi}^{\mathrm{NNLO}}_4\}_{ii}\right)\right|^2+(a\leftrightarrow b,3\leftrightarrow 4)\right),
\end{aligned}
\tag{6.83}
$$

and for the $q\bar{q}$- (four quark contribution) and $\bar{q}\bar{q}$-channel we have

$$
\mathrm{d}\hat{\sigma}^{S,ii,q\bar{q}q\bar{q}}_{\mathrm{NNLO}} =\mathcal{N}_{\mathcal{C},q\bar{q}}\,\mathrm{d}\Phi_4(\{p_i\}_{i=1}^4;p_a,p_b)
\tag{6.84}
$$

$$
\begin{aligned}
&\times 4\,Q_q\,C_F\,\mathcal{N}_{NLO}^{R_\mathrm{s}}\,\mathcal{N}_{NLO}^{R_\mathrm{ew}}\,J_2^{(2)}(\tilde{p}_1,\tilde{p}_2)\\
&\times \left(C_4^0(p_a,p_3,p_4,p_b)+C_4^0(p_b,p_4,p_a,p_3)\right)\,\left|\mathcal{M}_{\mathrm{LO},Z/\gamma}^{q\bar{q}\to\ell\bar{\ell}}\left(\{\widetilde{\Phi}_4^{\mathrm{NNLO}}\}_{ii}\right)\right|^2,\\
\mathrm{d}\hat{\sigma}_{\mathrm{NNLO}}^{S,ii,\bar{q}\bar{q}} =&\mathcal{N}_{\mathcal{C},q\bar{q}}\,\mathrm{d}\Phi_4(\{p_i\}_{i=1}^4;p_a,p_b) \qquad (6.85)\\
&\times 4\,Q_q\,C_F\,\mathcal{N}_{NLO}^{R_\mathrm{s}}\,\mathcal{N}_{NLO}^{R_\mathrm{ew}}\,J_2^{(2)}(\tilde{p}_1,\tilde{p}_2)\\
&\times \left(C_4^0(p_b,p_a,p_3,p_4)\,\left|\mathcal{M}_{\mathrm{LO},Z/\gamma}^{q\bar{q}\to\ell\bar{\ell}}\left(\{\widetilde{\Phi}_4^{\mathrm{NNLO}}\}_{ii}\right)\right|^2+(a\leftrightarrow b,3\leftrightarrow 4)\right).
\end{aligned}
$$

6.4 Numerical results

6.4.1 Input parameters and event selection

The numerical results presented in the following sections are produced using the same setup as in Section 5.3.1. In line with the calculation of the initial–final $\mathcal{O}(\alpha_\mathrm{s}\alpha)$ corrections presented in [55,56] we apply a photon recombination procedure identical to the one used in Refs. [21,29] in order to be able to add the results calculated in this work to the results of Refs. [21,29] consistently.

In detail, we apply the following photon recombination algorithm:

1. Photons close to the beam with a rapidity $|\eta_\gamma| > 3$ are treated as beam remnants and are not considered in the event selection any further.
2. For the photons that pass the first step, the angular distances to the charged leptons $R_{\ell^\pm\gamma} = \sqrt{(\eta_{\ell^\pm}-\eta_\gamma)^2+(\phi_{\ell^\pm}-\phi_\gamma)^2}$ are computed, where ϕ denotes the azimuthal angle in the transverse plane. If the smaller distance of $R_{\ell^\pm\gamma}$ between the photon and the closest lepton is smaller than 0.1, the photon is recombined with the lepton by adding the respective four-momenta, $\ell^\pm(k_i)+\gamma(k)\to\ell^\pm(k_i+k)$.
3. Finally, the event selection cuts from Eqs. (5.90)–(5.92) are applied to the resulting event kinematics.

6.4.2 Corrections to differential distributions

In Fig. 6.4 we show the relative corrections δ (normalized to LO) of type initial–initial $\mathcal{O}(\alpha_\mathrm{s}\alpha)$ to distributions in the invariant mass (left plot) and in the transverse momentum (right plot) of the final-state leptons for the neutral-current DY process. We depict the individually gauge-invariant weak × QCD (red curve) and photonic × QCD (green curve) corrections separately, as the weak × QCD corrections are calculated using the PA while the photonic × QCD corrections are calculated without approximation and are therefore valid beyond the resonance region. The photonic × QCD corrections are shown both for bare and dressed leptons (DL) where the latter are obtained using a recombination of the bare leptons and the radiated photon.
The corrections to the invariant-mass spectrum are of the permil or subpermil level and are therefore phenomenologically not relevant. In the resonance region, corrections to the transverse-momentum distribution are of the level of a few percent for both the photonic ×

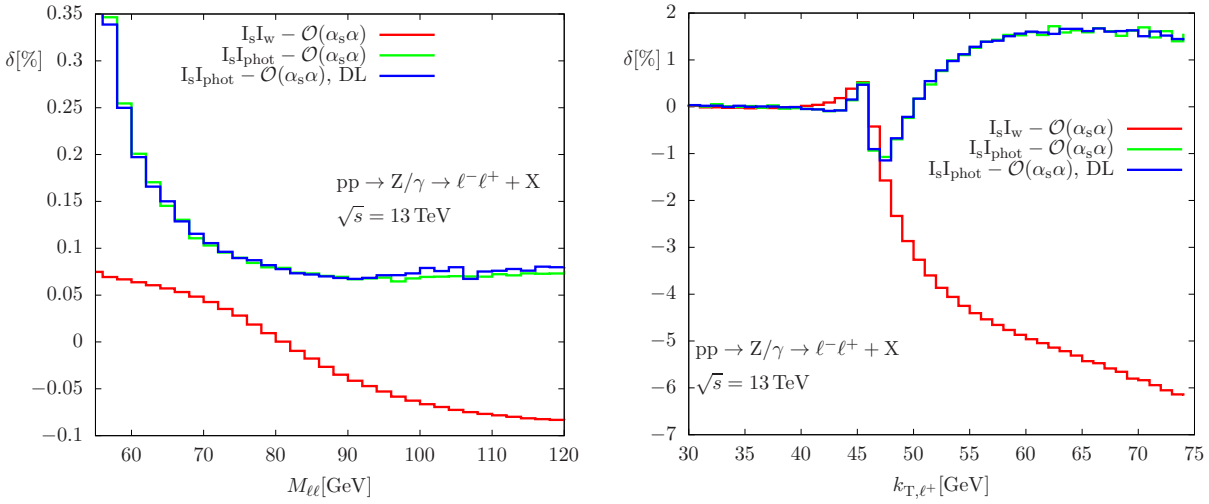

Figure 6.4: Relative initial–initial $\mathcal{O}(\alpha_s\alpha)$ corrections (normalized to the LO cross section) to distributions in the invariant mass of the Z boson (left) and in the transverse-lepton momentum (right). Depicted are QCD × weak $\mathcal{O}(\alpha_s\alpha_w)$ corrections (red curve) and corrections of type QCD × phot $\mathcal{O}(\alpha_s\alpha_p)$ without (green curve) and with (blue curve) photon recombination.

QCD and the weak × QCD corrections. Above the resonance, photonic × QCD corrections to the transverse-momentum distributions grow up to 2% and in case of weak × QCD up to 7%. However, we have to keep in mind that the weak × QCD corrections are calculated using the PA and it is therefore not reasonable to use them as an estimate of the full weak × QCD corrections far beyond the resonance region. Furthermore, we have normalized the corrections to the distributions to LO and as NLO QCD corrections to the transverse-momentum distribution of the final-state leptons induce corrections to the LO prediction of the order of 600% in the phase space region above the resonance (see e.g. Fig. 4.2 in [143]) a normalization to the NLO QCD correction (as we did for the $\mathcal{O}(N_f\alpha_s\alpha)$ corrections in Section 5.3.2) would reduce the corrections also in the off-shell region to the level of 1 percent.
In the class of considered corrections the photon present in the real–virtual and double-real photonic × QCD corrections is radiated off the initial state. Therefore, there is no collinear enhancement when the emitted photon is collinear to the final-state leptons leading to a small effect of photon recombination, i.e. we observe only a small difference between dressed and bare leptons in Fig. 6.4 and likewise in all distributions considered below.

The photonic × QCD double-real contributions involve diagrams with a gluon and a photon radiated off the initial state and the Z boson can recoil against both of these radiated particles leading to potentially large corrections also in the off-shell regions of transverse-momentum distributions. In contrast, in weak × QCD corrections the Z boson can recoil only against photonic initial-state radiation in the RV contribution. Therefore, naively one would expect the photonic × QCD corrections to dominate over the weak × QCD corrections. As shown in Fig. 6.4 this intuition is not reflected by the results as the corrections to the invariant-mass spectra (which are not sensitive to recoil effects) are actually dominated by the photonic × QCD corrections whereas the corrections to the transverse-momentum distributions of both the weak × QCD and the the photonic × QCD corrections

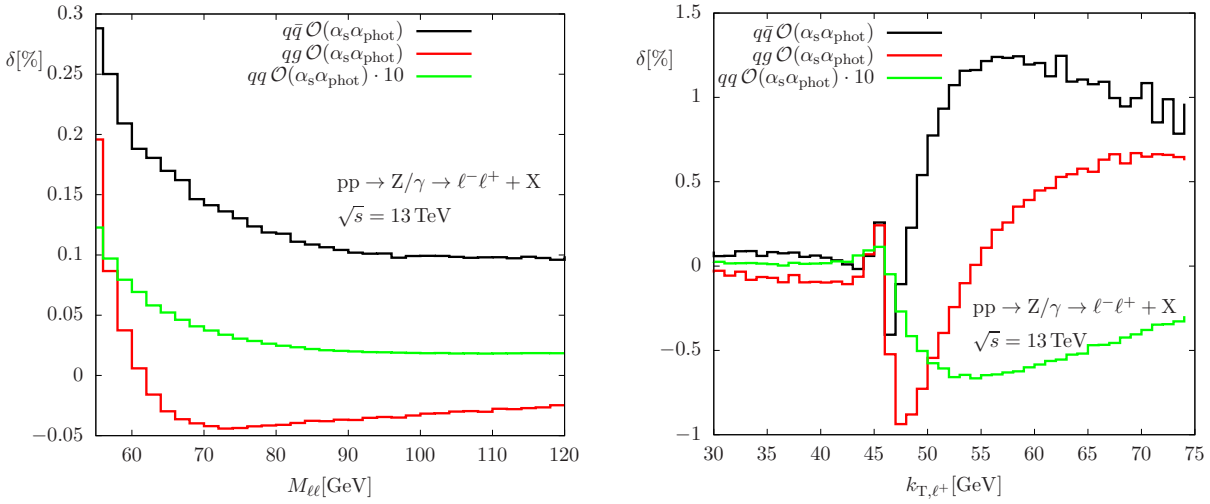

Figure 6.5: Relative initial–initial $\mathcal{O}(\alpha_s\alpha)$ corrections (normalized to the LO cross section) of type QCD × phot $\mathcal{O}(\alpha_s\alpha_p)$ to distributions in the invariant mass of the Z boson (left) and transverse-lepton momentum (right), split up into the three partonic initial states $qq/q\bar{q}/qg$ (green/black/red curve) for bare leptons and without recombination of photons.

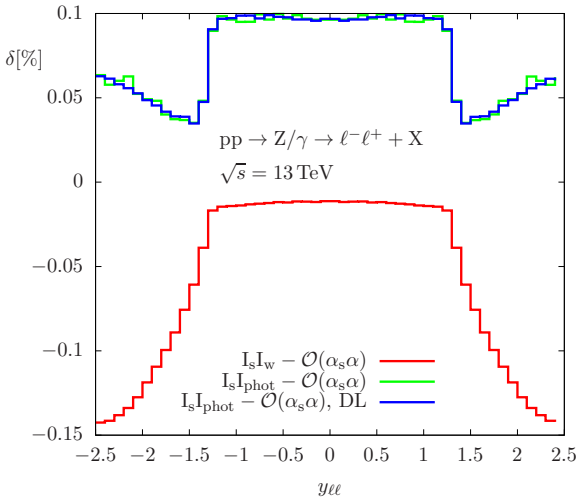

Figure 6.6: Relative initial–initial $\mathcal{O}(\alpha_s\alpha)$ corrections (normalized to the LO cross section) to the rapidity distribution of the lepton pair $\ell^+\ell^-$ with bare leptons represented by the green curve and dressed leptons (DL) in blue.

turn out to be of similar size above and in the vicinity of the resonance. In Fig. 6.5 we show the results for the photonic × QCD corrections broken down into the quark–gluon, the quark–antiquark, and the quark–quark-induced channels. We observe that the quark–quark-induced contribution is negligible compared to the quark–gluon or quark–antiquark induced channels. Furthermore, the quark–antiquark-induced channel contributes corrections to the invariant-mass distribution as well as the transverse-momentum distribution that are slightly larger than the the quark–gluon channel.
The relative corrections δ of type initial–initial $\mathcal{O}(\alpha_s\alpha)$ to the rapidity distribution of the final-state lepton pair $\ell^+\ell^-$ are depicted in Fig. 6.6. The corrections to the rapidity

distribution are of the subpermil level and are therefore phenomenologically negligible.

6.4.3 Corrections to the forward–backward asymmetry

The forward–backward asymmetry for $\ell^+\ell^-$ production at the LHC is defined as [18, 20]

$$A_{\mathrm{FB}}(M_{\ell\ell}) = \frac{\sigma_F(M_{\ell\ell}) - \sigma_B(M_{\ell\ell})}{\sigma_F(M_{\ell\ell}) + \sigma_B(M_{\ell\ell})} \tag{6.86}$$

with

$$\sigma_F(M_{\ell\ell}) = \int_0^1 \mathrm{d}\cos\theta^* \frac{\mathrm{d}\sigma}{\mathrm{d}\cos\theta^*}, \qquad \sigma_B(M_{\ell\ell}) = \int_{-1}^0 \mathrm{d}\cos\theta^* \frac{\mathrm{d}\sigma}{\mathrm{d}\cos\theta^*}. \tag{6.87}$$

The angle θ^* is the so-called Collins–Soper (CS) angle, which is defined as [18, 154]

$$\cos\theta^* = \frac{|p_{z,\ell\ell}|}{p_{z,\ell\ell}} \frac{2}{M_{\ell\ell}\sqrt{M_{\ell\ell}^2 + p_{\mathrm{T},\ell\ell}^2}} \Big(p^+(\ell^-)p^-(\ell^+) - p^+(\ell^+)p^-(\ell^-) \Big), \tag{6.88}$$

where

$$p^\pm = \frac{1}{\sqrt{2}}(E \pm p_z) \tag{6.89}$$

and all four-momenta are given in the LAB frame. Apart from Eq. (6.88) used to calculate the CS angle we also implemented an explicit Lorentz transformation to get the momenta of the incoming partons and the outgoing leptons in the CS frame and calculated the CS angle directly in this frame to check the results obtained with (6.88). For further details on the CS frame see App. G.

In Fig. 6.7 the LO prediction for the forward–backward asymmetry A_{FB} is compared to predictions for the forward–backward asymmetry including initial–initial $\mathcal{O}(\alpha_{\mathrm{s}}\alpha)$ corrections, where

$$A_{FB}^X = \frac{\sigma_F^{\mathrm{LO}} - \sigma_B^{\mathrm{LO}} + \sigma_F^X - \sigma_B^X}{\sigma_F^{\mathrm{LO}} + \sigma_B^{\mathrm{LO}} + \sigma_F^X + \sigma_B^X}. \tag{6.90}$$

As shown in Fig. 6.7 the impact of initial–initial $\mathcal{O}(\alpha_{\mathrm{s}}\alpha)$ corrections is quite small and therefore we mainly discuss the quantity

$$\Delta A_{FB}^X = A_{FB}^X - A_{FB}^{\mathrm{LO}}, \tag{6.91}$$

which directly shows the impact of corrections on the forward–backward asymmetry.

Figure 6.8 shows the corrections to the forward–backward asymmetry induced by QCD × photonic initial–initial corrections ($\Delta A_{\mathrm{FB}}^{I_{\mathrm{s}}I_{\mathrm{phot}}}$ in red) and corrections including QCD×weak initial–initial corrections ($\Delta A_{\mathrm{FB}}^{I_{\mathrm{s}}I_{\mathrm{w}}}$ in green). For invariant masses below the Z resonance the QCD × photonic corrections reach the percent level relative to the LO prediction for the forward–backward asymmetry whereas the QCD × weak corrections are at the level

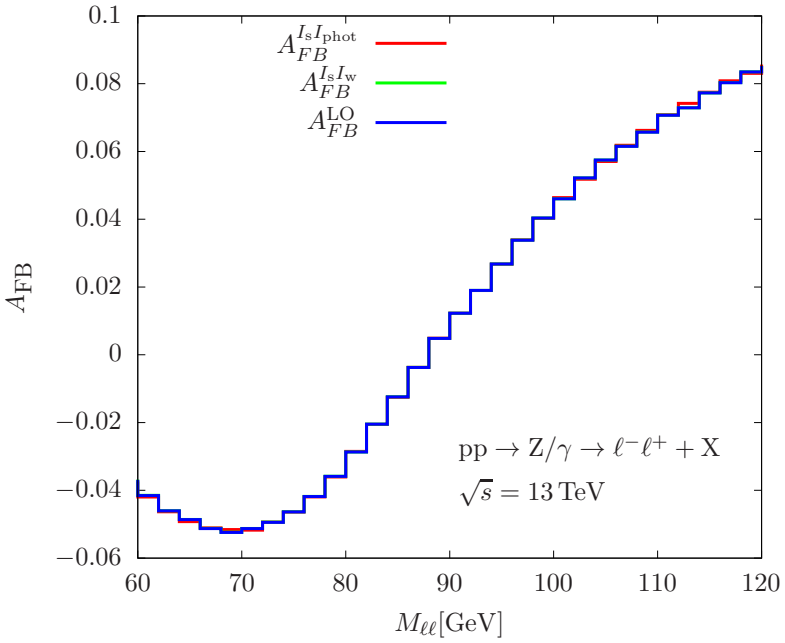

Figure 6.7: The Forward–backward asymmetry $A_{\rm FB}$ for $\ell^+\ell^-$ production at LO (blue), $A_{\rm FB}^{I_{\rm s}I_{\rm phot}}$ including QCD × photonic initial–initial corrections (red), and $A_{\rm FB}^{I_{\rm s}I_{\rm w}}$ including QCD × weak initial–initial corrections (green). The corrections to the LO prediction do not include photon recombination.

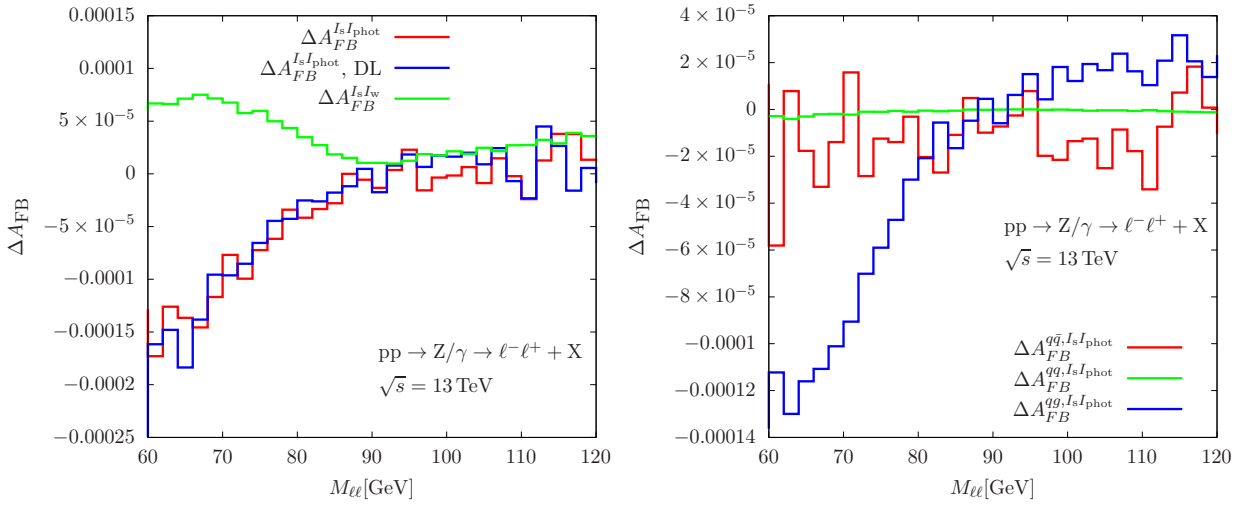

Figure 6.8: The left plot shows the corrected forward–backward asymmetry $\Delta A_{\rm FB}^{I_{\rm s}I_{\rm phot}}$ including QCD × photonic initial–initial corrections (red without and blue with photon recombination) and $\Delta A_{\rm FB}^{I_{\rm s}I_{\rm w}}$ including QCD × weak initial–initial corrections (green). In the right plot the different partonic channels $qq/q\bar{q}/qg$ (green/red/blue curve) are depicted for QCD × photonic corrections.

of a few permil over the full invariant-mass range of the final-state leptons. Recall that the QCD × photonic corrections are valid in the full invariant-mass range as the PA was only applied to the QCD × weak initial–initial corrections.
The left plot of Fig. 6.9 shows that there are cancellations between the $q\bar{q}$-induced double-

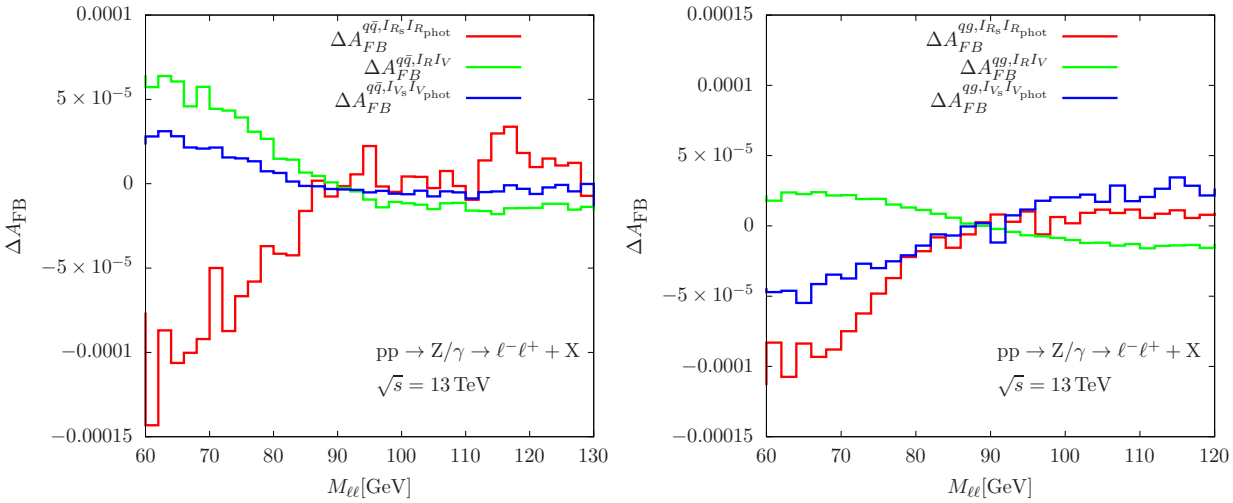

Figure 6.9: Double-real (red), real–virtual (green), and double-virtual (blue) QCD × photonic initial–initial corrections to the corrected forward–backward asymmetry $\Delta A_{\mathrm{FB}}^{I_{\mathrm{s}}I_{\mathrm{phot}}}$ for the $q\bar{q}$ (left) and the qg (right) initial states.

virtual, real–virtual, and double-real corrections using antenna subtraction whereas in the qg channel the double-real and double-virtual corrections amplify. Therefore, the qg channel is dominating the initial–initial $\mathcal{O}(\alpha_{\mathrm{s}}\alpha)$ correction as shown in the right plot in Fig. 6.8.

Even though the corrections to the forward–backward asymmetry induced by initial–initial $\mathcal{O}(\alpha_{\mathrm{s}}\alpha)$ corrections are rather small we have to keep in mind that for combined (e^+e^- and $\mu^+\mu^-$) A_{FB} measurements the absolute experimental uncertainties are of the order $\Delta A_{\mathrm{FB}}^{\ell,\mathrm{exp}} \approx 10^{-4}$ in the bin containing the Z resonance for certain rapidity cuts (see Table 2 in [155]). Furthermore, with the upcoming high luminosity (HL) LHC it will be possible to measure the forward–backward asymmetry A_{FB} even more precise and reduce the experimental uncertainty even further as the current total experimental error on A_{FB} is dominated by the statistical error [155]. Therefore, even though the initial–initial $\mathcal{O}(\alpha_{\mathrm{s}}\alpha)$ corrections to the forward–backward asymmetry are in the range $\Delta A_{\mathrm{FB}}^{II} \approx 10^{-5}$ to 10^{-4} they are still relevant for analyses at the upcoming HL LHC as already LHC data at $\sqrt{s} = 8\mathrm{TeV}$ reaches the mentioned accuracy of $\Delta A_{\mathrm{FB}}^{\ell,\mathrm{exp}} \approx 10^{-4}$, which will certainly improve at the HL LHC.

Chapter 7

Summary

The Drell–Yan-like production of lepton pairs is one of the most important standard-candle processes at the LHC. Among others, these processes provide the opportunity to gain insight on the mass and width of W bosons or allow for the search for new gauge bosons in the high invariant-mass range of the final-state leptons. Precision tests of the Standard Model using Drell–Yan processes are, however, only possible if the accuracy of theoretical predictions matches or even surpasses the precision of measurements. As searches of physics beyond the SM are performed in off-shell regions such as the tails of invariant-mass or transverse-momentum distributions the understanding of higher-order corrections in these regions of phase space is essential. Therefore, $\mathcal{O}(\alpha_s\alpha)$ corrections to Drell–Yan-like W/Z production have to be calculated not only in the resonance region of the intermediate massive vector bosons but also in off-shell regions where a PA is not applicable anymore.

This work consists of two main parts: We started with the discussion of the calculation of $\mathcal{O}(N_f\alpha_s\alpha)$ corrections to off-shell Drell–Yan processes as the first main part of this thesis. The second part was devoted to a discussion of $\mathcal{O}(\alpha_s\alpha)$ initial–initial corrections to Drell–Yan-like Z production in PA. The idea behind the slightly unconventional ordering of the two main parts is that the $\mathcal{O}(N_f\alpha_s\alpha)$ corrections contain vertex counterterm contributions which also have to be included in the calculation of the $\mathcal{O}(\alpha_s\alpha)$ initial–initial corrections.

As a first step towards a calculation of the complete set of $\mathcal{O}(\alpha_s\alpha)$ corrections to off-shell Drell–Yan processes the first part of this thesis was devoted to the calculation of the gauge-invariant $\mathcal{O}(N_f\alpha_s\alpha)$ two-loop corrections to single W/Z-boson production which are enhanced by the number of fermion flavours N_f in the SM. These corrections comprise all diagrams of $\mathcal{O}(\alpha_s\alpha)$ including closed fermion loops and additional gluon exchange or radiation. As $\mathcal{O}(N_f\alpha_s\alpha)$ corrections do not involve photon emission, the IR singularities are of one-loop complexity and therefore no two-loop subtraction schemes were needed to obtain predictions for differential distributions. However, to obtain a gauge-invariant description of the W/Z resonances in the vicinity of the resonance as well as in the off-shell regions we had to extend the complex-mass scheme to $\mathcal{O}(\alpha_s\alpha)$.
We evaluated corrections to single W/Z-boson production of $\mathcal{O}(N_f\alpha_s\alpha)$ in a differential manner and studied their effect on the (transverse) invariant-mass and transverse-momentum spectra of the W and Z boson, respectively. We observed that $\mathcal{O}(N_f\alpha_s\alpha)$

corrections to the integrated cross sections or rapidity distributions, which are dominated by resonant W/Z bosons, are at the permille level and thus phenomenologically negligible. The off-shell regions above the Jacobian peak of (transverse) invariant-mass distributions or the transverse-momentum distributions normalized to the LO prediction, however, receive corrections that grow up to 2% or up to 15%, respectively. As the LO prediction underestimates these distributions—higher-order corrections include initial-state radiation leading to recoil effects not present at LO, as discussed in Section 5.3.2—the size of those corrections reduces to a few percent when normalizing the distributions to full predictions. It is important to note that the impact of $\mathcal{O}(\alpha_s\alpha)$ corrections without N_f enhancement on the differential distributions are not smaller than corrections of $\mathcal{O}(N_f\alpha_s\alpha)$ as can be seen in [57,58]. At high energies NLO EW corrections are enhanced by Sudakov logarithms leading to large corrections of $\mathcal{O}(\alpha_s\alpha)$ without N_f enhancement also at NNLO.

In the vicinity of the resonance of a Drell–Yan-like produced Z boson it is possible to extract precision observables such as the effective weak mixing angle from the forward–backward asymmetry A_{FB} motivating the effort of calculating higher-order corrections valid in this region of phase space. In the second part of this thesis we have calculated $\mathcal{O}(\alpha_s\alpha)$ corrections of initial–initial type adding the final part to the previously calculated initial–final, final–final, and non-factorizable contributions [55,56] and therefore completing the PA at $\mathcal{O}(\alpha_s\alpha)$ for the neutral-current Drell–Yan process. We studied the impact of initial–initial $\mathcal{O}(\alpha_s\alpha)$ corrections on the forward–backward asymmetry A_{FB} in the resonance region of the Drell–Yan-like produced Z boson. To our best knowledge, there are no published results that study the effect of $\mathcal{O}(\alpha_s\alpha)$ corrections on the numerically challenging forward–backward asymmetry.
The so far missing gauge-invariant initial–initial $\mathcal{O}(\alpha_s\alpha)$ corrections in PA comprise contributions where the corrections are solely contained in the production mode of the Z boson and include genuine two-loop virtual–virtual corrections, real–virtual corrections, and double-real $\mathcal{O}(\alpha_s\alpha_{\text{phot}})$ corrections. The PA was only applied to the weak × QCD $\mathcal{O}(\alpha_s\alpha_w)$ corrections as these are only gauge invariant for on-shell Z bosons while the photonic × QCD $\mathcal{O}(\alpha_s\alpha_{\text{phot}})$ corrections are gauge invariant on their own without PA due to their proportionality to the charge of the initial-state quarks. The impact of the $\mathcal{O}(\alpha_s\alpha_{\text{phot}})$ corrections on the forward–backward asymmetry A_{FB} turned out to be of the order of one percent in the region below the resonance of the Z boson while corrections of $\mathcal{O}(\alpha_s\alpha_w)$ are of the level of a few permille over the whole invariant-mass range of the final-state leptons. Therefore, at least below the resonance of the Z boson the total $\mathcal{O}(\alpha_s\alpha)$ initial–initial correction to the forward–backward asymmetry is dominated by the $\mathcal{O}(\alpha_s\alpha_{\text{phot}})$ corrections. In the resonance region and above, the $\mathcal{O}(\alpha_s\alpha)$ initial–initial corrections to the forward–backward asymmetry are of the permille level.
As the photons are radiated off the initial state no collinear enhancement occurs when the emitted photon is collinear to the final-state leptons. Accordingly, we observed that the effect of photon recombination on the size of $\mathcal{O}(\alpha_s\alpha)$ initial–initial corrections to the various distributions we considered was negligible.
Apart from corrections to the forward–backward asymmetry we have studied the effect of the initial–initial $\mathcal{O}(\alpha_s\alpha)$ corrections on the transverse-momentum, the invariant-mass, and rapidity spectrum of the Z boson. While the corrections to the invariant mass and rapidity distribution of the Z boson are of the sub-permille level the $\mathcal{O}(\alpha_s\alpha_{\text{phot}})$ corrections

to transverse-lepton momentum distributions grow up to 2% above the resonance of the Z boson. In principle, we observed the $\mathcal{O}(\alpha_s\alpha_w)$ corrections to transverse-lepton momentum distributions to be even larger reaching up to 7%. However, as we used the PA to obtain a gauge-invariant prediction for the $\mathcal{O}(\alpha_s\alpha_w)$ initial–initial corrections, these predictions are not reliable far beyond the resonance region. In the vicinity of the resonance also the $\mathcal{O}(\alpha_s\alpha_w)$ initial–initial corrections to transverse-lepton momentum distributions were on the level of a few percent.

The numerical results presented in the previous chapters were obtained using a flexible Monte Carlo program that was fully developed in the scope of this work. It allows the calculation of corrections to arbitrary distributions induced by the discussed $\mathcal{O}(\alpha_s\alpha)$ corrections, by selected $\mathcal{O}(\alpha)$ corrections, and by the full NLO QCD $\mathcal{O}(\alpha_s)$ corrections. In particular the Monte Carlo program allows the prediction of corrections to the numerically challenging forward–backward asymmetry and also predictions for corrections to total cross sections.
In the future also the initial–initial $\mathcal{O}(\alpha_s\alpha)$ corrections to the charged-current Drell–Yan process should be calculated. It is expected that the impact of these corrections on the transverse-mass distribution of the W boson (and therefore also on the extraction of the W mass) is small compared to the impact of initial–final corrections. Nevertheless, this has to be checked in a dedicated calculation of the initial–initial corrections to charged-current processes. As $\mathcal{O}(\alpha_s\alpha_{phot})$ corrections to charged-current Drell–Yan processes involve diagrams including radiation of photons off W bosons an extension of the antenna subtraction formalism is needed.

Appendices

Appendix A

Conventions

A.1 Four-vectors

We write three-vectors in bold font (e.g. $\mathbf{p}$), four-vectors in italic font (e.g. p), and use the metric tensor

$$(g_{\mu\nu}) = (g^{\mu\nu}) = \mathrm{diag}(+1, -1, -1, -1). \tag{A.1}$$

Contravariant four-vectors are denoted with upper greek indices,

$$p^{\mu} = (p^0, \mathbf{p}), \tag{A.2}$$

whereas covariant four-vectors are denoted by lower indices

$$p_{\mu} = g_{\mu\nu} p^{\nu}. \tag{A.3}$$

The four-momentum of a particle with three-momentum $\mathbf{p}$

$$\mathbf{p} = (p^1, p^2, p^3)^T \tag{A.4}$$

and mass m is given by

$$p^{\mu} = (p^0, \mathbf{p})^T. \tag{A.5}$$

The zero component of the four-momentum p^{μ} is given by the energy of the particle and for a real particle fulfils the on-shell condition $p^2 = m^2$, with

$$p^0 = \sqrt{\mathbf{p}^2 + m^2} > 0, \tag{A.6}$$

where we introduced the scalar product between two four-vectors

$$p \cdot q = g_{\mu\nu} p^{\mu} q^{\nu} = p_{\nu} q^{\nu} = p^0 q^0 - \mathbf{pq}, \tag{A.7}$$

so that $p^2 = p_{\mu} p^{\mu}$. A four-vector p is called time-like if $p^2 > 0$, space-like if $p^2 < 0$, and light-like if $p^2 = 0$.

A.2 Dirac algebra in four dimensions

The defining relation of the Dirac algebra is given by,

$$\{\gamma^\mu, \gamma^\nu\} = \gamma^\mu\gamma^\nu + \gamma^\nu\gamma^\mu = 2g^{\mu\nu}, \tag{A.8}$$

and the gamma matrices are the generators of the Dirac algebra. In the chiral representation the gamma matrices are given by

$$\gamma^\mu = \begin{pmatrix} 0 & \bar{\sigma}^\mu \\ \sigma^\mu & 0 \end{pmatrix}, \qquad \sigma^\mu = (\sigma^0, \boldsymbol{\sigma}), \qquad \bar{\sigma}^\mu = (\sigma^0, -\boldsymbol{\sigma}), \tag{A.9}$$

where $\boldsymbol{\sigma} = (\sigma^1, \sigma^2, \sigma^3)$ is the vector of Pauli matrices,

$$\sigma^1 = \begin{pmatrix} 0 & 1 \\ 1 & 0 \end{pmatrix}, \qquad \sigma^2 = \begin{pmatrix} 0 & -\mathrm{i} \\ \mathrm{i} & 0 \end{pmatrix}, \qquad \sigma^3 = \begin{pmatrix} 1 & 0 \\ 0 & -1 \end{pmatrix}, \tag{A.10}$$

and σ^0 is the unit matrix. Moreover, we use the slashed notation for the contraction of gamma matrices with four-vectors,

$$\not{k} = k_\nu\gamma^\nu. \tag{A.11}$$

Furthermore, one can define a matrix which anti-commutes with all other gamma matrices given by,

$$\gamma_5 = -\frac{\mathrm{i}}{4!}\varepsilon_{\mu\nu\eta\rho}\gamma^\mu\gamma^\nu\gamma^\eta\gamma^\rho = \mathrm{i}\gamma^0\gamma^1\gamma^2\gamma^3, \tag{A.12}$$

which is used to define the left- and right-handed chirality projectors,

$$\omega_\pm = \frac{1}{2}\big(\mathbb{1} \pm \gamma_5\big). \tag{A.13}$$

In the chiral representation of the gamma matrices, γ_5 and the chiral projectors are given by

$$\gamma_5 = \begin{pmatrix} 1 & 0 \\ 0 & -1 \end{pmatrix}, \qquad \omega_+ = \begin{pmatrix} 1 & 0 \\ 0 & 0 \end{pmatrix}, \qquad \omega_- = \begin{pmatrix} 0 & 0 \\ 0 & 1 \end{pmatrix}. \tag{A.14}$$

A.3 The Weyl–van-der-Waerden formalism

All amplitudes in Chapter 5 and the real emission amplitudes in Chapter 6 were calculated using the Weyl–van-der-Waerden (WvdW) spinor formalism. In this section we therefore give a short overview over some basic ideas and definitions that are needed to calculate amplitudes involving massless external particles using the WvdW formalism. For a more complete presentation of the subject we refer to [153]. In the WvdW formalism all objects that belong to higher-dimensional representations of the Lorentz group are expressed in

terms of objects in the two-dimensional irreducible representations $D(\frac{1}{2},0)$ and $D(0,\frac{1}{2})$. The decomposition of all Lorentz structures into two-dimensional spinor objects allows the direct calculation of helicity amplitudes, i.e. the decomposition allows the numerical evaluation of helicity amplitudes. Therefore, also the squaring to obtain squared amplitudes can then be performed numerically. This is a clear advantage compared to the Dirac formalism where to obtain a expression for the squared amplitudes suitable for the implementation in a computer completeness relations for the external polarisation vectors and Dirac spinors have to be used.

The spinors that belong to the two fundamental two-dimensional representations $D(\frac{1}{2},0)$ and $D(0,\frac{1}{2})$ of the Lorentz group are denoted ψ_A and $\psi^{\dot{A}}$, respectively. The connection between the two representations is given by complex conjugation

$$\psi_{\dot{A}} = (\psi_A)^*, \qquad \psi^{\dot{A}} = (\psi^A)^*, \tag{A.15}$$

and lowering and raising of indices

$$\psi_A = \psi^B \epsilon_{BA} = (\psi^{\dot{B}})^* \epsilon_{BA}, \qquad \psi^{\dot{A}} = \epsilon^{\dot{A}\dot{B}} \psi_{\dot{B}} = \epsilon^{\dot{A}\dot{B}} (\psi_B)^*, \tag{A.16}$$

is achieved by contraction with the totally anti-symmetric tensor

$$\epsilon_{AB} = \epsilon_{\dot{A}\dot{B}} = \epsilon^{AB} = \epsilon^{\dot{A}\dot{B}} = \begin{pmatrix} 0 & 1 \\ -1 & 0 \end{pmatrix}. \tag{A.17}$$

The anti-symmetric tensor ϵ also allows the definition of a Lorentz-invariant spinor product

$$\langle \phi\psi \rangle = \phi_A \psi^A = \phi_A \epsilon^{AB} \psi_B = \phi_1\psi_2 - \phi_2\psi_1 = -\langle \psi\phi \rangle, \tag{A.18}$$

$$\langle \phi\psi \rangle^* = \phi_{\dot{A}} \psi^{\dot{A}} = \phi_{\dot{A}} \epsilon^{\dot{A}\dot{B}} \psi_{\dot{B}} = (\phi_1\psi_2 - \phi_2\psi_1)^* = -\langle \psi\phi \rangle^*. \tag{A.19}$$

For the spinor product we also use the notation

$$\langle \phi | \psi \rangle \equiv \langle \phi\psi \rangle. \tag{A.20}$$

Four-vectors and massless spin-1 particles

As four-vectors belong to the representation $D(\frac{1}{2},0) \otimes D(0,\frac{1}{2})$, they are represented by objects with two spinor indices in the WvdW formalism

$$K_{\dot{A}B} = k^\mu \sigma_{\mu,\dot{A}B} = \begin{pmatrix} k^0 + k^3 & k^1 + \mathrm{i}k^2 \\ k^1 - \mathrm{i}k^2 & k^0 - k^3 \end{pmatrix}, \qquad 2k_\mu p^\mu = K_{\dot{A}B} P^{\dot{A}B}, \tag{A.21}$$

where the transition matrices, used to obtain the representation of four-vectors in the spinor formalism, are given by the four-dimensional Pauli matrices

$$\sigma^{\mu,\dot{A}B} = (\sigma^0, \boldsymbol{\sigma}), \qquad \sigma^\mu_{A\dot{B}} = (\sigma^0, -\boldsymbol{\sigma}). \tag{A.22}$$

In case of massless particles, the matrix $K_{\dot{A}B}$ factorizes into a product of so-called momentum spinors

$$K_{\dot{A}B} = k_{\dot{A}} k_B, \qquad k_A = \sqrt{2k^0} \begin{pmatrix} e^{-i\phi} \cos\frac{\theta}{2} \\ \sin\frac{\theta}{2} \end{pmatrix}, \tag{A.23}$$

where we have used polar coordinates to express the momentum spinors

$$\mathbf{k} = |\mathbf{k}| \begin{pmatrix} \cos\phi \sin\theta \\ \sin\phi \sin\theta \\ \cos\theta \end{pmatrix}. \tag{A.24}$$

Moreover, in case the momenta are light-like, the contraction in (A.21) further simplifies to

$$2k_\mu p^\mu = |\langle pk \rangle|^2, \tag{A.25}$$

where in terms of polar coordinates the spinor product (A.18) of the momentum spinors is given by

$$\langle pk \rangle = 2\sqrt{p^0 k^0} \left(e^{-\mathrm{i}\phi_p} \cos\frac{\theta_p}{2} \sin\frac{\theta_k}{2} - e^{-\mathrm{i}\phi_k} \cos\frac{\theta_k}{2} \sin\frac{\theta_p}{2} \right). \tag{A.26}$$

As polarisation vectors $\varepsilon^\pm_\mu(k)$ for massless particles are also four-vectors their representation in the WvdW formalism is also given by objects with two spinor indices

$$\varepsilon_{+,\dot{A}B}(k) = \frac{\sqrt{2} g_{+,\dot{A}} k_B}{\langle g_+ k \rangle^*}, \qquad \varepsilon_{-,\dot{A}B}(k) = \frac{\sqrt{2} k_{\dot{A}} g_{-,B}}{\langle g_- k \rangle}, \tag{A.27}$$

$$\varepsilon^*_{+,\dot{A}B}(k) = \frac{\sqrt{2} k_{\dot{A}} g_{+,B}}{\langle g_+ k \rangle}, \qquad \varepsilon^*_{-,\dot{A}B}(k) = \frac{\sqrt{2} g_{-,\dot{A}} k_B}{\langle g_- k \rangle^*}, \tag{A.28}$$

where the appearance of gauge spinors $g_\pm$ is the manifestation of the missing longitudinal polarisation in the case of massless vector bosons. Apart from the condition $\langle g_\pm k \rangle \neq 0$, the gauge spinors are arbitrary and can be chosen differently for different helicity configurations within the same amplitudes.

Spin-$\frac{1}{2}$ particles

Dirac spinors Ψ are elements of the direct sum of $D(\frac{1}{2}, 0)$ and $D(0, \frac{1}{2})$, and can therefore be written in terms of two WvdW spinors as

$$\Psi = \begin{pmatrix} \phi_A \\ \psi^{\dot{A}} \end{pmatrix}. \tag{A.29}$$

Inserting the plane-wave ansatz $\Psi(x) = \exp(\mp \mathrm{i} kx) \Psi^{(\mp)}(k)$ into the Dirac equation for massless fermions $\mathrm{i}\partial\!\!\!/ \Psi(x) = 0$ leads to

$$K_{A\dot{B}} \psi^{(\pm),\dot{B}}(k) = 0, \qquad K^{\dot{A}B} \phi^{(\pm)}_B(k) = 0. \tag{A.30}$$

Helicity	Outgoing fermion	Incoming fermion
$\sigma = -$	$\overline{\Psi}^{+}_{k,-} = \begin{pmatrix} k^A & 0 \end{pmatrix}$	$\Psi^{+}_{k,-} = \begin{pmatrix} 0 \\ k^{\dot{A}} \end{pmatrix}$
$\sigma = +$	$\overline{\Psi}^{+}_{k,+} = \begin{pmatrix} 0 & k_{\dot{A}} \end{pmatrix}$	$\Psi^{+}_{k,+} = \begin{pmatrix} k_A \\ 0 \end{pmatrix}$
Helicity	Outgoing antifermion	Incoming antifermion
$\sigma = -$	$\Psi^{-}_{k,-} = \begin{pmatrix} k_A \\ 0 \end{pmatrix}$	$\overline{\Psi}^{-}_{k,-} = \begin{pmatrix} 0 & k_{\dot{A}} \end{pmatrix}$
$\sigma = +$	$\Psi^{-}_{k,+} = \begin{pmatrix} 0 \\ k^{\dot{A}} \end{pmatrix}$	$\overline{\Psi}^{-}_{k,+} = \begin{pmatrix} k^A & 0 \end{pmatrix}$

Table A.1: Helicity eigentstates for massless Dirac fermions.

The solutions to these equations are shown in Tab. A.1.

In the calculation of helicity amplitudes discrete symmetries like parity or the CP symmetry can be used to reduce the number of different helicity configurations that have to be calculated explicitly, as these symmetries relate different helicity configurations of the same process. Moreover, starting from a helicity amplitude where all helicity configurations are known, so-called crossing symmetries, which transform incoming into outgoing particles and vice versa, can be used to obtain helicity amplitudes of different processes. A summary and guideline of how these symmetries are to be used in an actual calculation can be found in [153].

A.4 Harmonic polylogarithms

In this section we give the definition of harmonic polylogarithms $\mathrm{H}(m_1, ..., m_w; y)$, $m_j = 0, \pm 1$ using the notation of [144]. The harmonic polylogarithms $\mathrm{H}(m; y)$ of lowest-weight ($w = 1$) are defined as

$$\mathrm{H}(0; y) \;=\; \ln y \;, \qquad \mathrm{H}(\pm 1; y) \;=\; \mp \ln(1 \mp y) \;. \tag{A.31}$$

Harmonic polylogarithms of higher-weight ($w \geq 2$) are recursively defined as

$$\mathrm{H}(m_1, ..., m_w; y) \;=\; \begin{cases} \dfrac{1}{w!} \ln^w y \;, & \text{if} \quad m_1, ..., m_w = 0 \\ \displaystyle\int_0^y dz \, f_{m_1}(z) \, \mathrm{H}(m_2, ..., m_w; z) \;, & \text{otherwise} \end{cases} \tag{A.32}$$

with

$$f_0(y) \;=\; \frac{1}{y} \;, \qquad f_{\pm 1}(y) \;=\; \frac{1}{1 \mp y} \;. \tag{A.33}$$

A.5 Scattering matrix, perturbation theory, and cross sections

A scattering process in quantum mechanics is described by the so-called "S-matrix", which transforms incoming states $|i\rangle$ entering a particle scattering into outgoing states $|f\rangle$. Technically the scattering is assumed to happen in a finite time interval. In the limit $t \to \infty$ the S-matrix coincides with the time evolution operator $U_I(t, -t)$ in the interaction picture. In cases where the interaction Hamiltonian density $\mathcal{H}_{\text{int}}$, contained in the time evolution operator $U_I(t, -t)$, is free of derivatives acting on fields one can write the S-matrix as

$$S = T\left[\exp\left(\mathrm{i}\int \mathrm{d}^4x \mathcal{L}_I\right)\right], \tag{A.34}$$

where T is the time ordering operator and we introduced the interaction Lagrangian $\mathcal{L}_I$ (in the interaction picture) obtained by decomposing the total Lagrangian into a free part $\mathcal{L}_0$, containing only bilinear terms of the fields, and the interaction Lagrangian $\mathcal{L}_I$,

$$\mathcal{L} = \mathcal{L}_0 + \mathcal{L}_I. \tag{A.35}$$

The Lehmann-Symanzik-Zimmermann (LSZ) reduction formula [156] relates S-matrix elements for scattering processes with n external particles and n-point correlation functions (Green functions), which can be evaluated perturbatively. The elements of the perturbative expansion of a Green function have a pictorial representation known as Feynman diagrams that are built from so-called "propagators" and "vertices". Propagators are represented by lines in Feynman diagrams and are derived from $\mathcal{L}_0$, whereas vertices, represented by dots joining three or more propagators, are derived from $\mathcal{L}_I$. The analytic expressions corresponding to propagators and vertices are the so-called "Feynman rules".

S-matrix elements can be decomposed into a sum of a part $\langle f|i\rangle$ describing the situation where no scattering occurs and the so-called "transition matrix element" (or equivalent "amplitude") $\mathcal{M}_{fi}$,

$$\langle f|S|i\rangle = \langle f|i\rangle + \mathrm{i}(2\pi)^3\delta^4(p_i - p_f)\mathcal{M}_{fi}. \tag{A.36}$$

The differential cross section of two unpolarized incoming particles with momenta q_1, q_2 and masses m_{q_1}, m_{q_2} and n particles in the final state with momenta $p_1, \ldots, p_n$ is given in terms of transition matrix elements by

$$\mathrm{d}\sigma(q_1, q_2, p_1, \ldots, p_n) = \frac{1}{S}\frac{1}{F(q_1, q_2)}\mathrm{d}\Phi_n(q_1, q_2, p_1, \ldots, p_n)\langle|\mathcal{M}_{ab\to f}(q_1, q_2, p_1, \ldots, p_n)|^2\rangle, \tag{A.37}$$

where we denote the squared amplitude of the process summed over all possible helicity states of particles in the final state and spin averaged over the initial states by $\langle|\mathcal{M}_{ab\to f}(q_1, q_2, p_1, \ldots, p_n)|^2\rangle$. To avoid double counting due to identical particles of type f in the final state the symmetry factor

$$S = n_f! \tag{A.38}$$

is introduced for each particle species f and the Lorentz-invariant flux factor is given by

$$F(q_1, q_2) = \sqrt{(q_1 q_2)^2 - (m_{q_1} m_{q_2})^2}. \tag{A.39}$$

For processes including two incoming particles with momenta q_1, q_2 and n particles in the final state with momenta $p_1, \ldots, p_n$ the differential phase space $\mathrm{d}\Phi_n$ f is given by

$$\mathrm{d}\Phi_n(q_1, q_2, p_1, \ldots, p_n) = (2\pi)^4 \delta^{(4)}\Big(q_1 + q_2 - \sum_{i=1}^{n} p_i\Big) \prod_{j=1}^{n} \frac{\mathrm{d}^4 p_j}{(2\pi)^4} \delta(p_j^2 - m_j^2)\theta(p_j^0). \tag{A.40}$$

In situations with only one incoming particle (i.e. in case of a particle decay) Eq. (A.37) simplifies to

$$\mathrm{d}\Gamma_{X\to f} = \frac{1}{S}\frac{1}{2m_x}\mathrm{d}\Phi_n(Q, p_1, \ldots, p_n)\langle|\mathcal{M}_{X\to f}|^2\rangle, \tag{A.41}$$

where Q is the momentum of the decaying particle and $\mathrm{d}\Gamma_{X\to f}$ denotes the differential decay width.

Appendix B

Hadron collider kinematics

We define the hadronic momenta with respect to the beam axis in the laboratory (lab) frame as

$$P_A = \frac{\sqrt{s}}{2}\begin{pmatrix}1\\0\\0\\1\end{pmatrix}, \qquad P_B = \frac{\sqrt{s}}{2}\begin{pmatrix}1\\0\\0\\-1\end{pmatrix}, \tag{B.1}$$

where $\sqrt{s}$ is the hadronic centre-of-mass (CM) energy. If parton a carries the momentum fraction x_a of the momentum of hadron A and b analogously the fraction x_b of the momentum of B, the momenta of the partons are given by

$$p_a = x_a\frac{\sqrt{s}}{2}\begin{pmatrix}1\\0\\0\\1\end{pmatrix}, \qquad p_b = x_b\frac{\sqrt{s}}{2}\begin{pmatrix}1\\0\\0\\-1\end{pmatrix}. \tag{B.2}$$

The Lorentz transformation that relates the momenta in the lab frame with the momenta in the partonic CM system reads

$$\begin{pmatrix}\hat{p}_i^0\\\hat{p}_i^1\\\hat{p}_i^2\\\hat{p}_i^3\end{pmatrix} = \begin{pmatrix}\gamma & 0 & 0 & -\gamma\beta\\0 & 1 & 0 & 0\\0 & 0 & 1 & 0\\-\gamma\beta & 0 & 0 & \gamma\end{pmatrix}\begin{pmatrix}p_i^0\\p_i^1\\p_i^2\\p_i^3\end{pmatrix} \tag{B.3}$$

where $i = a, b$ and the boost factor β, describing the relative velocity of the two colliding partons, is given by

$$\beta = \frac{|\mathbf{p}_{ab}|}{E_{ab}} = \frac{|x_a\mathbf{P}_A + x_b\mathbf{P}_B|}{x_aP_A^0 + x_bP_B^0} = \frac{x_a - x_b}{x_a + x_b} \tag{B.4}$$

and

$$\gamma = \frac{1}{\sqrt{1-\beta^2}}. \tag{B.5}$$

By defining the rapidity y via $\gamma = \cosh(y)$ and using $\beta = -\tanh(y)$ we can rewrite (B.3) as

$$\begin{pmatrix} \hat{p}^0 \\ \hat{p}^1 \\ \hat{p}^2 \\ \hat{p}^3 \end{pmatrix} = \underbrace{\begin{pmatrix} \cosh y & 0 & 0 & \sinh y \\ 0 & 1 & 0 & 0 \\ 0 & 0 & 1 & 0 \\ \sinh y & 0 & 0 & \cosh y \end{pmatrix}}_{\equiv B(y)} \begin{pmatrix} p^0 \\ p^1 \\ p^2 \\ p^3 \end{pmatrix}. \tag{B.6}$$

If we consider the four momentum $p^\mu = (m, 0, 0, 0)^{\mathrm{T}}$ of some massive particle with mass m in its rest frame and apply a boost in the longitudinal direction we obtain

$$\hat{p}^\mu = (m \cosh y, 0, 0, m \sinh y)^{\mathrm{T}} = B(y)^\mu_\nu \; p^\nu, \tag{B.7}$$

which can be used to write the rapidity in the more familiar form [157]

$$y = \frac{1}{2} \log \frac{e^y}{e^{-y}} = \frac{1}{2} \log \frac{\cosh y + \sinh y}{\cosh y - \sinh y} = \frac{1}{2} \log \frac{\hat{p}^0 + \hat{p}^3}{\hat{p}^0 - \hat{p}^3}. \tag{B.8}$$

We now show that the two parameters x_a, x_b can be obtained from the rapidity and the partonic center-of-mass energy $\hat{s} = x_a x_b s$, which has been used to obtain (5.9). Starting from $\beta = -\tanh(y)$, using $\sinh(y)^2 = \cosh(y)^2 - 1$, and (B.4) we obtain

$$\frac{\cosh(y)^2 - 1}{\cosh(y)^2} = \beta^2 = \frac{(x_a - x_b)^2}{(x_a + x_b)^2}. \tag{B.9}$$

Solving this equation for $\cosh(y)$ we arrive at

$$\cosh y = \frac{x_a + x_b}{2\sqrt{x_a x_b}} = \frac{1}{2} \left(\sqrt{\frac{x_a}{x_b}} + \sqrt{\frac{x_b}{x_a}} \right). \tag{B.10}$$

If we now use $\cosh y = \frac{1}{2}(e^y + e^{-y})$ we find

$$e^y = \sqrt{\frac{x_a}{x_b}}, \tag{B.11}$$

which, in combination with $\hat{s} = x_a x_b s$, leads us to

$$x_a = \sqrt{\frac{\hat{s}}{s}} e^y, \qquad\qquad x_b = \sqrt{\frac{\hat{s}}{s}} e^{-y}. \tag{B.12}$$

Further, we define the transverse energy of a particle with mass m, four-momentum p, and transverse momentum $\mathbf{p}_{\mathrm{T}}$ as

$$E_{\mathrm{T}}^2 = m^2 + (\mathbf{p}_{\mathrm{T}})^2. \tag{B.13}$$

The transverse mass of the two particles ℓ and ν is then given by

$$M_{\mathrm{T},\ell\nu}^2 = (E_{\mathrm{T},\ell} + E_{\mathrm{T},\nu})^2 - (\mathbf{p}_{\mathrm{T},\ell} + \mathbf{p}_{\mathrm{T},\nu})^2. \tag{B.14}$$

If we consider that neutrinos only show up as missing transverse energy in a measurement at the LHC, i.e. $E_{\mathrm{T},\nu} = E_{\mathrm{T,miss}}$, and assuming massless leptons this reduces to

$$\begin{aligned} M_{\mathrm{T},\ell\nu} =& \sqrt{2(p_{\mathrm{T},\ell} E_{\mathrm{T,miss}} - \mathbf{p}_{\mathrm{T},\ell} \cdot \mathbf{p}_{\mathrm{T,miss}})} \\ =& \sqrt{2 p_{\mathrm{T},\ell} E_{\mathrm{T,miss}} (1 - \cos\phi_{\ell\nu})}, \end{aligned} \tag{B.15}$$

where $\phi_{\ell\nu}$ is the angle between the missing momentum in the transverse plane and the lepton ℓ.

B.1 Kinematics of the Drell–Yan process at leading order

In this section we will discuss some rather simple kinematics of the LO Drell–Yan process that are, however, quite useful when it comes to understanding distributions of observables, e.g. in Section 5.3.2. In particular, we focus on the transverse-momentum distribution and try to find out what we know about the momentum of the intermediate W/Z boson if we measure a certain transverse momentum of the positively charged lepton. In the following we only consider the NC Drell–Yan process, but the discussion is completely analogous in the CC case.

Lets start by just writing down the equation implied by four-momentum conservation in the Lab-frame

$$p_a^{\mathrm{lab}} + p_b^{\mathrm{lab}} = p_{\mathrm{Z}}^{\mathrm{lab}} = p_{\ell^-}^{\mathrm{lab}} + p_{\ell^+}^{\mathrm{lab}}. \tag{B.16}$$

From momentum conservation combined with (B.2) it immediately follows that $\mathbf{p}_{\mathrm{T},\ell^+}^{\mathrm{lab}} = -\mathbf{p}_{\mathrm{T},\ell^-}^{\mathrm{lab}}$. We split our discussion in three different cases, where in the first case we assume that we measured $p_{\mathrm{T},\ell^+}^{\mathrm{lab}} > M_{\mathrm{Z}}/2$, in the second $p_{\mathrm{T},\ell^+}^{\mathrm{lab}} = M_{\mathrm{Z}}/2$, and in the last case $p_{\mathrm{T},\ell^+}^{\mathrm{lab}} < M_{\mathrm{Z}}/2$.

$\underline{p_{\mathrm{T},\ell^+}^{\mathrm{lab}} > M_{\mathrm{Z}}/2:}$

According to (B.16) and (B.2) the rest frame (RF) and the Lab frame are connected by a simple boost in the longitudinal (beam) direction (B.3), as $\mathbf{p}_{\mathrm{T,Z}}^{\mathrm{lab}} = 0$. This means that transverse components of four-momenta are invariant under boosts between the RF of the Z boson and the Lab frame, i.e.

$$p_{\mathrm{T},\ell^\pm}^{\mathrm{RF}} = p_{\mathrm{T},\ell^\pm}^{\mathrm{lab}} > \frac{M_{\mathrm{Z}}}{2}. \tag{B.17}$$

Therefore, for the positively charged lepton—which we assume to be massless—in the RF of the Z boson we have

$$0 = (p_{\ell^\pm}^{\mathrm{RF}})^2 = (p_{\ell^\pm,0}^{\mathrm{RF}})^2 - \underbrace{(\mathbf{p}_{\mathrm{T},\ell^\pm}^{\mathrm{RF}})^2}_{>M_{\mathrm{Z}}^2/4} - (p_{\ell^\pm,3}^{\mathrm{RF}})^2 < (p_{\ell^\pm,0}^{\mathrm{RF}})^2 - M_{\mathrm{Z}}^2/4, \tag{B.18}$$

which implies

$$p^{\mathrm{RF}}_{\ell^\pm,0} > M_{\mathrm{Z}}/2. \tag{B.19}$$

Combined with energy conservation in the RF of the Z boson one obtains

$$p^{\mathrm{RF}}_{\mathrm{Z},0} = p^{\mathrm{RF}}_{\ell^+,0} + p^{\mathrm{RF}}_{\ell^-,0} > M_{\mathrm{Z}}, \tag{B.20}$$

which leads to the conclusion that the Z boson must be off-shell for $p^{\mathrm{lab}}_{\mathrm{T},\ell^+} > M_{\mathrm{Z}}/2$

$$(p^{\mathrm{RF}}_{\mathrm{Z}})^2 = (p^{\mathrm{RF}}_{\mathrm{Z},0})^2 > M^2_{\mathrm{Z}}. \tag{B.21}$$

$\underline{p^{\mathrm{lab}}_{\mathrm{T},\ell^+} = M_{\mathrm{Z}}/2:}$

As discussed before, the boost between Lab and rest frame does not change transversal components, i.e. $p^{\mathrm{RF}}_{\mathrm{T},\ell^\pm} = M_{\mathrm{Z}}/2$. On-shellness of the leptons implies

$$0 = (p^{\mathrm{RF}}_{\ell^\pm})^2 = (p^{\mathrm{RF}}_{\ell^\pm,0})^2 - M^2_{\mathrm{Z}}/4 - (p^{\mathrm{RF}}_{\ell^\pm,3})^2. \tag{B.22}$$

Solving for the energy of the leptons

$$p^{\mathrm{RF}}_{\ell^\pm,0} = \sqrt{\frac{M^2_{\mathrm{Z}}}{4} + (p^{\mathrm{RF}}_{\ell^\pm,3})^2} \tag{B.23}$$

we obtain that, given we have $p^{\mathrm{lab}}_{\mathrm{T},\ell^+} = M_{\mathrm{Z}}/2$, then

$$(p^{\mathrm{RF}}_{\mathrm{Z},0})^2 = (p^{\mathrm{RF}}_{\ell^+,0} + p^{\mathrm{RF}}_{\ell^-,0})^2 = M^2_{\mathrm{Z}} \qquad \text{iff} \qquad p^{\mathrm{RF}}_{\ell^\pm,3} = 0. \tag{B.24}$$

Therefore, the Z boson can be on-shell if the longitudinal components of the four-momenta of the leptons vanishes in the RF of the Z boson.

$\underline{p^{\mathrm{lab}}_{\mathrm{T},\ell^+} < M_{\mathrm{Z}}/2:}$

Following the same strategy as before, leads to

$$0 = (p^{\mathrm{RF}}_{\ell^\pm})^2 > (p^{\mathrm{RF}}_{\ell^\pm,0})^2 - M^2_{\mathrm{Z}}/4 - (p^{\mathrm{RF}}_{\ell^\pm,3})^2, \tag{B.25}$$

which implies

$$p^{\mathrm{RF}}_{\ell^\pm,0} < \sqrt{\frac{M^2_{\mathrm{Z}}}{4} + (p^{\mathrm{RF}}_{\ell^\pm,3})^2}. \tag{B.26}$$

This means, that the Z boson can still be on-shell for some non-vanishing $p^{\mathrm{RF}}_{\ell^\pm,3}$, since

$$(p^{\mathrm{RF}}_{\mathrm{Z}})^2 = (p^{\mathrm{RF}}_{\mathrm{Z},0})^2 = (p^{\mathrm{RF}}_{\ell^+,0} + p^{\mathrm{RF}}_{\ell^-,0})^2 \overset{!}{=} M^2_{\mathrm{Z}} \tag{B.27}$$

has to be fulfilled for the Z boson to be on-shell.

B.2 Jet recoil effects in initial-state radiation processes

In the discussion in the last section we saw that the region $p_{\mathrm{T},\ell^+}^{\mathrm{lab}} \leq M_{\mathrm{Z}}/2$ allows for on-shell Z bosons, but $p_{\mathrm{T},\ell^+}^{\mathrm{lab}} > M_{\mathrm{Z}}/2$ does not include on-shell kinematics. This changes when we consider the DY process at NLO and include contributions with initial-state radiation of photons or jets, e.g. the diagrams depicted in Fig. 5.4. Lets assume again that we have measured the momentum of some positively charged lepton with $p_{\mathrm{T},\ell^+}^{\mathrm{lab}} > M_{\mathrm{Z}}/2$. Including for instance an additional gluon with momentum k_g radiated in the initial state, momentum conservation is now given by

$$p_a^{\mathrm{lab}} + p_b^{\mathrm{lab}} = p_{\mathrm{Z}}^{\mathrm{lab}} + k_g = p_{\ell^-}^{\mathrm{lab}} + p_{\ell^+}^{\mathrm{lab}} + k_g. \tag{B.28}$$

At LO we had $\mathbf{p}_{\mathrm{T},\ell^+}^{\mathrm{lab}} = -\mathbf{p}_{\mathrm{T},\ell^-}^{\mathrm{lab}}$, which is not valid anymore if we include initial-state radiation. According to the last equation and (B.2) the transverse component of the four-momentum of the gluon and the Z boson have to cancel in the lab frame. This means, that for a non-vanishing transverse momentum of the gluon in the lab frame, a simple boost in longitudinal directions is not sufficient to get from the lab frame to the RF of the Z boson, as in the RF we should have $p_{\mathrm{T,Z}}^{\mathrm{RF}} = 0$ but in the lab frame $p_{\mathrm{T,Z}}^{\mathrm{lab}} \neq 0$. Therefore, the Lorentz transformation that connects the RF of the Z boson and the lab frame $B_{\mathrm{lab}\to\mathrm{RF}}$ contains a boost in the transverse direction.

Let now $\mathbf{p}_{\mathrm{T},\ell^+}^{\mathrm{RF}}$ be the transverse component of the four-momentum of the positively charged lepton in the RF of the Z boson,

$$\mathbf{p}_{\mathrm{T},\ell^+}^{\mathrm{RF}} = B_{\mathrm{lab}\to\mathrm{RF}}\, \mathbf{p}_{\mathrm{T},\ell^+}^{\mathrm{lab}} \neq \mathbf{p}_{\mathrm{T},\ell^+}^{\mathrm{lab}}. \tag{B.29}$$

Even though $p_{\mathrm{T},\ell^+}^{\mathrm{lab}} > M_{\mathrm{Z}}/2$ the energy of the lepton

$$p_{\ell^\pm,0}^{\mathrm{RF}} = \sqrt{(\mathbf{p}_{\mathrm{T},\ell^\pm}^{\mathrm{RF}})^2 + (p_{\ell^\pm,3}^{\mathrm{RF}})^2} \tag{B.30}$$

can still fulfill the condition (B.27) for the on-shellness of the Z boson in its RF, as boosting from the lab frame to the RF of the Z boson might reduce the size of the transverse components of the leptons four-momenta such that $p_{\mathrm{T},\ell^+}^{\mathrm{RV}} \leq M_{\mathrm{Z}}/2$.

Appendix C

Dimensional regularization

Dimensional regularization [70, 71] is a procedure which relates divergences in loop integrals to finite expressions by analytic continuation in the dimension of space-time to $d \neq 4$ dimensions,

$$\int \frac{\mathrm{d}^4 k}{(2\pi)^4} \to \int \frac{\mathrm{d}^d k}{(2\pi)^d}, \tag{C.1}$$

where the limit $d \to 4$ reproduces the original divergences. After the application of this regularization procedure, loop integrals become meromorphic functions of d. In this work we use the conventional dimensional regurlarization (CDR) scheme [158], where all momenta, four-vectors, and Lorentz covariants that appear in a divergent integral are analytically continued to d dimensions. In order to keep coupling constants dimensionless an arbitrary mass scale μ is introduced,

$$g_s \to \mu^{\frac{4-d}{2}} g_s, \qquad e \to \mu^{\frac{4-d}{2}} e. \tag{C.2}$$

In d dimensions the four Dirac matrices are replaced by d generators of the Dirac algebra of dimensionality $2^{\frac{d}{2}}$. The naive continuation of the vanishing anticommutator of γ-matrices and γ_5 in four dimensions,

$$\{\gamma_\mu, \gamma_5\} = 0, \tag{C.3}$$

to d dimensions and also maintaining cyclicity of the trace would lead to [159, 160]

$$\mathrm{Tr}(\gamma^\mu \gamma^\nu \gamma^\rho \gamma^\sigma \gamma_5) = 0, \tag{C.4}$$

where the trace function is defined in such a way that the application to the unit matrix in d dimensions is still four as in 4 dimensions, i.e. in d dimensions we have

$$g_{\mu\nu} = \mathrm{diag}(1, -1, \ldots, -1), \qquad \{\gamma^\mu, \gamma^\nu\} = 2g^{\mu\nu} \mathbb{1}_d, \qquad \mathrm{Tr}(\mathbb{1}_d) = 4. \tag{C.5}$$

Equation (C.4) is inconsistent with the relation in four dimension

$$\mathrm{Tr}(\gamma^\mu \gamma^\nu \gamma^\rho \gamma^\sigma \gamma_5) = 4\mathrm{i}\varepsilon^{\mu\nu\rho\sigma}, \tag{C.6}$$

which is the reason why the treatment of γ_5 in dimensional regularization is quite complicated and several different schemes differing in the properties of γ_5 and the trace operator in d dimensions are proposed in the literature [70, 160–163]. For an overview of the different schemes see e.g. [60].

As we use the FeynArts/FormCalc packages to calculated one-loop amplitudes we mention for completeness that FeynArts/FormCalc uses the so-called naive scheme [163] where γ_5 is assumed to be anticommuting with all γ^μ in d dimensions,

$$\{\gamma_5, \gamma_\mu\} = 0, \quad \mu = 0, 1, \ldots, d-1. \tag{C.7}$$

This scheme is consistent at the one-loop level [60].

C.1 Traces and γ_5 in initial–initial $\mathcal{O}(\alpha_s\alpha_w)$ corrections

We start the discussion by considering first only corrections of $\mathcal{O}(N_f\alpha_s\alpha)$. As discussed in Section 5.2.1 these corrections always involve closed fermionic loops that show up only in gauge-boson self-energies. Typically, projectors are used to reduce the calculation of the self-energies to the calculation of their longitudinal and transversal parts [118]. Due to the simple Lorentz structure of these self-energies the projectors only contain terms that are proportional to the metric tensor g_{μ_1,μ_2}, $\mu_i \in \{\mu, \nu, \rho, \sigma\}$, or to $p_{\mu_1}p_{\mu_2}$, where p_μ denotes the external momentum that flows in and out of the self-energy diagram. Therefore, traces of the form $\mathrm{Tr}(\gamma^\mu\gamma^\nu\gamma^\rho\gamma^\sigma\gamma_5)$—that might show up in the calculation of the self-energy diagrams—are always contracted either with the metric tensor g_{μ_1,μ_2}, $\mu_i \in \{\mu, \nu, \rho, \sigma\}$, or with $p_{\mu_1}p_{\mu_2}$. Both the contraction between the problematic trace term and the metric tensor g_{μ_1,μ_2} and also the contraction of the traces with $p_{\mu_1}p_{\mu_2}$ vanish. Therefore, traces of the form $\mathrm{Tr}(\gamma^\mu\gamma^\nu\gamma^\rho\gamma^\sigma\gamma_5)$ do not contribute to the calculation of $\mathcal{O}(N_f\alpha_s\alpha)$ corrections as there are not enough external momenta to produce non-vanishing contributions.

Throughout this work the guiding principle in the treatment of γ_5 was to combine UV- or IR-divergent terms in such a way that their combination is free of UV or IR divergences before calculating traces that include γ_5. If we now consider $\mathcal{O}(\alpha_s\alpha_w)$ corrections that do not involve closed fermionic loops in gauge-boson self-energies (these contributions have been discussed above), then there are no sources for traces of the form $\mathrm{Tr}(\gamma^\mu\gamma^\nu\gamma^\rho\gamma^\sigma\gamma_5)$ on the amplitude level. Therefore, in $\mathcal{O}(\alpha_s\alpha_w)$ corrections these traces are typically coming from closed fermionic loops that are produced in the interference of amplitudes contributing to squared matrix elements. By constructing combinations which are free of divergences before evaluating problematic traces we are able to evaluate these combinations in four dimensions. In four dimensions we can use all the usual properties of the trace (cyclicity and (C.6)) and the problem of continuing the definition of the trace to d dimensions is avoided. As an example we now show how we can rearrange terms in the calculation of the double-virtual initial–initial QCD × weak $\mathcal{O}(\alpha_s\alpha_w)$ corrections to obtain IR- and UV-finite combinations. The individual contributions to this set of $\mathcal{O}(\alpha_s\alpha_w)$ corrections and their calculation is discussed in Section 6.3.1. A similar procedure can be applied to the real–virtual $\mathcal{O}(\alpha_s\alpha_w)$ corrections discussed in Section 6.3.2.

In the calculation of the $\mathcal{O}(\alpha_s\alpha_w)$ correction to the $q\bar{q} \to \ell\bar{\ell}$ squared amplitude (6.12) we

used the renormalized $\mathcal{O}(\alpha_s\alpha_w)$ formfactor (6.11). The correction to the squared amplitude $M^{q\bar{q}\to\ell\bar{\ell}}_{V_s\otimes V_w,\mathrm{II,PA}}$ is therefore free of UV divergences and only contains IR divergences. In order to isolate these IR divergences we write $M^{q\bar{q}\to\ell\bar{\ell}}_{V_s\otimes V_w,\mathrm{II,PA}}$ as

$$\begin{aligned} M^{q\bar{q}\to\ell\bar{\ell}}_{V_s\otimes V_w,\mathrm{II,PA}}\Big|_{\text{IR div.}} &= 2\mathrm{Re}\Big\{\mathcal{M}^{q\bar{q}\to\ell\bar{\ell}}_{V_s\otimes V_w,\mathrm{II,PA}}\left(\mathcal{M}^{q\bar{q}\to\ell\bar{\ell}}_{\mathrm{LO},Z}\right)^*\Big\}\Big|_{\text{IR div.}} \\ &\quad + 2\mathrm{Re}\Big\{\mathcal{M}^{q\bar{q}\to\ell\bar{\ell}}_{V_w,\mathrm{I,PA}}\left(\mathcal{M}^{q\bar{q}\to\ell\bar{\ell}}_{V_s,\mathrm{I,PA}}\right)^*\Big\}\Big|_{\text{IR div.}} \\ &\quad + \text{IR- and UV-finite terms} \\ &= 2\mathrm{Re}\{\delta^{Z\bar{q}q}_{V_s}(q^2)\}\times\underbrace{2\mathrm{Re}\Big\{\mathcal{M}^{q\bar{q}\to\ell\bar{\ell}}_{V_w,\mathrm{I,PA}}\left(\mathcal{M}^{q\bar{q}\to\ell\bar{\ell}}_{\mathrm{LO},Z}\right)^*\Big\}}_{\text{IR and UV finite}} \\ &\quad + \text{IR- and UV-finite terms.} \end{aligned} \tag{C.8}$$

It is important to note that interference products as $\mathcal{M}^{q\bar{q}\to\ell\bar{\ell}}_{V_s,\mathrm{I,PA}}\left(\mathcal{M}^{q\bar{q}\to\ell\bar{\ell}}_{V_w,\mathrm{I,PA}}\right)^*$ already contain closed fermionic loops that lead to problematic traces including γ_5. Therefore, we do not evaluate these traces as long as we haven't canceled all IR divergences and are still in $d\neq 4$ dimensions to regularize these divergences. If we do not evaluate these traces we also do not need a prescription of how to evaluate them in $d\neq 4$ dimensions.
The IR divergences in (C.8) are canceled by the integrated subtraction term (6.24), where the sum is schematically given by

$$\begin{aligned} &M^{q\bar{q}\to\ell\bar{\ell}}_{V_s\otimes V_w,\mathrm{II,PA}}\Big|_{\text{IR div.}} - \boldsymbol{\mathcal{J}}^{(1)}_{2,ii}(z_a,z_b)\,2\mathrm{Re}\Big\{\mathcal{M}^{q\bar{q}\to\ell\bar{\ell}}_{V_w,\mathrm{I,PA}}\left(\mathcal{M}^{q\bar{q}\to\ell\bar{\ell}}_{\mathrm{LO},Z}\right)^*\Big\} \\ &= \underbrace{\left(2\mathrm{Re}\{\delta^{Z\bar{q}q}_{V_s}(q^2)\} - \boldsymbol{\mathcal{J}}^{(1)}_{2,ii}(z_a,z_b)\right)}_{\text{IR and UV finite}}\times\underbrace{2\mathrm{Re}\Big\{\mathcal{M}^{q\bar{q}\to\ell\bar{\ell}}_{V_w,\mathrm{I,PA}}\left(\mathcal{M}^{q\bar{q}\to\ell\bar{\ell}}_{\mathrm{LO},Z}\right)^*\Big\}}_{\text{IR and UV finite}} \\ &\quad + \text{IR- and UV-finite terms.} \end{aligned} \tag{C.9}$$

We have now combined terms so that all UV and IR divergences are canceled. Therefore, at this point we can omit dimensional regularization and set $d=4$ such that the problematic trace contained in $\mathcal{M}^{q\bar{q}\to\ell\bar{\ell}}_{V_w,\mathrm{I,PA}}\left(\mathcal{M}^{q\bar{q}\to\ell\bar{\ell}}_{\mathrm{LO},Z}\right)^*$ can now safely be evaluated in $d=4$ dimensions.
It is important that we were able to factorize the IR-divergent QCD corrections from the amplitude and that $\mathcal{M}^{q\bar{q}\to\ell\bar{\ell}}_{V_w,\mathrm{I,PA}}$ is a renormalized amplitude and therefore free of UV divergences. Due to the factorization of QCD corrections and renormalization we were able to combine terms in such a way that the dimensional regulator is not needed any more and traces can be evaluated in $d=4$.

Appendix D

Explicit form of the gauge-boson self-energies at $\mathcal{O}(\alpha_s\alpha)$

The auxiliary functions used to express the gauge-boson self-energies in Section 5.2.4 depend on two-loop two-point integrals of the form

$$S_{abcde}(p^2, m_1^2, m_2^2) = \left(\frac{(2\pi\mu)^{2\epsilon}}{\mathrm{i}\pi^2}\right)^2 \int \mathrm{d}^D q_1 \int \mathrm{d}^D q_2 \, \frac{1}{(q_1^2)^a \, (q_2^2 - m_1^2)^b} \times \frac{1}{[(q_2+p)^2 - m_2^2]^c \, [(q_1+q_2)^2 - m_1^2]^d \, [(q_1+q_2+p)^2 - m_2^2]^e}, \quad \text{(D.1)}$$

where a graphical representation of these integrals is shown in Fig. D.1. The prefactor of the integrals is chosen such that reducible integrals contained in the integral family S_{abcde} decompose into the product of the standard one-loop integrals as defined in Refs. [60]. In the W-boson self-energy at zero-momentum transfer used in the application of the G_μ input-parameter scheme one additionally needs the two-mass two-loop tadpole integrals T_{abc}, defined by

$$T_{abc}(m_1^2, m_2^2) = \left(\frac{(2\pi\mu)^{2\epsilon}}{\mathrm{i}\pi^2}\right)^2 \int \mathrm{d}^D q_1 \int \mathrm{d}^D q_2 \, \frac{1}{(q_1^2)^a \, (q_2^2 - m_1^2)^b [(q_1+q_2)^2 - m_2^2]^c}. \quad \text{(D.2)}$$

One can choose a set of master integrals such that the auxiliary functions f_k ($k = 1, \ldots, 4$) can be expressed in terms of these master integrals [115],

$$f_1(s, m^2) = \frac{1-\epsilon}{2s} \, S_{10110} + \frac{1-\epsilon}{2(3-2\epsilon)\epsilon} \left[2 - 3\epsilon + 2\epsilon^2 + 4(1-\epsilon)(1+2\epsilon)\frac{m^2}{s}\right] S_{11110}$$

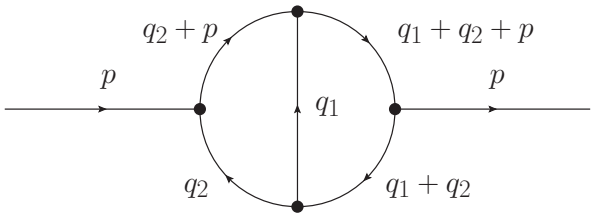

Figure D.1: Two-loop sunset topology, corresponding to the self-energy integral S_{abcde} defined in Eq. (D.1).

$$
\begin{aligned}
&+\frac{1}{4\epsilon}\left[-\frac{(1-\epsilon)(2-\epsilon+2\epsilon^2)}{3-2\epsilon}-\frac{2m^2}{(3-2\epsilon)s}+\frac{2(1-2\epsilon)m^2}{4m^2-s}\right]S_{01111}\\
&+\frac{m^2}{\epsilon s}\left[\frac{2-6\epsilon+7\epsilon^2-2\epsilon^3}{3-2\epsilon}-\frac{2(2-3\epsilon+2\epsilon^2)m^2}{4m^2-s}\right]S_{01120}\\
&+\frac{m^2}{2\epsilon s}\left[-\frac{2-3\epsilon+2\epsilon^2}{(1-2\epsilon)(3-2\epsilon)}+\frac{4(1-\epsilon)m^2}{4m^2-s}\right]S_{02020}, \qquad \text{(D.3)}
\end{aligned}
$$

$$
\begin{aligned}
f_2(s,m^2) = {}& \frac{(1-2\epsilon)}{(3-2\epsilon)s}S_{10110}+\frac{1}{3-2\epsilon}\left[-\frac{6-9\epsilon+2\epsilon^2}{\epsilon}+\frac{4(1-2\epsilon)m^2}{s}\right]S_{11110}\\
&+\frac{1}{\epsilon}\left[\frac{(1-\epsilon)(3-3\epsilon+2\epsilon^2)}{3-2\epsilon}-\frac{2(1-2\epsilon)m^2}{4m^2-s}\right]S_{01111}\\
&-2m^2\left[\frac{2}{(3-2\epsilon)s}-\frac{2-3\epsilon+2\epsilon^2}{\epsilon(4m^2-s)}\right]S_{01120}\\
&+m^2\left[\frac{1}{(3-2\epsilon)(1-\epsilon)s}-\frac{2(1-\epsilon)}{\epsilon(4m^2-s)}\right]S_{02020}, \qquad \text{(D.4)}
\end{aligned}
$$

$$
f_3(s,m^2) = -(3-2\epsilon)\left[\frac{\epsilon}{1-2\epsilon}+\frac{2m^2}{4m^2-s}\right]S_{01120}+\frac{2(3-2\epsilon)m^2}{(1-2\epsilon)(4m^2-s)}S_{02020}, \qquad \text{(D.5)}
$$

$$
f_4(s,m^2) = (3-2\epsilon)\left[\frac{1}{1-2\epsilon}+\frac{2m^2}{4m^2-s}\right]S_{01120}-\frac{2(3-2\epsilon)m^2}{(1-2\epsilon)(4m^2-s)}S_{02020}, \qquad \text{(D.6)}
$$

with suppressed arguments of the integral functions $S_{abcde}(s,m^2,m^2)$. Analytic expressions for all master integrals in the last expressions and also the ones in the following expressions can be found in [115]. The auxiliary function f_k $(k=5,6)$ are given by

$$
\begin{aligned}
f_5(s,m_1^2,m_2^2) = {}& \left[1-\epsilon+\frac{(1-2\epsilon)(m_1^2+m_2^2)}{2(3-2\epsilon)s}\right]\frac{S_{10110}}{8s}\\
&+\frac{1}{16(3-2\epsilon)\epsilon}\Bigg[(2-3\epsilon+2\epsilon^2)\left(2(1-\epsilon)-(1-2\epsilon)\frac{m_1^2}{s}-\frac{m_1^4}{s^2}\right)\\
&\quad-(2-3\epsilon)(1-2\epsilon)^2\frac{m_2^2}{s}+4(1-2\epsilon^2)\frac{m_1^2m_2^2}{s^2}-(2-5\epsilon+6\epsilon^2)\frac{m_2^4}{s^2}\Bigg]S_{11101}\\
&-\frac{1}{16\epsilon}\left[\frac{(1-\epsilon)(2-\epsilon+2\epsilon^2)}{3-2\epsilon}+\frac{(1-2\epsilon)(1-\epsilon^2)}{3-2\epsilon}\frac{m_1^2+m_2^2}{s}\right.\\
&\quad\left.+4(1-2\epsilon)\frac{m_1^2m_2^2}{\lambda}\right]S_{01111}\\
&+\frac{m_2^2}{8\epsilon s}\left[\frac{2(2-6\epsilon+7\epsilon^2-2\epsilon^3)}{3-2\epsilon}-\frac{(2-3\epsilon+2\epsilon^2)m_1^2}{(3-2\epsilon)s}+\frac{(2-7\epsilon+2\epsilon^2)m_2^2}{(3-2\epsilon)s}\right.\\
&\quad\left.-\frac{2(2-3\epsilon+2\epsilon^2)m_1^2(m_1^2-m_2^2-s)}{\lambda}\right]S_{01102}\\
&+\frac{m_1^2m_2^2}{8\epsilon s^2}\left[\frac{(1-2\epsilon)(2-\epsilon)}{(3-2\epsilon)(1-\epsilon)}+\frac{2(1-\epsilon)s(m_1^2+m_2^2-s)}{\lambda}\right]S_{00220}\\
&-\frac{m_2^2}{16\epsilon s}\left[\frac{(2-17\epsilon+26\epsilon^2-8\epsilon^3)m_2^2+(2-3\epsilon+2\epsilon^2)(m_1^2+2(1-\epsilon)s)}{(1-2\epsilon)(3-2\epsilon)(1-\epsilon)s}\right.
\end{aligned}
$$

$$+\frac{8(1-\epsilon)m_1^2m_2^2}{\lambda}\Bigg]S_{00202}, \tag{D.7}$$

$$\begin{aligned} f_6(s,m_1^2,m_2^2) = \frac{3-2\epsilon}{4}\Bigg\{&\left[\frac{(1-2\epsilon)s-m_1^2+m_2^2}{2(1-2\epsilon)s}+\frac{m_1^2(s-m_1^2+m_2^2)}{\lambda}\right]S_{01102}\\ &+\frac{m_1^2}{1-2\epsilon}\left[\frac{1}{2(1-\epsilon)s}+\frac{m_1^2+m_2^2-s}{\lambda}\right]S_{00220}\\ &-\frac{m_2^2}{1-2\epsilon}\left[\frac{1}{2(1-\epsilon)s}+\frac{2m_1^2}{\lambda}\right]S_{00202}\Bigg\} \end{aligned} \tag{D.8}$$

with the Källen function

$$\lambda = (s-m_1^2-m_2^2)^2-4m_1^2m_2^2 \tag{D.9}$$

and the arguments of the integral functions given by $S_{abcde}(s,m_1^2,m_2^2)$. Note that the interchange $(m_{d_j} \leftrightarrow m_{u_j})$ of the up- and down-type quark masses in (5.72) and (5.73) also concerns the arguments of the integral functions; this change of arguments can, however, be achieved by rearranging labels in S_{abcde} using the symmetries of the two-loop two-point integral family

$$S_{abcde}(p^2,m_1^2,m_2^2) = S_{adebc}(p^2,m_1^2,m_2^2) = S_{acbed}(p^2,m_2^2,m_1^2) = S_{aedcb}(p^2,m_2^2,m_1^2). \tag{D.10}$$

For massless fermions, we only need the functions f_1 and f_5,

$$f_1(s,0) = 4f_5(s,0,0) = \left(\frac{4\pi\mu^2}{-s-\mathrm{i}0}\right)^{2\epsilon}\Gamma(1+\epsilon)^2\left[\frac{1}{8\epsilon}+\frac{55}{48}-\zeta_3+\mathcal{O}(\epsilon)\right]. \tag{D.11}$$

The auxiliary functions f_k $(k=7,8)$ are given by

$$\begin{aligned} f_7(m_1^2,m_2^2) = &\frac{m_2^4}{4(2-\epsilon)}\left[\frac{m_2^2}{(1-\epsilon)\lambda_0}+\frac{(3-2\epsilon)(1-\epsilon)}{(1-2\epsilon)(m_1^2-m_2^2)}\right]S_{00202}\\ &-\frac{m_1^2m_2^4}{4(2-\epsilon)(1-\epsilon)\lambda_0}S_{00220}+\frac{1-\epsilon}{8(2-\epsilon)}T_{111}(m_1^2,m_2^2), \end{aligned} \tag{D.12}$$

$$f_8(m_1^2,m_2^2) = \frac{(3-2\epsilon)m_2^2}{4(2-\epsilon)(1-2\epsilon)\lambda_0}\Big\{\Big[(1-\epsilon)m_2^2-(2-\epsilon)m_1^2\Big]S_{00202}+m_1^2\,S_{00220}\Big\}, \tag{D.13}$$

where λ_0 is obtained by evaluating λ in (D.9) at $s=0$,

$$\lambda_0 = (m_1^2-m_2^2)^2, \tag{D.14}$$

and the integrals S_{abcde} have the arguments $S_{abcde}(0,m_1^2,m_2^2)$.

Appendix E

Results for convolutions of integrated antennas

This appendix contains results for the convolutions of integrated three-parton antennas and mass-factorization kernels. Before stating the explicit results we start by proofing the two identities relevant for the evaluation of convolutions of functions $f(x,y), h(x,y), g(x)$ and plus distribution given in (6.37) and (6.38). We begin with the proof of (6.37),

$$[f \otimes h](z_a, z_b) = \int_{z_1}^1 \mathrm{d}x_1 \int_{z_2}^1 \mathrm{d}x_2 \, f(x_1,x_2)\, h\left(\frac{z_1}{x_1}, \frac{z_2}{x_2}\right), \tag{E.1}$$

which can be derived in the following way

$$\begin{aligned}
[f \otimes h](z_1,z_2) &= \int_0^1 \mathrm{d}x_1 \mathrm{d}x_2 \, \mathrm{d}y_1 \mathrm{d}y_2 \, f(x_1,x_2)\, h(y_1,y_2)\delta(z_1 - x_1 y_1)\delta(z_2 - x_2 y_2) \\
&= \prod_{i=1}^2 \left(\int_0^1 \mathrm{d}x_i \int_0^{x_i} \frac{\mathrm{d}v_i}{x_i} \delta(z_i - v_i) \right) f(x_1,x_2)\, h\left(\frac{v_1}{x_1}, \frac{v_2}{x_2}\right) \\
&= \prod_{i=1}^2 \left(\underbrace{\int_0^{z_i} \mathrm{d}x_i \int_0^{x_i} \frac{\mathrm{d}v_i}{x_i} \delta(z_i - v_i)}_{v_i < x_i < z_i \Rightarrow \delta(z_i - v_i) = 0} + \int_{z_i}^1 \mathrm{d}x_i \int_0^{x_i} \frac{\mathrm{d}v_i}{x_i} \delta(z_i - v_i) \right) \\
&\qquad \times f(x_1,x_2)\, h\left(\frac{v_1}{x_1}, \frac{v_2}{x_2}\right) \\
&= \int_{z_1}^1 \mathrm{d}x_1 \int_{z_2}^1 \mathrm{d}x_2 \, f(x_1,x_2)\, h\left(\frac{z_1}{x_1}, \frac{z_2}{x_2}\right).
\end{aligned} \tag{E.2}$$

Similarly, the proof of (6.38),

$$[\mathcal{D}_n \otimes g](z) = \int_z^1 \mathrm{d}x \frac{\log^n(1-x)}{1-x} \left[\frac{1}{x} g\left(\frac{z}{x}\right) - g(z) \right] + \frac{g(z)\log^{n+1}(1-z)}{n+1} \tag{E.3}$$

reads

$$[\mathcal{D}_n \otimes g](z) = \int_0^1 \mathrm{d}x \, \mathrm{d}y D_n(x) g(y) \delta(z - xy) \tag{E.4}$$

$$
\begin{aligned}
&= \int_0^1 \mathrm{d}x\,\mathrm{d}y \frac{\log^n(1-x)}{1-x} g(y) \left[\delta(z-xy) - \delta(z-y)\right] \\
&= \underbrace{\int_0^z \mathrm{d}x \int_0^x \frac{\mathrm{d}v}{x} \frac{\log^n(1-x)}{1-x} g\left(\frac{v}{x}\right) \delta(z-v)}_{v<x<z \Rightarrow \delta(z-v)=0} \\
&\quad + \int_z^1 \mathrm{d}x \int_0^x \frac{\mathrm{d}v}{x} \frac{\log^n(1-x)}{1-x} g\left(\frac{v}{x}\right) \delta(z-v) - g(z) \int_0^1 \mathrm{d}x \frac{\log^n(1-x)}{1-x} \\
&= \int_z^1 \mathrm{d}x \frac{\log^n(1-x)}{1-x} \left[\frac{1}{x} g\left(\frac{z}{x}\right) - g(z)\right] - g(z) \int_0^z \mathrm{d}x \frac{\log^n(1-x)}{1-x} \\
&= \int_z^1 \mathrm{d}x \frac{\log^n(1-x)}{1-x} \left[\frac{1}{x} g\left(\frac{z}{x}\right) - g(z)\right] + \frac{g(z)\log^{n+1}(1-z)}{n+1}.
\end{aligned}
$$

Note that (6.38) can also be rewritten as

$$
\left[\mathcal{D}_n \otimes g\right](z) = \int_z^1 \mathrm{d}x \frac{\log^n(1-\frac{z}{x})}{1-\frac{z}{x}} \left[\frac{1}{x} g(x) - \frac{z}{x^2} g(z)\right] + \frac{g(z)\log^{n+1}(1-z)}{n+1}. \tag{E.5}
$$

Especially if the function g convoluted with the plus-distribution $\mathcal{D}_n$ is rather complicated using this form instead of (6.38) sometimes leads to more compact results of the integrals as we have shifted the fraction z/x from the function g to the logarithm in the last equation.

E.1 Results for convolutions

The convolutions of integrated antennae and mass-factorization kernels or convolutions of two mass-factorization kernels in (6.27) to (6.30) can be expanded in $\epsilon = \frac{4-d}{2}$, e.g.

$$
\begin{aligned}
\left[\Gamma^{(1)}_{ki} \otimes \mathcal{A}^0_{qq,g}\right]_1(s; z_1, z_2) = \left(\frac{s}{\mu}\right)^{-\epsilon} \Bigg(& \frac{\left[\Gamma^{(1)}_{ki} \otimes \mathcal{A}^0_{qq,g}\right]_1^{-4}}{\epsilon^4} + \frac{\left[\Gamma^{(1)}_{ki} \otimes \mathcal{A}^0_{qq,g}\right]_1^{-3}}{\epsilon^3} \\
& + \frac{\left[\Gamma^{(1)}_{ki} \otimes \mathcal{A}^0_{qq,g}\right]_1^{-2}}{\epsilon^2} + \frac{\left[\Gamma^{(1)}_{ki} \otimes \mathcal{A}^0_{qq,g}\right]_1^{-1}}{\epsilon^1} \\
& + \left[\Gamma^{(1)}_{ki} \otimes \mathcal{A}^0_{qq,g}\right]_1^{0} + \mathcal{O}(\epsilon^1) \Bigg).
\end{aligned} \tag{E.6}
$$

We note that due to the symmetry of the integrated three-parton antenna $\mathcal{A}^0_{qq,g}(x_1, x_2) = \mathcal{A}^0_{qq,g}(x_2, x_1)$ we have

$$
\left[\Gamma^{(1)}_{ki} \otimes \mathcal{A}^0_{qq,g}\right]_2(s; z_1, z_2) = \left[\Gamma^{(1)}_{ki} \otimes \mathcal{A}^0_{qq,g}\right]_1(s; z_2, z_1), \tag{E.7}
$$

which reduces the number of convolutions that have to be calculated explicitly. As the results for the coefficients are rather lengthy we present them only in terms of master integrals that can be evaluated with (6.33) to (6.36), (6.37), and (6.38):

$$
\left[\Gamma^{(1)}_{qq} \otimes \mathcal{A}^0_{qq,g}\right]_1^{-4} = 0, \tag{E.8}
$$

$$\big[\Gamma^{(1)}_{qq} \otimes \mathcal{A}^0_{qq,g}\big]^{-3}_1 = \frac{1}{4}\big(-3\,\delta(1-z_1) - 4\,\mathcal{D}_0(1-z_1) + 2z_1 + 2\big)\,\delta(1-z_2), \tag{E.9}$$

$$\begin{aligned}\big[\Gamma^{(1)}_{qq} \otimes \mathcal{A}^0_{qq,g}\big]^{-2}_1 = {}& \delta(1-z_2)[h_1 \otimes h_1](z_1) - 2\,\delta(1-z_2)[\mathcal{D}_0 \otimes h_1](z_1) \\ & + \frac{1}{8}(8[\mathcal{D}_0 \otimes \mathcal{D}_0](z_1)\,\delta(1-z_2) - 3z_1\,\delta(1-z_2) - 3z_2\,\delta(1-z_1) \\ & + \mathcal{D}_0(1-z_2)(6\,\delta(1-z_1) - 4z_1 - 4) \\ & + \mathcal{D}_0(1-z_1)(6\,\delta(1-z_2) + 8\,\mathcal{D}_0(1-z_2) - 4z_2 - 4) \\ & - 3\,\delta(1-z_1) - 3\,\delta(1-z_2) + 2z_1z_2 + 2z_1 + 2z_2 + 2),\end{aligned} \tag{E.10}$$

$$\begin{aligned}\big[\Gamma^{(1)}_{qq} \otimes \mathcal{A}^0_{qq,g}\big]^{-1}_1 = {}& \frac{1}{48}(-48[\mathcal{D}_0 \otimes \mathcal{D}_1](z_1)\ \delta(1-z_2) + \frac{1}{z_1-1}\big\{18(\log(2)z_1^2 + \log(2) \\ & + z_1^2 + (z_1^2-1)\log(1-z_1) - (z_1^2+1)\log(z_1+1) - 2z_1 + 1)\delta(1-z_2)\big\} \\ & + \frac{1}{z_2-1}\big\{18(\log(2)z_2^2 + \log(2) + z_2^2 + (z_2^2-1)\ \log(1-z_2) \\ & - (z_2^2+1)\log(z_2+1) - 2z_2 + 1)\delta(1-z_1)\big\} - 36\ \mathcal{D}_1(1-z_2)\delta(1-z_1) \\ & - 2\pi^2(z_1+1)\delta(1-z_2) + 4\pi\ {}^2\mathcal{D}_0(1-z_1)\delta(1-z_2) \\ & - 36\mathcal{D}_1(1-z_1)\ \delta(1-z_2) + 3\pi^2\delta(1-z_1)\delta(1-z_2) \\ & - 48[\mathcal{D}_0 \otimes \mathcal{D}_0](z_1)\mathcal{D}_0(1-z_2) + \frac{1}{z_2-1}\big\{24\mathcal{D}_0(1-z_1)\ (\log(2)z_2^2 \\ & + \log(2) + z_2^2 + (z_2^2-1)\log(1-z_2) - (z_2^2+1)\log\ (z_2+1) - 2z_2 + 1)\big\} \\ & + 18(z_2+1)\mathcal{D}_0(1-z_1) + 18(z_1+1)\ \mathcal{D}_0(1-z_2) \\ & - 36\mathcal{D}_0(1-z_1)\mathcal{D}_0(1-z_2) + 24(z_1+1)\ \mathcal{D}_1(1-z_2) \\ & - 48\mathcal{D}_0(1-z_1)\mathcal{D}_1(1-z_2) + 24[\mathcal{D}_0 \otimes \mathcal{D}_0](z_1)(z_2+1) \\ & - \frac{1}{z_2-1}\big\{12(z_1+1)(\log(2)\ z_2^2 + \log(2) + z_2^2 \\ & + (z_2^2-1)\log(1-z_2) - (z_2^2+1)\log(z_2+1) - 2\ z_2 + 1)\big\} \\ & - \frac{1}{(z_1+1)(z_2+1)(z_1+z_2)^2}\big\{18(z_1^4(2z_2^2 + 2z_2 + 1) \\ & + 2z_1^3(z_2^2 + 3\ z_2 + 1) \\ & + 2z_1^2(z_2^4 + z_2^3 + z_2^2 + z_2 + 1) \\ & + 2z_1z_2^2(z_2^2 + 3\ z_2 + 1) + z_2^2(z_2^2 + 2z_2 + 2))\big\}) \\ & - \delta(1-z_2)[\mathcal{D}_0 \otimes h_2](z_1) + \delta(1-z_2)[\ \mathcal{D}_1 \otimes h_1](z_1) \\ & + \delta(1-z_2)[h_1 \otimes h_2](z_1) + 2\ \mathcal{D}_0(1-z_2)[\mathcal{D}_0 \otimes h_1](z_1) \\ & - [(\mathcal{D}_0 \otimes h_3(z_2,x_1)](z_1,z_2)) - \mathcal{D}_0(1-z_2)[h_1 \otimes h_1](z_1) \\ & + [h_1 \otimes h_3(z_2,x_1)](z_1,z_2) - h_1(z_2)[\mathcal{D}_0 \otimes h_1](z_1),\end{aligned} \tag{E.11}$$

$$\begin{aligned}\big[\Gamma^{(1)}_{qq} \otimes \mathcal{A}^0_{qq,g}\big]^{0}_1 = {}& \frac{1}{48}\Bigg(-24[\mathcal{D}_0 \otimes \mathcal{D}_1](z_1)(z_2+1) - 18\ \mathcal{D}_1(1-z_1)(z_2+1) \\ & + 48[\mathcal{D}_0 \otimes \mathcal{D}_1](z_1)\ \mathcal{D}_0(1-z_2) - 4\pi^2\mathcal{D}_0(1-z_1)\mathcal{D}_0(1-z_2) \\ & + 36\ \mathcal{D}_0(1-z_2)\mathcal{D}_1(1-z_1) + 48[\mathcal{D}_0 \otimes \mathcal{D}_0](z_1)\mathcal{D}_1(1-z_2) \\ & - 18(z_1+1)\mathcal{D}_1(1-z_2) + 36\ \mathcal{D}_0(1-z_1)\mathcal{D}_1(1-z_2)\end{aligned} \tag{E.12}$$

$$
\begin{aligned}
&+ 24\mathcal{D}_0(1-z_1)\mathcal{D}_2(1-z_2)\\
&- 3\pi^2\mathcal{D}_0(1-z_2)\delta(1-z_1) + 18\ \mathcal{D}_2(1-z_2)\delta(1-z_1)\\
&+ 24[\mathcal{D}_0\otimes\mathcal{D}_2](z_1)\delta(1-z_2) - 8(z_1+1)\zeta_3\delta(1-z_2)\\
&+ 16\zeta_3\mathcal{D}_0(1-z_1)\delta(1-z_2) - 3\pi^2\ \mathcal{D}_0(1-z_1)\delta(1-z_2)\\
&+ 18\mathcal{D}_2(1-z_1)\delta(1-z_2) + 12\ \zeta_3\delta(1-z_1)\delta(1-z_2)\\
&- 4[\mathcal{D}_0\otimes\mathcal{D}_0](z_1)\pi^2\delta(1-z_2)\\
&- \frac{1}{z_1-1}\big\{18\mathcal{D}_0(1-z_2)\ (\log(2)z_1^2 + z_1^2 - 2z_1\\
&+ \log(2) + (z_1^2-1)\log\ (1-z_1) - (z_1^2+1)\log(z_1+1) + 1)\big\}\\
&- \frac{1}{z_2-1}\big\{18\ \mathcal{D}_0(1-z_1)(\log(2)z_2^2 + z_2^2 - 2z_2 + \log(2)\\
&+ (z_2^2-1)\log\ (1-z_2) - (z_2^2+1)\log(z_2+1) + 1)\big\}\\
&- \frac{1}{z_2-1}\big\{24[\mathcal{D}_0\otimes\mathcal{D}_0](z_1)(\log(2)z_2^2 + z_2^2 - 2\ z_2 + \log(2)\\
&+ (z_2^2-1)\log(1-z_2) - (z_2^2+1)\log\ (z_2+1) + 1)\big\}\\
&- \frac{1}{(z_1-1)(z_1+1)(z_2-1)(z_1+z_2)^2(z_2+1)}\\
&\times\Big\{18(-2z_2^3z_1^5 + \log(2)z_1^5 + \log(2)\ z_2z_1^5 + z_2z_1^5 - 2z_2^3\log(1-z_2)z_1^5\\
&+ z_2\log(1-z_2)\ z_1^5 + \log(1-z_2)z_1^5 - 2z_2^3\log(z_2+1)z_1^5\\
&+ 4z_2^3\log\ (z_1+z_2)z_1^5 + z_1^5 - 4z_2^4z_1^4 + 2\log(2)z_2^2z_1^4 + 4z_2^2\ z_1^4 + \log(2)z_1^4\\
&+ 3\log(2)z_2z_1^4 + z_2z_1^4 - 4z_2^2\log\ (1-z_2)z_1^4 + 3z_2\log(1-z_2)z_1^4\\
&+ \log(1-z_2)z_1^4 - 6z_2^2\ \log(z_2+1)z_1^4 + 12z_2^2\log(z_1+z_2)z_1^4 - z_1^4\\
&- 2z_2^5z_1^3 + 2\log(2)z_2^3z_1^3 + 6z_2^3z_1^3 + 4\log(2)z_2^2z_1^3 - 2\ z_2^2z_1^3\\
&+ 2\log(2)z_1^3 + 4\log(2)z_2z_1^3 - 2z_2z_1^3 - 2z_2^5\ \log(1-z_2)z_1^3\\
&+ 2z_2^3\log(1-z_2)z_1^3 + 4z_2^2\log(1-z_2)\ z_1^3 - 4z_2\log(1-z_2)z_1^3\\
&- 2z_2^5\log(z_2+1)z_1^3 - z_2^3\ \log(z_2+1)z_1^3 - z_2^2\log(z_2+1)z_1^3\\
&- 7z_2\log(z_2+1)\ z_1^3 - \log(z_2+1)z_1^3 + 4z_2^5\log(z_1+z_2)z_1^3\\
&+ 12z_2\log\ (z_1+z_2)z_1^3 + 2\log(2)z_2^4z_1^2 + 4z_2^4z_1^2\\
&+ 4\log(2)z_2^3\ z_1^2 - 2z_2^3z_1^2 + 6\log(2)z_2^2z_1^2 - 2z_2^2z_1^2\\
&+ 2\log(2)\ z_1^2 + 6\log(2)z_2z_1^2 - 4z_2^4\log(1-z_2)z_1^2 + 4z_2^3\log\ (1-z_2)z_1^2\\
&+ 2z_2^2\log(1-z_2)z_1^2 - 2\log(1-z_2)z_1^2 - 8\ z_2^4\log(z_2+1)z_1^2\\
&- 3z_2^3\log(z_2+1)z_1^2 - 3z_2^2\log\ (z_2+1)z_1^2\\
&- 3z_2\log(z_2+1)z_1^2 - 3\log(z_2+1)z_1^2 + 12\ z_2^4\log(z_1+z_2)z_1^2\\
&+ 4\log(z_1+z_2)z_1^2 + \log(2)z_2^5\ z_1 + z_2^5z_1 + 3\log(2)z_2^4z_1\\
&+ z_2^4z_1 + 4\log(2)z_2^3z_1 - 2\ z_2^3z_1 + 6\log(2)z_2^2z_1\\
&+ 4\log(2)z_2z_1 + z_2^5\log(1-z_2)\ z_1 + 3z_2^4\log(1-z_2)z_1\\
&- 4z_2^3\log(1-z_2)z_1 - z_2^5\log\ (z_2+1)z_1 - 3z_2^4\log(z_2+1)z_1\\
&- 9z_2^3\log(z_2+1)z_1 - 3\ z_2^2\log(z_2+1)z_1 - 2z_2\log(z_2+1)z_1
\end{aligned}
$$

$$
\begin{aligned}
&+ 12z_2^3 \log\,(z_1+z_2)z_1 + \log(2)z_2^5 + z_2^5 + \log(2)z_2^4 - z_2^4 \\
&+ 2\log(2)\; z_2^3 + 2\log(2)z_2^2 - (z_2-1) \\
&\times \big((2z_2^2+2z_2+1)z_1^5 + (4z_2+1)\; z_1^4 + 2z_2(z_2^3+z_2^2-2)z_1^3 \\
&+ (4z_2^3 - 2z_2 - 2)z_1^2 - z_2^3\;(z_2+4)z_1 - z_2^2(z_2^2+2z_2+2)\big)\log(1-z_1) \\
&- ((2z_2^3+z_2+1)\; z_1^5 + (8z_2^2+3z_2+1)z_1^4 \\
&+ (2z_2^5 + z_2^3 + 3z_2^2 + 9z_2 + 1)\; z_1^3 + (6z_2^4 + z_2^3 + 3z_2^2 + 3z_2 + 3)z_1^2 \\
&+ z_2(7z_2^2 + 3z_2 + 2)\; z_1 + z_2^2(z_2+3))\log(z_1+1) + z_2^5\log(1-z_2) \\
&+ z_2^4\log\,(1-z_2) - 2z_2^2\log(1-z_2) - z_2^5\log(z_2+1) \\
&- z_2^4\log\,(z_2+1) - z_2^3\log(z_2+1) \\
&- 3z_2^2\log(z_2+1) + 4z_2^2\log\,(z_1+z_2))\Big\}\Big) \\
&+ \frac{1}{12}\pi^2\delta(1-z_2)[\mathcal{D}_0\otimes h_1](z_1) - \delta(1-z_2)[\mathcal{D}_0\otimes h_4](z_1) \\
&- \frac{1}{2}\;\delta(1-z_2)[\mathcal{D}_2\otimes h_1](z_1) + \delta(1-z_2)\;[h_1\otimes h_4](z_1) \\
&- \frac{3}{4}h_4(z_1)\delta(1-z_2) \\
&- \frac{3}{4}h_4(z_2)\delta(1-z_1) - 2\;\mathcal{D}_1(1-z_2)[\mathcal{D}_0\otimes h_1](z_1) \\
&+ \mathcal{D}_0(1-z_2)[\mathcal{D}_0\otimes h_2](z_1) \\
&- [(\mathcal{D}_0\otimes h_5(y_1,z_2)](z_1,z_2)) - \;\mathcal{D}_0(1-z_2)[\mathcal{D}_1\otimes h_1](z_1) \\
&+ \mathcal{D}_1(1-z_2)\;[h_1\otimes h_1](z_1) \\
&- \mathcal{D}_0(1-z_2)[h_1\otimes h_2](z_1) + \frac{1}{12}\pi^2 h_1(z_1)\mathcal{D}_0(1-z_2) \\
&- \;\frac{1}{2}h_1(z_1)\mathcal{D}_2(1-z_2) - h_4(z_2)\;\mathcal{D}_0(1-z_1) \\
&+ [h_1\otimes h_5(y_1,z_2)](z_1,z_2) - h_2(z_2)[\mathcal{D}_0\otimes h_1](z_1) \\
&+ h_1(z_2)[\mathcal{D}_1\otimes h_1](z_1) + h_1(z_1)h_4(z_2).
\end{aligned}
$$

$$\big[\Gamma_{qg}^{(1)}\otimes\mathcal{A}_{qq,g}^0\big]_2^{-4} = 0, \tag{E.13}$$

$$\big[\Gamma_{qg}^{(1)}\otimes\mathcal{A}_{qq,g}^0\big]_2^{-3} = -\,h_1^{\mathrm{qg}}(z_2)\delta(1-z_1), \tag{E.14}$$

$$
\begin{aligned}
\big[\Gamma_{qg}^{(1)}\otimes\mathcal{A}_{qq,g}^0\big]_2^{-2} = &-\frac{1}{2}h_1^{\mathrm{qg}}(z_2)(-2\mathcal{D}_0(1-z_1)+z_1+1) \\
&+ \delta(1-z_1)([\mathcal{D}_0\otimes h_1^{\mathrm{qg}}](z_2) - [h_1^{\mathrm{qg}}\otimes h_1](z_2)),
\end{aligned} \tag{E.15}
$$

$$
\begin{aligned}
\big[\Gamma_{qg}^{(1)}\otimes\mathcal{A}_{qq,g}^0\big]_2^{-1} = &\frac{1}{12}h_1^{\mathrm{qg}}(z_2)(\pi^2\delta(1-z_1) - 12\;\mathcal{D}_1(1-z_1) \\
&+ \frac{1}{z_1-1}\big\{6(\log(2)z_1^2 + \log(2) + z_1^2 \\
&+ (z_1^2-1)\log\,(1-z_1) - (z_1^2+1)\log(z_1+1) - 2z_1 + 1)\big\})
\end{aligned} \tag{E.16}
$$

$$
\begin{aligned}
&+ -\delta(1-z_1)[\mathcal{D}_1 \otimes h_1^{\mathrm{qg}}](z_2) - \delta(1-z_1)[h_1^{\mathrm{qg}} \otimes h_2](z_2) \\
&+ (h_1(z_1) - \mathcal{D}_0(1-z_1))\ [\mathcal{D}_0 \otimes h_1^{\mathrm{qg}}](z_2) + \mathcal{D}_0(1-z_1)\ [h_1^{\mathrm{qg}} \otimes h_1](z_2) \\
&- ([h_1^{\mathrm{qg}} \otimes h_5(x_2, z_1)](z_1, z_2)),
\end{aligned}
$$

$$
\begin{aligned}
\left[\Gamma_{qg}^{(1)} \otimes \mathcal{A}_{qq,g}^{0}\right]_2^0 = &- \frac{1}{12}\pi^2\delta(1-z_1)[\mathcal{D}_0 \otimes h_1^{\mathrm{qg}}](z_2) + \frac{1}{2}\delta(1-z_1)[\mathcal{D}_2 \otimes h_1^{\mathrm{qg}}](z_2) \\
&+ \frac{1}{3}\zeta_3 h_1^{\mathrm{qg}}(z_2)\ \delta(1-z_1) - \delta(1-z_1)[h_1^{\mathrm{qg}} \otimes h_4](z_2) \\
&+ \mathcal{D}_1(1-z_1)[\mathcal{D}_0 \otimes h_1^{\mathrm{qg}}](z_2) + (\mathcal{D}_0(1-z_1) - h_1(z_1))[\mathcal{D}_1 \otimes h_1^{\mathrm{qg}}](z_2) \\
&- \frac{1}{12}\pi^2 h_1^{\mathrm{qg}}(z_2)\ \mathcal{D}_0(1-z_1) + \frac{1}{2}h_1^{\mathrm{qg}}(z_2)\ \mathcal{D}_2(1-z_1) \\
&- \mathcal{D}_1(1-z_1)[h_1^{\mathrm{qg}} \otimes h_1](z_2) + \mathcal{D}_0(1-z_1)[h_1^{\mathrm{qg}} \otimes h_2](z_2) \\
&- [h_1^{\mathrm{qg}} \otimes h_5]_2(z_1, z_2) + h_2(z_1)[\mathcal{D}_0 \otimes h_1^{\mathrm{qg}}](z_2) - h_1^{\mathrm{qg}}(z_2)h_4(z_1),
\end{aligned}
\tag{E.17}
$$

$$
\left[\Gamma_{qq}^{(1)} \otimes \mathcal{A}_{gq,g}^{0}\right]_1^{-4} = 0, \tag{E.18}
$$

$$
\left[\Gamma_{qq}^{(1)} \otimes \mathcal{A}_{gq,g}^{0}\right]_1^{-3} = 0, \tag{E.19}
$$

$$
\left[\Gamma_{qq}^{(1)} \otimes \mathcal{A}_{gq,g}^{0}\right]_1^{-2} = -\frac{1}{4}h_1^{\mathrm{qg}}(z_2)(3\delta(1-z_1) + 4\mathcal{D}_0(1-z_1) - 4h_1(z_1)), \tag{E.20}
$$

$$
\begin{aligned}
\left[\Gamma_{qq}^{(1)} \otimes \mathcal{A}_{gq,g}^{0}\right]_1^{-1} = &- [\mathcal{D}_0 \otimes h_3^{\mathrm{qg}}(x_1, z_2)](z_1, z_2) + [h_3^{\mathrm{qg}}(y_1, z_2) \otimes h_1](z_1, z_2) \\
&- h_1^{\mathrm{qg}}(z_2)[\mathcal{D}_0 \otimes h_1](z_1) + \frac{1}{4}(h_2^{\mathrm{qg}}(z_2)(-3\delta(1-z_1) \\
&- 4\mathcal{D}_0(1-z_1) + 4h_1(z_1)) + h_1^{\mathrm{qg}}(z_2)(3\mathcal{D}_0(1-z_1) \\
&+ 4[\mathcal{D}_0 \otimes \mathcal{D}_0](z_1)) - 3h_3^{\mathrm{qg}}(z_1, z_2)),
\end{aligned}
\tag{E.21}
$$

$$
\begin{aligned}
\left[\Gamma_{qq}^{(1)} \otimes \mathcal{A}_{gq,g}^{0}\right]_1^{0} = &\frac{1}{4}(-3h_5^{\mathrm{qg}}(z_2)\ \delta(1-z_1) + h_2^{\mathrm{qg}}(z_2)(3\mathcal{D}_0(1-z_1) \\
&+ 4[\mathcal{D}_0 \otimes \mathcal{D}_0](z_1)) - (h_1^{\mathrm{qg}}(z_2)(3\ \mathcal{D}_1(1-z_1) \\
&+ 4[\mathcal{D}_0 \otimes \mathcal{D}_1](z_1))) - 4\ h_5^{\mathrm{qg}}(z_2)\mathcal{D}_0(1-z_1) - 3\ h_5^{\mathrm{qg}}(z_1, z_2) \\
&+ 4h_1(z_1)h_5^{\mathrm{qg}}(z_1, z_2)) - [\mathcal{D}_0 \otimes h_5^{\mathrm{qg}}(y_1, z_2)](z_1, z_2) \\
&+ [h_1 \otimes h_5^{\mathrm{qg}}](y_1, z_2)(z_1, z_2) - h_2^{\mathrm{qg}}(z_2)[\mathcal{D}_0 \otimes h_1](z_1) \\
&+ h_1^{\mathrm{qg}}(z_2)[\mathcal{D}_1 \otimes h_1](z_1).
\end{aligned}
\tag{E.22}
$$

$$
\left[\Gamma_{qq}^{(1)} \otimes \mathcal{A}_{gq,g}^{0}\right]_2^{-4} = 0, \tag{E.23}
$$

$$
\left[\Gamma_{qq}^{(1)} \otimes \mathcal{A}_{gq,g}^{0}\right]_2^{-3} = 0, \tag{E.24}
$$

$$
\left[\Gamma_{qq}^{(1)} \otimes \mathcal{A}_{gq,g}^{0}\right]_2^{-2} = -\frac{1}{4}\delta(1-z_1)(4[\mathcal{D}_0 \otimes h_1^{\mathrm{qg}}](z_2) + 3h_1^{\mathrm{qg}}(z_2) - 4[h_1^{\mathrm{qg}} \otimes h_1](z_2)), \tag{E.25}
$$

$$
\begin{aligned}
\left[\Gamma_{qq}^{(1)} \otimes \mathcal{A}_{gq,g}^{0}\right]_2^{-1} = &- \delta(1-z_1)[\mathcal{D}_0 \otimes h_2^{\mathrm{qg}}](z_2) - [\mathcal{D}_0 \otimes h_3^{\mathrm{qg}}(z_1, x_2)](z_1, z_2) \\
&+ \delta(1-z_1)[h_2^{\mathrm{qg}} \otimes h_1](z_2) + \mathcal{D}_0(1-z_1)[\mathcal{D}_0 \otimes h_1^{\mathrm{qg}}](z_2)
\end{aligned}
\tag{E.26}
$$

$$
\begin{aligned}
&- \mathcal{D}_0(1-z_1)[h_1^{\mathrm{qg}} \otimes h_1](z_2) + [h_3^{\mathrm{qg}}(z_1,y_2) \otimes h_1](z_1,z_2) \\
&- \frac{3}{4}(h_2^{\mathrm{qg}}(z_2)\delta(1-z_1) - h_1^{\mathrm{qg}}(z_2)\mathcal{D}_0(1-z_1) + h_3^{\mathrm{qg}}(z_1,z_2)), \\
\left[\Gamma_{qq}^{(1)} \otimes \mathcal{A}_{gq,g}^0\right]_2^0 = &- \delta(1-z_1)[\mathcal{D}_0 \otimes\ h_4^{\mathrm{qg}}](z_2) + \delta(1-z_1)[h_1 \otimes h_4^{\mathrm{qg}}](z_2) \\
&- [\mathcal{D}_0 \otimes h_5^{\mathrm{qg}}](z_1,y_2)](z_1,z_2) - \mathcal{D}_1(1-z_1)[\mathcal{D}_0 \otimes h_1^{\mathrm{qg}}](z_2) \\
&+ \mathcal{D}_0(1-z_1)[\mathcal{D}_0 \otimes h_2^{\mathrm{qg}}](z_2) + \mathcal{D}_1(1-z_1)[h_1^{\mathrm{qg}} \otimes h_1](z_2) \\
&- \mathcal{D}_0(1-z_1)[h_2^{\mathrm{qg}} \otimes h_1](z_2) + [h_1 \otimes h_5^{\mathrm{qg}}(z_1,y_2)](z_1,z_2) \\
&- \frac{3}{4}(h_5^{\mathrm{qg}}(z_2)\ \delta(1-z_1) + h_1^{\mathrm{qg}}(z_2)\ \mathcal{D}_1(1-z_1) \\
&- h_2^{\mathrm{qg}}(z_2)\ \mathcal{D}_0(1-z_1) + h_5^{\mathrm{qg}}(z_1,z_2)).
\end{aligned}
\tag{E.27}
$$

$$
\left[\Gamma_{qg}^{(1)} \otimes \mathcal{A}_{gq,g}^0\right]_1^{-4} = 0, \tag{E.28}
$$

$$
\left[\Gamma_{qg}^{(1)} \otimes \mathcal{A}_{gq,g}^0\right]_1^{-3} = 0, \tag{E.29}
$$

$$
\left[\Gamma_{qg}^{(1)} \otimes \mathcal{A}_{gq,g}^0\right]_1^{-2} = \delta(1-z_1)(-([h_1^{\mathrm{qg}} \otimes h_1^{\mathrm{qg}}](z_2))), \tag{E.30}
$$

$$
\begin{aligned}
\left[\Gamma_{qg}^{(1)} \otimes \mathcal{A}_{gq,g}^0\right]_1^{-1} = &- \delta(1-z_1)[h_2^{\mathrm{qg}} \otimes h_1^{\mathrm{qg}}](z_2) + \mathcal{D}_0(1-z_1)[h_1^{\mathrm{qg}} \otimes h_1^{\mathrm{qg}}](z_2) \\
&- ([h_3^{\mathrm{qg}}(z_1,x_2) \otimes h_1^{\mathrm{qg}}](z_1,z_2)),
\end{aligned}
\tag{E.31}
$$

$$
\begin{aligned}
\left[\Gamma_{qq}^{(1)} \otimes \mathcal{A}_{gq,g}^0\right]_1^{0} = &- \delta(1-z_1)[h_4^{\mathrm{qg}} \otimes h_1^{\mathrm{qg}}](z_2) - \mathcal{D}_1(1-z_1)[h_1^{\mathrm{qg}} \otimes h_1^{\mathrm{qg}}](z_2) \\
&+\ \mathcal{D}_0(1-z_1)[h_2^{\mathrm{qg}} \otimes h_1^{\mathrm{qg}}](z_2) - ([h_5^{\mathrm{qg}} \otimes h_1^{\mathrm{qg}}](z_1,z_2))
\end{aligned}
\tag{E.32}
$$

$$
\left[\Gamma_{qq}^{(1)} \otimes \Gamma_{qq}^{(1)}\right]_1^{-4} = 0, \tag{E.33}
$$

$$
\left[\Gamma_{qq}^{(1)} \otimes \Gamma_{qq}^{(1)}\right]_1^{-3} = 0, \tag{E.34}
$$

$$
\begin{aligned}
\left[\Gamma_{qq}^{(1)} \otimes \Gamma_{qq}^{(1)}\right]_1^{-2} = &\ \delta(1-z_2)([h_1 \otimes h_1](z_1) - 2[\mathcal{D}_0 \otimes h_1](z_1)) \\
&+ \frac{1}{16}\delta(1-z_2)(9\delta(1-z_1) + 24\ \mathcal{D}_0(1-z_1) \\
&+ 16[\mathcal{D}_0 \otimes \mathcal{D}_0](z_1) - 24h_1(z_1)),
\end{aligned}
\tag{E.35}
$$

$$
\left[\Gamma_{qq}^{(1)} \otimes \Gamma_{qq}^{(1)}\right]_1^{-1} = 0, \tag{E.36}
$$

$$
\left[\Gamma_{qq}^{(1)} \otimes \Gamma_{qq}^{(1)}\right]_1^{0} = 0. \tag{E.37}
$$

$$
\left[\Gamma_{qq}^{(1)} \otimes \Gamma_{qq}^{(1)}\right]_2^{-4} = 0, \tag{E.38}
$$

$$
\left[\Gamma_{qq}^{(1)} \otimes \Gamma_{qq}^{(1)}\right]_2^{-3} = 0, \tag{E.39}
$$

$$\begin{aligned}\left[\Gamma_{qq}^{(1)} \otimes \Gamma_{qq}^{(1)}\right]_2^{-2} =& \delta(1-z_1)([h_1 \otimes h_1](z_2) - 2\ [\mathcal{D}_0 \otimes h_1](z_2)) \\ &+ \frac{1}{16}\delta(1-z_1)(9\delta(1-z_2) + 24\ \mathcal{D}_0(1-z_2) \\ &+ 16[\mathcal{D}_0 \otimes \mathcal{D}_0](z_2) - 24h_1(z_2)),\end{aligned} \tag{E.40}$$

$$\left[\Gamma_{qq}^{(1)} \otimes \Gamma_{qq}^{(1)}\right]_2^{-1} = 0, \tag{E.41}$$

$$\left[\Gamma_{qq}^{(1)} \otimes \Gamma_{qq}^{(1)}\right]_2^{0} = 0. \tag{E.42}$$

$$\left[\Gamma_{qq}^{(1)} \otimes \Gamma_{qq}^{(1)}\right]_2^{-4} = 0, \tag{E.43}$$

$$\left[\Gamma_{qq}^{(1)} \otimes \Gamma_{qq}^{(1)}\right]_2^{-3} = 0, \tag{E.44}$$

$$\left[\Gamma_{qq}^{(1)} \otimes \Gamma_{qq}^{(1)}\right]_2^{-2} = \frac{3}{4}h_1^{\mathrm{qg}}(z_2)\delta(1-z_1) + \delta(1-z_1)([\mathcal{D}_0 \otimes h_1^{\mathrm{qg}}](z_2) - [h_1^{\mathrm{qg}} \otimes h_1](z_2)), \tag{E.45}$$

$$\left[\Gamma_{qq}^{(1)} \otimes \Gamma_{qq}^{(1)}\right]_2^{-1} = 0, \tag{E.46}$$

$$\left[\Gamma_{qq}^{(1)} \otimes \Gamma_{qq}^{(1)}\right]_2^{0} = 0. \tag{E.47}$$

$$h_1(x) = \frac{1+x}{2}, \tag{E.48}$$

$$h_1^{\mathrm{qg}}(x) = x^2 - x + \frac{1}{2}, \tag{E.49}$$

$$\begin{aligned}h_2(x) =& -\frac{1}{2(x-1)}\big(\log(2)x^2 + \log(2) + x^2 \\ &+ (x^2-1)\log(1-x) - (x^2+1)\log\ (x+1) - 2x + 1\big),\end{aligned} \tag{E.50}$$

$$\begin{aligned}h_2^{\mathrm{qg}}(x) =& \frac{1}{2}(-2\log(2)x^2 + 2\log(2)x - \log(2) + (-2x^2+2x-1)\ \log(1-x) \\ &+ (2x^2 - 2x + 1)\log(x+1) - 1),\end{aligned} \tag{E.51}$$

$$\begin{aligned}h_3(x,y) =& \frac{1}{2(x+1)(y+1)(x+y)^2} \\ &\times \big\{x^4(2y^2+2y+1) + 2x^3(y^2+3y+1) + 2x^2(y^4+y^3+y^2+y+1) \\ &+ 2\ xy^2(y^2+3y+1) + y^2(y^2+2y+2)\big\},\end{aligned} \tag{E.52}$$

$$\begin{aligned}h_3^{\mathrm{qg}}(x,y) =& \frac{1}{2(x+1)(x+y)^3}\big\{2x^5y^3 + 2x^4y^2(2y^2+y-1) \\ &+ x^3(4y^5+4y^4-2y^3-4\ y^2-1) \\ &+ x^2y(4y^4+8y^3-8y^2-4y-1) \\ &+ xy^2(4y^3+2y^2-4y-1) + y^3\ (2y^2-2y+1)\big\},\end{aligned} \tag{E.53}$$

$$
\begin{aligned}
h_4(x) = &\frac{1}{24(x-1)}\{6\log(2)^2x^2 + 6\log(2)^2 + 12\log(2)x^2 \\
&- 12(\log(2)\ (x^2+1) + (x-1)^2)\log(x+1) \\
&+ 12\log(1-x)(\log(2)(x^2+1) \\
&- (x^2+1)\ \log(x+1) + (x-1)^2) - 24\log(2)x \\
&+ 12\log(2) - \pi^2x^2 + 6(x^2-1)\ \log^2(1-x) \\
&+ 6(x^2+1)\log^2(x+1) + \pi^2\},
\end{aligned} \tag{E.54}
$$

$$
\begin{aligned}
h_4^{\mathrm{qg}}(x) = &\frac{1}{24}(12\log(2)^2x^2 - 12\log(2)^2x + 6\log(2)^2 - 12(2\ \log(2)x^2 \\
&- 2\log(2)x + \log(2) + 1)\log(x+1) \\
&+ 12\log(1-x)(2\ \log(2)x^2 - 2\log(2)x + \log(2) \\
&+ (-2x^2 + 2x - 1)\log(x+1) + 1) + 12\ \log(2) \\
&- 2\pi^2x^2 + 6(2x^2 - 2x + 1)\log^2(1-x) \\
&+ 6(2x^2 - 2x + 1)\ \log^2(x+1) + 2\pi^2x - \pi^2),
\end{aligned} \tag{E.55}
$$

$$
\begin{aligned}
h_5(x,y) = &\frac{1}{2(x-1)(x+1)(y-1)(y+1)(x+y)^2} \\
&\times \big\{ - 2y^3x^5 + \log(2)x^5 + \log(2)yx^5 + yx^5 - 2y^3\log\ (1-y)x^5 \\
&+ y\log(1-y)x^5 + \log(1-y)x^5 \\
&- 2y^3\log(y+1)x^5 + 4\ y^3\log(x+y)x^5 \\
&+ x^5 - 4y^4x^4 + 2\log(2)y^2x^4 + 4y^2\ x^4 + \log(2)x^4 + 3\log(2)yx^4 \\
&+ yx^4 - 4y^2\log(1-y)x^4 + 3y\ \log(1-y)x^4 \\
&+ \log(1-y)x^4 - 6y^2\log(y+1)x^4 \\
&+ 12y^2\log\ (x+y)x^4 - x^4 - 2y^5x^3 + 2\log(2)y^3x^3 + 6y^3x^3 \\
&+ 4\log(2)y^2\ x^3 - 2y^2x^3 + 2\log(2)x^3 \\
&+ 4\log(2)yx^3 - 2yx^3 - 2y^5\log\ (1-y)x^3 \\
&+ 2y^3\log(1-y)x^3 + 4y^2\log(1-y)x^3 \\
&- 4y\log(1-y)\ x^3 - 2y^5\log(y+1)x^3 \\
&- y^3\log(y+1)x^3 - y^2\log(y+1)x^3 - 7y\ \log(y+1)x^3 \\
&- \log(y+1)x^3 + 4y^5\log(x+y)x^3 \\
&+ 12y\log\ (x+y)x^3 + 2\log(2)y^4x^2 + 4y^4x^2 + 4\log(2)y^3x^2 \\
&- 2y^3x^2 + 6\ \log(2)y^2x^2 - 2y^2x^2 + 2\log(2)x^2 \\
&+ 6\log(2)yx^2 - 4y^4\ \log(1-y)x^2 + 4y^3\log(1-y)x^2 \\
&+ 2y^2\log(1-y)x^2 - 2\log\ (1-y)x^2 - 8y^4\log(y+1)x^2 \\
&- 3y^3\log(y+1)x^2 - 3y^2\log\ (y+1)x^2 \\
&- 3y\log(y+1)x^2 - 3\log(y+1)x^2 \\
&+ 12y^4\log(x+y)\ x^2 + 4\log(x+y)x^2 \\
&+ \log(2)y^5x + y^5x + 3\log(2)y^4x \\
&+ y^4x + 4\ \log(2)y^3x - 2y^3x + 6\log(2)y^2x + 4\log(2)yx
\end{aligned} \tag{E.56}
$$

$$
\begin{aligned}
&+ y^5 \log\,(1-y)x + 3y^4 \log(1-y)x - 4y^3 \log(1-y)x \\
&- y^5 \log(y+1)x - 3\,y^4 \log(y+1)x - 9y^3 \log(y+1)x \\
&- 3y^2 \log(y+1)x \\
&- 2y \log\,(y+1)x + 12y^3 \log(x+y)x + \log(2)y^5 + y^5 + \log(2)y^4 \\
&- y^4 + 2\,\log(2)y^3 + 2\log(2)y^2 - (y-1)((2y^2+2y+1)x^5 \\
&+ (4y+1)x^4 + 2y\,(y^3+y^2-2)x^3 \\
&+ (4y^3-2y-2)x^2 - y^3(y+4)x \\
&- y^2(y^2+2y+2))\log\,(1-x) - ((2y^3+y+1)x^5 \\
&+ (8y^2+3y+1)x^4 + (2y^5+y^3+3y^2+9y+1)\,x^3 \\
&+ (6y^4+y^3+3y^2+3y+3)x^2 + y(7y^2+3y+2)x \\
&+ y^2(y+3))\log\,(x+1) \\
&+ y^5 \log(1-y) + y^4 \log(1-y) - 2y^2 \log(1-y) \\
&- y^5 \log\,(y+1) - y^4 \log(y+1) - y^3 \log(y+1) \\
&- 3y^2 \log(y+1) + 4y^2 \log\,(x+y)\big\},
\end{aligned}
$$

$$
\begin{aligned}
h_5^{\mathrm{qg}}(x,y) = \frac{1}{2(x^2-1)(x+y)^3}\big\{ &- 2y^3x^6 - 2y^3\log(1-y)x^6 \\
&- 2y^3\log(y+1)x^6 + 4y^3\,\log(x+y)x^6 - 6y^2x^5 \\
&- 4y^4\log(1-y)x^5 + 2y^2\log(1-y)\,x^5 - 4y^4\log(y+1)x^5 \\
&+ 2y^2\log(y+1)x^5 + 8y^4\log(x+y)\,x^5 - 4y^2\log(x+y)x^5 \\
&+ 2\log(2)y^2x^4 + \log(2)x^4 - 2\log(2)\,yx^4 - 6yx^4 - 4y^5\log(1-y)x^4 \\
&+ 4y^3\log(1-y)x^4 + 2y^2\log\,(1-y)x^4 \\
&+ \log(1-y)x^4 - 4y^5\log(y+1)x^4 \\
&+ 4y^3\log(y+1)\,x^4 - 2y^2\log(y+1)x^4 \\
&+ 4y\log(y+1)x^4 - \log(y+1)x^4 \\
&+ 8y^5\,\log(x+y)x^4 \\
&- 8y^3\log(x+y)x^4 - 4y\log(x+y)x^4 \\
&+ x^4 + 6\,\log(2)y^3x^3 - 4\log(2)y^2x^3 + \log(2)x^3 + \log(2)yx^3 \\
&+ 3y\,x^3 - 4y^4\log(1-y)x^3 + 6y^3\log(1-y)x^3 + y\log(1-y)\,x^3 \\
&- \log(1-y)x^3 - 4y^4\log(y+1)x^3 \\
&- 6y^3\log(y+1)x^3 + 8y^2\,\log(y+1)x^3 \\
&- y\log(y+1)x^3 - 3\log(y+1)x^3 \\
&+ 8y^4\log(x+y)\,x^3 - 8y^2\log(x+y)x^3 \\
&+ 4\log(x+y)x^3 - x^3 + 6\log(2)y^4x^2 - 3\,\log(2)y^2x^2 \\
&+ 3y^2x^2 + 3\log(2)yx^2 + 3yx^2 \\
&+ 6y^4\log(1-y)\,x^2 - 4y^3\log(1-y)x^2 - 3y^2\log(1-y)x^2 \\
&- y\log(1-y)x^2 - 6\,y^4\log(y+1)x^2 \\
&- 4y^3\log(y+1)x^2 + 3y^2\log(y+1)x^2 \\
&- 7y\,\log(y+1)x^2 + 8y^3\log(x+y)x^2
\end{aligned}
\tag{E.57}
$$

$$
\begin{aligned}
&+ 8y\log(x+y)x^2 + 2\log(2)\ y^5x + 4\log(2)y^4x \\
&- 5\log(2)y^3x + y^3x + 3\log(2)y^2x \\
&+ 3y^2\ x - 2(y^3x^5 + y^2(2y^2-1)x^4 \\
&+ y(2y^4 - 2y^2 - 1)x^3 + (2y^4 - 2y^2 + 1)\ x^2 \\
&+ 2(y^3 + y)x + 2y^2)\log(x+1)x \\
&+ 2y^5\log(1-y)x + 4y^4\log\ (1-y)x - 5y^3\log(1-y)x \\
&- y^2\log(1-y)x - 2y^5\log(y+1)x - 4\ y^4\log(y+1)x \\
&+ 5y^3\log(y+1)x - 7y^2\log(y+1)x + 8y^2\log\ (x+y)x \\
&+ 2\log(2)y^5 - 2\log(2)y^4 + \log(2)y^3 + y^3 \\
&+ (-2y^3x^6 + (2\ y^2 - 4y^4)x^5 + (-4y^5 + 4y^3 + 2y^2 + 1)x^4 \\
&+ (-4y^4 + 6y^3 + y - 1)x^3 \\
&+ y(6\ y^3 - 4y^2 - 3y - 1)x^2 + y^2(2y^3 + 4y^2 - 5y - 1)x \\
&+ y^3(2y^2 - 2y + 1))\ \log(1-x) + 2y^5\log(1-y) - 2y^4\log(1-y) \\
&+ y^3\log(1-y) - 2y^5\ \log(y+1) + 2y^4\log(y+1) - y^3\log(y+1)\big\}.
\end{aligned}
$$

Appendix F

Convolutions in integrated subtraction terms

In this appendix we show that the convolution over z_a and z_b between the integrated antenna string $\boldsymbol{\mathcal{J}}_2^{(1)}$ and the partonic cross section, as in (4.82), can be shifted to become a convolution between the antenna string and the PDFs, i.e. we prove (4.84). This leads to a more stable numerical evaluation of the occurring convolution integrals than (4.82), where the integrated antenna string is convoluted with the partonic cross section. Starting from (4.82) one can obtain (4.84) just as the result of a change of variables (use $u_i = \zeta_i\, z_i$, and subsequently renaming $u_i \to \zeta_i$, $i = a, b$),

$$\begin{aligned}
&\int_0^1 \frac{\mathrm{d}\zeta_a}{\zeta_a}\frac{\mathrm{d}\zeta_b}{\zeta_b}\int_0^1 \frac{\mathrm{d}z_a}{z_a}\frac{\mathrm{d}z_b}{z_b} f_a\left(\zeta_a\right) f_b\left(\zeta_b\right) \boldsymbol{\mathcal{J}}_2^{(1)}(Q^2, z_a, z_b)\, \mathrm{d}\hat{\sigma}^{\mathrm{LO}}(z_a\zeta_a P_a, z_b\zeta_b P_b) \\
&\overset{\text{(F.2)}}{=} \int_0^1 \frac{\mathrm{d}\zeta_a}{\zeta_a}\frac{\mathrm{d}\zeta_b}{\zeta_b}\int_{\zeta_a}^1 \frac{\mathrm{d}z_a}{z_a}\int_{\zeta_b}^1 \frac{\mathrm{d}z_b}{z_b} f_a\left(\frac{\zeta_a}{z_a}\right) f_b\left(\frac{\zeta_b}{z_b}\right) \boldsymbol{\mathcal{J}}_2^{(1)}(\tilde{Q}^2, z_a, z_b)\, \mathrm{d}\hat{\sigma}^{\mathrm{LO}}(\zeta_a P_a, \zeta_b P_b), \quad \text{(F.1)}
\end{aligned}$$

where $\tilde{Q}^2 = 2\,\zeta_a\zeta_b\, P_a P_b$ and $Q^2 = z_a z_b\, \tilde{Q}^2$. However, when applying a change of variables to an integrand that contains "+"-distributions care has to be taken. The following result shows that (F.1) is still valid even though the integrated antenna string might contain "+"-distributions,

$$\begin{aligned}
&\int_0^1 \frac{\mathrm{d}\zeta_a}{\zeta_a}\int_0^1 \frac{\mathrm{d}z_a}{z_a} f_a\left(\zeta_a\right) (Q^2)^{-\epsilon} \mathcal{D}_n(1-z_a) f(z_a\zeta_a) \\
&= \int_0^1 \frac{\mathrm{d}\zeta_a}{\zeta_a}\int_0^1 \mathrm{d}z_a f_a\left(\zeta_a\right) \frac{\log^n(1-z_a)}{1-z_a}\left(\frac{(Q^2)^{-\epsilon} f(z_a\zeta_a)}{z_a} - (\zeta_a Q_b^2)^{-\epsilon} f(\zeta_a)\right) \\
&= \int_0^1 \mathrm{d}z_a \frac{\log^n(1-z_a)}{1-z_a}\Bigg(\underbrace{\frac{1}{z_a}\int_0^1 \frac{\mathrm{d}\zeta_a}{\zeta_a} f_a\left(\zeta_a\right)(Q^2)^{-\epsilon} f(z_a\zeta_a)}_{\text{use } u_a = \zeta_a z_a} - \int_0^1 \frac{\mathrm{d}\zeta_a}{\zeta_a} f_a\left(\zeta_a\right)(\zeta_a Q_b^2)^{-\epsilon} f(\zeta_a)\Bigg) \\
&= \int_0^1 \mathrm{d}z_a \frac{\log^n(1-z_a)}{1-z_a}\left(\frac{1}{z_a}\int_0^{z_a} \frac{\mathrm{d}u_a}{u_a} f_a\left(\frac{u_a}{z_a}\right)(u_a Q_b^2)^{-\epsilon} f(u_a) - \int_0^1 \frac{\mathrm{d}\zeta_a}{\zeta_a} f_a\left(\zeta_a\right)(\zeta_a Q_b^2)^{-\epsilon} f(\zeta_a)\right) \\
&= \int_0^1 \frac{\mathrm{d}z_a}{z_a}\mathcal{D}_n(1-z_a) \underbrace{\int_0^{z_a} \frac{\mathrm{d}\zeta_a}{\zeta_a}}_{=\int_0^1 \frac{\mathrm{d}\zeta_a}{\zeta_a}\theta(z_a-\zeta_a)} f_a\left(\frac{\zeta_a}{z_a}\right)(\zeta_a Q_b^2)^{-\epsilon} f(\zeta_a)
\end{aligned}$$

$$= \int_0^1 \frac{\mathrm{d}z_a}{z_a}\frac{\mathrm{d}\zeta_a}{\zeta_a}\mathcal{D}_n(1-z_a)\theta(z_a-\zeta_a)f_a\left(\frac{\zeta_a}{z_a}\right)(\zeta_a Q_b^2)^{-\epsilon}f(\zeta_a)$$
$$= \int_0^1 \frac{\mathrm{d}\zeta_a}{\zeta_a}\int_{\zeta_a}^1 \frac{\mathrm{d}z_a}{z_a}\mathcal{D}_n(1-z_a)f_a\left(\frac{\zeta_a}{z_a}\right)(\zeta_a Q_b^2)^{-\epsilon}f(\zeta_a), \tag{F.2}$$

where we use $Q_b^2 = \frac{Q^2}{z_a\zeta_a}$ and $f(x)$ is some function (e.g. the partonic cross section). This rather lengthy calculation can now be extended (getting even a bit more lengthy) to the case including also the integration over z_b and ζ_b, which then completes the proof of (F.1) for terms in the antenna string $\boldsymbol{\mathcal{J}}_2^{(1)}$ which are proportional to "+"-distributions.

Integrated antenna strings can contain regular functions, δ-distributions, and "+"-distributions of z_a, z_b. The δ- and "+"-distributions are defined on integrals over the unit interval so that we have to understand how to evaluate these on subsets $(u,1)$ of the interval $(0,1)$ in order to evaluate (F.1) numerically. For regular functions the (numerical) evaluation of the integral is trivial, where for δ- and "+"-distributions we make use of

$$\int_u^1 \mathrm{d}x\,\delta(1-x)f(x) = \int_0^1 \mathrm{d}x\,\delta(1-x)f(x) - \underbrace{\int_0^u \mathrm{d}x\,\delta(1-x)f(x)}_{=0,\text{ since } u<1}$$
$$= \int_0^1 \mathrm{d}x\,\delta(1-x)f(x), \tag{F.3}$$
$$\int_u^1 \mathrm{d}x\,g(x)\left[\frac{f(x)}{1-x}\right]_+ = \int_0^1 \mathrm{d}x\,g(x)\left[\frac{f(x)}{1-x}\right]_+ - \int_0^u \mathrm{d}x\,g(x)\left[\frac{f(x)}{1-x}\right]_+$$
$$= \int_0^1 \mathrm{d}x\,g(x)\left[\frac{f(x)}{1-x}\right]_+ - \int_0^u \mathrm{d}x\,g(x)\frac{f(x)}{1-x}, \tag{F.4}$$

where one needs

$$\int_0^u \mathrm{d}x\,g(x)\left[\frac{f(x)}{1-x}\right]_+ = \int_0^1 \mathrm{d}x\,\theta(x)\theta(u-x)g(x)\left[\frac{f(x)}{1-x}\right]_+$$
$$= \int_0^1 \mathrm{d}x\,f(x)\frac{\theta(x)\theta(u-x)g(x) - \theta(1)\overbrace{\theta(u-1)}^{=0,\text{ since } u<1}g(1)}{1-x}$$
$$= \int_0^u \mathrm{d}x\,\frac{f(x)g(x)}{1-x} \tag{F.5}$$

in the last step. Using (F.3) and (F.4) we can rewrite (4.84) to obtain a form that is suitable for numerical evaluation

$$\int_0^1 \frac{\mathrm{d}\zeta_a}{\zeta_a}\frac{\mathrm{d}\zeta_b}{\zeta_b}\int_{\zeta_a}^1 \frac{\mathrm{d}z_a}{z_a}\int_{\zeta_b}^1 \frac{\mathrm{d}z_b}{z_b}f_a\left(\frac{\zeta_a}{z_a}\right)f_b\left(\frac{\zeta_b}{z_b}\right)\boldsymbol{\mathcal{J}}_2^{(1)}(\tilde{Q}^2,z_a,z_b)\,\mathrm{d}\hat{\sigma}^{\mathrm{LO}}(\zeta_a P_a,\zeta_b P_b)$$
$$= \int_0^1 \frac{\mathrm{d}\zeta_a}{\zeta_a}\frac{\mathrm{d}\zeta_b}{\zeta_b}\Bigg[\int_0^1 \frac{\mathrm{d}z_a}{z_a}\int_0^1 \frac{\mathrm{d}z_b}{z_b}f_a\left(\frac{\zeta_a}{z_a}\right)f_b\left(\frac{\zeta_b}{z_b}\right)\boldsymbol{\mathcal{J}}_2^{(1)}(\tilde{Q}^2,z_a,z_b)\,\mathrm{d}\hat{\sigma}^{\mathrm{LO}}(\zeta_a P_a,\zeta_b P_b)$$
$$- \underbrace{\int_0^{\zeta_a} \frac{\mathrm{d}z_a}{z_a}\int_0^{\zeta_b} \frac{\mathrm{d}z_b}{z_b}f_a\left(\frac{\zeta_a}{z_a}\right)f_b\left(\frac{\zeta_b}{z_b}\right)}_{=0}\widetilde{\boldsymbol{\mathcal{J}}}_2^{(1)}(\tilde{Q}^2,z_a,z_b)\,\mathrm{d}\hat{\sigma}^{\mathrm{LO}}(\zeta_a P_a,\zeta_b P_b)\Bigg]$$

$$= \int_0^1 \frac{\mathrm{d}\zeta_a}{\zeta_a}\frac{\mathrm{d}\zeta_b}{\zeta_b}\frac{\mathrm{d}z_a}{z_a}\frac{\mathrm{d}z_b}{z_b} f_a\left(\frac{\zeta_a}{z_a}\right) f_b\left(\frac{\zeta_b}{z_b}\right) \mathbb{1}_{\zeta_a/z_a<1}\mathbb{1}_{\zeta_b/z_b<1}\boldsymbol{\mathcal{I}}_2^{(1)}(\tilde{Q}^2, z_a, z_b)\,\mathrm{d}\hat{\sigma}^{\mathrm{LO}}(\zeta_a P_a, \zeta_b P_b), \tag{F.6}$$

where the contribution in the third line vanishes because $\zeta_i/z_i > 1$, $i = a, b$, and therefore $f_i(\zeta_i/z_i) = 0$, as the probability of a parton to have a larger momentum than its mother hadron is zero. The functions $\mathbb{1}_{\zeta_a/z_a<1}\mathbb{1}_{\zeta_b/z_b<1}$ in the last line ensure that $f_a(\zeta_a/z_a) = f_b(\zeta_b/z_b) = 0$ when $\zeta_i/z_i > 1$, $i = a, b$, to prevent the evaluation of the integrand in regions where the PDFs are undefined. Even though $\widetilde{\boldsymbol{\mathcal{I}}}_2^{(1)}$ does not contribute in the final result, for completeness we mention that it is given by

$$\widetilde{\boldsymbol{\mathcal{I}}}_2^{(1)}(\tilde{Q}^2, z_a, z_b) = \boldsymbol{\mathcal{I}}_2^{(1)}(\tilde{Q}^2, z_a, z_b)\Big|_{\delta(1-z_i)\to 0,\ \mathcal{D}_n(1-z_i)\to\frac{\log^n(1-z_i)}{1-z_i}}. \tag{F.7}$$

Appendix G

Collins–Soper frame and the forward–backward asymmetry

In the partonic centre-of-mass (CM) frame the angle $\hat{\theta}$ between the quark and the lepton ℓ^- can be used to define the partonic forward and backward direction, the forward and backward cross section

$$\hat{\sigma}_F(M_{\ell\ell}) = \int_0^1 \mathrm{d}\cos\hat{\theta}\frac{\mathrm{d}\sigma}{\mathrm{d}\cos\hat{\theta}} \qquad \hat{\sigma}_B(M_{\ell\ell}) = \int_{-1}^0 \mathrm{d}\cos\hat{\theta}\frac{\mathrm{d}\sigma}{\mathrm{d}\cos\hat{\theta}}, \tag{G.1}$$

and the corresponding partonic forward–backward asymmetry $\hat{A}_{FB}$ in analogy to (6.86). If we consider DY-like Z-boson production at LO the partonic CM frame is also the RF of the Z boson such that the angle $\hat{\theta}$ is actually measured in the RF of the Z boson. At a hadron collider we do not have information about the exact partonic initial state and therefore can not determine the angle of a lepton with respect to a incoming quark in the partonic CM frame.

To tackle the problem of defining an angle θ^*—our definition below follows the proposal by Collins and Soper and we define θ^* as the so-called Collins–Soper angle—suitable to define a forward–backward asymmetry at hadron colliders, it is desirable to find a reference frame that has as many similarities as possible to the partonic CM where we defined $\hat{\theta}$, i.e. we search for a rest frame of the Z boson where at LO the definition of $\hat{\theta}$ and the angle θ^* agree. The commonly used choice is the so-called Collins–Soper (CS) frame, and the Collins–Soper angle as given in (6.88) is actually the polar angle in exactly this frame. The Collins–Soper frame is a rest frame of the final-state lepton system (or equivalently the intermediate Z boson) with the property that the z-axis is chosen so that it bisects the angle between the incoming partonic momentum $\mathbf{p}_a^{\mathrm{CS}}$ and the negative of the second incoming momentum $-\mathbf{p}_b^{\mathrm{CS}}$. Without real radiation (i.e. $p_{\mathrm{T},\ell\ell} = 0$) the leptonic rest-frame is also the partonic rest-frame and therefore the definition of $\hat{\theta}$ and θ^* agree, such that the CS frame fulfills the requirements that we formulated above in this situation. For an illustration of the CS frame and the CS angle θ^* see Fig. G.1. The remaining complication at hadron colliders is the missing information whether p_a is actually the momentum associated to a initial-state quark. Considering the shape of the PDFs, at large x it is more likely that a quark obtains a higher momentum fraction of the

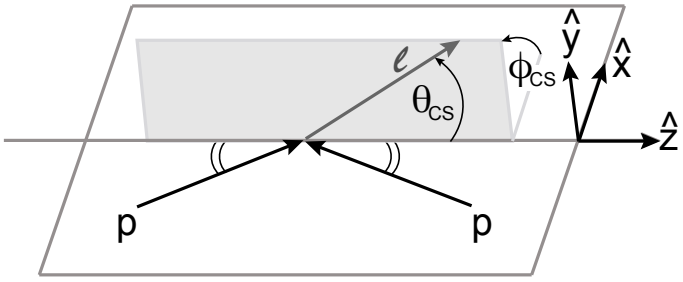

Figure G.1: Schematic illustration of the Collins–Soper frame and the Collins–Soper angle $\theta^* = \theta_{\mathrm{CS}}$. The picture has been taken from [164].

parent proton than the anti-quark. Therefore, at the LHC one extracts the direction of the inital-state quark from the boost direction of the $\ell^+\ell^-$ pair.

We now proceed with the construction of the Lorentz transformation from the LAB frame to the CS frame [47]. We start with a rotation which transforms the three-momentum of the Z boson $\mathbf{q}_Z^{\mathrm{LAB}} = \mathbf{p}_{\ell^-}^{\mathrm{LAB}} + \mathbf{p}_{\ell^+}^{\mathrm{LAB}}$ such that it has only components in the x–z plane, i.e. we rotate around the z axis with

$$\Lambda^{\mu}_{\mathrm{LAB}\to\mathrm{long},\nu} = \begin{pmatrix} 1 & 0 & 0 & 0 \\ 0 & \cos\phi_Z & \sin\phi_Z & 0 \\ 0 & -\sin\phi_Z & \cos\phi_Z & 0 \\ 0 & 0 & 0 & 1 \end{pmatrix}. \tag{G.2}$$

To calculate the angle ϕ_Z we need the decomposition into longitudinal and transverse components

$$q_Z^{\mu} = q_{\mathrm{L}}^{\mu} + q_{\mathrm{T}}^{\mu} = \begin{pmatrix} q_Z^0 \\ 0 \\ 0 \\ q_Z^3 \end{pmatrix} + \begin{pmatrix} 0 \\ q_Z^1 \\ q_Z^2 \\ 0 \end{pmatrix}, \qquad Q_{\mathrm{T}} = \sqrt{q_{\mathrm{T}}^{\mu}\, q_{\mathrm{T},\mu}}, \tag{G.3}$$

and obtain

$$\phi_Z = \begin{cases} \arccos\frac{q_{\mathrm{T},1}}{Q_{\mathrm{T}}}, & Q_{\mathrm{T}} > 0 \text{ and } q_{\mathrm{T},2} \geq 0 \\ -\arccos\frac{q_{\mathrm{T},1}}{Q_{\mathrm{T}}}, & Q_{\mathrm{T}} > 0 \text{ and } q_{\mathrm{T},2} < 0. \end{cases} \tag{G.4}$$

After the application of the rotation $\Lambda_{\mathrm{LAB}\to\mathrm{long}}$ to q_Z^{LAB} we obtain a four-vector that is an element of the t-x-z space in the "longitudinal" frame. We now want to construct a boost $\Lambda_{\mathrm{long}\to\mathrm{RF}}$ from the longitudinal frame to a rest frame of the Z boson, which we obtain

from a general Lorentz boost in direction $\mathbf{v} = \mathbf{q}_Z^{\text{long}}/q_{Z,0}^{\text{long}}$ by

$$\begin{aligned}\Lambda^{\mu}_{\text{long}\to\text{RF},\nu} &= \begin{pmatrix} \gamma & -\mathbf{v}\gamma \\ -\mathbf{v}\gamma & \mathbb{1}_3 + \frac{\mathbf{v}\cdot\mathbf{v}^{\text{T}}}{|\mathbf{v}|^2}(\gamma-1) \end{pmatrix} \\ &= \frac{1}{Q_Z}\begin{pmatrix} q_{Z,0} & -Q_{\text{T}} & 0 & -q_{Z,3} \\ -Q_{\text{T}} & Q_Z + \frac{Q_{\text{T}}}{q_{Z,0}+Q_Z} & 0 & \frac{Q_{\text{T}}q_{Z,3}}{q_{Z,0}+Q_Z} \\ 0 & 0 & Q_Z & 0 \\ -q_{Z,3} & \frac{Q_{\text{T}}q_{Z,3}}{q_{Z,0}+Q_Z} & 0 & Q_Z + \frac{Q_{\text{T}}}{q_{Z,0}+Q_Z} \end{pmatrix}\end{aligned} \tag{G.5}$$

with $Q_Z = \sqrt{q_Z^2}$, $\gamma = q_{Z,0}^{\text{long}}/Q_Z$, and all entries in the last matrix have to be understood in the longitudinal frame. The last step is to rotate from the RF of the Z boson to the CS frame, where the z-axis bisects the momenta of the incoming partons p_a^{CS} and $-p_b^{\text{CS}}$. After the application of the first rotation and $\Lambda_{\text{LAB}\to\text{long}}$ and the subsequent boost $\Lambda_{\text{long}\to\text{RF}}$ to a RF of the Z boson we obtain momenta of the form

$$q_Z^{\text{RF},\mu} = \begin{pmatrix} q_Z^{\text{RF},0} \\ 0 \\ 0 \\ 0 \end{pmatrix}, \qquad p_{\ell^\pm}^{\text{RF},\mu} = \begin{pmatrix} p_{\ell^\pm}^{\text{RF},0} \\ p_{\ell^\pm}^{\text{RF},1} \\ 0 \\ p_{\ell^\pm}^{\text{RF},3} \end{pmatrix}, \tag{G.6}$$

with no non-vanishing components in the y-direction in the RF. Note that $p_a^{\text{RF}} + p_b^{\text{RF}}$ coincides with q_Z^{RF} without IS radiation. It is therefore reasonable to rotate around the y-axis by an angle α to get to the CS frame,

$$\Lambda^{\mu}_{\text{RF}\to\text{CS},\nu} = \begin{pmatrix} 1 & 0 & 0 & 0 \\ 0 & \cos\alpha & 0 & \sin\alpha \\ 0 & 0 & 1 & 0 \\ 0 & -\sin\alpha & 0 & \cos\alpha \end{pmatrix}, \tag{G.7}$$

where we have to choose α such that the z-axis bisects the momenta p_a^{CS} and p_b^{CS}. This leads to the condition

$$\frac{\mathbf{p}_a^{\text{CS}}\mathbf{e}_3^{\text{CS}}}{|\mathbf{p}_a^{\text{CS}}|} = \cos\left(\angle(\mathbf{p}_a^{\text{CS}}, \mathbf{e}_3^{\text{CS}})\right) \overset{!}{=} \cos\left(\angle(\mathbf{p}_b^{\text{CS}}, \mathbf{e}_3^{\text{CS}})\right) = \frac{-\mathbf{p}_b^{\text{CS}}\mathbf{e}_3^{\text{CS}}}{|\mathbf{p}_b^{\text{CS}}|}. \tag{G.8}$$

By writing the last equation in terms of momenta in the RF of the Z boson constructed above

$$\frac{\Lambda^3_{\text{RF}\to\text{CS},\mu}\, p_a^{\text{RF},\mu}}{|\mathbf{p}_a^{\text{RF}}|} \overset{!}{=} \frac{-\Lambda^3_{\text{RF}\to\text{CS},\mu}\, p_b^{\text{RF},\mu}}{|\mathbf{p}_b^{\text{RF}}|} \tag{G.9}$$

we can obtain a quadratic equation in $x = \cos\alpha$

$$x \cdot c_{a,1} - \sqrt{1-x^2}\cdot c_{a,2} \overset{!}{=} -x\cdot c_{b,1} + \sqrt{1-x^2}\cdot c_{b,2} \tag{G.10}$$

with the coefficients ($i = a, b$)

$$c_{i,1} = \frac{p_i^{\mathrm{RF},3}}{|\mathbf{p}_i^{\mathrm{RF}}|}, \tag{G.11}$$

$$c_{i,2} = \frac{p_i^{\mathrm{RF},1}}{|\mathbf{p}_i^{\mathrm{RF}}|}. \tag{G.12}$$

By solving (G.10) we can determine the required rotation angle α. The complete transformation from the LAB frame to the CS frame is now given by

$$\Lambda^{\mu}_{\mathrm{LAB}\to\mathrm{CS},\nu} = \Lambda^{\mu}_{\mathrm{RF}\to\mathrm{CS},\sigma}\, \Lambda^{\sigma}_{\mathrm{long}\to\mathrm{RF},\eta}\, \Lambda^{\eta}_{\mathrm{LAB}\to\mathrm{long},\nu}. \tag{G.13}$$

As the CS frame is a special RF of the Z boson, the lepton momenta in the FS (without real radiation) have to be back to back and both get an equal share of the energy of the intermediate Z boson. Considering that the momenta in (G.6) are only rotated around the y-axis to get to the CS frame we have

$$p_{\ell^\pm}^{\mathrm{CS},\mu} = \frac{M_{\ell\ell}}{2} \begin{pmatrix} 1 \\ \pm \sin\theta^* \\ 0 \\ \pm \cos\theta^* \end{pmatrix}. \tag{G.14}$$

Therefore, the CS angle θ^* can be determined from the FS lepton momenta in the CS frame by

$$\cos\theta^* = \frac{p_{\ell^-}^{\mathrm{CS},3}}{M_{\ell\ell}/2}. \tag{G.15}$$

The last equation can be used to numerically check the validity of (6.88).

Bibliography

[1] S. L. Glashow, *Partial-symmetries of weak interactions*, *Nuclear Physics* **22** (1961) 579–588.

[2] I. J. Glashow, S. L. and L. Maiani, *Weak interactions with lepton-hadron symmetry*, *Physical review D* **2** (1970) 1285.

[3] A. Salam, *Elementary particle theory*, *Almyuist and Wiksell, Stockholm* (1968).

[4] S. Weinberg, *A model of leptons*, *Physical Review Letters* **19** (1967).

[5] G. Arnison, et al., *Experimental observation of isolated large transverse energy electrons with associated missing energy at s= 540 GeV*, *Physics Letters B* **122** (1983) 103–116.

[6] M. Banner, et al., *Observation of single isolated electrons of high transverse momentum in events with missing transverse energy at the CERN pp collider*, *Physics Letters B* **122** (1983) 476–485.

[7] G. Arnison, et al., *Experimental observation of lepton pairs of invariant mass around* $95 GeV/c^2$ *at the CERN SPS collider*, *Physics Letters B* **126** (1983) 398–410.

[8] P. Bagnaia, et al., *Evidence for* $Z^0 \to e^+e^-$ *at the CERN* $\bar{p}p$ *collider*, *Phys. Lett. B* **129** (1983) 130–140.

[9] **ATLAS** Collaboration, *Observation of a new particle in the search for the Standard Model Higgs boson with the ATLAS detector at the LHC*, *arXiv preprint arXiv:1207.7214* (2012).

[10] S. Chatrchyan, et al., *Observation of a new boson at a mass of 125 GeV with the CMS experiment at the LHC*, *Physics Letters, Section B: Nuclear, Elementary Particle and High-Energy Physics* **716** (2012) 30–61.

[11] **TeV4LHC Working Group** Collaboration, S. Abdullin et al., *Tevatron-for-LHC Report: Preparations for Discoveries*, 8, 2006. `hep-ph/0608322`.

[12] **TeV4LHC-Top, Electroweak Working Group** Collaboration, C. Gerber et al., *Tevatron-for-LHC Report: Top and Electroweak Physics*, 5, 2007. `arXiv:0705.3251`.

[13] M. Dittmar, F. Pauss, and D. Zurcher, *Towards a precise parton luminosity determination at the CERN LHC*, *Phys. Rev. D* **56** (1997) 7284–7290, [hep-ex/9705004].

[14] V. A. Khoze, A. D. Martin, R. Orava, and M. Ryskin, *Luminosity monitors at the LHC*, *Eur. Phys. J. C* **19** (2001) 313–322, [hep-ph/0010163].

[15] M. Boonekamp, F. Chevallier, C. Royon, and L. Schoeffel, *Understanding the Structure of the Proton: From HERA and Tevatron to LHC*, *Acta Phys. Polon. B* **40** (2009) 2239–2321, [arXiv:0902.1678].

[16] S. Haywood et al., *Electroweak physics*, in *CERN Workshop on Standard Model Physics (and more) at the LHC (Final Plenary Meeting)*, pp. 117–230, 10, 1999. hep-ph/0003275.

[17] **ATLAS** Collaboration, *Measurement of the effective leptonic weak mixing angle using electron and muon pairs from Z-boson decay in the ATLAS experiment at* $\sqrt{s} = 8$ *TeV*, .

[18] U. Baur, S. Keller, and W. Sakumoto, *QED radiative corrections to Z boson production and the forward backward asymmetry at hadron colliders*, *Phys. Rev. D* **57** (1998) 199–215, [hep-ph/9707301].

[19] V. Zykunov, *Electroweak corrections to the observables of W boson production at RHIC*, *Eur. Phys. J. direct* **3** (2001) 9, [hep-ph/0107059].

[20] U. Baur et al., *Electroweak radiative corrections to neutral current Drell-Yan processes at hadron colliders*, *Phys. Rev. D* **65** (2002) 033007, [hep-ph/0108274].

[21] S. Dittmaier and M. Krämer, *Electroweak radiative corrections to W boson production at hadron colliders*, *Phys. Rev. D* **65** (2002) 073007, [hep-ph/0109062].

[22] U. Baur and D. Wackeroth, *Electroweak radiative corrections to* $p\bar{p} \to W^{\pm} \to \ell^{\pm}\nu$ *beyond the pole approximation*, *Phys. Rev. D* **70** (2004) 073015, [hep-ph/0405191].

[23] A. Arbuzov et al., *One-loop corrections to the Drell-Yan process in SANC. I. The Charged current case*, *Eur. Phys. J. C* **46** (2006) 407–412, [hep-ph/0506110]. [Erratum: Eur.Phys.J.C 50, 505 (2007)].

[24] C. Carloni Calame, G. Montagna, O. Nicrosini, and A. Vicini, *Precision electroweak calculation of the charged current Drell-Yan process*, *JHEP* **12** (2006) 016, [hep-ph/0609170].

[25] V. Zykunov, *Weak radiative corrections to Drell-Yan process for large invariant mass of di-lepton pair*, *Phys. Rev. D* **75** (2007) 073019, [hep-ph/0509315].

[26] C. Carloni Calame, G. Montagna, O. Nicrosini, and A. Vicini, *Precision electroweak calculation of the production of a high transverse-momentum lepton pair at hadron colliders*, *JHEP* **10** (2007) 109, [arXiv:0710.1722].

[27] A. Arbuzov, et al., *One-loop corrections to the Drell–Yan process in SANC. (II). The Neutral current case*, *Eur. Phys. J. C* **54** (2008) 451–460, [arXiv:0711.0625].

[28] S. Brensing, S. Dittmaier, M. Krämer, and A. Mück, *Radiative corrections to W^- boson hadroproduction: Higher-order electroweak and supersymmetric effects*, *Phys. Rev. D* **77** (2008) 073006, [arXiv:0710.3309].

[29] S. Dittmaier and M. Huber, *Radiative corrections to the neutral-current Drell-Yan process in the Standard Model and its minimal supersymmetric extension*, *JHEP* **01** (2010) 060, [arXiv:0911.2329].

[30] R. Boughezal, Y. Li, and F. Petriello, *Disentangling radiative corrections using the high-mass Drell-Yan process at the LHC*, *Phys. Rev. D* **89** (2014) 034030, [arXiv:1312.3972].

[31] W. Placzek and S. Jadach, *Multiphoton radiation in leptonic W boson decays*, *Eur. Phys. J. C* **29** (2003) 325–339, [hep-ph/0302065].

[32] C. Carloni Calame, G. Montagna, O. Nicrosini, and M. Treccani, *Higher order QED corrections to W boson mass determination at hadron colliders*, *Phys. Rev. D* **69** (2004) 037301, [hep-ph/0303102].

[33] C. Duhr, F. Dulat, and B. Mistlberger, *Charged Current Drell-Yan Production at N^3LO*, arXiv:2007.13313.

[34] R. Hamberg, W. van Neerven, and T. Matsuura, *A complete calculation of the order α_s^2 correction to the Drell-Yan K factor*, *Nucl. Phys. B* **359** (1991) 343–405. [Erratum: Nucl.Phys.B 644, 403–404 (2002)].

[35] R. Gavin, Y. Li, F. Petriello, and S. Quackenbush, *W Physics at the LHC with FEWZ 2.1*, *Comput. Phys. Commun.* **184** (2013) 208–214, [arXiv:1201.5896].

[36] R. Gavin, Y. Li, F. Petriello, and S. Quackenbush, *FEWZ 2.0: A code for hadronic Z production at next-to-next-to-leading order*, *Comput. Phys. Commun.* **182** (2011) 2388–2403, [arXiv:1011.3540].

[37] S. Catani et al., *Vector boson production at hadron colliders: a fully exclusive QCD calculation at NNLO*, *Phys. Rev. Lett.* **103** (2009) 082001, [arXiv:0903.2120].

[38] K. Melnikov and F. Petriello, *Electroweak gauge boson production at hadron colliders through $O(\alpha_s^2)$*, *Phys. Rev. D* **74** (2006) 114017, [hep-ph/0609070].

[39] K. Melnikov and F. Petriello, *The W boson production cross section at the LHC through $O(\alpha_s^2)$*, *Phys. Rev. Lett.* **96** (2006) 231803, [hep-ph/0603182].

[40] C. Anastasiou, L. J. Dixon, K. Melnikov, and F. Petriello, *High precision QCD at hadron colliders: Electroweak gauge boson rapidity distributions at NNLO*, *Phys. Rev. D* **69** (2004) 094008, [hep-ph/0312266].

[41] R. V. Harlander and W. B. Kilgore, *Next-to-next-to-leading order Higgs production at hadron colliders*, *Phys. Rev. Lett.* **88** (2002) 201801, [hep-ph/0201206].

[42] T. Ahmed, M. Mahakhud, N. Rana, and V. Ravindran, *Drell-Yan Production at Threshold to Third Order in QCD*, *Phys. Rev. Lett.* **113** (2014) 112002, [arXiv:1404.0366].

[43] S. Catani et al., *Threshold resummation at N^3LL accuracy and soft-virtual cross sections at N^3LO*, *Nucl. Phys. B* **888** (2014) 75–91, [arXiv:1405.4827].

[44] M. Guzzi, P. M. Nadolsky, and B. Wang, *Nonperturbative contributions to a resummed leptonic angular distribution in inclusive neutral vector boson production*, *Phys. Rev. D* **90** (2014) 014030, [arXiv:1309.1393].

[45] A. Kulesza and W. Stirling, *Soft gluon resummation in transverse momentum space for electroweak boson production at hadron colliders*, *Eur. Phys. J. C* **20** (2001) 349–356, [hep-ph/0103089].

[46] S. Catani, D. de Florian, G. Ferrera, and M. Grazzini, *Vector boson production at hadron colliders: transverse-momentum resummation and leptonic decay*, *JHEP* **12** (2015) 047, [arXiv:1507.06937].

[47] C. Balazs and C. Yuan, *Soft gluon effects on lepton pairs at hadron colliders*, *Phys. Rev. D* **56** (1997) 5558–5583, [hep-ph/9704258].

[48] F. Landry, R. Brock, P. M. Nadolsky, and C. Yuan, *Tevatron Run-1 Z boson data and Collins-Soper-Sterman resummation formalism*, *Phys. Rev. D* **67** (2003) 073016, [hep-ph/0212159].

[49] G. Bozzi et al., *Production of Drell-Yan lepton pairs in hadron collisions: Transverse-momentum resummation at next-to-next-to-leading logarithmic accuracy*, *Phys. Lett. B* **696** (2011) 207–213, [arXiv:1007.2351].

[50] S. Mantry and F. Petriello, *Transverse Momentum Distributions from Effective Field Theory with Numerical Results*, *Phys. Rev. D* **83** (2011) 053007, [arXiv:1007.3773].

[51] T. Becher, M. Neubert, and D. Wilhelm, *Electroweak Gauge-Boson Production at Small q_T: Infrared Safety from the Collinear Anomaly*, *JHEP* **02** (2012) 124, [arXiv:1109.6027].

[52] W. Bizoń, et al., *Fiducial distributions in Higgs and Drell-Yan production at N^3LL+NNLO*, *JHEP* **12** (2018) 132, [arXiv:1805.05916].

[53] W. Bizon, et al., *The transverse momentum spectrum of weak gauge bosons at N ^{3} LL + NNLO*, *Eur. Phys. J. C* **79** (2019) 868, [arXiv:1905.05171].

[54] **ATLAS** Collaboration, N. Besson, M. Boonekamp, E. Klinkby, T. Petersen, and S. Mehlhase, *Re-evaluation of the LHC potential for the measurement of Mw*, *Eur. Phys. J. C* **57** (2008) 627–651, [arXiv:0805.2093].

[55] S. Dittmaier, A. Huss, and C. Schwinn, *Mixed QCD-electroweak $O(\alpha_s\alpha)$ corrections to Drell-Yan processes in the resonance region: pole approximation and non-factorizable corrections*, *Nucl. Phys. B* **885** (2014) 318–372, [arXiv:1403.3216].

[56] S. Dittmaier, A. Huss, and C. Schwinn, *Dominant mixed QCD-electroweak $O(\alpha_s\alpha)$ corrections to Drell–Yan processes in the resonance region*, *Nucl. Phys. B* **904** (2016) 216–252, [arXiv:1511.08016].

[57] R. Bonciani, et al., *Mixed Strong-Electroweak Corrections to the Drell-Yan Process*, *Phys. Rev. Lett.* **128** (2022) 012002, [arXiv:2106.11953].

[58] L. Buonocore, M. Grazzini, S. Kallweit, C. Savoini, and F. Tramontano, *Mixed QCD-EW corrections to $pp \to \ell\nu_\ell + X$ at the LHC*, *Phys. Rev. D* **103** (2021) 114012, [arXiv:2102.12539].

[59] A. Denner, S. Dittmaier, M. Roth, and L. H. Wieders, *Electroweak corrections to charged-current $e^+e^- \to 4$ fermion processes: Technical details and further results*, *Nucl. Phys. B* **724** (2005) 247–294, [hep-ph/0505042]. [Erratum: Nucl.Phys.B 854, 504–507 (2012)].

[60] A. Denner and S. Dittmaier, *Electroweak Radiative Corrections for Collider Physics*, *Phys. Rept.* **864** (2020) 1–163, [arXiv:1912.06823].

[61] O. W. Greenberg, *Spin and unitary-spin independence in a paraquark model of baryons and mesons*, *Physical Review Letters* **13** (1964) 598.

[62] M. Han and Y. Nambu, *Three-triplet model with double $SU(3)$ symmetry*, *Physical Review* **139** (1965) B1006.

[63] H. Fritzsch, M. Gell-Mann, and H. Leutwyler, *Advantages of the color octet gluon picture*, in *Murray Gell-Mann: Selected Papers*, pp. 262–265. World Scientific, 2010.

[64] L. D. Faddeev and V. N. Popov, *Feynman diagrams for the yang-mills field*, *Physics Letters B* **25** (1967) 29–30.

[65] G. Hooft, *Renormalizable lagrangians for massive yang-mills fields*, *Nuclear Physics B* **35** (1971) 167 – 188.

[66] K. Aoki, Z. Hioki, R. Kawabe, M. Konuma, and T. Muta, *ELECTROWEAK RADIATIVE CORRECTIONS TO HIGH-ENERGY νe SCATTERINGS*, *Prog. Theor. Phys.* **65** (1981) 1001.

[67] D. Ross and J. Taylor, *Renormalization of a unified theory of weak and electromagnetic interactions*, *Nuclear Physics B* **51** (1973) 125 – 144.

[68] K. I. Aoki, Z. Hioki, M. Konuma, R. Kawabe, and T. Muta, *Electroweak Theory. Framework of On-Shell Renormalization and Study of Higher Order Effects*, *Prog. Theor. Phys. Suppl.* **73** (1982) 1–225.

[69] A. Denner, *Techniques for calculation of electroweak radiative corrections at the one loop level and results for W physics at LEP-200*, *Fortsch. Phys.* **41** (1993) 307–420, [arXiv:0709.1075].

[70] G. 't Hooft and M. Veltman, *Regularization and renormalization of gauge fields*, *Nuclear Physics B* **44** (1972) 189 – 213.

[71] C. Bollini and J. Giambiagi, *Nuovo cim. b12 (1972) 20*, *Lett. Nuovo Cim* **4** (1972) 289.

[72] A. Denner, *Techniques for the Calculation of Electroweak Radiative Corrections at the One-Loop Level and Results for W-physics at LEP 200*, *Fortschritte der Physik* **41** (1993) 307–420.

[73] R. K. Ellis, W. J. Stirling, and B. R. Webber, *QCD and collider physics*. Cambridge university press, 2003.

[74] R. K. Ellis, W. J. Stirling, and B. R. Webber, *QCD and collider physics*, vol. 8. Cambridge University Press, 2, 2011.

[75] A. Sirlin, *Radiative corrections in the* $\mathrm{SU}(2)_L \times \mathrm{U}(1)$ *theory: A simple renormalization framework*, *Physical Review D* **22** (Aug, 1980) 971–981.

[76] A. Sirlin, *Theoretical considerations concerning the Z0 mass*, *Phys. Rev. Lett.* **67** (1991) 2127–2130.

[77] R. G. Stuart, *Gauge invariance, analyticity and physical observables at the Z0 resonance*, *Phys. Lett. B* **262** (1991) 113–119.

[78] P. Gambino and P. A. Grassi, *The Nielsen identities of the SM and the definition of mass*, *Phys. Rev. D* **62** (2000) 076002, [hep-ph/9907254].

[79] A. Denner, S. Dittmaier, M. Roth, and D. Wackeroth, *Predictions for all processes* $e^+e^- \to 4$ *fermions* $+ \gamma$, *Nucl. Phys. B* **560** (1999) 33–65, [hep-ph/9904472].

[80] A. Denner and S. Dittmaier, *The Complex-mass scheme for perturbative calculations with unstable particles*, *Nucl. Phys. B Proc. Suppl.* **160** (2006) 22–26, [hep-ph/0605312].

[81] G. Passarino, C. Sturm, and S. Uccirati, *Higgs Pseudo-Observables, Second Riemann Sheet and All That*, *Nucl. Phys. B* **834** (2010) 77–115, [arXiv:1001.3360].

[82] J. R. Currie, *Antenna Subtraction for NNLO Calculations at the LHC*. PhD thesis, Durham U. (main), 2012.

[83] L. D. Landau, *On analytic properties of vertex parts in quantum field theory*, *Nucl. Phys.* **13** (1959) 181–192.

[84] A. Gehrmann-De Ridder, T. Gehrmann, and E. W. N. Glover, *Antenna subtraction at NNLO*, *JHEP* **09** (2005) 056, [hep-ph/0505111].

[85] B. W. Harris and J. F. Owens, *The Two cutoff phase space slicing method*, *Phys. Rev. D* **65** (2002) 094032, [hep-ph/0102128].

[86] U. Baur, S. Keller, and D. Wackeroth, *Electroweak radiative corrections to W boson production in hadronic collisions*, *Phys. Rev. D* **59** (1999) 013002, [hep-ph/9807417].

[87] G. Altarelli and G. Parisi, *Asymptotic Freedom in Parton Language*, *Nucl. Phys. B* **126** (1977) 298–318.

[88] S. Catani, *The Singular behavior of QCD amplitudes at two loop order*, *Phys. Lett. B* **427** (1998) 161–171, [hep-ph/9802439].

[89] Z. Bern, V. Del Duca, and C. R. Schmidt, *The Infrared behavior of one loop gluon amplitudes at next-to-next-to-leading order*, *Phys. Lett. B* **445** (1998) 168–177, [hep-ph/9810409].

[90] F. A. Berends and W. T. Giele, *Multiple Soft Gluon Radiation in Parton Processes*, *Nucl. Phys. B* **313** (1989) 595–633.

[91] J. M. Campbell and E. W. N. Glover, *Double unresolved approximations to multiparton scattering amplitudes*, *Nucl. Phys. B* **527** (1998) 264–288, [hep-ph/9710255].

[92] R. P. Feynman, *Very high-energy collisions of hadrons*, *Phys. Rev. Lett.* **23** (1969) 1415–1417.

[93] J. D. Bjorken and E. A. Paschos, *Inelastic Electron Proton and gamma Proton Scattering, and the Structure of the Nucleon*, *Phys. Rev.* **185** (1969) 1975–1982.

[94] C. A. and K. Melnikov, *Higgs boson production at hadron colliders in NNLO QCD*, *Nucl. Phys. B* **646** (2002) 220–256, [hep-ph/0207004].

[95] A. Gehrmann-De Ridder, E. W. N. Glover, and J. Pires, *Real-Virtual corrections for gluon scattering at NNLO*, *JHEP* **02** (2012) 141, [arXiv:1112.3613].

[96] J. Currie, E. W. N. Glover, and S. Wells, *Infrared Structure at NNLO Using Antenna Subtraction*, *JHEP* **04** (2013) 066, [arXiv:1301.4693].

[97] T. Kinoshita, *Mass singularities of Feynman amplitudes*, *J. Math. Phys.* **3** (1962) 650–677.

[98] T. D. Lee and M. Nauenberg, *Degenerate Systems and Mass Singularities*, *Phys. Rev.* **133** (1964) B1549–B1562.

[99] R. K. Ellis, H. Georgi, M. Machacek, H. D. Politzer, and G. G. Ross, *Factorization and the Parton Model in QCD*, *Phys. Lett. B* **78** (1978) 281–284.

[100] D. A. Kosower, *Antenna factorization of gauge theory amplitudes*, *Phys. Rev. D* **57** (1998) 5410–5416, [hep-ph/9710213].

[101] A. Gehrmann-De Ridder, T. Gehrmann, E. W. N. Glover, and G. Heinrich, *Infrared structure of $e^+e^- \to 3$ jets at NNLO*, *JHEP* **11** (2007) 058, [arXiv:0710.0346].

[102] D. A. Kosower, *Multiple singular emission in gauge theories*, *Phys. Rev. D* **67** (2003) 116003, [hep-ph/0212097].

[103] A. Daleo, T. Gehrmann, and D. Maitre, *Antenna subtraction with hadronic initial states*, *JHEP* **04** (2007) 016, [hep-ph/0612257].

[104] A. Gehrmann-De Ridder, T. Gehrmann, and E. W. N. Glover, *Infrared structure of $e^+e^- \to 2$ jets at NNLO*, *Nucl. Phys. B* **691** (2004) 195–222, [hep-ph/0403057].

[105] A. Gehrmann-De Ridder, T. Gehrmann, and E. W. N. Glover, *Quark-gluon antenna functions from neutralino decay*, *Phys. Lett. B* **612** (2005) 36–48, [hep-ph/0501291].

[106] A. Gehrmann-De Ridder, T. Gehrmann, and E. W. N. Glover, *Gluon-gluon antenna functions from Higgs boson decay*, *Phys. Lett. B* **612** (2005) 49–60, [hep-ph/0502110].

[107] A. Gehrmann-De Ridder, T. Gehrmann, and G. Heinrich, *Four particle phase space integrals in massless QCD*, *Nucl. Phys. B* **682** (2004) 265–288, [hep-ph/0311276].

[108] A. Daleo, A. Gehrmann-De Ridder, T. Gehrmann, and G. Luisoni, *Antenna subtraction at NNLO with hadronic initial states: initial-final configurations*, *JHEP* **01** (2010) 118, [arXiv:0912.0374].

[109] A. Gehrmann-De Ridder, T. Gehrmann, and M. Ritzmann, *Antenna subtraction at NNLO with hadronic initial states: double real initial-initial configurations*, *JHEP* **10** (2012) 047, [arXiv:1207.5779].

[110] R. Boughezal, A. Gehrmann-De Ridder, and M. Ritzmann, *Antenna subtraction at NNLO with hadronic initial states: double real radiation for initial-initial configurations with two quark flavours*, *JHEP* **02** (2011) 098, [arXiv:1011.6631].

[111] E. W. N. Glover and J. Pires, *Antenna subtraction for gluon scattering at NNLO*, *JHEP* **06** (2010) 096, [arXiv:1003.2824].

[112] T. Gehrmann and P. F. Monni, *Antenna subtraction at NNLO with hadronic initial states: real-virtual initial-initial configurations*, *JHEP* **12** (2011) 049, [arXiv:1107.4037].

[113] S. Weinzierl, *NNLO corrections to 3-jet observables in electron-positron annihilation*, *Phys. Rev. Lett.* **101** (2008) 162001, [arXiv:0807.3241].

[114] A. Gehrmann-De Ridder, T. Gehrmann, E. W. N. Glover, and J. Pires, *Double Virtual corrections for gluon scattering at NNLO*, *JHEP* **02** (2013) 026, [arXiv:1211.2710].

[115] S. Dittmaier, T. Schmidt, and J. Schwarz, *Mixed NNLO QCD×electroweak corrections of $\mathcal{O}(N_f\alpha_s\alpha)$ to single-W/Z production at the LHC*, *JHEP* **12** (2020) 201, [arXiv:2009.02229].

[116] A. Arbuzov and R. Sadykov, *Inverse bremsstrahlung contributions to Drell-Yan like processes*, *J. Exp. Theor. Phys.* **106** (2008) 488–494, [arXiv:0707.0423].

[117] S. Dittmaier, *Electric charge renormalization to all orders*, *Phys. Rev. D* **103** (2021) 053006, [arXiv:2101.05154].

[118] A. Djouadi and P. Gambino, *Electroweak gauge bosons selfenergies: Complete QCD corrections*, *Phys. Rev. D* **49** (1994) 3499–3511, [hep-ph/9309298]. [Erratum: Phys.Rev.D 53, 4111 (1996)].

[119] A. B. Goncharov, *Multiple polylogarithms, cyclotomy and modular complexes*, *Math. Res. Lett.* **5** (1998) 497–516, [arXiv:1105.2076].

[120] A. B. Goncharov, M. Spradlin, C. Vergu, and A. Volovich, *Classical Polylogarithms for Amplitudes and Wilson Loops*, *Phys. Rev. Lett.* **105** (2010) 151605, [arXiv:1006.5703].

[121] C. W. Bauer, A. Frink, and R. Kreckel, *Introduction to the GiNaC framework for symbolic computation within the C++ programming language*, *J. Symb. Comput.* **33** (2002) 1–12, [cs/0004015].

[122] S. Buehler and C. Duhr, *CHAPLIN - Complex Harmonic Polylogarithms in Fortran*, *Comput. Phys. Commun.* **185** (2014) 2703–2713, [arXiv:1106.5739].

[123] P. Maierhöfer, J. Usovitsch, and P. Uwer, *Kira—A Feynman integral reduction program*, *Comput. Phys. Commun.* **230** (2018) 99–112, [arXiv:1705.05610].

[124] P. Maierhöfer and J. Usovitsch, *Kira 1.2 Release Notes*, arXiv:1812.01491.

[125] W. Tschernow, *Evaluation of scalar Feynman integrals via differential equations*, Master's thesis, Freiburg U., 2016.

[126] A. Djouadi and C. Verzegnassi, *Virtual Very Heavy Top Effects in LEP / SLC Precision Measurements*, *Phys. Lett. B* **195** (1987) 265–271.

[127] A. Djouadi, $O(\alpha\alpha_s)$ *Vacuum Polarization Functions of the Standard Model Gauge Bosons*, *Nuovo Cim. A* **100** (1988) 357.

[128] T. Chang, K. Gaemers, and W. van Neerven, *QCD Corrections to the Mass and Width of the Intermediate Vector Bosons*, *Nucl. Phys. B* **202** (1982) 407–436.

[129] B. A. Kniehl, J. H. Kühn, and R. Stuart, *QCD corrections, virtual heavy quark effects and electroweak precision measurements*, *Phys. Lett. B* **214** (1988) 621–629.

[130] B. A. Kniehl, *Two Loop Corrections to the Vacuum Polarizations in Perturbative QCD*, *Nucl. Phys. B* **347** (1990) 86–104.

[131] **Particle Data Group** Collaboration, J. Beringer et al., *Review of Particle Physics (RPP)*, *Phys. Rev. D* **86** (2012) 010001.

[132] R. D. Ball et al., *Parton distributions with LHC data*, *Nucl. Phys. B* **867** (2013) 244–289, [arXiv:1207.1303].

[133] **NNPDF** Collaboration, R. D. Ball et al., *Parton distributions with QED corrections*, *Nucl. Phys. B* **877** (2013) 290–320, [arXiv:1308.0598].

[134] S. Dittmaier, A. Huss, and J. Schwarz, *Mixed NNLO QCD×electroweak corrections to single-Z production in pole approximation: differential distributions and forward–backward asymmetry*, in preparation.

[135] P. A. Grassi, B. A. Kniehl, and A. Sirlin, *Width and partial widths of unstable particles in the light of the Nielsen identities*, *Phys. Rev. D* **65** (2002) 085001, [hep-ph/0109228].

[136] A. Aeppli, F. Cuypers, and G. J. van Oldenborgh, *O(Gamma) corrections to W pair production in e^+e^- and gamma gamma collisions*, *Phys. Lett. B* **314** (1993) 413–420, [hep-ph/9303236].

[137] H. G. J. Veltman, *Mass and width of unstable gauge bosons*, *Z. Phys. C* **62** (1994) 35–52.

[138] A. Denner, S. Dittmaier, and M. Roth, *Nonfactorizable photonic corrections to $e^+e^- \to WW \to$four fermions*, *Nucl. Phys. B* **519** (1998) 39–84, [hep-ph/9710521].

[139] D. Wackeroth and W. Hollik, *Electroweak radiative corrections to resonant charged gauge boson production*, *Phys. Rev. D* **55** (1997) 6788–6818, [hep-ph/9606398].

[140] D. Wackeroth and W. Hollik, *Electroweak radiative corrections to resonant charged gauge boson production*, *Physical Review D* **55** (1997) 6788.

[141] A. Kotikov, J. H. Kuhn, and O. Veretin, *Two-Loop Formfactors in Theories with Mass Gap and Z-Boson Production*, *Nucl. Phys. B* **788** (2008) 47–62, [hep-ph/0703013].

[142] L. Naterop, A. Signer, and Y. Ulrich, *handyG —Rapid numerical evaluation of generalised polylogarithms in Fortran*, *Comput. Phys. Commun.* **253** (2020) 107165, [arXiv:1909.01656].

[143] M. Huber, *Radiative corrections to the neutral-current Drell-Yan process*. PhD thesis, Freiburg U., 2010.

[144] E. Remiddi and J. Vermaseren, *Harmonic polylogarithms*, *Int. J. Mod. Phys. A* **15** (2000) 725–754, [hep-ph/9905237].

[145] M. Höschele, J. Hoff, A. Pak, M. Steinhauser, and T. Ueda, *MT: A Mathematica package to compute convolutions*, *Comput. Phys. Commun.* **185** (2014) 528–539, [arXiv:1307.6925].

[146] J. Küblbeck, M. Böhm, and A. Denner, *Feyn Arts: Computer Algebraic Generation of Feynman Graphs and Amplitudes*, *Comput. Phys. Commun.* **60** (1990) 165–180.

[147] T. Hahn, *Generating Feynman diagrams and amplitudes with FeynArts 3*, *Comput. Phys. Commun.* **140** (2001) 418–431, [hep-ph/0012260].

[148] T. Hahn and M. Perez-Victoria, *Automated one-loop calculations in four and d dimensions*, *Computer Physics Communications* **118** (1999) 153–165.

[149] A. Denner, S. Dittmaier, and L. Hofer, *Collier: a fortran-based Complex One-Loop LIbrary in Extended Regularizations*, *Comput. Phys. Commun.* **212** (2017) 220–238, [arXiv:1604.06792].

[150] A. Denner and S. Dittmaier, *Reduction of one loop tensor five point integrals*, *Nucl. Phys. B* **658** (2003) 175–202, [hep-ph/0212259].

[151] A. Denner and S. Dittmaier, *Reduction schemes for one-loop tensor integrals*, *Nucl. Phys. B* **734** (2006) 62–115, [hep-ph/0509141].

[152] A. Denner and S. Dittmaier, *Scalar one-loop 4-point integrals*, *Nucl. Phys. B* **844** (2011) 199–242, [arXiv:1005.2076].

[153] S. Dittmaier, *Weyl-van der Waerden formalism for helicity amplitudes of massive particles*, *Phys. Rev. D* **59** (1998) 016007, [hep-ph/9805445].

[154] J. C. Collins and D. E. Soper, *Angular Distribution of Dileptons in High-Energy Hadron Collisions*, *Phys. Rev. D* **16** (1977) 2219.

[155] **CMS** Collaboration, V. Khachatryan et al., *Forward–backward asymmetry of Drell–Yan lepton pairs in pp collisions at* $\sqrt{s} = 8$ *TeV*, *Eur. Phys. J. C* **76** (2016) 325, [arXiv:1601.04768].

[156] H. Lehmann, K. Symanzik, and W. Zimmermann, *Zur formulierung quantisierter feldtheorien*, *Il Nuovo Cimento (1955-1965)* **1** (1955) 205–225.

[157] T. Plehn, *Lectures on LHC Physics*, *Lect. Notes Phys.* **844** (2012) 1–193, [arXiv:0910.4182].

[158] J. C. Collins, *Renormalization: an introduction to renormalization, the renormalization group and the operator-product expansion*. Cambridge university press, 1985.

[159] F. Jegerlehner, *Facts of life with* γ_5, *The European Physical Journal C-Particles and Fields* **18** (2001) 673–679.

[160] D. Kreimer, *The* γ_5*-problem and anomalies—a clifford algebra approach*, *Physics Letters B* **237** (1990) 59–62.

[161] J. Körner, D. Kreimer, and K. Schilcher, *A practicable*γ *5-scheme in dimensional regularization*, *Zeitschrift für Physik C Particles and Fields* **54** (1992) 503–512.

[162] P. Breitenlohner and D. Maison, *Dimensional renormalization and the action principle*, *Communications in Mathematical Physics* **52** (1977) 11–38.

[163] M. Chanowitz, M. Furman, and I. Hinchliffe, *The axial current in dimensional regularization*, *Nuclear Physics B* **159** (1979) 225–243.

[164] **ATLAS** Collaboration, G. Aad et al., *Measurement of the angular coefficients in Z-boson events using electron and muon pairs from data taken at* $\sqrt{s} = 8$ *TeV with the ATLAS detector*, *JHEP* **08** (2016) 159, [arXiv:1606.00689].

German Abstract

Der Drell-Yan-Prozess ist einer der wichtigsten Streuprozesse am LHC und erlaubt unter anderem die genaue Vermessung der Masse und Zerfallsbreite des W-Bosons und die Suche nach neuen Teilchen, wie z.B. Z' Bosonen, in der Region großer (transversaler) invarianter Massen der Leptonen im Endzustand. Um die Präzisionsmessungen am LHC sinnvoll mit Theorievorhersagen vergleichen zu können, müssen die theoretischen und experimentellen Unsicherheiten von einer ähnlichen Größenordnung sein. Auf theoretischer Seite waren die bis vor wenigen Jahren nicht vorhandenen Vorhersagen für Korrekturen der Ordnung $\mathcal{O}(\alpha_s\alpha)$ die größte Quelle für theoretische Unsicherheiten in Vorhersagen von Verteilungen für Drell-Yan-artig produzierte Leptonen.

In [55,56] wurden mit Hilfe der so genannten Polapproximation (PA), bei der die Amplituden der Drell-Yan-Prozesse um die Resonanz der W/Z Bosonen entwickelt und die nicht resonanten Terme vernachlässigt werden, die dominanten Beiträge in der Resonanzregion berechnet. In Rahmen dieser Arbeit wurden die Ergebnisse in [55, 56] durch die bisher noch fehlenden "initial–initial" Korrekturen der Ordnung $\mathcal{O}(\alpha_s\alpha)$ zur Drell-Yan-artigen Z-Produktion komplettiert. Die Klasse der "initial–initial" Korrekturen enthalten dabei sowohl eine QCD als auch eine elektroschwache (EW) Korrektur in der Produktion des W/Z-Bosons. Die Korrekturen lassen sich weiter in eichinvariante QCD $\times$ schwache $\mathcal{O}(\alpha_s\alpha_w)$ und QCD $\times$ photonische $\mathcal{O}(Q_q^2\alpha_s\alpha_{phot})$ Korrekturen aufspalten, wobei sich Korrekturen vom Typ QCD $\times$ photonisch aufgrund ihrer Proportionalität zur Ladung der Quarks im Eingangszustand der Drell-Yan-Prozesse ohne PA berechnen lassen. Das Auftreten von Infrarotdivergenzen erfordert die Anwendung einer geeigneten Subtraktionsmethode, wobei im Rahmen dieser Arbeit die Antennen-Subtraktionsmethode verwendet wurde.
Neben der Berechnung von Vorhersagen für "initial–initial" $\mathcal{O}(\alpha_s\alpha)$ Korrekturen zu invarianten Masse- und Transversalimpuls-Verteilungen der Leptonen im Endzustand wurden Korrekturen derselben Ordnung zur numerisch herausfordernden Vorwärts-Rückwärts-Asymmetrie berechnet. Während die Korrekturen zu invarianten Masse- und Transversalimpuls-Verteilungen der Leptonen im Endzustand phänomenologisch vernachlässigbar sind, erreichen die Korrekturen zur Vorwärts-Rückwärts-Asymmetrie für kleine invariante Massen des Z-Bosons eine Größe von etwa 1% und sind damit insbesondere für den kommenden HL-LHC phänomenologisch relevant. Außerdem wurde der Effekt von Photonrekombination auf die Vorhersagen für die Korrekturen zur Vorwärts-Rückwärts-Asymmetrie untersucht und ein vernachlässigbarer Unterschied zu den Resultaten ohne Rekombination festgestellt.

Da sich Drell-Yan-Prozesse auch zur Suche neuer Teilchen eignen und diese insbesondere in der Region weit oberhalb der Resonanzen der W/Z Boson zu erwarten sind, ist es notwendig Korrekturen der Ordnung $\mathcal{O}(\alpha_s\alpha)$ auch jenseits der Resonanzregion und damit auch ohne die Anwendung einer PA zu berechnen. Als Schritt in Richtung einer vollen $\mathcal{O}(\alpha_s\alpha)$ Rechnung ohne Anwendung einer Approximation wurden im ersten Teil der Arbeit $\mathcal{O}(N_f\alpha_s\alpha)$ Korrekturen zum Drell-Yan-Prozess berechnet. Diese Klasse eichinvarianter $\mathcal{O}(\alpha_s\alpha)$ Zwei-Schleifen-Korrekturen zeichnet sich durch ihre Proportionalität zur Zahl N_f der Fermionfamilien im Standardmodell der Teilchenphysik aus. Die zu den Korrekturen der Ordnung $\mathcal{O}(N_f\alpha_s\alpha)$ beitragenden Diagramme erhalten ihre Proportionalität zu N_f durch das Vorhandensein von geschlossenen Fermion-Schleifen. Diese Einschränkung reduziert die Komplexität der zu berücksichtigenden Diagramme und erlaubt beispielsweise die Behandlung der auftretenden Infrarotdivergenzen mit Ein-Schleifen-Subtraktions-Methoden, obwohl $\mathcal{O}(N_f\alpha_s\alpha)$ Korrekturen Zwei-Schleifen-Diagramme enthalten. Außerdem wurde das in Ein-Schleifen-Rechnungen zur eichinvarianten Behandlung von W/Z-Resonanzen genutzte "Complex-Mass-scheme" zur Ordnung $\mathcal{O}(\alpha_s\alpha)$ verallgemeinert.
Die $\mathcal{O}(N_f\alpha_s\alpha)$ Korrekturen zum integrierten totalen Wirkungsquerschnitt oder zu Rapiditätsverteilungen der Leptonen im Endzustand stellen sich als phänomenologisch vernachlässigbar heraus, da diese Observablen durch resonante W/Z-Bosonen dominiert werden und $\mathcal{O}(N_f\alpha_s\alpha)$ Korrekturen in dieser Region vernachlässigbar klein sind. Die Korrekturen der Ordnung $\mathcal{O}(N_f\alpha_s\alpha)$ zu (transversalen) invarianten Masse- und Transversalimpuls-Verteilungen der Leptonen im Endzustand hingegen wachsen im Bereich großer (transversaler) invarianter Massen bzw. transversaler Impulse auf bis zu 2% respektive 15%.

Acknowledgements

First of all, I want to thank Prof. Dr. Stefan Dittmaier for the opportunity to work in his research group on this very interesting topic, for always taking time to answer my questions, and for his essential hints guiding me in the right direction. There are countless moments spread over the last few years where I was able to benefit from the passion and deep knowledge Stefan has of physics in general and especially of particle physics. I am truly grateful for these last years that led to this thesis. Thanks a lot Stefan!

I am also deeply indebted to Dr. Alexander Huss for the fruitful discussions and his patience during the debugging phase (and also before) of the code used to calculate the results presented in Chapter 6. Without his knowledge of antenna subtraction and particle physics this thesis would not have been possible. Thank you Alex!

I would also like to express my special thanks to Dr. Timo Schmidt for his support in the early stages of preparing this thesis.

I am grateful for all the helpful discussions about particles physics, tigers vs. bears vs. gorillas (I still think a mountain gorilla has a fair chance against a tiger!), and submarines with all group members and especially with Jonas Rehberg, Max Reyer, Sebastian Schuhmacher, José Luis Hernando, Tim Engel, Maria Dias Astros, and Julian Bollig.

Finally, I want to thank my family, in particular my parents, my sister, and Janina. Their support, care, and encouragement especially in times of frustration was vital. Without them the endeavour of completing this thesis would not have been possible.